The differential modulation of receptor tyrosine kinase Axl in human mesenchymal stromal cell responses to modified titanium surfaces

This thesis is submitted in part fulfillment of the requirements for the degree of PhD at UCL.

By

Mohammad Ramine Khan BSc, MSc

August 2011

UCL Eastman Dental Institute

Division of Biomaterials and Tissue Engineering

Declaration

‘I, Mohammad Ramine Khan confirm that the work presented in this thesis is my own. Where information has been derived from other sources, I confirm that this has been indicated in the thesis.'

_____

Mohammad Ramine Khan

Date

Dedication

I dedicate this thesis to my late father, Dr Habib Ullah Khan Afridi (29th December, 1951 to 14th December, 2011), who drew my path in science, and saw and encouraged me through to the point of completing this work. I am forever grateful to my supervisors and the examiners, Prof Timothy Arnett (UCL) and Dr Matt Dalby (Univ. of Glasgow), for letting me this honorable chance of making him a very proud man.

Acknowledgements

I am grateful to the University College London and the UCL Eastman Dental Institute for allowing me the opportunity of scientific research in a first class academic institution. I thank Straumann AG (Walderberg) for providing the valuable titanium biomaterial substrates for this study. Further, I am grateful to the international Team for Implantology (ITI) for funding this project, as well as the University of London's Central Research Fund for their generous award for the gene array analyses.

More so, my whole hearted gratefulness extends to the following individuals whose contributions made this thesis a reality.

My family- I am very blessed and lucky to have you. I feel especially for my late father who guided me through my career in science, and hopefully will so beyond. I am extremely grateful to my wife, mother, brothers and sister for bearing me through this tough period.

My supervisors, Dr. Peter Mark Brett, Prof. Nikos Donos and Dr. Vehid Salih; forever in debt to them for the chance that they gave me at scientific research, their guidance and teaching, and their friendship. I would extend special thanks to Peter for accepting me into his research, at a time when most were closing their doors.

A friend who gave me much needed motivation and technical help was Mohamad Hussein Parkar from biomaterials and tissue engineering. I extend a special thanks to Dr Nicola Mordan for her help in electron microscopy, Dr Hadwa Muawad for RNA isolation and PCR techniques; Mr. Paul Darkins and Dr Paul Buxton for their histological and technical advice, respectively.

My friends who were there for me, thick or thin: Hsyun Shen, Dr Khalid Al-Qahtani, Dion Telesford, Bilal Hassan, Muhammad Bilal Nawazish, Atif Ahmad, Mohd Sardar Khan, Dr Harsh D Amin, Hy Jaynara, Dean, Robb, Lee, Kaha et al., and Krunal 'Krondi' Patel. Finally, I thank the many souls whose names I may have not mentioned here but was part of this journey.

Abstract

Osseointegration is the process of *de novo* bone regeneration on the surface of an endosseous titanium (Ti) implant *in vivo*. This neo formation of bone underlies the physical integration of a Ti implant in bone at a level sufficient to restore loss of function; for example, of mastication due to absent teeth. The outer atoms of a bulk of Ti metal form a stable and passive surface oxide layer that serves as a substrate for the amalgamation of tissue reparative components, which entail the formation of an osseous bond between tissue and fixture. This interaction was empirically demonstrated to be highly affected by the characteristics of the surface an implant in experimental studies querying the varied effects of additive or subtractive physical modifications, as well as altered chemical compositions, of Ti implant surfaces on osseointegration. Subsequent clinical and experimental practices have demonstrated that rough surfaced implants perform comparatively 'better' than their smooth surfaced counterparts by promoting bone growth on the fixture. Moreover, a particular surface modification that yields high surface energy combined with a widely tested micron scaled topographical roughness (modSLA) has been shown to further promote the timely enhancement of osseointegration compared to its hydrophobic rough counterpart (SLA). The biological mechanisms underlying this apparent enhancement of osseointegration by modified Ti implant surfaces are still subject to intense study due to the materials' implications in bone related tissue engineering applications. Amongst the several views being opined is a proposition mainly arising from *in vitro* experimentation, which suggests modified Ti implant surfaces possess an 'intrinsic' osteoinductive potential that affects uncommitted reparative cells by inducing a temporal and magnitudinal enhancement in cellular differentiation and function; in turn, implying the early formation of functional osteoblasts and bone tissue matrix in an *in vivo* scenario. The observations of differential cellular behavior include the apparent modulation by the modified surfaces, of a cell surface receptor tyrosine kinase Axl in human osteoblasts. The proposed role of the receptor in negatively regulating osteogenic mineralisation in uncommitted pericytic cells suggests an association with the altered response of cells to these substrates. The aim of this project was to examine and test the hypothesised differential modulation of Axl in the responses of human marrow derived mesenchymal stromal cells to modified Ti implant substrates.

Table of contents

List of figures

List of tables

List of abbreviations

^{o} C	Degree Celsius
αMEM	alpha Minimum Essential Medium
Ala	Alanine
Axl-MAb	Axl antagonist with monoclonal antibodies
BIC	bone implant contact
BS-SEM	back scattered scanning electron microscope
C1-TEN	tensin like C1 domain containing phosphatase
CFU	Colony forming unit
CPC	cetylpyridinium chloride
cm^2	Centimetre square
Ct	Threshold cycle in real time polymerase chain reaction
d	Day
Divalent cation-free PBS	Ca and Mg ion free phosphate buffered saline
DMEM	Dulbecco's modified Eagle medium
dpi	Dots per inch
ECM	extracellular matrix
EDTA	Ethylenediaminetetraacetic acid
ELISA	Enzyme-linked immunosorbent assay
FBS	Foetal bovine serum
FOP	Fibrodysplasia ossificans progressiva
Gas6	Growth arrest specific type 6
Glu	Glutmaic acid
GM	growth medium
GDF15	growth differentiation factor type 15
Grb2	Growth factor receptor-bound protein 2
h	Hour
H_2SO_4	Sulphuric acid
HCl	Hydrochloric acid
hMSC	human mesenchymal stromal cell
HSC	hematopoietic stem cell
kDa	Kilo Dalton
Lck	Lymphocyte-specific protein tyrosine kinase
Ile	Isoleucine
Leu	Leucine
Lys	Lysine
min	minute
ml	Milli litre
mm	Millimetre
mM	Milli Molar
MSC	Mesenchymal stromal cell
mMSC	Mature mesenchymal stromal cell

modSLA	Hydrophilic modified SLA surface
MTT	Dimethylthiazol diphenyltetrazolium bromide
N	Number of donors
n	Number of experimental replicates
Nck2	Cytoplasmic signaling protein
NPP	Nitrophenyl phosphate
OM	Osteogenic medium
OC	Osteocalcin
OPG	Osteoprotegrin
PBS	Phosphate buffered saline
P	Polished Ti
pH	Power of hydrogen
PLC-γ	Phospholipase gamma
PI3K	Phosphatidyl inositol 3 kinase
R_a	Arithmetic mean of vertical distance between least and highest points in a surface profile
RanBPM	Ran binding phosphoprotein
RANK	Receptor Activator of Nuclear Kappa
RANKL	Receptor Activator of Nuclear Kappa Ligand
RGD domain	Arginine-Glycine-Aspartic acid motif
rhGas6	Recombinant human growth arrest specific 6 protein
RTK	Receptor tyrosine kinase
RT-PCR	Real time polymerase chain reaction
SH_2	Src homology domain
SiO_2	Silica oxide
SLA	Surface prepared by sand blasting and acid etching
SEM	Scanning electron microscope
SOCS-1	Suppressor of cytokine signaling 1
c-Src	Cellular homolog of Src
TAM receptor	Tyro, Axl, Mer family of receptors
TCP	Tissue culture plastic
TGFβ1	Transforming growth factor beta type 1
Trp	Tryptophan
Tyr	Tyrosine
UK	United Kingdom
µm	Micrometer
µM	Micro Molar
USA	United Staes of America
w	week
Wnt5a	Wingless- type MMTV integration site family member 5A

1 Introduction

1.1 Bone

1.1.1 Bone tissue

Bone or osseous tissue may be defined as an extracellular matrix composed of a scaffold of tri-fibrillar collagen molecules with interspersed non-collagenous proteins and calcium phosphate mineral (Hall, 2005). It is a hard connective tissue in vertebrates that in combination with vascular, lymphatic, connective or nervous structures forms the organ, bone. A total of 213 different bones combine to form the skeletal system of the human that constitutes ~ 18 % of the weight of an adult body (Tortora and Derrickson, 2009a; Clarke, 2008). The anatomical aspects of a prototypic bone are divisible into seven structural entities (illustrated in figure 1-1). Of these, the diaphysis, epiphyses and metaphyses form the larger bone structure, with the articular cartilage and periosteum occurring on the outside and, medullary cavity and endosteum within. These structural entities occur in various relative proportions in the diverse range of bones that form the human skeleton (Clarke, 2008).

Bone tissue is macroscopically organised into two distinct architectural forms. These are cortical and cancellous that constitute 80 % and 20 % of the adult human skeleton, respectively (Clarke, 2008)(figure 1-2). The former is relatively dense and compact while the latter is spongy with a ‘honey comb’ of branching bars and/or plates called ‘trabeculae’ (Vassilios et al., 2001). The architecture of cancellous bone accommodates a higher level of vascular tissue compared to cortical bone, which nourishes bone marrow and its embedded populations of various stem cells (Tortora and Derrickson, 2009a). Cortical and cancellous bones are chemically identical; roughly estimated to comprise of 25 %, 25 % and 50 % of water, collagen fibres and crystallized mineral salts, respectively. The predominant mineral salt is a combination of calcium phosphate and calcium hydroxide, which combine with di-cations and carbonates to form the mineral half of bone called hydroxyapatite (chemical formula: $Ca_5(PO_4)_3(OH)$) (Tortora and Derrickson, 2009a).

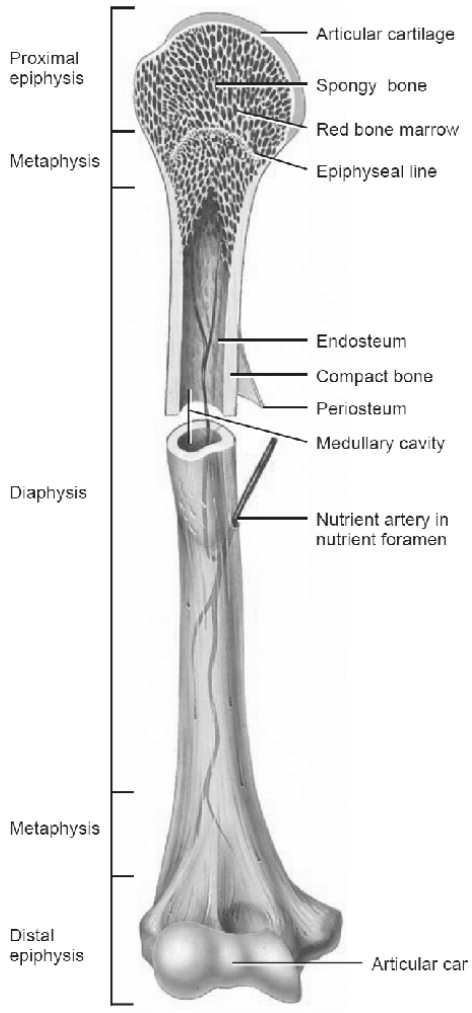

Figure 1-1 Macro-structural organisation of bone

Image shows a long bone (humerus, arm) with structural segments highlighted along a descending vertical axis on the left hand side of image; and sub-cortical structures of a transverse section on the right hand side. The centre diaphysis constitutes the hollow body. It predominantly consists of cortical osseous. The epiphyses form the poles of a long bone. They are cancellous, made of trabecular bone with relatively higher vascularisation and marrow content. The metaphyses are cartilaginous sub-epiphyseal zones of bone growth that later turn to a calcified epiphyseal line at adulthood. Prior to this, the metaphyses instigate longitudinal growth of a bone. The articular cartilage is a thin layer of hyaline cartilage covering the epiphyses. It occurs at articular joints to reduce friction between adjoined bones during motion. The periosteum is an almost continuous bi-layer membrane surrounding the external surface of bone except at joints. Its outer layer is composed of a dense irregular fibrous connective tissue that mainly serves as a substrate for tendon and ligament attachment. The inner osteogenic layer is highly vascularised and contains osteogenic cells. The medullary cavity is the hollow cylindrical space within the diaphysis. The endosteum is a single cell layer membrane that lines the internal bone surface facing the medullary cavity. Image taken with permission from (Tortora and Derrickson, 2009a).

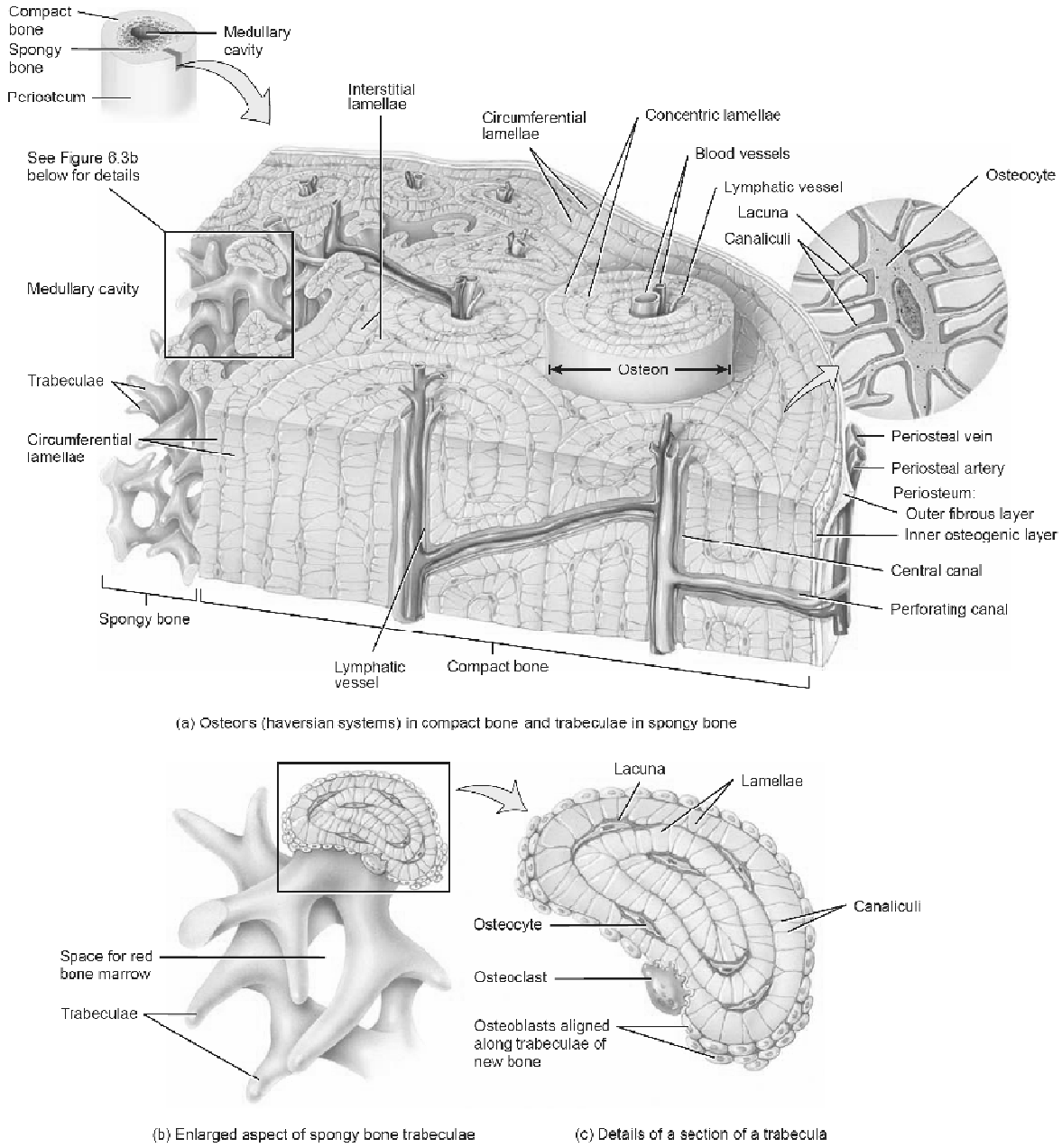

Figure 1-2 Micro-structural organisation of bone

Figure shows a cross section along the transverse and sagittal planes of a hypothetical disaphyseal segment of a bone. (a) The axis from right to left shows periosteum followed by compact cortical bone in the middle and spongy bone to the left. An osteon, Haversian canal, resident blood and lymphatic vessels are surrounded by concentric rings of lamellae. Spaces between lamellae are either lacunae (osteocyte sites) or emanating canaliculi, indicated in the magnified representation on the upper right hand side are trabecular rods that lamellae are arranged into. (b & c) Magnified views of the cross section of trabecular bone indicating the irregular arrangement of lamellae. Figure re-produced with permission from (Tortora and Derrickson, 2009a).

The micro-architecture of cortical bone ascribes it a unique stiffness to sustain large forces compared to cancellous bone. Cortical bone is composed of many repeating structural units called osteons or Haversian systems (figure 1-2). Each osteon is essentially a cylinder with many internal concentric rings encircling a central canal that averages 0.2 mm in diameter and 10 mm in length (Clarke, 2008). The centre hollow canal of the osteon is the Haversian canal and may be occupied by small blood vessels, nerves or a lymphatic vessel. This canal is surrounded by concentric layers of mineralised extracellular matrix sheets called lamellae. In between the lamellae occur spaces called lacunae. These spatial confinements contain the terminal state of the bone producing osteoblast, called the osteocyte, which becomes entrapped in the ECM during osteogenesis. Individual osteocytes are physically linked via intercellular filaments through cellular gap junctions, radiating in all directions from lacunae occur in small channels called canaliculi, extending like a network throughout cortical bone. Several osteons are separated from each other by interstitial lamellae, and the collection of all osteons is encircled by circumferential lamellae that lie directly beneath the periosteum. This arrangement of osteons is not present in cancellous bone. Instead, lamellae are arranged in an irregular concentric manner to form beams or rods, the spatial arrangement of which gives it the spongy macroscopic appearance. Blood vessels, nerves and lymphatic channels diffuse from the periosteum into bone through the transverse perforating Volkmann's canals. These connect with equivalent structures in the Haversian canals or in the medullary cavity to form a closed circulatory circuit (Sikavitsas et al., 2001; Tortora and Derrickson, 2009a).

The collection of 'cranio-facial' bones, which are of interest to this study, are fourteen in number: these include two nasal bones, two maxillae, two zygomatic bones, the mandible, two lacrimal bones, two palatine bones, two inferior nasal conchae, and the vomer (Tortora and Derrickson, 2009b). These bones vary in structure in the ratios of cortical to cancellous bone, which clinical dentistry has classified in to four types based on radiographic appearance and resistance to surgical drilling (Lekholm et al., 1985). Type 1 is homogenous compact cortical bone that occurs in relative majority in the anterior mandible and maxillae. The other types consist of varying ratios of cortical to cancellous bone, and occur mainly towards the posterior of jaw, primarily of the maxillae.

Type 2 consists of a thick layer of cortical bone surrounding a core of dense cancellous. Type 3 consists of a thin layer of cortical bone around dense cancellous. Type 4 consists of a thin layer of cortical bone surrounding a core of low density cancellous. In general, type 1 occurs predominantly in the anterior portion of the jaw, and transitions through types 2 and 3 to type 4 towards the posterior (Lekholm et al. 1985).

The physiological functions of bone can be roughly categorised into mechanical, synthetic and metabolic (Clarke, 2008). Bone provides shape and protection to inner organs and in combination with muscular activity creates movement. The skull bone is further endowed with the reception and transmission of sound waves through a process called ‘bone conduction’ (Stenfelt, 2011). From the synthetic perspective, it serves as a life-long reservoir of progenitor cells that form blood and mesenchymal tissues (De Silva Merielles, 2008). The metabolic aspects are several but primarily pertain to the maintenance of calcium and phosphorus levels in blood. Interplay between paracrine hormonal feedback loops of the parathyroid hormone and thyroid-secreted calcitonin, strive to maintain plasma calcium ion concentrations within the homeostatic range of 9 and 11 mg / 100 ml by instructing the absorption or release of ions through osteogenesis or bone remodeling, respectively (Tortora and Derrickson, 2009a). In addition, bone also has been considered to have endocrine function through fibroblast growth factor 23 and osteocalcin (OC), which are suggested to have a role in the regulation of serum calcium and phosphorus levels (Fukumoto and Martin, 2009).

1.1.2 Ontogeny

The process of osseous tissue formation is called osteogenesis or ossification (Gilbert, 2000; Shapiro, 2008). This occurs in four discreet scenarios: embryonic bone formation, post natal bone development, bone remodeling and fracture repair (Dimitriou et al., 2005). It may additionally take place in the form of ectopic bone formation in certain pathological states such as vascular calcification (Vattikut and Towler, 2004), as well as in a *de novo* form on the surface of endosseous implants.

1.1.2.1 Embryonic bone development

The process of osteogenesis is initiated in the embryo. Fetal bone is derived from the paraxial mesoderm. Three distinct lineages of embryonic cells generate different segments of the osseous skeletal assembly. The somites form the axial skeleton, lateral plate mesoderm the limb skeleton, and the cranial neural tube form the branchial and cranio-facial bones (Gilbert, 2000; Clarke, 2008; Chung et al., 2004).

Fetal bone development initiates from embryonic mesenchymal stem cells in two distinct modes; intramembranous and endochondral ossifications (Mackie et al., 2011; Shapiro, 2008). The former underlies the formation of bones of the skull and mandible while the latter concerns formation of the limbs and axial skeleton. In intramembranous osteogenesis, neural crest derived mesenchymal cells proliferate and condense into sheets that form compact nodules. These form either blood capillaries or osteoblasts. The osteoblasts form an ‘ossification’ centre and secrete osteoid, a collagen rich calcium-nucleating proteoglycan matrix, eventually becoming entrapped within it as ‘osteocytes’ (Clarke, 2008). The osteoid serves as a high affinity platform for the deposition of calcium mineral salts, which calcify the osteoid to form ‘woven bone’. This type of bone is characterised by irregularly orientated collagen fibrils, large space between fibrils and vascular structures, and low mineral quantity that confer low mechanical integrity to the skeleton (Chung et al., 2004; Sikavitsas et al., 2001). The mesenchymal precursors at the periphery form the periosteum over these bones (Gilbert, 2000; Shapiro, 2008).

The process of endochondral ossification forms the vertebral column, pelvis and limb bones. It comprises bone formation through an endochondral intermediary in a process that takes place over five steps. It initiates with the aggregation of mesenchymal precursors in the shape of prospective bones and their commitment to a chondrocytic lineage by the action of lineage specific transcription factors (Mackie et al., 2011). This is followed by the cells compaction to dense nodules and differentiation to terminal chondrocytes. This pre-cartilaginous stage is characterised by the downregulation of expression of the SOX9 transcription factor, believed to signify the transition from chondro- to osteo- genesis (Hattori et al., 2010). In the third phase, differentiated chondrocytes

divide and secrete hyaline cartilage forming a framework referred to as the cartilage model. The chondrocytes continually proliferate and secrete ECM molecules to advance the interstitial growth of the cartilage model, as well as outer peripheral cartilage formation through appositional growth originating from an embryonic structure called perichondrium. These cells later cease replication in the fourth stage and turn into large hypertrophic chondrocytes, which secrete collagen type X and fibronectin to enable mineralisation (Shapiro, 2008; Mackie et al., 2011).

Hypertrophic chondrocytes in the centre of the developing organ die by apoptosis due to the lack of nutrient supply(Mackie et al., 2011). Their apoptosis forms empty lacunae that fuse to form small cavities. In the fifth stage, angiogenesis causes the generation of new osteoblasts in the middle and peripheral zones of the model, which instigate the continual replacement of cartilage with osseous (Clarke, 2008). In combination with the small cavities, the osteoblasts lead to form a trabecular matrix within the developing organ while peripherally replacing the perichondrium with the cortical osseous generating periosteum (Gilbert, 2000; Tortora and Derrickson, 2009a; Chung et al., 2004).

1.1.2.2 Post natal bone development

The epiphyseal plate is a layer of hyaline cartilage with chondrocytes. It underpins the increase in post-natal bone length through the interstitial growth of cartilage and its replacement with osseous on the disaphyseal side of the plate via endochondral ossification (Shapiro, 2008). The periosteum increases bone thickness by forming osteoblasts that deposit osseous on the periphery of the organ (Tortora and Derrickson, 2009a; Clarke, 2008).

Bone is continually ‘recycled’ through the tightly regulated process of remodeling through which initially laid woven bone is converted to a stronger lamellar bone (Sikavitsas et al., 2001). This is a synergistic process, mediated by hormonal feedback loops that involves bone resorption by the osteoclast and formation in layers by osteoblasts (Clarke, 2008). The dynamics of this process differs in different regions of the skeleton and with age. It is highest in regions of high density of cancellous bone, presumably to accommodate change in incurred forces by the sensitive tissue type, and during post fetal to early youth (Sikavitsas et al., 2001).

Combinations of the three primary parts of bone development occur during all forms of bone fracture healing, which has been grouped into primary and secondary based on the type of ossification (Dimitriou et al., 2005; Fazzalari, 2011). Primary fracture healing occurs exclusively in cortical bone and is mediated by the periosteum. This is similar to intramembranous ossification with the exception of the membrane sheets being replaced in this instance with layers osteoblasts covering all edges of the fracture and striving to regenerate osseous continuity in the organ. The secondary form of bone healing, which mainly occurs in long bone fractures, is a combination of endochondral and intramembranous ossification that involves the formation of a semi-cartilagenous intermediate and its resulting transformation into a hard callus (Dimitriou et al., 2005).

Bone formation may additionally take place in pathological instances as ectopic ossification in tissues other than bone. This has been recorded, for example, in fibrodysplasia ossificans progressiva (FOP) (Shore et al., 2006) and related muscular calcifications, as well as in instances of vascular calcification (Johnson et al., 2006). These pathological states represent situations that entail the formation of bone with related marrow and vascular components in soft tissues such as muscle, tendon, and cardio-vascular system (Chen et al., 2008). A further case, which is the subject of this study, is the formation of bone on the surface of endosseous dental implants leading to their stable integration. This has been proposed to represent a *de novo* form of osteogenesis (Davies, 2003).

1.1.3 Cells

Bone contains an array of different cell types. These include non-osseous cells, such as vascular, nervous and immune cells, and osseous specific cells: marrow stroma, osteoblasts, osteocytes and osteoclasts. The latter maintain the physiological integrity of the skeletal system through life (Aubin, 2001). The marrow stroma resides in vascular rich cancellous bone. These are reticular stromal connective tissue cells that sequester adult stem cells (Aubin, 2001). Two types of stem cells are believed to occur within bone marrow stoma; the hematopoietic and mesenchymal stem cells. The former gives rise to blood progenitor cells while the latter is believed to instigate the lifelong replenishment of mesenchymal tissue precursors. The osteoblasts and osteocytes are bone

generative cells that represent two different stages in the life cycle of the same cell type, while osteoclasts are bone degenerative cells originating from monocytes (Fujita and Janz, 2007).

The osteoblast originates from an adult mesenchymal stem cell (MSC) through the tightly regulated sequential process of osteogenic differentiation (Marie, 2008). This is a complex molecular process, believed to surround a key axis involving Wnt/β-catenin positive signaling, which modulates bone morphogenic protein type 2 (BMP2), p53, osterix and alkaline phosphatase axis (Fujita and Janz, 2007). The induction of this axis entails a sequence of cellular 'transformations', in which an MSC initially commits to a pre-osteoblastic progenitor phase characterised by the expression of collagen type 1, osteonectin and alkaline phosphatase with high cell proliferation rates (AR Guntur and CJ Rosen, 2011; Shapiro, 2008). This state leads to the pre-mature phase of a functional osteoblast that produces osteoid tissue. Osteoid formation is divisible into two phases; collagen matrix elaboration, and pre-calcification assembly (Clarke, 2008). Initially collagen fibril subunits are translated and secreted by the cells into the ECM where they align and polymerise to form a fibrillar collagenous scaffold. The cells produce Alkaline phosphatase and matrix components including bone sialoproteins (types 1 and 2), and Osteocalcin amongst the many. In the pre-mineralisation phase of a maturing osteoblast, these components are secreted by means of budding cytoplasmic-membrane vesicles (50 – 200 nm size) that attach at points in the osteoid to form calcium nucleation sites (Sikavitsas et al., 2001). In the matrix bound vesicles, Ca^{2+} ions and inorganic phosphate are combined to form 'octa-calcium phosphate', which then penetrates the vesicle membrane, and combines with the highly osteogenic microenvironment to grow into hydroxylapatite (Anderson et al., 2005; Chen et al., 2008). This molecular interplay accommodates two modes of osteogenic extracellular matrix mineralization, which initiates with homogeneous mineralization of calcium nucleation mediated by non-collagenous calcium binding (sialo) proteins and later through calcium ions in the environment via heterogeneous mineralization (Shapiro, 2008; Sikavitsas et al., 2001). The mature osteoblast co-secretes several different factors (Clarke, 2008), but of importance are the soluble osteoclastogenic inhibitory factors that determine the balance between bone formation and resorption Two important ones being osteoprotegrin (OPG, pseudo-receptor for Receptor Activator of Nuclear Kappa Ligand (RANKL)) and growth differentiation factor 15 (GDF-

15) (Caetano-Lopes et al., 2007). The former (OPG) binds RANKL expressed on the surface of osteoblasts, preventing its interaction with its cognate receptor RANK, a cell surface molecule expressed on monocyte-macrophage lineage cells (Takahashi et al., 2011). The mature osteoblast would be later faced with a probability of further maturing to the terminal form of an osteocyte, estimated to be achieved by 20 percent of cells while 80 percent perish by apoptosis. The osteocytes are characterised by their cellular processes traversing in all directions, from lacunae to lacunae, forming a network of what many regard as a bone sensory systems that regulates the larger part of bone physiology by sensing changes in physiological levels of calcium or hormones, as well as enacting as a 'mechanosensor'; transducing mechanical forces felt from the external environment to an instigated biological response (Sikavitsas et al. 2001).

The osteoclast undertakes bone resorption. It originates from the fusion of hematopoietic monocytic cell populations through the effects of macrophage-colony stimulating factor (M-CSF) and ligand of receptor activator of nuclear factor kappa B (RANKL), eventually taking the form of a multinucleated bipolar cell with a high quantity of mitochondria and lysosomes (Novack and Teitelbaum, 2008). This process is negatively regulated by a ligand to RANKL called osteoprotegrin (OPG). The dorsal face of the cell in contact with bone is ruffled with emanating cellular processes. It overlies a bone resorption pit, enclosed on all ends by sealing zones. An osteoclast resorbs bone by secreting hydrogen ions into the pit, thus reducing the pH and then secreting acidic enzymes that extract the calcium phosphate crystals first and then digest the organic phase(Novack and Teitelbaum, 2008). The resulting ions and protein fragments are endocytosed and released into the extracellular fluid through the ventral side of the cell (Sikavitsas et al., 2001).

1.2 Osseointegration

1.2.1 Discovery

Per Ingvar Branemark coined the term osseointegration to define the phenomenon of titanium (Ti) metal integration in living bone tissue. The observations leading to this discovery were made in vital microscopy experiments performed in the early1950s aimed at examining bone repair and

microvascularisation in rabbits (Branemark, 1983). A vital microscope is an optical device that consists of a metallic chamber housing an objective lens. The device would be implanted transdermally with the objective set over a site of interest. Visual examinations in situ in real time would be conducted by mounting the implanted device to a specialised microscope (Branemark et al., 1964).

The early designs of vital microscopes relied on incident and reflected light, and were restricted in application to capillary beds in the ears and eyes of subject animals. For his purpose, Branemark used a modified design vital microscope, in which the metal chamber was made from Ti metal, and transillumination was used as a source of light. The choice of Ti was largely based on the metal's known corrosion resistive properties considered capable of withstanding the variable *in vivo* environment, as well as its large scale availability due to the developing air industry of that time (Ulf Bagge, 1989).

The Branemark chamber would be implanted *in vivo*, supported by appendages screwed into bone, with the lens placed over a site of interest comprising cortical bone ground to a thickness of ~ 10 - 20 um with respect to the underlying marrow. This allowed the visualisation of bone microvasculature and marrow, and their inter-relationship in tissue repair (Branemark and Harders, 1963). When retrieving the devices, Branemark and colleagues noticed host bone to have grown into spaces present on the Ti devices rendering them 'inseparably incorporated' in living bone tissue (Branemark et al., 1969). This observation was followed by a series of successful experiments in animals, and trials in humans with screw shaped Ti fixtures for edentulism (lack of teeth). These successful attempts led Branemark, and a Swiss scientist named A Schroeder, to present clinical and histological evidence, respectively, to the concept of intra-osseous integration of Ti implants (Branemark et al., 1977); (Branemark, 2005).

1.2.2 Definition

1.2.2.1 Present working definitions

Osseointegration does not have one single definition. It has been variably defined by different observers, using different scientific methods and scales. These have predominantly included long-term clinical trials, evaluation of implant-bone interfacial mechanical parameters, and histological & morphological details of the bone-implant interface (Santos et al., 2002).

The initial definition provided by Branemark following a 10 year review of screw shaped Ti dental implants in humans was that it is a system of implanting a Ti made screw shaped device in bone to form a 'direct structural and functional connection between living tissue and the surface of the implant' (Branemark et al., 1977). This definition was modified to include a mechanical evaluation of healing that considered osseointegration to have occurred if there was no progressive relative motion between the fixture and surrounding living bone and marrow under functional levels i.e. oral movements, such as mastication, in a 'load bearing condition' (carrying an artificial tooth) (Branemark, 2005). Histological and microscopic examinations further defined it as the state attained by clinically successful implant devices, characterised by 'the close apposition of new and reformed bone with (an implanted) fixture that at the light microscopic level has no intervening connective or fibrous tissue' (Branemark, 2005; Santos et al., 2002).

1.2.2.2 Limitations of definitions

These attempts at defining the phenomenon presented a 'consequent' view of clinically scaled osseointegration; i.e. measurements of variables in successful cases of implantation. This state of success had been known very early to be a function of a multitude of factors, which primarily include (i) host bone variables; (ii) site of implantation; (iii) competence of surgical procedure; (iv) implant material; (v) implant design and finish; (vi) implant loading time and conditions; and (vi) host hygiene (Albrektsson et al., 1981; Wennerberg and Albrektsson, 2009; McNutt and Chou, 2003) . This apparent lack of a 'true' perspective of this process partly underlies the inexplicable state of

implant failure (Santos et al., 2002); the other reason is the incredible variability between studies and specimen, preventing any collective inference (Wennerberg and Albrektsson, 2009).

Take the following for example: a failed outcome is reported to be relatively higher for the posterior than anterior maxillae (Tinsley et al., 1999) suggesting that an implant that may be retained well in the anterior mandible (reported >90% success rate) may not perform in a comparable manner in the posterior maxilla (reported 35% success rate) of the same patient (McNutt and Chou, 2003).These anatomical sites differ in the ratio of cortical to trabecular bone, (ironically) based on a classification derived to counter the tissue related factor of implant failure by providing a reference for evaluating implant sites (Lekholm et al., 1985). The multi-factorial variability of the possible outcomes of this process bears an obvious burden: with all lateral aspects aside, what is osseointegration?

1.2.2.3 Biological perspective

The biological events constituting osseointegration are not fully known (Brett PM et al., 2004; Wall et al., 2009; Raghavendra et al., 2005). This is largely due to the widely acknowledged effectiveness of dental implants that are applied in a relatively larger proportion to single tooth replacements, thus negating the incentive to oppose general ethical standards for intrusive study of its complexities in living organisms. But also due to the relative higher interest in the commercial status of working endosseous implants compared to the work the implant conducts i*n vivo*. A derivative of this fact is the lack of consensus on implant design parameters, evaluation methods and efficacy studies (Wennerberg and Albrektsson, 2009).

A biologic perspective may consider osseointegration synonymous to a novel form of wound healing, which combines primary or cortical bone-fracture healing with *de novo* bone regeneration, to form an osseous continuity between implant and tissue (Marco et al., 2005);(Dimitriou et al., 2005; Davies, 2003; Davies, 2007). Systemic in nature, it is suggested to initiate with the recruitment of tissue reparative elements to the bone-implant interface, where a synergy between the ‘response of the host to the implant and behavior of the biomaterial *in vivo*’ determines the outcome of the process (Puelo and Nanci, 1999).

1.2.3 Biological paradigm of osseointegration

A model depicting the process of osseointegration has been drawn from histological and ultra-structural studies of Ti implants retrieved from animal and human sources. It proposes a tandem sequence of *in vivo* events instigated systemically in bone tissue in response to implant placement. These are osteoinduction, osteoconduction and bone remodeling (Davies, 2003; Davies, 2007; Davies, 1998; Albrektsson and Johansson, 2001). Osteoinduction is the initial event constituting the migration of tissue progenitor cells to the implant surface and their attachment, proliferation and subsequent differentiation on the substrate. It is followed by osteoconduction, which is the formation of woven bone at the bone-implant interface leading to an osseous union between implant and adjacent tissue. Osteoconduction is further divided to (i) contact osteogenesis, the *de novo* bone formation on the surface of the implant, and (ii) distance osteogenesis, the formation of bone on the surface of old bone apposing the implant. These steps occur within the initial stages of implant placement, in parallel to processes constituting normal tissue repair (such as angiogenesis; debris clearance; immunity). They are followed at a later stage of healing by physiological bone remodeling, an osteoclast and osteoblast mediated replacement of the woven osseous continuity with structurally robust lamellar bone over the course of time.

1.2.4 Practicality of biological paradigm

The biological paradigm of osseointegration is described below in a hypothetical scenario of the placement of a cpTi root form endosseous dental implant into an anterior mandibular bone site, assuming a controlled surgical process, good patient health, bone tissue variables and a smooth Ti implant surface. An endosseous implant is commonly a screw shaped threaded cylindrical object (figure 1-3). It is placed in the alveolar ridge of jaw bone where it remains submerged under the oral mucosa till the point of being loaded with an abutment. It is inserted in bone by surgically drilling a cavity transcending only one cortical plate. The implant is generally of a diameter slightly wider than that of the cavity, and upon insertion through a ‘screwing’ process, laterally displaces cortical bone to form a tight junction. This effect is called press-fit. It causes compaction and circumferential necrosis of bone in a region 0.1 mm from implant surface, laterally extending 2/3rd of the length of

the implant in contact with cortical bone. The distal 1/3rd segment of the implant contacts trabecular bone and marrow, displacing them anterior to their previous position.

Figure 1-3 A standard Ti endosseous dental implant

Image shows an artificial tooth attached via an abutment to a threaded endosseous Ti implant. The bottom threaded Ti implant is the first to be placed in bone. Its subsequent healing, clinically assessed by examining relative micro-motion and x-ray scans of bone-material interface, may occur anywhere between 3-6 months depending on the type of the implant surface. Till then, it remains submerged beneath the oral epithelium. The abutment and artificial tooth are added after complete osseointegration is achieved by the implant. Image taken from (Liu et al., 2004) and re-reproduced with permission.

The press-fit effect achieved in the cortical plate with the proximal 2/3rd of the device attributes 'primary' stability to the implant, defined as a mechanically rigid fixation with significant lack of relative micro-motion at implant-bone interface (Marco et al., 2005). This insertion of the implant in bone initiates a cascade of healing responses from the host tissue. The initial responses that precede osseointegration are (i) haematoma & clot resolution, which stabilize the fresh wound, followed by (ii) granulation tissue formation, which forms a vascularised embedment for the forthcoming osteoprogenitor cells (Raghavendra et al., 2005)

The haematoma forms in the space at the bone implant interface from blood being discharged from severed vessels. Small molecules such as water, ions and serum proteins adsorb the electrostatically negative surface of the implant, saturating it almost instantaneously. In the mean time, platelets amass at the implant site and attach to the implant surface through Von Willebrand factor, and RGD (Arginine-Glycine-Aspartic acid) motif containing implant adsorbed proteins (Lindhe et al., 2000). Platelets initiate a coagulation cascade, releasing factors and cytokines (platelet-derived growth factor and Transforming growth factor-beta), which form a positive feedback loop, further recruiting & activating platelets as well as inflammatory and uncommitted cells (Lindhe et al., 2000). Subsequently, a fibrin clot is formed at the interface that stabilises by three days post implantation (Davies, 2003) (Raghavendra et al., 2005).

It is in these initial three days that angiogenesis is initiated from the ends of sheared vessels emanating from proximally displaced trabecular bone and marrow. This transforms the stable fibrin clot into a highly vascularised ‘Granulation’ tissue, which persists for a period of three weeks post implantation (Lindhe et al., 2000). Un-differentiated adult stem cells recruited to the wound are believed to use this fibrin meshwork to reach the implant surface (Davies, 2003), where overwhelming differentiation cues induce their osteogenic commitment and osteoprogenitor proliferation, eventually forming osteoblasts that deposit mineralised matrix on the implant surface. This phase of progenitor cell migration to the surface of the implant and osteoblastic differentiation constitutes osteoinduction while that of mineralized bone deposition is osteoconduction (Albrektsson and Johansson, 2001).

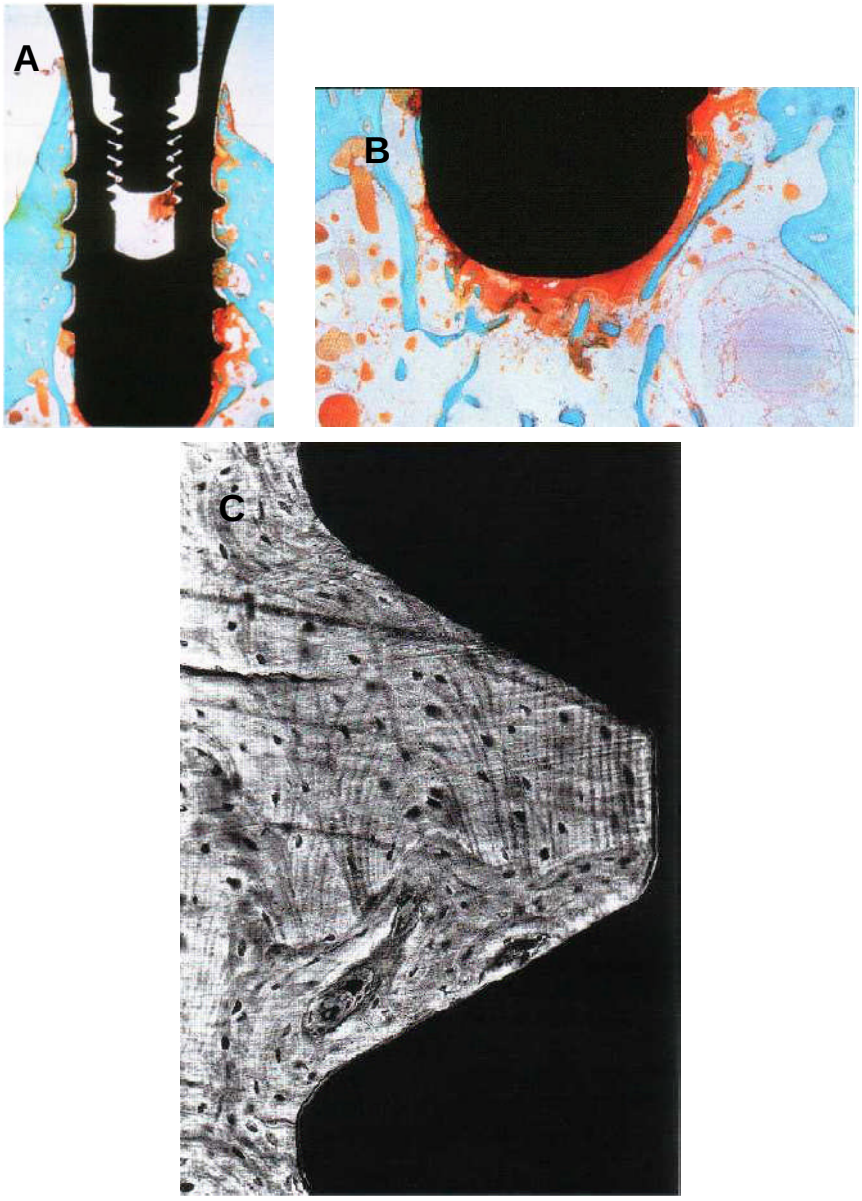

Figure 1-4 Comparison of early and later tissue implant sections

Histological slides of bone-implant interface retrieved from experimental subjects. (A and B) 24 h post implantation in the alveolar ridge of the mandible. Images show mineralisation front in (toluidine) blue, blood clot in red, marrow as white, and implant as black. Images indicate spaces present at interface, occupied largely by blood clot. (C) Complete osseointegration, with bone to implant contact without any intervening tissues. Black is implant. Grey is bone. Lacunae are the dark dots in the grey mass. Concentric lamellae are apparent. Images re-produced with permission (Lindhe et al. 2000).

The osteoblasts initiate *de novo* bone formation on the implant surface by initially depositing a non-collagenous dense layer (10 to 100 nm thick) composed primarily of osteopontin and integrin-binding bone sialoprotein type 2, two high affinity calcium nucleating proteins. This is followed by

the deposition of layers of osteoid (collagen and associated proteins) that later mineralise to osseous. This process is called contact osteogenesis while that occurring on the opposing bone surface, which is reminiscent to primary bone healing, is termed distance osteogenesis (Davies, 2007; Dimitriou et al., 2005). The initial type of bone formed during osteoconduction is woven bone that is composed of loosely packed collagen fibrils lacking an ordered spatial arrangement with low mineral density. Woven bone formation continues till two months, during which it is progressively replaced by lamellar bone through the osteoclast mediated remodeling of bone. This subsequently leads to complete healing by six months post implantation that is clinically scaled as a fixture with lack of relative motion with reference to surrounding bone and radiographic lack of intervening soft tissues at the bone - implant interface (Sakka and Coulthard, 2011; Marco et al., 2005). It is after such an assessment that an abutment and artificial tooth are loaded to restore masticatory function.

Osseointegration can only happen due to the presence of *de novo* bone regeneration on the implant surface during contact osteogenesis. In an adult organism, osseous tissue, particularly from the cranio-facial region, is reformed by osteoblasts on pre-existing bone largely through the process of primary cortical wound healing, in which adjacent ends of a fractured bone re-establish osseous continuity through intramembranous ossification (Dimitriou et al., 2005). However, in contact osteogenesis, osseous formation is initiated on an inanimate metallic surface, and to an extent that the continuity formed is sufficient to withstand strong forces of jaw motion without major impediment to host tissue.

1.3 Implant surface modifications

1.3.1 Titanium biocompatibility

Biocompatibility is a contextual term that generally defines a material's ability, due to its inherent physical and chemical properties as well as commercial viability, to perform with an appropriate response in a specific application (Brunette et al., 2000). The high probability of integration of Ti metal to bone was an important discovery at that time as prior metal implants had predominantly led to 'fibrous-integration', i.e. the encapsulation of a metallic implant by a fibrous ECM. The occurrence of fibrous tissue at the material-tissue interface was considered to be recognition and rejection of

the metal by the body, as the nature of this soft tissue was incapable of providing adequate integration and functionality to the implant (Santos et al., 2002). Indeed, it was the widespread occurrence of fibrous-integration that led to the initial skepticism surrounding osseointegration when it was first discovered, and remained until after a decade of clinical trials and innovative experimental findings were presented. Osseointegration highlighted Ti, and its properties attributing 'biocompatibility' with bone were studied.

From the physical perspective, Ti metal has an inherently low modulus of elasticity and low stiffness that render it ideal to receive mechanical forces, and distribute them across to surrounding bone, hence permitting the functional replacement of a missing tooth (Liu et al., 2004). However, the primary factor considered to underpin the biocompatibility of Ti metal is the chemical nature of its 'native' surface oxide layer. Ti is a transition element and is highly reactive in an elemental state, spontaneously forming a stable ~ 3 - 7 nm thick oxide layer on the surface. This layer is credited to impart the metal with corrosion and ion-leaching resistance, biological inertness (non-immunogenic) and the observed potential to assimilate with bone compared to other metals (Brunette et al., 2000; Marco et al., 2005). The oxide layer enacts as a barrier by encasing the elemental reactive and toxic bulk from the bio-chemically variable *in vivo* environment, but more importantly serves as an organic substrate that is recognised as self by the body's tissue-reparative apparatus, and which leads to the amalgamation of molecules, cells and eventually bone (Liu et al., 2004). The assembly of this apparatus is stepwise, in which protein adhere and saturate the implant surface, making way for adhesive interactions between the cell and newly-conditioned substrate (Puelo and Nanci, 1999). Verily, it is this interaction, as stated in 1.2.2.3, which largely determines the outcome.

1.3.2 Implant failure to surface modification

The terms implant success and failure that are applied to assess the presence or absence of osseointegration, respectively, have been deemed obscure (Santos et al., 2002). Their ambiguity stems from the lack of a true characterisation of osseointegration but also from the high variability in the designs and criteria applied to examine implant efficacy from study to study (Wennerberg and

Albrektsson, 2009). Appropriate histological and microscopic methods developed towards the late 1970s to evaluate the bone implant interface indicated the presence of fibrous tissue that encompassed 60-70 percent of the implant surface compared to 25-30 % of bone implant contact (BIC) (Schwartz et al., 1999). Though the relative little BIC was found to provide adequate biocompatibility in the short term, complicated by the series of variables linked with implant integration, an endemic rate of ~ 10 to 30 % failure were attached with mandibular and maxillary implants, respectively, in the long term (McNutt and Chou, 2003).

Attempts to overcome the endemic of implant failure led to the empirical alteration of implant surface characteristics in early and mid 1980s (Schwartz et al., 1999). A surface is a physical aspect of matter comprising the outermost layer of atoms of the bulk of an object or medium that interacts with that of another material bulk (Brunette et al., 2000). In Ti implants, the surface forms the larger part of the implant in contact with living tissue. The importance of implant surfaces in osseointegration led to a set of physical and chemical parameters being applied to define it (Brunette et al., 2000) . These parameters are tabulated in table 1-1.

Table 1-1 Properties of an implant surface

Primary physical-chemical properties of an implant surface. Adapted from (Brunette et al., 2000)

Surface Characteristic	Definition
Chemical Composition	Measure of the types, electrochemical states and assemblies of various atoms and chemical moieties present on surface.
Chemical Structure/Order	Measure of the spatial orientation & arrangement of chemical moieties present on the surface.
Topography	Physical texture or landscape in terms of pits waves, peaks, pores and undulation.
Surface Energy	Measure of the electrochemical kinetics of the surface. It includes the quantitative measurement of adsorption of bio-molecules, wettability/contact angle of liquid (polar vs. non-polar) & surface energy
Mechanical Properties	An estimate of the mechanical elasticity and contractility of the surface forming atomic layers
Surface Dynamics	Mobility of atoms across and along a surface. It is influenced major by physical properties of the metal.

The surface characteristics of Ti implants that have undergone substantial modification over the past two decades are surface topography and surface energy. Chemical composition has been altered and tested in various scenarios but shown to be inferior in the long run compared with nude Ti (Liu et al., 2004).

1.3.3 Topographical modifications

Surface topography is a physical measure indicative of the spatial configuration / geometric landscape or architecture of a substrate. It is a term that is difficult to define as it encompasses physical and chemical interactions between at least two entities, and will inadvertently be different from material to material and the prospective application (Assender et al., 2012). The significance of topography in directing cell fate was first reported by 1911 by R.G.Harrison who noted the movement of embryonic cells on spider web fibers holding a piece of neural tube tissue (Harrison, 1911). This phenomenon was termed contact guidance in 1934 by Paul Weiss, who later hypothesised this movement to be controlled and under the guidance of adsorbed proteins (Curtis and Wilkinson, 1998).

In the case of Ti, modifications and testing over the years, arising mainly from the acknowledgement of the importance of surface characteristics on osseointegration (Albrektsson et al., 1981), led to two levels of surface topographical modifications for endosseous implant design; micro and nano metric scaled topographical modifications. Micro topography is the measure of physical landscape of a surface within the dimensional range of 1 - 10 µm along a vertical axis from a mean surface plane. It is characterised by textural features such as pits, peaks, pores & waviness. Nano topography, on the other hand, is a physico- chemical measure of the geometric landscape of a surface within a spatial dimensional range of 1 - 100 nm (10 to 1000 Å, angstrom) from a mean plane. At this spatial range, physical features influence chemical forces emanating from surface constituent atoms and molecules, which inadvertently alter surface energy. Surface energy, though influenced by topography, is strictly a chemical variable that increases the surface's electrostatic negativity and apolarisation to water; rendering it wettable and highly hydrophilic. This

parameter is determined by measuring the 'contact angle' between a water droplet and a surface that reflects the ratio of adhesive forces between surface - water and cohesive forces between water - water molecules: the higher the adhesive than cohesive forces, the smaller the contact angle and more 'hydrophilic' a substrate, and vice versa (Liu et al., 2004; Brunette et al., 2000; Guehennec et al., 2007).

Micro and nano topographical modifications are created by treatment methods in an additive or subtractive manner with respect to a reference polished surface. Table 1-2 lists the common methods used to modify Ti dental implant surfaces. Among these, the subtractive treatment of blasting a surface with solid particles and 'pickling' it in a solution of strong acids has shown to introduce topographical characteristics that render a Ti implant with comparatively better contact with bone and anchorage relative to plane polished surfaces *in vivo* (Buser et al., 1991; Gotfredsen et al., 1995; Wannerberg et al., 1996).

A surface treatment that has become an industrial standard is the SLA surface prepared by Straumann AG (Waldenburg, Switzerland). SLA is an acronym for **s**and blasted **l**arge grit **a**cid etched. This substrate is generated by blasting a plane Ti surface with large alumina particles of ~ 250 µm in diameter with compressed air, and then 'attacking' the surface oxide layer with acidic treatment in HCl / H_2SO_4, followed by multiple rinses in distilled water (Rupp et al., 2006). This treatment yields a surface of the appearance of osteoclast resorbed bone and gives it a mean roughness value (R_a: arithmetic mean of the absolute height of all points in a surface profile) of 4.12 µm along the z-axis, in comparison to 0.03 µm of the plane polished Ti surface. An SEM micrograph of a polished and its derived SLA surface are shown in figure 1-5. The rough surfaces, though different in their potentials to adsorb water, have the same topography. An easy way to describe their roughness is as a surface resorbed by osteoclasts, with large craters formed by the blasting of alumina particles, superimposed by many tiny 'crypt' like indentations formed by acid etching that collectively yield a highly uneven topography (Ferguson et al., 2006; Rupp et al., 2006).

Table 1-2 Overview of surface modification for titanium Implants

Table from (Liu et al., 2004)

Surface modification methods	Modified layer	Objective
Mechanical methods		
Machining **Grinding** **Polishing** **Blasting**	Rough or smooth surfaces formed by subtraction process	Produce specific surface topographies; clean and roughnen surface; improve adhesion in bonding
Chemical methods		
Chemical treatment		
Acidic treatment	<10 nm of surface oxide layer	Remove oxide scales and contamination
Alkaline treatment	~ 1 μm of sodium titanate gel	Improve biocompatibility, bioactivity or bone conductivity
Hydrogen peroxide	~ 5 nm of dense inner oxide and porous outer layer	Improve biocompatibility, bioactivity or bone conductivity
Sol-gel	~ 10 μm of thin film, such as calcium phosphate, Ti-oxide and silica	
Anodic oxidation	10 nm to 40 nm of TiO_2 layer, adsorption and incorporation of electrolyte anions	Produce specific surface improved corrosion resistance; topographies; biocompatibility, bioactivity or bone conductivity
Biochemical methods	Modification through silanized titania, photochemistry, self-assembled monolayers, protein-resistance, etc.	Induce specific cell and tissue response by means of surface-immobilized peptides, proteins, or growth factors
Physical methods		
Thermal spray **Flame spray** **Plasma spray** **HVOF** **DGUN**	~30 to ~200 μm of coatings, such as titanium, HA, calcium silicate, Al_2O_3, ZrO_2, TiO_2	Improve wear resistance, corrosion resistance and biological properties
Plasma Vapour Deposition		
Evaporation **Ion plating** **Sputtering**	~1 nm of TiN, TiC, TiCN, diamond and diamond-like carbon thin film	Improve wear resistance, corrosion resistance and blood compatibility
Ion implantation and deposition **Beam line ion implantation**	~10 nm of surface modified layer and/or implantation 1μm of thin film	Modify surface composition; improve wear, corrosion resistance, and biocompatibility
Glow discharge plasma treatment	~1 nm to ~100 nm of surface modified layer	Clean, sterilize, oxide, nitride surface; remove native oxide layer

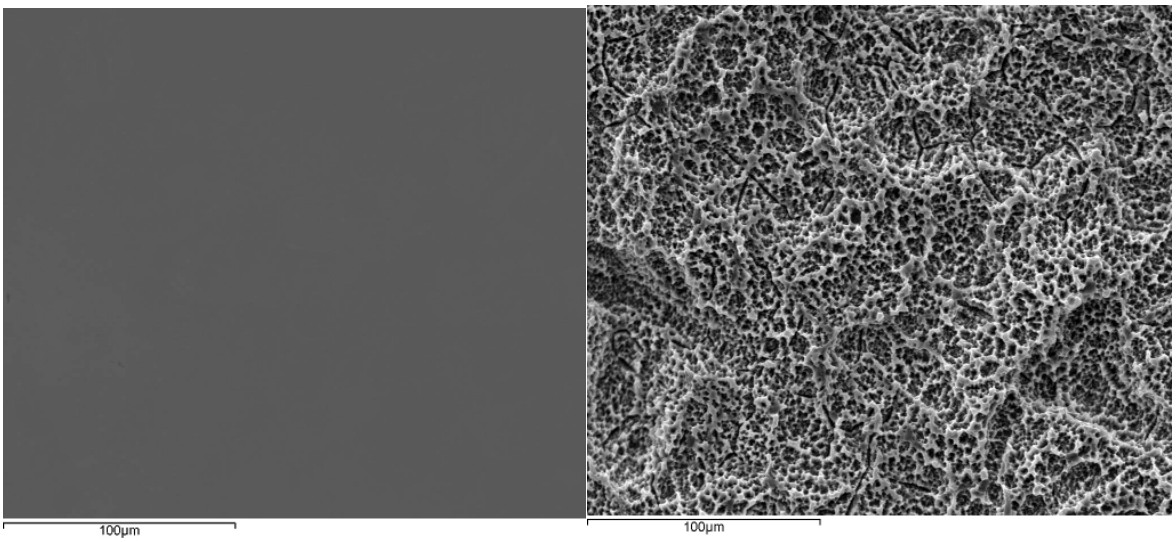

Figure 1-5 Surface modifications of Ti implants

Images are scanning electron micrographs of Ti discs used in this study. Non-sputter coated Ti discs of 15 mm diameter, with one side bearing a fabrication of the original implant modification, were taken at x1000 magnification. The left image is of a polished Ti surface while the right is of an SLA rough hydrophobic surface. The modSLA is identical to the SLA and hence not shown. The P surface has a mean R_a of < 0.5 µm. The SLA has a R_a of ~ 4.2 µm.

The SLA preparatory method inadvertently introduces nano-topographical features on an implant surface that have the potential to alter surface energy (Mendonca G et al., 2008). These nano-topographical features, yielded on every SLA surface, are normally masked by atmospheric contaminants that adsorb the substrate upon exposure to air but can be 'unmasked' by modifying the preparatory method to exclude atmospheric contact of surface and prevent contaminants from adsorbing it. This is achieved in the case of 'modified SLA' (modSLA), prepared just as SLA but being rinsed in an N_2 atmosphere rather than air and securely stored in an isotonic solution of NaCl in water, pH=4-6 (Rupp et al., 2006). By preventing contamination, the modSLA has a relatively large quantity of hydroxyl ions retained on the surface oxide compared to an SLA (Rupp et al., 2006; Zhao et al., 2007). These hydroxyl ions greatly increase the modSLA substrate's surface free energy, rendering it hydrophilic as assessed by a dynamic water contact angle analysis. In this analysis, an object of length 'l' is immersed and the emersed in a liquid of a certain surface tension. In this process, the angle at which the liquid advances or recedes with respect to the material surface is measured. A large angle between the surface of the material and line of liquid represents

hydrophobicity, high cohesive (liquid-liquid) to adhesive (liquid-material) forces. A small angle indicates relative hydrophilicity, where adhesive forces between the liquid-material overcome cohesive forces between liquid molecules. In most cases the liquid used is water, which yields measurements of 0^{o} for the modSLA compared to 138.3 $\pm$ 4.2^{o} angles for SLA and 96 ^{o} angle for P surface (Buser et al., 2004; Zhao et al., 2007).

1.3.4 *In vivo* effects of modified Ti surfaces

The variability in the methods employed to create and characterise various modified surfaces by different manufacturers underlies a lack of consensus in the findings derived from manufacture to manufacturer (Wennerberg and Albrektsson, 2009). This section reviews the *in vivo* findings derived using Straumann AG manufactured SLA and modSLA implant surfaces compared to their control, a polished machined surface (P).

The effects of the SLA surface have been evaluated through clinical trials in humans and experimental observations in subject animals. The modSLA surface has been assessed largely in pre-clinical settings in experimental subjects (Bornstein et al., 2010). In the clinical trials, the SLA surface had been observed to present healing periods of 6 – 8 weeks compared to 6 months for the conventional plane surface implant, demonstrating a 99 % success rate over a five year follow up. The pre clinical trials conducted thus far indicate the modSLA to be capable of inducing significantly more healing than SLA at 2 weeks post implantation, making it possible to load the fixture with an abutment by the third week (subjects = 40 in number) in the posterior mandible with a 96 % success rate over a three year follow up (Bornstein et al., 2010); (Wennerberg and Albrektsson, 2009).

Experimental analyses comparing both surfaces *in vivo* have followed two common methods; a histo-morphometric assessment of bone implant contact, and interfacial strength between tissue and fixture by removal torques. These have more recently moved to *in vivo* molecular analyses, using tissue specimen retrieved from subjects at various time intervals for genetic and molecular examinations.

The 'traditional' analyses have applied histological and morphometric evaluations to implant integration in various animal subjects, comparing different loading times, a range of bone qualities, and time points of analysis etc. The examinations indicate a significantly higher bone implant contact % (BIC) and removal torque values in the case of the modSLA compared with SLA by as early as two weeks post implantation (Buser et al., 2004; Ferguson et al., 2006; Bornstein et al., 2008).

The recent analyses have applied basic science to query *in vivo* events by retrieving implants and examining specimen with molecular techniques. One such assessment has indicated more stable hematoma clot formations on the modSLA suggesting that the surface's enhancement effects extend to the spatial orientation of clot constituting elements at the interface (Schwartz et al., 2010). This effect of modSLA also occurs with implant bound bone debris formed during placement. These have been shown to be retained at a significantly higher ratio compared to soft tissue on the modSLA than SLA and are suggested to mediate the comparative increase in BIC (Bosshardt et al., 2011). These observations have been further substantiated by gene expression analyses of retrieved samples that indicate a temporal up-regulation in skeletogenesis related genes' expression compared to SLA as early as 4 d post implantation (Ivanovski et al., 2011).

1.3.5 *In vitro* effects of modified Ti surfaces

In vitro studies on the biological effects of Ti implant surface characteristics on cellular responses imply these have an intrinsic influence on cellular function (Mendonca et al. 2008). Experimental evaluations have mostly followed a typical methodology of fabricating implant surfaces on a disc of a size suitable for use in a 1.96 cm^2 surface area of a well of a 24-well tissue culture treated plate. Cells are suspended in either growth or osteogenic inductive media and seeded on the discs under the influence of gravity. The cell types predominantly studied include osteoblastic cell lines (MG63) and primary alveolar bone derived osteoblast cultures, but other cell types have also been applied such as, human umbilical cord endothelial cells (Zhang et al., 2010), dendritic cells (Kou et al., 2011) and more recently bacterial bio-films (Almaguer-Flores et al., 2011).

This model of study is two-dimensional, and has been deemed artificial and incapable of recreating osseointegration in the absolute context (Wennerberg and Albrektsson, 2009). The obvious advantage of this model is its simplicity of setup that allows the examination of various cell types under controlled conditions and at different sub-cellular levels. The major disadvantage is that this system does not model the complex interaction between the many cell types involved in the *in vivo* situation. Even though it is a simple and easy accessible model, experimental questions have to be tested in isolation. A 3-d model of the cell surface interactions, perhaps involving compressed collagen matrices and more than one cell type, would present a better model for examining more complex questions.

The parameters of cellular responses that have been predominantly assessed *in vitro* are adsorption of proteins, cellular attachment, morphological adaptation, viability and proliferation and, osteogenic mineralisation. These correlate with the steps that constitute the current paradigm of osseointegration. The inferences drawn from such studies on the SLA and modSLA substrates are summarised in the following points.

1.3.5.1 Molecular and cellular adsorption

The adsorption characteristics of serum equivalent proteins, such as bovine serum albumin with analytical protein quantification assays have shown these adhere uniformly to all surfaces at any time measured. However, that the quantity of adsorbed protein is usually higher on the rough surfaces, believed to be due to the extra surface area offered by the substrate (Nishimoto et al., 2007). Cellular attachment of osteoblastic cells, assessed with microscopic techniques at >1 h post contact, have demonstrated a higher attachment number on the rough compared to smooth (Lai et al., 2009; Miron et al., 2010). Moreover, cells are reported to adapt a more stretched morphology on the rough with cytoplasmic processes emanating into topographical features within the vicinity. The polished Ti surface seem to cause cellular spreading as opposed to stretch, yielding a near uniform ‘fried egg’ like morphology at 3 hours post contact (Wall et al., 2009). Rough surfaces are reported to also elicit defined actin filament reorganizations with a relatively aberrant focal adhesion kinases

distribution compared to the smooth surfaces (Lai et al., 2009; Nishimoto et al., 2007; Miron et al., 2010).

1.3.5.2 Viability and proliferation

Cellular viability and proliferative rate of cells is significantly higher on the smooth than rough surfaces (Zhao et al., 2007). This has been observed in almost every study examining the effects of rough surface topographies on cellular function (Masaki et al., 2005; Brett PM et al., 2004; Olivares-Navarrete et al., 2011; Miron et al., 2010; Vlacic-Zischke et al., 2010; Zhang et al., 2010; Wall et al., 2009; Schwartz et al., 2009b; Lai et al., 2009). These studies have applied the traditional two-dimensional cell culture model with analyses usually made over the initial week following contact with the MTT assay as the preferred method.

1.3.5.3 Osteogenic mineralisation

The osteogenic differentiation of cells on the different substrates have been evaluated by genetic expression of bone physiology related genes such as Runx2, osteopontin, bone sialoproteins, as well as microarrays of whole transcriptomes; quantitative assessments of osteoblastic phenotypic protein markers, mainly with alkaline phosphatase, osteocalcin, osteoprotegrin and transforming growth factor β-1 measurements; and functional evaluations of osteogenic phenotypic characteristics such as calcium deposition and calcified nodule formation via Alizarin Red S staining of monolayers, or spectrophotometric analysis of deposited calcium.

These analyses, in summary, point towards a phenomenon, described in relative detail in section 1.3.6, that in summary infers a novel enhancement of osteogenic differentiation to be induced in cells cultured on the rough Ti modified surfaces. The observations drawn for osteoblastic cells cultured on the SLA and modSLA surfaces are that

a. The rough surfaces induce a relative up-regulation in the expression of a select set of genes, many key to bone physiology. Examples of solitary genes being differentially modulated are the instance fibroblast growth factor receptor type 5 (Brett et al. 2004);

Wnt5a, Runx2, osteopontin and bone sialoprotein type 2 (Wall et al. 2009; (Harle et al., 2004)

b. increased matrix mineralisation assessed by significantly higher levels of Alizarin Red S retention by monolayers cultured on rough surfaces (Miron et al., 2010; Wall et al., 2009), and
c. an elevation in the levels of different osteoblast specific protein markers, such as alkaline phosphatase, osteoprotegrin and osteocalcin, on the rough modSLA than SLA (Rausch-Fan et al., 2007)(Schwartz et al. 2009).

Recent studies have shown the selective engagement of cell surface integrin subunits ITGA2 and ITGB1 by Ti, and their enhanced modulation by surface roughness and hydrophilicity, to be linked with the TGF-b1 regulation of OPG synthesis (Schwartz et al., 2009b). The authors later showed that a particular Wnt3a based pathway that attenuates osteogenic differentiation through negative regulators Dkk -1 and -2 proteins (Fujita and Janz, 2007) is also negatively influenced by the osteoinductive potential of the modified surfaces (Olivares-Navarrete et al., 2010b). The overall inference drawn is that rough and additionally rough-hydrophilic modified Ti surfaces induce a temporal and magnitudinal enhancement in the *in vitro* osteogenic responses of human osteoblastic cells.

1.3.5.4 Immunological effects

The enhancement effects of modified Ti surfaces extends to dendritic cells, which seem to produce higher levels of anti-inflammatory cytokines and anti-osteoclastogenic regulators in response to the rough surfaces (Kou et al., 2011).

1.3.6 Mechanisms of effects of surface modifications

A number of different theories have been proposed in an attempt to define the significance of implant surface roughness on osseointegration. Three of these are prominent (Mendonca G et al., 2008). The initial hypothesis is the ‘bio-mechanistic’ view, which proposes that rough surfaces present a higher surface area for bone to contact with and thus, promote BIC % and mechanical

fixation of the implant by a process of physical interlock. A mathematical model has been drawn that hypothetically tested this idea by measuring the interfacial shear strength between bone and an implant surface with mathematical algorithms. This relayed the dimensions of pits sized 1.5 µm deep and 3 – 5 µm wide to be optimum for implant integration, which corroborated with the findings of studies employing substrates of a similar surface architecture (Hansson and Norton, 1999). Mechanical interlock of the implant with bone is an ultimate requirement for the successful assessment of osseointegration. Recent developments in cell-implant observations have, however, deemed mechanical interlock a downstream consequence of initial healing events rather than an underpinning factor for the enhanced osseointegration of rough surfaces.

The second view promotes the proposition of '*de novo* bone formation'. It suggests that surface topography offers a faster substrate for fibrin fibres, formed during the initial platelet cascade, to adhere to. Accordingly, migrating MSCs are suggested to use these fibres as scaffolds to translocate to the surface where they differentiate to an osteoblast phenotype. The newly formed osteoblasts deposit an all important cement line or lamina lamitans on an implant surface (Davies et al 2005; Davies et al 2003; Davies et al 1996). It proposes this cement line formation to occur in four arbitrarily sub-divided stages, promoted by the rough surfaces due to the fibrin mediated early and denser influx of osteo-precursors. This process initiates with the secretion of a collagen-free organic matrix that serves as a calcium nucleation platform for mineralisation. This entails calcium phosphate crystalisation that in turn attracts collagen fiber assembly to form osteoid on the cement line at the interface. The mineralisation of the osteoid forms an osseous link of the implant surface with adjacent bone that is subsequently replaced with secondary, lamellar bone through remodeling. The core of this proposition is the formation of an amorphous collagen-free layer of sialoproteins, reminiscent of a cement line formed at the juncture of old and new bone, which precedes direct bone formation on the implant. There is an exception to this theory. Contrary to it is the proposition originating from ultrastructural scanning microscopic studies (SEM) that report a non-uniformly distributed layer of amorphous material some 20 – 400 nm thick, peripheral to the cement line. This layer may occur spread over different sections in positively identified samples and is suggested to be composed primarily of proteoglycans that precede the cement line formation

(Sennerby et al., 1992). This finding implicates a delay in fibrin attachment and polymerisation and therefore, negates it a primary role in mediating increased osseointegration by the rough surfaces.

The third view comes from *in vitro* experimental findings that, in brief, suggest rough surfaces induce a temporal and magnitudinal enhancement in osteogenic cell activity and function. It suggests that osteoblastic cells are influenced to produce an osseous tissue microenvironment on the *in vitro* substrate (Boyan et al., 2003a) reminiscent of their innate response to osteoclast resorbed pits *in vivo* (Boyan et al., 2003b). A mode of cellular activity implicated here is mechanotransduction. This proposes that rough surfaces exert minute mechanical stimuli / forces on surrounding bone tissue, which are sensed by local osteocytes that transduce the physical stimulus from the cell membrane to load-responsive genes in the nucleus by means of a mechanosome; a protein complex attached with mechano-sensory receptors (Pavlako FM et al., 2003). This novel concept has been gaining support as various osteogenic effectors, such as the Runx2 osteogenic master transcription factor, are shown to be modulated by mechanical forces, and in some instances over riding cytokine or hormonal influence (Ziros et al., 2008). The role of mechanical forces in osteogenic developmental processes has implicated the Rock and RhoA GTPAses in mediating cell shape and cytoskeletal-tension related adaptive enhancements in osteogenic differentiation (McBeath et al., 2004) by means of downstream non-canonical Wnt ligand WNT5A (Santos et al., 2010).

1.4 Mesenchymal stromal cells

1.4.1 Definition

Adult tissue resident stem cells are generally defined as lineage unspecified, functionally un-differentiated, mononuclear cells. They play an intrinsic role in the parental tissue's homeostatic repair by serving as a self-renewable source for prospective progenitor cells capable of differentiating into constitutive cell types *in vivo*, while also being able to home in to other tissues to participate in extra-parental tissue repair (Loeffler and Roeder, 2002). Human bone marrow contains at-least two adult tissue stem cell populations. These are the well characterised

hematopoietic stem cell (HSC) and the putative marrow derived mesenchymal stromal cell (MSC) (Horwitz et al., 2005). HSCs occur as circulating non-adherent somatic stem cells and have been found to be restricted to forming blood constituting myeloid and lymphoid precursors. The MSCs are mainly identifiable by their *in vitro* properties, particularly the cell types distinct characteristic to strongly attach to tissue culture plastic (TCP) as opposed to HSCs (De Silva Merielles, 2008). These cells are generally defined as TCP adherent mononuclear cells, negative for HSC markers, with a high replicative potential that can lead to single cell derived clonal colonies, and that are multipotent to differentiate to osteoblastic, adipocytic and chondrocytic like cells *in vitro* when induced with appropriate stimulants (Jones and McGonagle, 2008); (Lazennec G and Jorgensen, 2008; Horwitz et al., 2005).

1.4.2 Identity

In vivo, however, MSCs have not yet been well characterised, and lack a true identity. They are thought to be a heterogeneous population of multipotent cells that form part of a supporting reticular network, thought to regulate HSC differentiation, and are functionally implicated in the homeostatic repair of mesoderm tissues. This perception of MSCs is largely based on information that is known from experimental observations rather than an investigation of the true function of the cellular entity (Lazennec G and Jorgensen, 2008; De Silva Merielles, 2008; Caplan, 2008; Benayahu et al., 2007).

The heterogeneity of MSC isolates infers that a tissue culture plastic adherent bone marrow isolate is a population of different cell types that vary in lineage commitment and differentiation potentials. This population is proposed to contain a small proportion of the extremely rare true somatic adult stem cell, combined with a larger proportion of early stem derived progenitor cells of mesoderm tissues and their somewhat committed precursors (Benayahu et al., 2007). This heterogeneity is considered to be a function of the methods applied to isolate and study these cells and is an obstacle in delineating the cells true biological importance. The identity of the MSC has also largely not been addressed due to the lack of a singular discriminative marker as the present set of markers may represent an overlapping repertoire of proteins between the three theoretical sub-populations within an adherent isolate, all the while ignoring their heterogeneity such as the

transcription and post translational modification of important lineage determining regulators. Attempts at characterizing the cell type on the basis of a consensus of cell surface expressed molecular markers has revealed three categories of proteins that differentiate MSCs from cells of a similar *in vitro* profile. These are elaborated in tables 9-1, 9-2 and 9-3 (Appendix I) as positive, negative and undetermined markers, respectively. At the present, these markers, in particular Stromal cell antigen (Stro-1) (Simmons and Torok-Storb, 1991), are applied in assessing the multipotentiality of a TCP adherent population of marrow isolate derived cells; however, in combination with single cell colony forming unit assays, and tri lineage differentiation assays. The MSC's capacity to differentiate to osteoblastic, adipocytic and chondrocytic like cells not being tested *in vivo* at a single cell level further emphasises the lack of absolute compared to relative understanding of the cell type (Benayahu et al., 2007; Lazennec G and Jorgensen, 2008; Jones and McGonagle, 2008; Kolf et al., 2007). The present nomenclature assigned to the TCP adherent marrow isolate is the mesenchymal stromal cell abbreviated as MSC, with the prefix h indicative of human origin (Horwitz et al., 2005).

1.4.3 Biology

Cell transplantation and grafting experiments, as well as the isolation of MSC like cells from other anatomical sites such as adipose tissue, periosteum, tendon, muscle, synovial membrane, skin and lungs have lead to the perception that these represent a population of cells, possibly derived from a common embryonic ancestor, differentially distributed across the body during development, and responsible for carrying out post-natal repair of mesoderm tissue (De Silva Merielles, 2008; Caplan, 2008). A cell type that has been recently hypothesized as being 'parental' in lineage to MSCs is the perivascular cell, or pericyte. This cell occurs the outer lining on endothelial cells in capillaries and micro vessels and is regarded as a vasculature resident predecessor of true mesenchymal stem cells (Crisan, 2008). Pericytes have been isolated on the cell surface expression of $3G5^{+}$, $CD146^{+}$ $CD34^{-}$ from human fetal and adult tissues, and shown to be capable of clonogenic self renewal, forming single cell derived colonies, and undergoing osteogenic, adipogenic, chondrogenic and myogenic lineage differentiation *in vitro* (Crisan, 2008; Collet et al., 2003; Farrington-Rock et al., 2004). This proposition implies the MSC to be part of a regenerative system that like the many

systemic organisations (immune and nervous systems etc), is engaged in replacement of tissue to recuperate loss of organ function; albeit to a limited extent.

1.4.4 Cellular characteristics *in vitro*

It has been estimated that true multipotent MSC comprises 0.01 % to 0.001 % of the tissue culture plastic adherent mononuclear marrow cell isolate positive for Stro-1 cell surface anitigen (Simmons et al. 1991). These cells are proposed to have a fibrobrlastic, trigonal morphology in culture (figure 1-9) (Pittenger et al., 1999). Colter and colleagues, using morpho-metric parameters, have catergorised three distinct types of cells in an isolate of marrow derived MSCs seeded at clonal densities (1 to 10 cells.cm^{-2}). The initial two are said to be small 'recycling stem cells' that are characterised by the presence of a prominent nucleus and high nucleus to cytoplasm ratio. These are essentially identical differing primarily in their cytoplasmic granularity, with the type 1 agranular and type 2 highly granular; but also slightly with respect to their repertoire of cell surface markers (Colter et al., 2001).. The third morphological form that an MSC may take in culture is that of a large spindle or flattened like cell that Colter et al. termed as a mature marrow stromal cell (Sekiya et al. 2002; Colter et al. 2001; Colter et al. 2000). The recycling stem cells occur at a very small proportion of the culture at any given time.

It should be stated here that these denominations are rather arbitrary. Though worthy of appreciation, these are incapable of deciphering the complexity of a culture of MSC as an isolate of these cells is heterogeneous with respect to cellular lineage and multipotentiality, and has a colony forming unit percentage of at most 45 (see 'Specimen characterisation data sheets' in appendix VI).However, the cells cultured in the process of this thesis displayed the morphological characteristics described by Colter et al. when seeded at clonal densities, as shown in figures 1-6 and 1-7, which show dividing duplets of cells interspersed within a semi-confluent culture of human MSCs, with an obvious relative difference between the mitotic cells from the rest of the specimen.

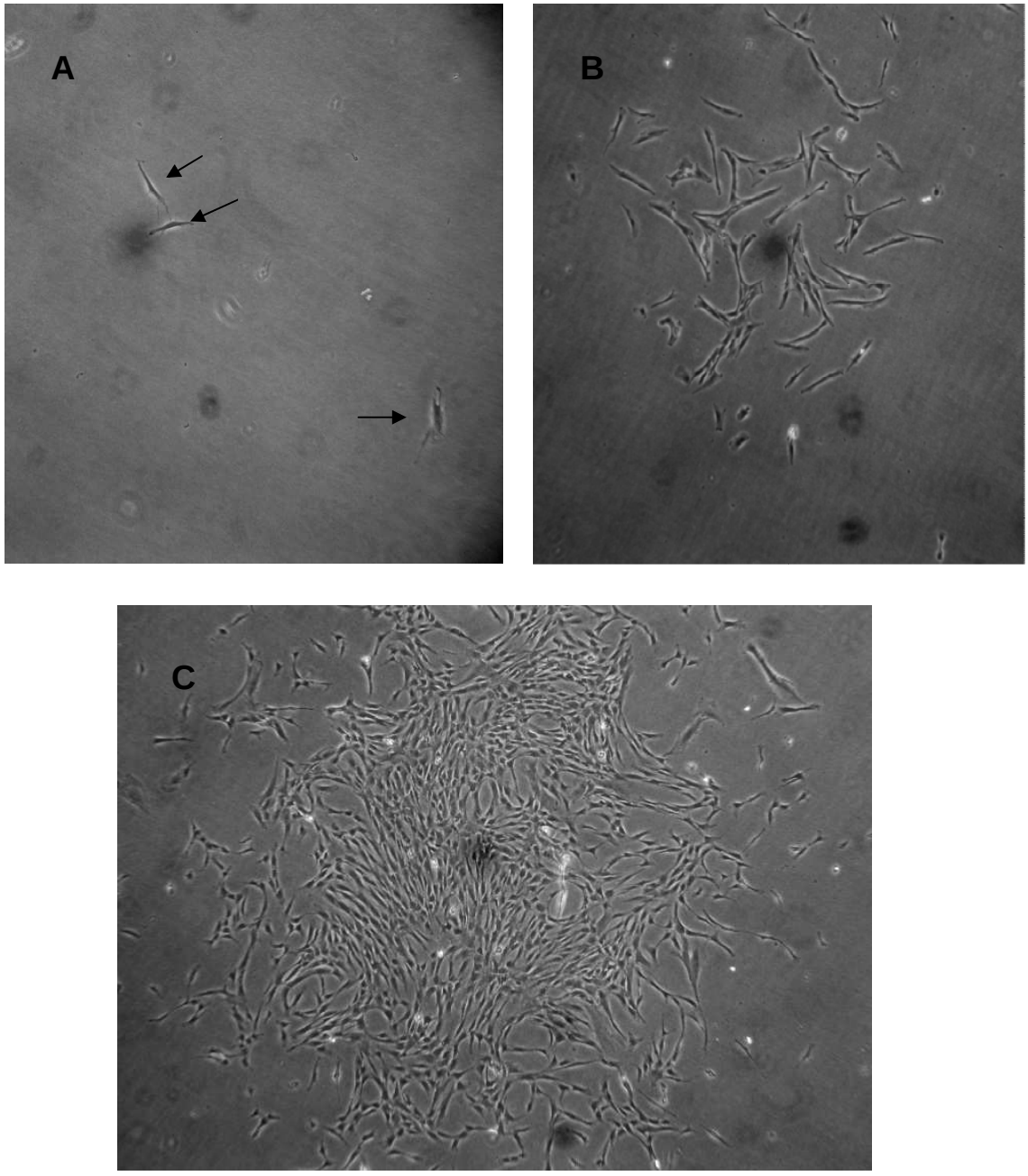

Figure 1-6 Human mesenchymal stromal cells in culture

Mesenchymal stromal cells contain colony forming units, which can be discriminated from within the heterogeneous population by seeding the specimen at clonal densities. Images are light micro-graphs of pre-characterised human MSCs, obtained from Tulane University (US) and isolated based on plastic adherence from iliac crest derived bone marrow aspirates. Cells were cultured at a density of 10 cells/cm^{-2} in a T-75 flask. (A) x10 objective at 3 d post seeding indicating three cells in near vicinity (black arrows). (B) x10 objective at cells at 7 d shows a young colony of multiple cells, highly likely of single cell origin. (C) x4 objective view of a colony of cells at 14 d post seeding. Images taken by author.

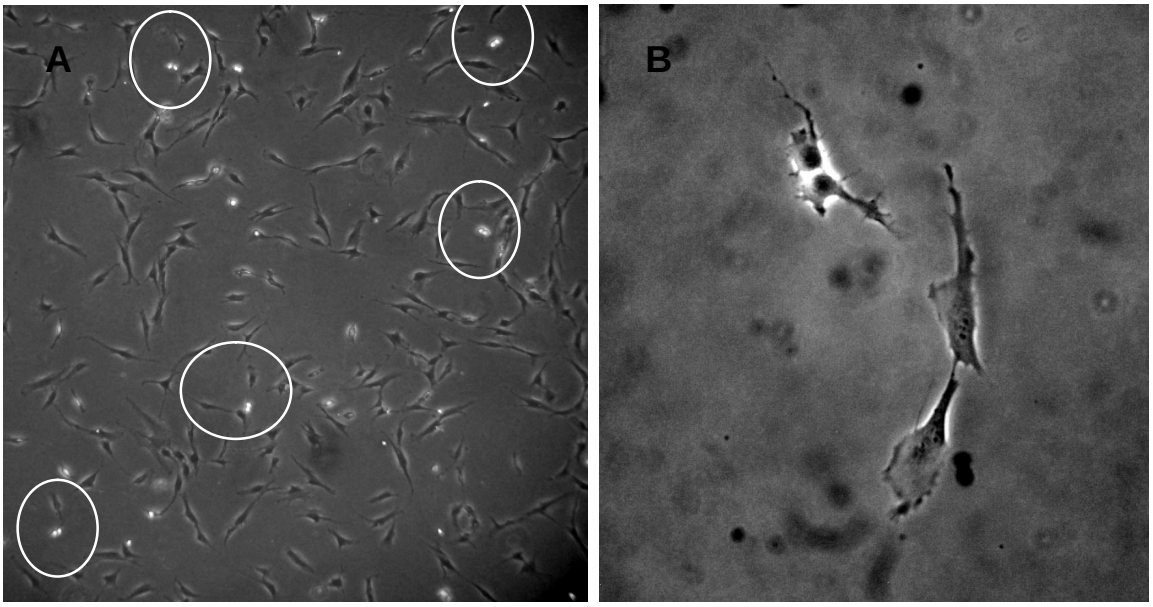

Figure 1-7 Duplets in a human mesenchymal stromal cell culture

(A) Image is x4 objective view of hMSCs cultured in a T150 flask (Donor 2 (7043); Passage 1) at 1 d post seeding. (Colter et al. 2000) proposed a system of nomenclature that considered a bone marrow adherent cell isolate to contain 'recycling' cells, i.e. mononuclear cells with self-renewal and replicative capacity that are many times smaller than the slow-replicative larger 'mature MSCs' of the culture. The cultures of hMSCs used in this study contained cells that were highly replicative in the lag phase of replication. White circles indicate mitotic duplets reminiscent of the description of a recycling stem cell provided in (Colter et al. 2000). (B) Image is a x100 objective view of two hMSC duplets in culture in a T150 flask (Donor 2 (7043); Passage 1) at 1 d post seeding. Cells were seeded at 100 cells.cm^{-2} in GM. Mitotic duplets interspersed within the adherent culture were readily observed in the initial three days of culture. The image shown indicates two such duplets in close proximity. The pair on the upper side of the image seems to be in the late stages of division while the lower seem to have almost-completely divided. Images taken by author.

The hMSCs have been shown to differentiate into osteoblastic, adipocytic, chondrocytic, tendon and myogenic like cells *in vitro* (Kolf et al., 2007), as well as to trans-differentiate *in vitro*, in response to changes in lineage induction from an osteoblastic to that of an adipocytic / chondrocytic cell (Song and Tuan, 2004). This study aimed to exploit the osteogenic ability of human MSCs. The experiments conducted in this study used a synthetic glucocorticoid called dexamethasone to induce differentiation in a medium co-containing a phosphate donor in the form of β-glycerolphosphate and ascorbic acid for collagen metabolism (Colter et al., 2001)(figure 1-8).

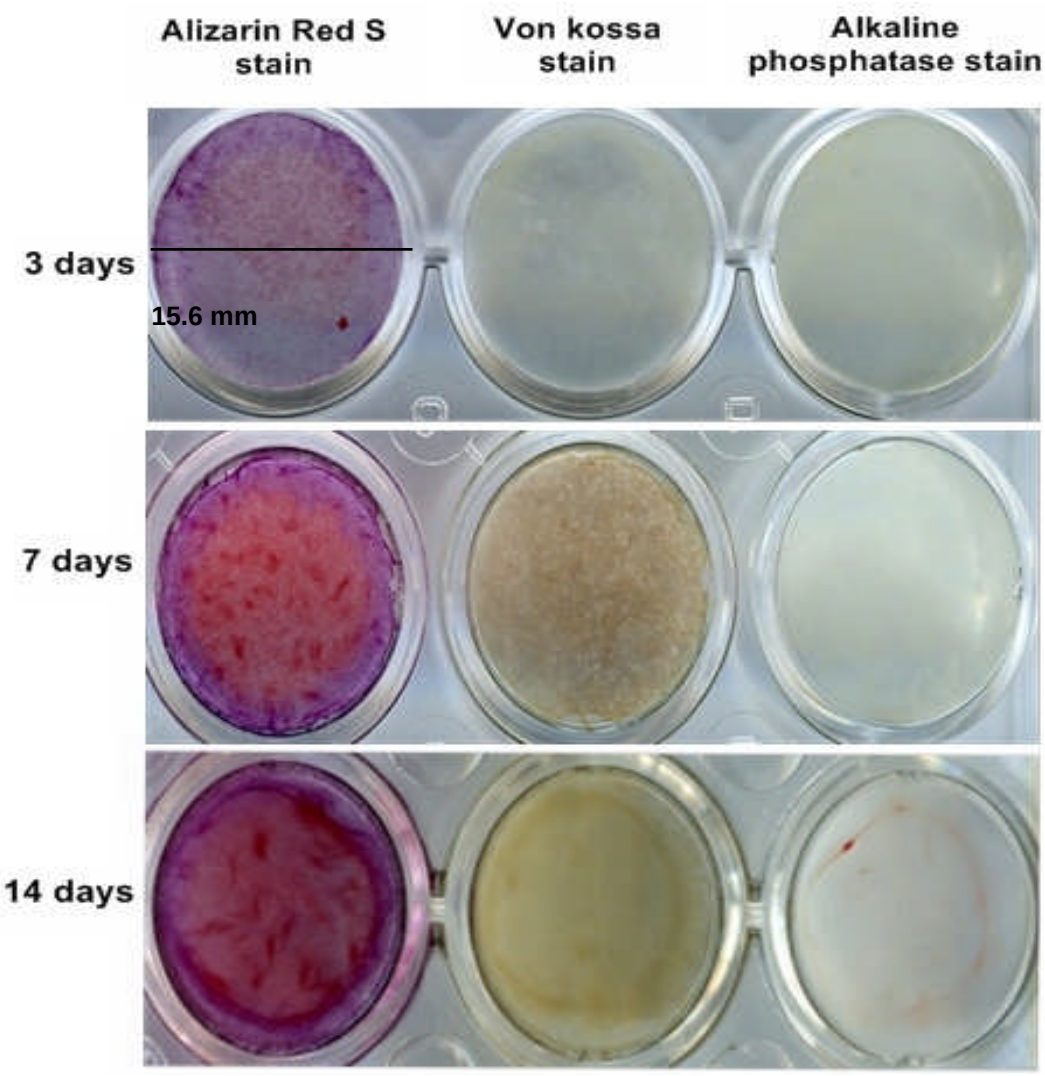

Figure 1-8 Assessment of osteogenic mineralisation in human MSCs

Image is a combination of scans of 24-well plates with hMSCs cultured at a higher density in osteogenic inductive medium for 3, 7 and 14 days. The first, second and third columns indicate the Alizarin Red S for calcium, Von Kossa for phosphates and alkaline phosphatase stains, respectively. The methods of these stains are described in sections 2.7.1, 2.7.3, and 2.7.4, respectively. The images were scanned and processed as described in section 2.3.3 and 2.3.4. The scans indicate a gradual change in the phenotype of the human MSCs from an initially non-osteogenic at 3 days to a mineralising cell at 14. The cells initially lack calcium mineralisation but 7 d, a relatively denser Alizarin stain in particular zones within the monolayer are seen. This is coupled with a relatively denser von kossa stain but not an apparent alkaline phosphatase stain. By fourteen days, the cells mineralise further. The denser circumferential Alizarin Red Stain is paralleled by relatively denser Von Kossa and alkaline phosphatase (ALP) stain, with the last apparent as a red colored line in a parallel pattern. Images were produced by author.

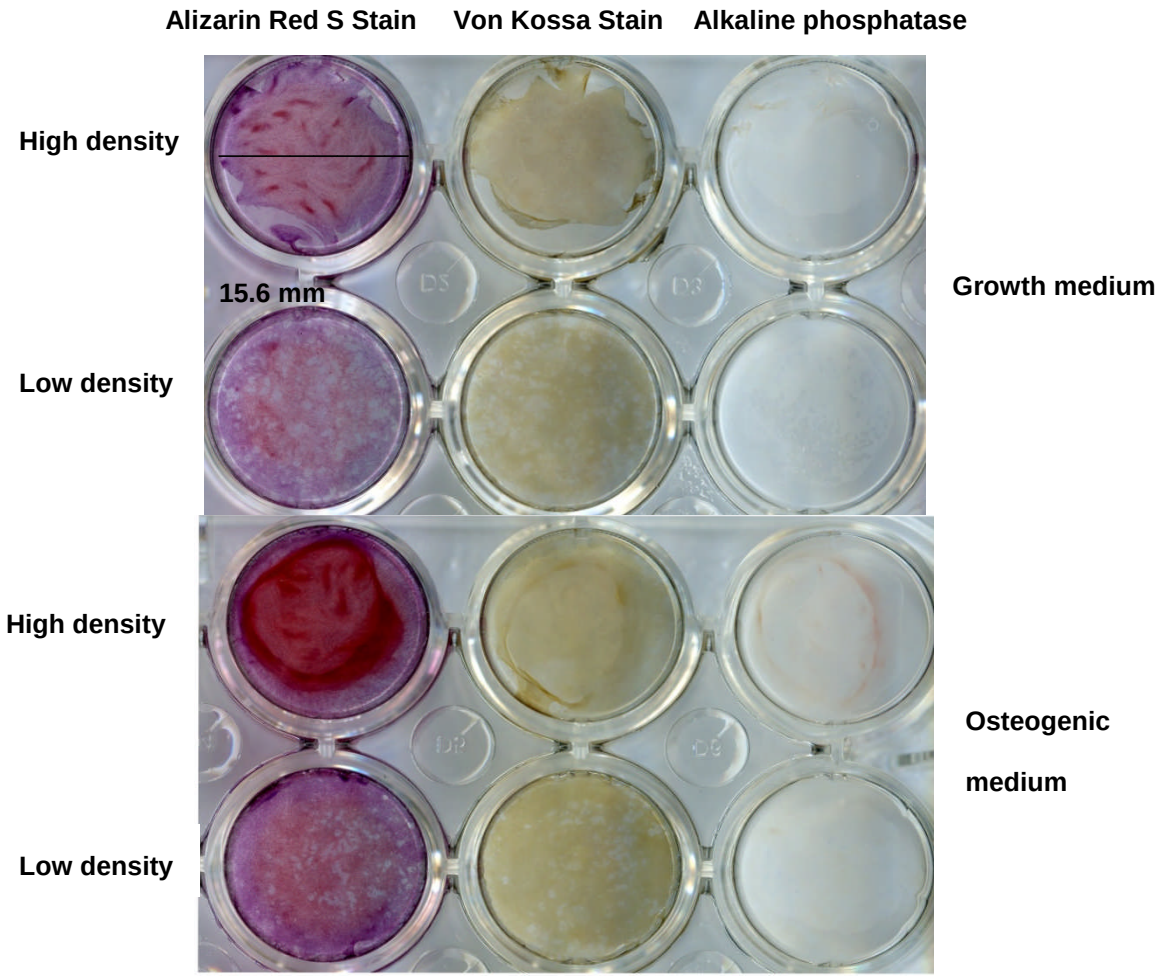

Figure 1-9 Differential effects of media on human MSC osteogenic differentiation

Image is a combination of scans of 24-well plates with hMSCs cultured at low and high densities (10,000 vs. 25,000 cells.cm^{-2}) in growth (GM) and osteogenic (OM) inductive medium 14 days. Monolayers were stained with Alizarin Red S, von Kossa, and alkaline phosphatase (ALP) as described in sections 2.7.1, 2.7.3, and 2.7.4, respectively. The images were scanned and processed described in section 2.3.3 and 2.3.4. GM is used for the propagation of hMSCs without the induction of a differentiation program. At high densities, hMSCs mineralise at high densities as evident in the foci of dense Alizarin, von kossa as well as ALP stain. This pattern of staining is not repeated in cultures that were setup at low densities. OM causes detectable mineralisation at higher densities than low. This is indicated by the strong circumferential calcium, phosphate and ALP stain in high density, and its relative lesser presence in low density cultures. The experimental findings indicate the importance to avoid confluence of cells in culture, and reflect the difficulties faced to expand hMSCs in their initial phenotypic form. Images were produced by author.

MSCs can undergo osteogenic commitment in ceramic or Titanium diffusion chambers placed under the periosteum, and have been used in pre-clinical trials for tissue regenerative purposes, of which the prominent examples include myocardial infarction (Williams and Hare, 2011), pulmonary tissue (Tzouvelekis et al., 2011), and osteogenesis imperfecta (Aslan et al., 2006; Soejitno et al., 2010). It should be noted that the potential of these cells to undergo differentiation *in vitro* depends on their length in culture; a common opinion is that these cells substantially lose their ability to undergo chondrogenic differentiation after the third passage, whereby their tendency to undergo adipogenic differentiation increases, with osteogenic differentiation thought to be capable up to five passages (Mark Clemens, visiting lecturer from University College London, personal communication).

1.4.5 Implicated function in osseointegration

The MSC has been hypothetically assigned a major role in the establishment of osseointegration. It is hypothesised that MSCs, originating from proximal and distal niches, migrate to the implant-bone interface. Here, they differentiate to osteoblastic cells that deposit the initial osseous matrix on the implant surface and adjacent bone, eventually forming an osteoid joint between fixture and tissue. The enhanced integrative effects of rough implant surfaces indirectly implies the parallel differential enhancement in MSC activity by these implant surfaces. The biological mechanisms underlying this suggested functional enhancement are largely unknown. Fewer studies have been conducted examining the effects of rough Ti surfaces on MSC activity than committed osteoblastic cell lines. The nature, implied role and the ability to induce osteogenic differentiation in MSCs renders them an important experimental specimen, which may yield findings closer to the truth than that obtained with committed osteoblastic cell lines (Tuan, 2011).

1.4.6 MSC responses to modified Ti surfaces

To assess the role of surface topography on osteogenic responses, an early study was undertaken with human marrow derived mesenchymal stromal cells (hMSC); with the rationale that any differences between the osteogenic potential of the surfaces would be exhibited by cells of a limited capacity of phenotypic function (Wall et al 2009). The study analysed early responses at 3 hours, 1,

3 and 5 days post seeding, to a polished Ti surface (P), rough-hydrophobic SLA and the then-newly introduced SLActive surface (now widely referred to as modified SLA; modSLA) by assessing differences in attachment & morphology, proliferation, mineralisation, viability/apoptosis and global gene expression. It demonstrated hMSCs bear distinct morphological differences between the surfaces with a higher viability and proliferative rate of cells on polished than rough. In addition, the authors suggested that this restriction in cell number changes on the rough was in part due to cellular apoptosis and necrosis occurring very early after cell-surface contact, incurring an increase in Stro-1 positive cells (Wall et al. 2 009). Furthermore, the study showed rough surfaces to cause significantly higher levels of calcium deposition, assessed by Alizarin Red S staining, on rough (modSLA > SLA) compared to polished surfaces. Global gene expression profiles with microarrays demonstrated the selective upregulation of osteogenic genes by rough compared to polished surfaces; notably amongst which were a set of cytoskeletal markers, Fibroblast Growth Factor type 5 (FGF5), Wingless- type MMTV integration site family member 5A (Wnt5a), beta-catennin, all three components of collagen type 6, RUNX2 transcription factor, osteopontin and the integrin-dependant bone sialoprotein protein type 2.

Collectively, the results suggested cells to have been primed towards an enhanced osteogenic program of differentiation by micro-topography, and to added extent nano-topography, of the SLA and modSLA surface preparations, respectively. Additional studies of hMSCs to the Ti surfaces have implicated candidate integrin subunits (ITGA2 and ITGB1) in the differential response of cells to Ti surface modifications by regulating downstream synthesis of osteoprotegrin through intermediary TGF-b1 (Olivares-Navarrete et al., 2010a). The authors have recently implicated WNT5A, a molecule first observed selectively upregulated on the modSLA by (Wall et al. 2009), in the effects of rough surfaces on hMSC osteogenic responses (Olivares-Navarrete et al., 2011). This, in parallel with the known induction of osteogenic differentiation by WNT5A and rock-Rho GTPase (Santos et al., 2010), and the implied role of the latter in stretch mediated differentiation in uncommitted cells (McBeath, 2004), strongly suggest that a (i) surface topography enhances phenotypic differentiation and that (ii) this mechanism is (partly) regulated by mechanotransduction based signaling, generated from rough topographical features.

1.5 Axl/Gas6 signal transduction pathway

1.5.1 Description

Axl is a cell surface Receptor Tyrosine Kinase (RTKs) discovered as an oncogene associated with the progression of Chronic Myelogenous Leukemia in humans (Liu et al., 1988). It is classed as a member of the 'TAM' family of RTKs that includes homologous c-Mer and Tyro3. The TAM receptors notably differ from other RTKs in the structure of the extra cellular domain that consists of two N-terminal Immunoglobulin repeats juxtaposed to two Fibronectin type 3 repeats, resembling adhesion molecules found within the neural system; as well as a unique conserved intracellular kinase domain sequence of Lys-Trp (Ile/Leu) Ala (Ile/Lue) Glu-Ser (O'Bryan et al., 1991). Axl is a ubiquitously expressed protein, detected at notable levels in the hippocampus and cerebellum of brain, monocytes / macrophages, platelets, endothelial cells, heart, skeletal muscle, liver, kidney and testis of humans. Furthermore, it has been detected to be ectopically expressed in different human cancers, including myelogenous leukaemia, colon, lung, esophageal, thyroid and breast (Hafizi and Dahlback, 2006). A strong Axl expression is reported to occur in normal bone marrow stromal cells that assayed negative for CD34 antigen (Neubauer et al., 1997).

Gas6 (growth arrest specific gene 6) is a secreted growth factor identified through a process of subtractive hybridisation in mammalian cells subjected to serum-deprivation induced growth arrest (Schneider et al., 1988). It was found to bind TAM receptors in an affinity dependent order; Axl>>Tyro3>Mer (Stitt et al., 1995). Gas6 resembles a blood anti-coagulation factor called Protein S by 44 % sequence homology. Gas6 is structurally composed of an N-terminal vitamin-K dependent γ-carboxylated glutamic acid domain (Gla domain), two epidermal growth factor-like repeats and two C-terminal globular laminin G-like domains (Linger et al., 2008). γ-Carboxylation is a necessary post translational modification required to activate the Gas6 ligand. It is deregulated in states of altered homeostasis, particularly in the state of vascular calcification, a process quite synonymous with osteogenesis (Demer and Tintut, 2008; Johnson et al., 2006). The underlying transcriptional control of the molecule is unknown (Berk, 2001).

1.5.2 Signal transduction pathway

Activation of Axl is reported to occur in either a conventional or atypical manner (i.e. a ligand dependent or ligand independent manner, respectively) (Linger et al., 2008). The conventional activation of the receptor occurs with a Gas6 molecule binding to an Axl molecule followed by dimerisation of two 1:1 Axl / Gas6 receptor-ligand complexes. This leads to autophosphorylation of three tyrosine residues (Tyr-779, Tyr-821, Tyr-866) within the C-terminal cytoplasmic domain of the receptor. Axl may form such dimers with fellow TAM members and also with the receptor for Interleukin 15 suggesting it to vary in functional potential through a 'cross-talk' mechanism with other cellular pathways (Budagian, 2005a). The atypical form of Axl activation is observed to occur *in vitro* in cells that exogenously express the receptor protein. The binding nature may either be homophilic with two Axl molecules dimerising, or heterotypic between an Axl molecule & a TAM family member. The biological significance *in vivo* of such atypical binding is unknown (Linger et al 2008). The cleaved extra cellular domain of Axl is plasma soluble and is an additional mode of function; although presently of an unclear purpose (Budagian, 2005b).

The phosphotyrosines of an auto-Phosphorylated Axl dimer, in particular tyrosine 821, act as substrate docking sites for phosphatidyl inositol 3 kinase (PI3K), phospholipase gamma (PLC-γ), Growth factor receptor-bound protein 2 (Grb2), cellular homolog of Src (c-Src), lymphocyte-specific protein tyrosine kinase (Lck), suppressor of cytokine signaling 1 (SOCS-1), cytoplasmic signaling protein Nck2, phosphoprotein RanBPM and tensin domain like phosphatase C1-TEN. These molecules contain phosphotyrosine binding SH_2 domains that interact 'preferentially' with Y821 phosphotyrosine of Axl (Hafizi and Dahlback, 2006). The downstream effectors present an association of Axl with various cellular processes that are primarily known to include cell survival; proliferation; cytoskeletal dynamics and cellular migration (figure 1-12).

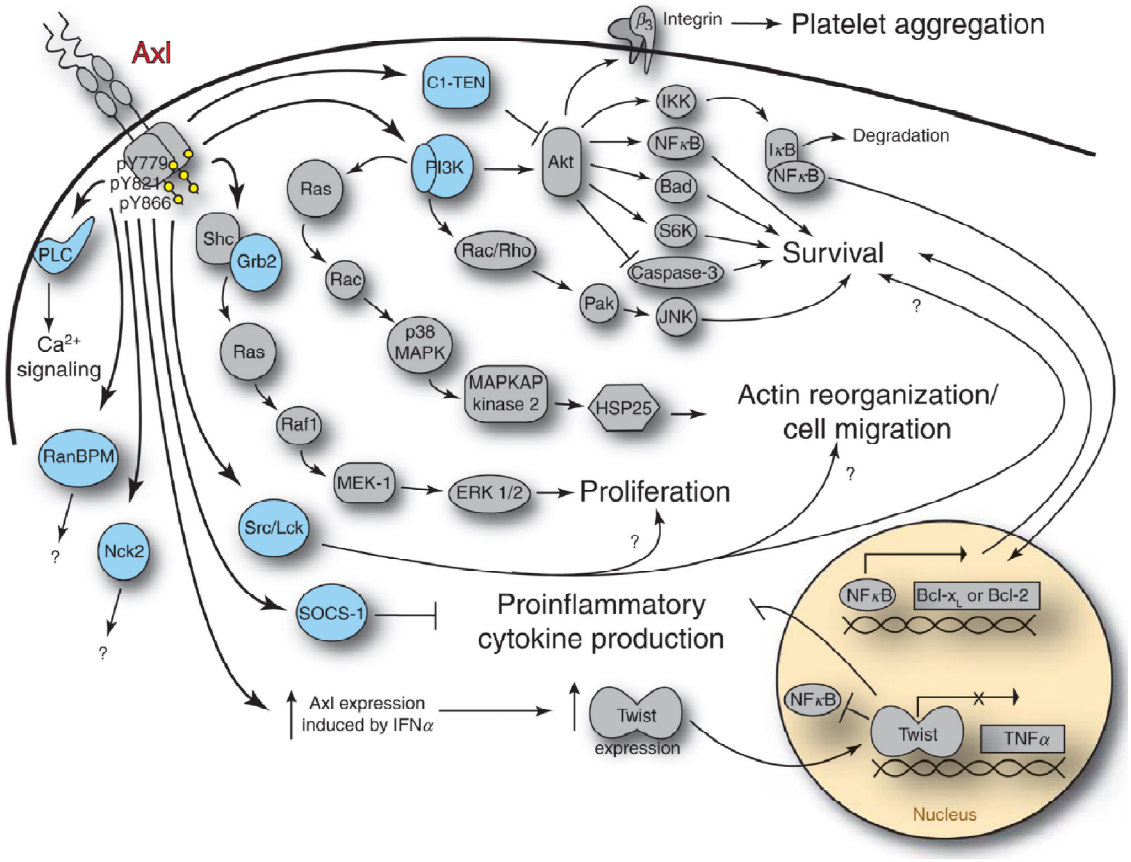

Figure 1-10 Axl signal transduction pathway

Ligand dependent dimerisation of cell surface Axl leads to recruitment of primary downstream signal transducers (blue circles). These catalyse the formation of inositol tri-phosphates that are required for the recruitment of PI3K (Phosphatidylinositol3 Kinase). Axl induced PI3K instigates survival signaling by activating anti-apoptotic Akt kinase, which stabilises NfκB that further upregulates anti-apoptotic Bcl-XL and Bcl-2. The primary molecules RanBPM and Nck2 link Axl with PUNCH & Integrin-linked kinase (FAK) proteins that collectively serve as signaling platforms at focal adhesion sites, thus affecting cytoskeletal dynamics. Src/Lck are presumed to act through the Ras/ERK pathway to transduce mitogenic signals. Ras/ERK is dispensable and not required for Axl survival but is implicated in cytoskeletal reorganisation through the modulation of small GTPases Rho and Rac. TWIST is an anti-inflammatory IFNα induced basic helix-loop-helix DNA binding transcription factor that inhibits NFκB-dependent transcription of TNFα and is also a negative regulator of osteogenic differentiation. Figure taken with permission from (Linger et al., 2008). Annotations derived from (Linger et al., 2008; Hafizi and Dahlback, 2006; Lee et al., 1999).

1.5.3 Biological implications in cell substrate responses

Axl was highlighted as a gene expressed early on at significantly higher levels in human alveolar osteoblasts in contact with rough Ti surfaces (Brett et al. 2004). It was observed to have been significantly downregulated by hMSCs at 5 days on the rough compared to polish Ti (Wall et al. 2009; Supplementary data). These observation correlate with the biological functions attributed to the pathway; as a potent anti-apoptotic protein (Shankar S L, 2006), role in the modulation of cytoskeletal re-organisation through rock-Rho GTPase (Linger et al., 2008; Goruppi et al., 2001)(Linger et al 2008; Goruppi et al 1999), cellular adhesion (McCloskey et al., 1997)(McCloskey et al 1997) and, of interest to this study, osteogenic differentiation of uncommitted cells (Collet et al., 2006; Collet et al., 2003).

The association of the Axl / Gas6 pathway with survival through activation of PI3K and up-regulation of anti-apoptotic BCL proteins implies it may be modulated by cells in response to surface induced apoptosis. But of more importance is the observation of receptor down-regulation prior to calcification in bovine pericytic cells *in vitro*, reversed by the addition of receptor agonist in the form of recombinant proteins (Collet et al. 2003; Collet et al. 2006) and supported by the demonstration of inhibition of calcification *in vivo* by statins through restoration of Gas6/Axl signaling (Son et al., 2006). These imply a possible involvement of the receptor in the differences observed in the osteogenic responses of cells to the rough surfaces. The small GTPase Rho-A and its downstream effector ROCK have been shown to be modulated by ‘stretched’ stromal cells compared to rounded cells, leading to the induction of an osteogenic phenotype in the former, and an adipogenic in the latter (McBeath et al 2004) presumably due to down-regulation of a master adipogenic instigator PPAR-γ (Peroxisome proliferator-activated receptor gamma) (David, 2007). The modulation of small GTPase Rho-A has been linked with Axl signaling through Ras/ERK by cytoskeletal stress (Goruppi et al., 2001). These observations strongly implicate the functional significance of the pathway in the differences observed on the rough surface.

1.6 Statement of thesis

1.6.1 Observations

Osseointegration is a complex biological phenomenon, reminiscent of neo bone formation, and composed of a series of overlapping cellular and molecular events, which seek to integrate an inanimate biocompatible material (predominately Ti), of specific dimensions, into living bone. The dynamics of osseointegration are highly affected by topographical modifications of Ti implants. Clinical evidence had indicated an increase in peri-implant bone accrual, larger bone to implant contact and faster bone conduction on rough compared to smooth implants. Furthermore, recently completed pre-clinical studies have shown that a hydrophilic rough surface can additionally promote osseointegration compared to the rough-hydrophobic surface modification; these substrates bear the exact physical topography but different chemistries. *In vitro* examinations of certain osteogenic parameters in osteoblastic and mesenchymal stromal cells cultured on smooth and modified Ti substrates indicate a novel enhancement by rough implant topographies, suggestive of a relative promotion in osteogenic phenotypic differentiation and function, which are additionally supported by the hydrophilic nature of the modified rough modSLA surface. An observation of selective upregulation at the gene level implicates the differential modulation of a cell surface tyrosine kinase receptor called Axl, a molecule functionally associated with cellular osteogenic differentiation in uncommitted pericytes, in these enhanced osteogenic responses of uncommitted cells to the rough Ti surfaces.

1.6.2 Hypothesis

The cell surface receptor Axl is differentially modulated in the osteogenic responses of human bone marrow derived mesenchymal stromal cells (hMSCs) to different Ti implant surface modifications.

1.6.3 Aims

The aims were to (i) investigate differences in the phenotypic and osteogenic responses of cells to the different substrates; (ii) compare the modulation of the Axl / Gas6 pathway in cells cultured on different substrates; (iii) examine the effects of deregulating the Axl / Gas6 pathway on cell-

substrate responses; and (iv) assess the functional significance of Axl in the altered responses of hMSCs to modified Ti surfaces.

1.6.4 Objectives

The objectives of this project are listed below.

a. Form an understanding of hMSC phenotypic responses to the different substrates by examining cellular attachment, morphological differences in spreading, and cellular viability and proliferation.
b. Form an understanding of hMSC osteogenic responses to the different substrates by comparing the expression of osteogenic markers, cellular mineralisation and soluble osteoblastic protein secretion over the course of culture.
c. Examine the hypothesised differential modulation of Axl and Gas6 genes by rough surfaces in hMSCs by comparing temporal differences in gene and protein expression of the receptor, its ligand and a downstream effector called TWIST1 that is implicated in osteo-inhibitory effects of the pathway. Furthermore, examine the effects of Axl receptor de-regulation on cellular proliferation, mineralisation and osteoblastic soluble protein secretion over the course of culture.
d. Attempt to query the differential modulation of Axl in cell to surface responses by assessing the effects of receptor de-regulation on the expression of stem cell pluripotency associated genes.

These experimental investigations were conducted in an *in vitro* two dimensional cell culture model that consisted of cells, suspended in liquid medium and plated under the influence of gravity onto a substrate immobilized in a sterile culture vessel. The experimental substrates assessed in this study were tissue culture plastic (TCP), polished cpTi (P), hydrophobic sand blasted large-acid etched (SLA) and hydrophilic SLA (modSLA). The TCP was used as a control for substrate material-type dependent effects on cell responses. This was because (i) it is the substrate that houses primary cells outside their natural environment, and is their ‘cognate’ substrate *in vitro*; (ii) TCP may

inadvertently incur changes in primary cells as they adapt to their new substrate; and (iii) it is the prime reference for comparison as aspects of bone development in human cells have been largely conducted on TCP. The polished surface was used as a reference control for Ti surface modifications' influenced effects on cellular responses.

2 Materials and methods

2.1 Modified titanium surfaces

2.1.1 Preparation

Titanium discs fabricated with the modified implant topographies were manufactured and provided by Institut Straumann AG (Walderberg, Switzerland). The implant surfaces were re-produced on discs that were of a 1.8 cm^2 surface area (15 mm diameter), designed to use in ~ 1.96 cm^2 24-well tissue culture treated plates. Three types of titanium surfaces were used in this study. The first was a control surface with a smooth topography referred in this study as the polished (P) surface, due to its near mirror-like reflectivity. The other two types were micro-rough surfaces. The first of these was a rough hydrophobic surface SLA, an acronym for **S**and-blasted **L**arge grit **A**cid-etched. The next of the rough surfaces was the rough hydrophilic modified SLA (modSLA) surface. It is produced in conditions that disallow surface contamination by hydrocarbons and thus, increases surface free energy, which in turn renders the surface hydrophilic, i.e. relatively more amenable to the flow of water molecules compared to the hydrophobic SLA.

A detailed description of the manufacturing methods and characterisation of these surfaces is provided in (Rupp et al., 2006). In brief, the Ti discs were punched out from sheets of commercially pure Ti (of grade III). The crude discs were polished to a mirror on one side with SiO_2 grinding paper with a grit diameter of 15 - 600 µm. These discs were further treated with diamond paste in oil and finally with a SiO_2 suspension to obtain a fine mirror-like surface. The polished Ti surface has been analysed by scanning electron microscopy to to have a R_a value, representing the average vertical distance between the lowest and highest points within topography, of 0.6 µm. The SLA discs were prepared by blasting a polished surfaces with large alumina particles, average in a diameter by 250 µm, and then acid-etching in a hot solution of hydrochloric (HCl) and sulphuric (H_2SO_4) acids. Following acid etching, the discs would be washed several times in de-ionised water and air dried. The modSLA surface was produced on polished discs with a method similar to that used for the SLA surface, with the exception of the final rinse being conducted under nitrogen

protection. By minimizing chances of contamination by atmospheric oxygen and organic chemical moieties, the modSLA has a higher surface energy. The modified discs were supplied sealed in glass tubes, immersed in isotonic NaCl at pH 4 - 6. The mean R_a value of the SLA and modSLA titanium surfaces is reported to be similar at 3.22 $\pm$ 0.88 µm (Rupp et al. 2006). The hydrophilicity due to high surface energy of the modSLA surface has been evaluated with advancing contact angle measurements by (Rupp et al. 2006) to be 91.31, 139.88 and 0 degrees for the polished, SLA and modSLA surfaces, respectively.

2.1.2 Passivation

The polished and SLA titanium discs were passivated prior to experimentation to remove excess hydrocarbon buildup on the surfaces. This was performed by washing discs in a 10 % (v / v) solution of 10 M nitric acid in distilled water, followed by several washes in de-ionised water. Discs were air-dried in a sterile environment and later ultra-violet irradiated for 1 hour on each side prior to use. The modSLA discs were supplied submerged in saline in sterile glass tubes and were required to be kept submerged in a liquid medium through the course of experimental setup to prevent transformation of the surface oxide layer.

2.1.3 Raman spectroscopic characterisation of surfaces

An attempt at assessing the chemical ‘cleanness’ of the modSLA compared to SLA surface was conducted in this study using Raman spectroscopy. This technique analyses the spectrum of emitted photons generated by incident monochromatic light to obtain an identity of the chemical nature of the target, such as oxides, hydrocarbons, etc, in comparison with the non-excited state, referred to as the background. The analysis in this study was conducted in a LabRAM HR spectrometer (Horiba Jobin Yvo; UK) fitted with a 633 nm incident laser. The analysis was performed on an area measuring five 40 x 40 µm squares at the center of an SLA and modSLA disc in air. The analysis was performed at x50 objective with a grating of 1800 Raman shifts (also known as wave numbers that bear the units = cm^{-1}).

A Raman spectrum for the polished surface could not be obtained due to the highly reflective nature of the surface, which strongly interfered with an optical receiver of the device. A spectrum for the modSLA surface could also not be obtained due to no difference between background and excitation states; suggesting a ‘very clean’ preparation without a trace of detectable surface contaminants. The SLA surface, however, showed differences with respect to the larger background. The results of this analysis are shown in figure 2-1. The first is observed at 1400 Raman Shifts and was suggestive of a carbon contaminant. The second and third peaks were observed at 450 and 600 Raman Shifts and reflected the presence of a form of Ti oxide, most likely anatase due to its high incidence in biomaterial preparations. A surface plot representing the regions of the SLA surface where these peaks were detected is shown in figure 2-1 (b and d). It indicates that the carbon contamination was at a lower extent but homogenously distributed while the anatase and titanium oxide contaminants occur at high intensities in interspersed foci.

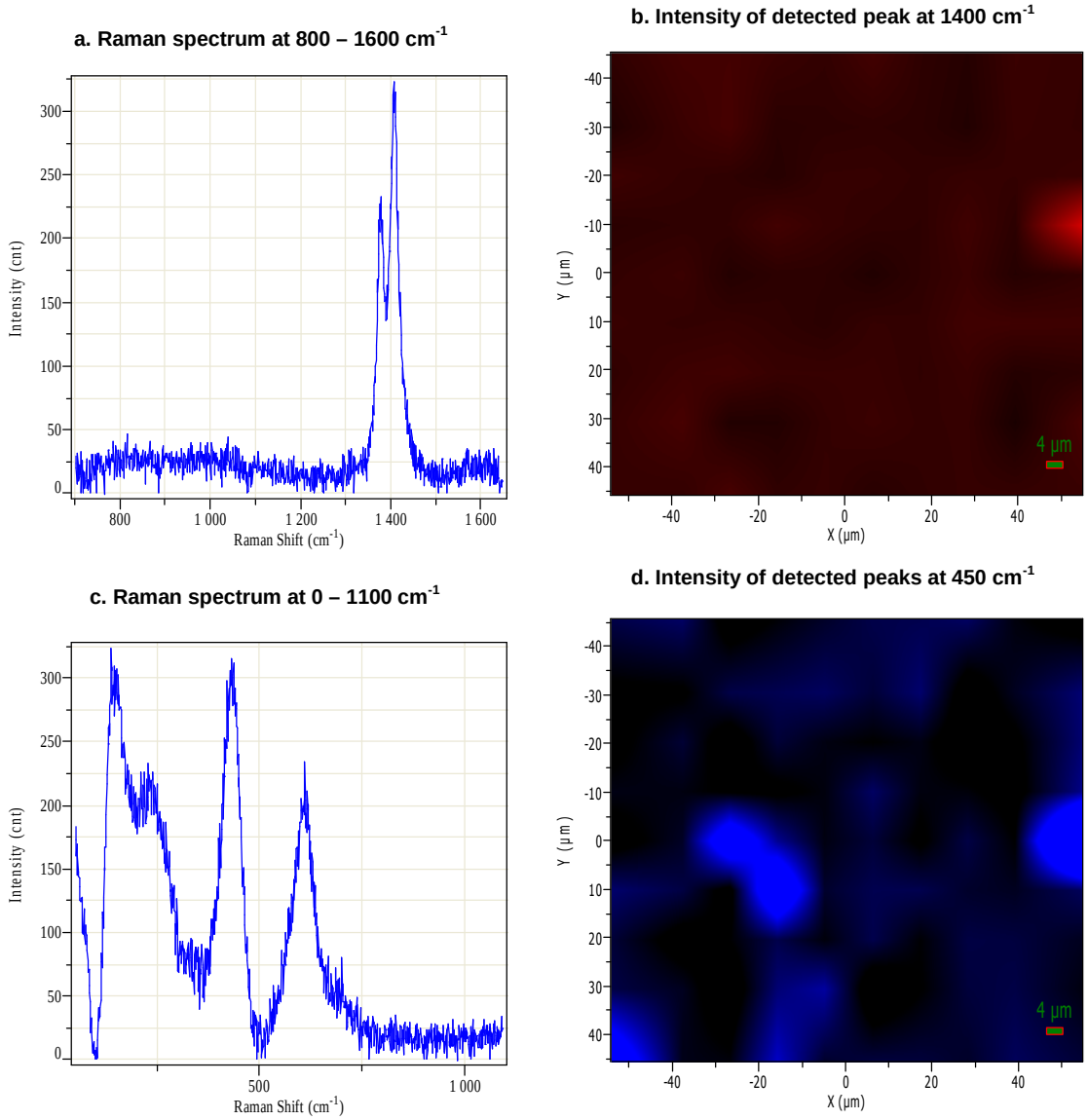

Figure 2-1 Raman spectrum of SLA Ti surface

Raman spectrogram of the SLA titanium surface was conducted to examine chemical differences compared to the modSLA. The graphs in (a) and (c) display the intensity of reflected signal on the y-axis plotted against the frequency of incident radiation on the x-axis (Raman shift, cm^{-1}). These graphs indicate the presence of chemical moieties excited by the laser. (a) The peak represents hydrocarbon contamination while those in (c) likely represent anatase and other Ti oxides. The images (b) and (d) are surface plots that attempt to show the physical distribution of detected chemical groups against their non-excited background. These images indicate presence of the chemical moieties within a specified area of the surface. Image (b) shows a small level of homogeneously distributed hydrocarbons represented in red against a black background. Image (d) shows interspersed regions of high titanium oxide in blue against a black background. The analysis shows that the SLA titanium surface, compared to its hydrophobic counterpart modSLA, has a relative degree of adsorbed hydrocarbons and complex titanium oxides.

2.2 Cell culture

This project entailed the culture primary human bone marrow derived mesenchymal stromal cells (hMSCs). The aspects of cell culture applied are explained over the following sub-sections. Accompanying tables of information are provided in appendix III ‘tabulation of cell culture materials’, from tables 9-5 to 9-9.

2.2.1 Environment & consumables

Cell culture was used for the maintenance, propagation, experimentation and storage of adherent primary human cells in sterile conditions. This work was conducted in a fully equipped tissue culture laboratory. The macro equipment used for tissue culture is tabulated in table 9-4. Most tissue culture consumables were acquired sterile. Non-sterilised items, including micropipette tips, forceps, were autoclaved and oven dried at 60^{o} C prior to use. The general consumables used for cell culture are detailed in table 9-5. The flasks and tubes were procured sterile and were disposed following a single use. The cell culture media and reagents used are tabulated in table 9-5. The instruments and consumables used for the sterilisation of equipment are tabulated in table 9-6.Practice

A cycle of cell culture normally constituted reviving a cryopreserved cellular specimen, and propagating it in an appropriate medium and vessel for a period of time in humidified conditions. During this period, medium would be replaced twice every week to replenish cellular nourishment and remove metabolic waste. Under ideal conditions, cultured cells increased in numbers forming confluent monolayers. These were detached, and either re-propagated (sub-culture), used in experimentation, or cryopreserved. The details of cell culture practice undertaken are elaborated in the following sub-sections.

2.2.1.1 Culture media

All liquid reagents and media were pre-warmed in water bath for ~ 30 min prior to use. Complete growth medium (GM) comprised αMEM basal medium supplemented with fetal bovine serum (FBS)

and antibiotics at 10 and 1 % of the final volume, respectively. The osteogenic inductive medium (OM) comprised Dulbecco's Modified Eagle's Medium low glucose supplemented with 10 % lot selected fetal calf serum, 1 % antibiotics, 0.1 % fungicide, dexamethasone at 10 nM; β-glycerolphosphate at 10 mM; and ascrobate-2-phosphate at 50 µM. The volumes of medium used per culture vessel substrate area are tabulated in table 9-7.

2.2.1.2 Specimen revival and propagation

Cellular specimens were normally stored in male-capped cryovials in liquid nitrogen. These stored cells were revived by half immersing a cryovial in a water bath and transferring thawed contents to pre-warmed growth medium in a 15 ml tube. The number of cells in suspension would be estimated with a hemocytometer by combining 10 µl of suspension with 10 µl trypan blue and counting total number of non-stained cells in the corner four 1 mm^2 boxes of the 9 boxed-grid. The average count was used in the formulas tabulated in table 2-1 to estimate the quantity of cells in suspension.

Table 2-1 Cell number calculations

Formulae used to quantify cells in a 1:1 cell suspension with Trypan blue with a haemocytometer. Here C = cell concentration. A = average count from 4x 1 mm^2 boxes of a haemocytometer. Df = dilution factor (2 throughout this study). Cn = total cell number

Variable	Formula
Estimated cell concentration	C (cells/ml) = A (cells) x Df x 10^4.ml^{-1}
Estimated total cell number	Cn (cells) = C x Vf

2.2.1.3 Sub-culture

Cellular detachment from a substrate was carried out with a Trypsin/EDTA solution. This was performed by twice washing cells with divalent-cation-free PBS and incubating the monolayer with Trypsin/EDTA solution at the proportion of 1 ml reagent per 25 cm^2 of substrate area in humidified conditions for up to 5 min. Detached cells were collected in growth medium and pelleted at 1000 x g for 5 min; and later re-suspended in a smaller known volume of growth medium. Cells were counted as described in 2.2.2.2. A known number of cells were added to culture vessels containing pre-warmed medium. The volume of inoculate was calculated with the arithmetic formula; Vi x Ci = Vf x

Cf, if Ni = Nf, where V = volume of suspension, C = concentration of suspension, N = number of cells, i = initial and f = final. Cultures would be incubated in humidified conditions with bi-weekly medium changes till attaining a ~80 percent confluence. The population doubling level of cells of a specimen were determined with the equation $(Log_{10}N_F - Log_{10} N_o)/Log2$, where N_F = number of cells harvested, and N_o = number of cells initially seeded.

2.2.1.4 Cryopreservation

Cells were cryopreserved in freezing medium formed by supplementing growth medium with FBS and DMSO to a final percentage of 30 and 5 percent, respectively. Pelleted detached cells were suspended at a density of 1 – 5 x 10^5 cells per ml in freezing medium. An aliquot of 1 ml of suspension would be added to individually marked cryovials, which were capped and stored at -80^o C for 24 h before being transferred to cryogenic liquid nitrogen tanks.

2.2.2 Culture of mesenchymal stromal cells

Human bone marrow derived stromal cells (hMSCs) from three unrelated donors (N = 3; Caucasian; male; 20-30 year age group) were obtained from the Centre for Gene Therapy, Tulane University (New Orleans, USA). These cells were isolated from bone marrow aspirates on their ability to adhere to tissue culture plastic compared to non-adherent hematopoietic adult stem cells. The hMSCs had been pre-characterised for colony forming unit formations, osteogenic, chondrogenic and adipogenic differentiation, and the expression of a repertoire of stromal cell surface markers by the suppliers (Appendix IV: Cell specimen characterization data sheets).

The cells were cultured according to the parameters suggested in (Colter et al., 2000; Colter et al., 2001; Colter et al., 2000; Sekiya et al., 2002; Sekiya et al., 2002). Cells were expanded at a low density (100 cells.cm^{-2}) in GM with αMEM as basal medium. Cultures were harvested for experimentation on attaining 80 % confluence with trypsin/EDTA. Experiments were performed with cultures that had undergone a maximum of three passages or at most 15 population doublings. Osteogenic differentiation was induced by seeding cells at a relatively higher density of ~1.25 x 10^4 cells.cm^{-2} in OM.

The cumulative population doublings were evaluated for the first vial of each of the three hMSC donor specimens used in this study. This was performed by setting up parallel cultures of specimens in T150 flasks at 100 cells.cm^{-2} in GM; recording cell numbers harvested at subculture, and calculating cumulative figures for population doublings as described in 2.2.2.3. The results of this analysis are presented in figure 2-2. It indicates two of the donor specimens (7043 and 7081) to be highly similar in population doubling characteristics. This was not the same for the specimen 7032, which although seeming to be highly replicative in the first passage, failed to thrive at a comparable level in later passages.

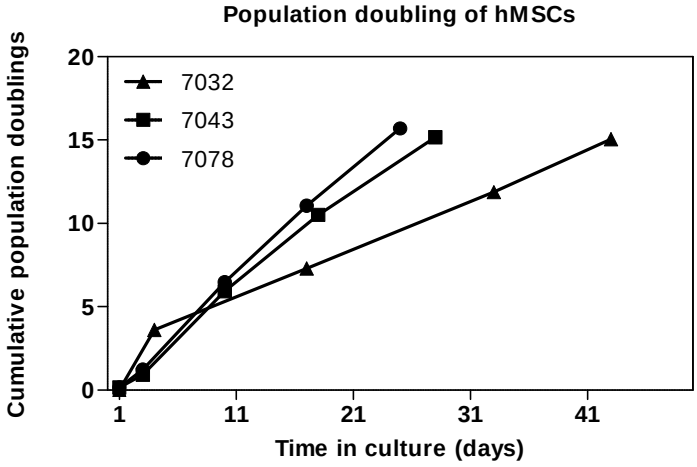

Figure 2-2 Cumulative population doublings of cultured hMSCs

The cells were plated at 100 cells.cm^{-2} in GM in T150 flasks till confluent colonies appeared. Cell numbers were determined with haemocytometric counts at the start and end of culture. The values were used to calculate the cumulative population doublings of each specimen over five passages. Donor 7032 exhibited a lag in population doublings following the second passage. Donor cells 7043 and 7081 exhibited similar proliferative characteristics through all passages. This finding indicates differences in the replicative, and hence probably, the phenotypic characteristics of the different hMSC specimens.

2.2.3 Cell culture optimisation

The *in vitro* behavior of cells is highly influenced by fetal bovine serum (FBS) (Kuznetsov et al., 2008; Caterson et al., 2002). This protein rich mixture acts as a source of hormones, growth factors, and peptide metabolites for cultured cells. The lack of a system to characterise and categorise FBS based on the relative proportions of all constituents entails a level of variability in cell culture

conditions and hence, experimental results. To control the variable affects of different lots of FBS on cell culture and experimental settings, a serum batch test was undertaken to acquire a serum lot optimum to support low density growth and *in vitro* osteogenic mineralisation of hMSCs. The list of sera types tested is provided in table 9-4 (appendix II). The protocol for testing sera types comprised a 10 d colony forming unit (CFU) assay, a 10 d proliferation curve and a 14 d osteogenic-like differentiation assay. The methodologies applied are described in sections 2.4, 2.5.3, and 2.7.2, respectively. The hMSCs used for this experiment were expanded in respective FBS types prior to experimentation to negate the effects of serum adaptation.

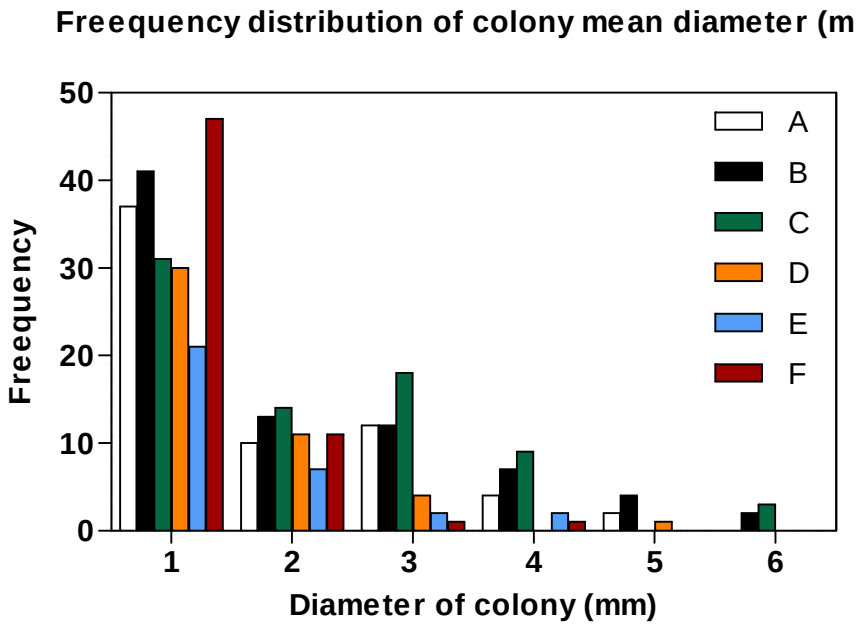

Figure 2-3 Frequency distribution bar chart of colony size

Each bar shows CFU numbers per FBS type per size of diameter (mm). Approximately 100 cells were seeded per T75 flask in GM and cultured for 10 days. Samples were fixed/stained with crystal violet in methanol. Images of CFU cultured flasks were analysed with Image pro plus. Total colonies were counted and mean diameters (mm) of all counted colonies were determined with image software. Readings were analysed with Graphpad Prism for frequency distributions (Bin minimum = 1 mm; Bin range = 1 mm). Sera A to D cultured cells produced colonies of higher sizes at a higher frequency than sera types E and F.

The CFU analysis revealed all serum types to be able to support hMSC growth at clonal densities. This is inferred from the observation of near equal numbers of colony formations by all serum types

that averaged 2 mm in diameter (figure 2-3). The cumulative number of colony forming units larger than 2 mm was 32, 38, 36, 16, 11 and 13 for A, B, C, D, E and F, respectively, indicating a difference in the potential of serum types to support colony growth above the standard 2 mm mean diameter mark.

The images of the colonies formed by FBS types A, B and C displayed a relatively denser stain as shown in figure 2-4. The hMSCs cultured in these sera also formed relatively well defined circular colonies compared to E and F as shown in figure 2-4.

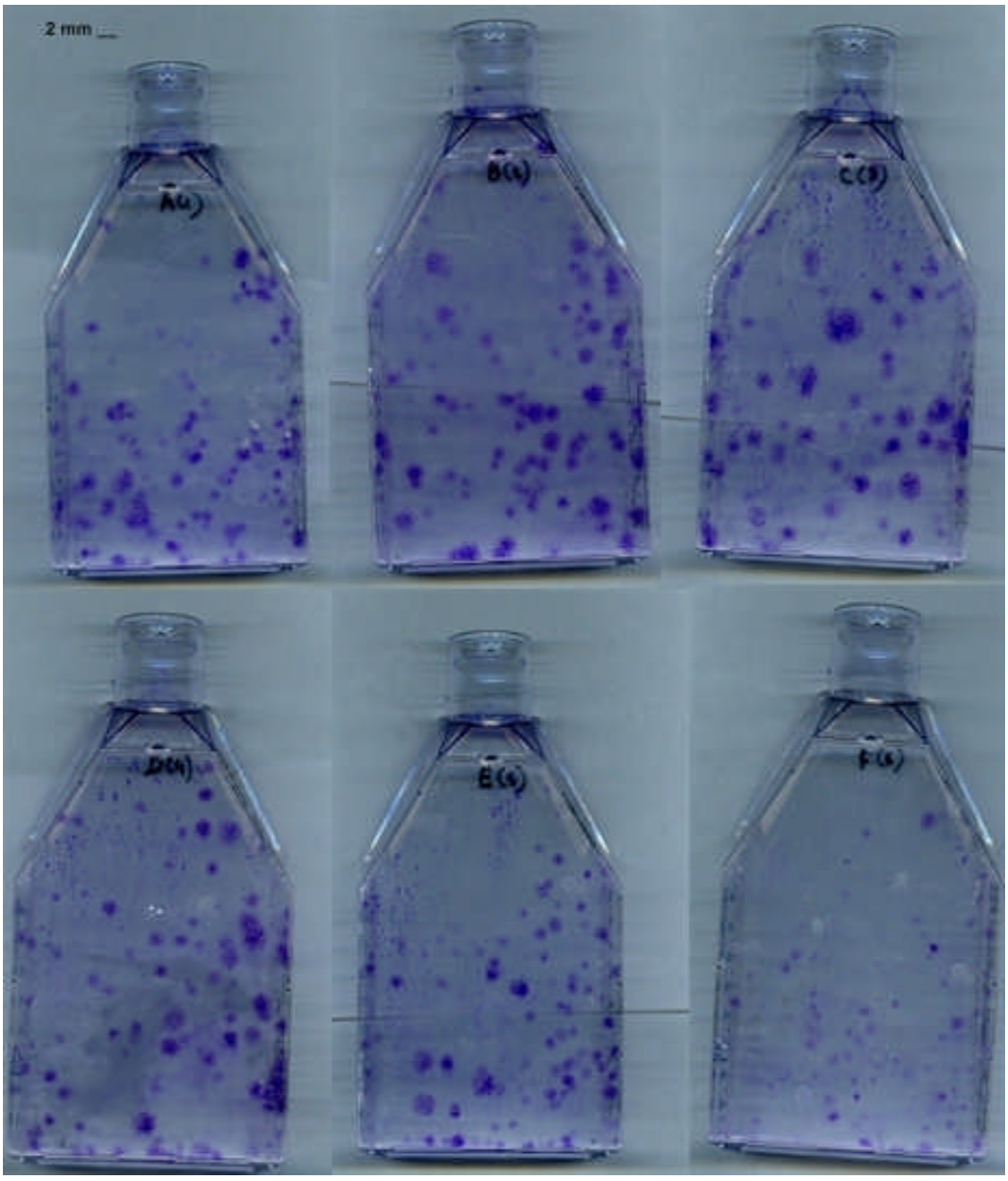

Figure 2-4 Colony formations in different FBS types

Images of crystal violet stained colonies formed by ~100 hMSCs seeded in a T-75 tissue culture flask for 10 days.Sera types A, B and C produced highly prominent colonies compared to E and F. Scale bar (2 mm) is provided in the upper left corner of the image.

The osteogenic mineralisation of cells indicated that hMSCs deposited higher levels of mineral in serum types A to D compared to lower levels in types E and F. A quantitative assessment of deposited calcium levels is provided in figure 2-5, which shows a significantly higher quantity of calcium detected in samples cultured with serum types A to C compared with E and F.

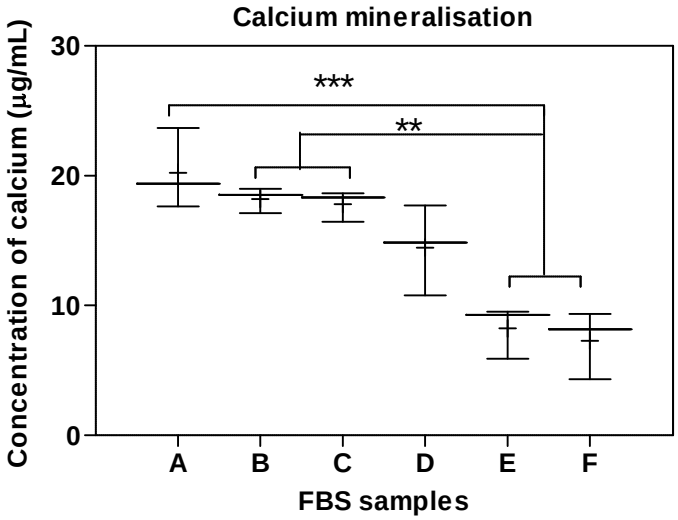

Figure 2-5 Calcium mineralisation in different sera types

Figure is a box and whisker plot of calcium concentrations determined in 0.5 ml lysates of samples cultured in OM supplemented with different sera types for 14 d. Approximately 2.5 x 10^4 hMSCs were cultured in 24 well plates in triplicate. Serum types A, B and C had induced significantly higher levels of matrix mineralisation compared to E and F indicating these to be highly supportive of osteogenic differentiation. Readings are presented as minimum to maximum range of data points with large and small horizontal lines depicting median and mean, respectively. ** = $p < 0.01$, and *** = $p < 0.001$; $N = 1$, n = 3.

Additionally, in a separate experiment, monolayers of hMSCs (donor type 2, 7043) were cultured in osteogenic inductive medium supplemented with different sera. Monolayers were stained with Alizarin Red S as stated in section 2.7.1. The results of this analysis are shown in figure 2-6. It shows a higher intensity of staining in samples A to C and least stain in samples E and F.

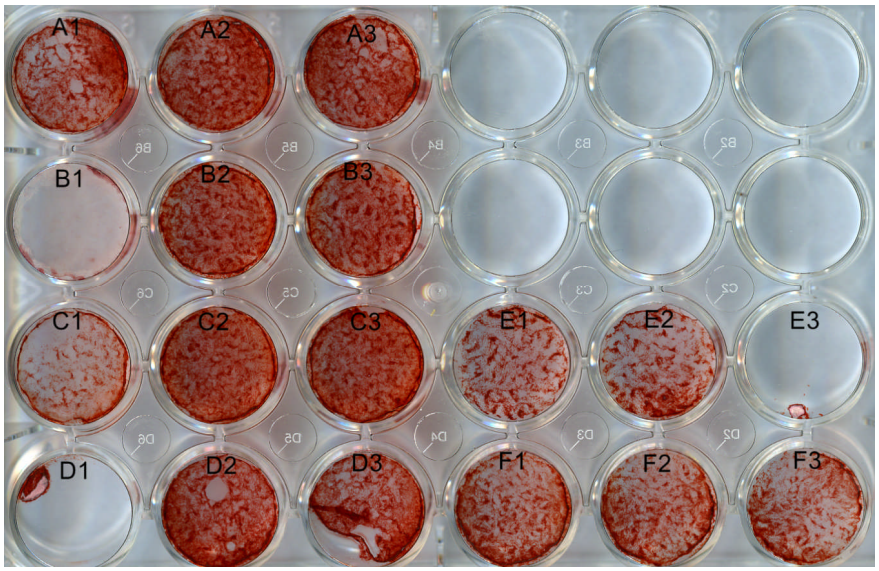

Figure 2-6 Staining for calcium mineralisation in different sera types

Image is a scan of a 24-well plate with hMSCs cultured in osteogenic medium supplemented with one of the seven serum types. Triplicate cultures were maintained for 14 d, and then stained for Alizarin Red S according to the protocol stated in section 2.7.1.Scans were acquired according to the method described in section 2.3.3. Samples A through to D displayed high levels of stain indicative of a high level of calcium mineralisation. The absence of a monolayer in B1, D1 and E3 is attributable to the process of de-lamination, seen to also be occurring in samples D2 and D3, which can be loosely defined as the detachment of a confluent monolayer of adherent cells from its *in vitro* substrate. Sampls E and F show the least relative stain suggestive of a weaker capability of promoting osteogenic mineralisation in hMSCs.

2.3 Microscopy and imaging

2.3.1 Light microscopy

Light microscopy was used to visualize cellular confluence and morphology at different stages of culture with an inverted light microscope. Normal observations were conducted with x4 and x10 magnification objective lenses.

2.3.2 Scanning electron microscopy

Scanning electron microscopy (SEM) was conducted on a Cambridge Stereoscan S90B (Cambridge Instruments; UK). Samples were imaged either uncoated with Back-scattered SEM or following a sputter coat. The former analysis highlights organic entities as dark objects against a

bright inorganic (Ti) background, and was useful for the quantitative estimation of cells attached to the different discs. The latter was directed at qualitative evaluations, such as shape, spreading etc. An SEM analysis would be initiated by washing a sample (cells cultured on a Ti disc) several times with divalent-cation-free PBS with gentle aspiration. The sample would then be fixed in 4% glutaryldehyde in 0.14 M sodium cacodylate buffer (pH 7.3) (Sigma) at 4^{o} C overnight. The sample would be dehydrated in a graded series of alcohols (50 %, 70 %, 90 % and twice 100 %) and finally critically dried in hexamethyldisilazane (TAAB Laboratories) for 5 min. The dehydrated samples were normally stored in a case mounted onto stubs in a sealed dessicator. Samples were then sputter coated sputter-coated with gold/palladium using a Polaron E5100 coating device (Polaron CVT, Milton Keynes, UK). Samples were stored in a dessicator till viewing.

2.3.3 Plate scanning with document scanner

A further imaging method (advised by Prof. Timothy Arnett, UCL, Dept. of Anatomy) employed the usage of a flat bed document scanner (Epsom photo 4200). For this purpose, samples exclusively comprising cells cultured on tissue culture plastic dishes were stained, washed, and air dried dishes placed on a scanner with a piece of white paper laid on top of the samples (forming a white colored background). Images were acquired at 800 dots per inch (dpi). Images were cropped to highlight samples.

2.3.4 Image analysis

Images were analysed with the Image Pro Plus software, version 4. Many of the panels of images used in this thesis were prepared using Photopad Editor version 2.01 distributed by NCH Software (www.nchsoftware.com).

2.4 Colony forming unit analysis

The hMSCs are a highly proliferative cell type capable of forming single cell derived colonies when plated at extremely low cell seeding densities. The measure of colony forming ability of a cell population is indicative of the relative proportion of uncommitted/replicative cells; and is evaluated by a colony forming unit (CFU) assay (Colter et al., 2001). A typical CFU assay was performed by

culturing ~100 cells in a T-75 flask for 10 days at 37^0C and 5% CO_2 with bi-weekly medium changes. At 10 days, cultures were fixed & stained in a solution of 3% Crystal Violet in 100% Methanol, followed by several washes in distilled water and finally air dried. Comparative parameters included number, density and diameter ($\geq$ 2 mm).

The CFU analyses were primarily undertaken for fetal bovine serum batch selection and included the further steps of analysing images representing 80% of surface area of a substrate with Image-Pro Plus software. The analyses conducted were of colony number and mean colony diameter, defined as the average of several diameters measured at 2^o intervals around the centre of a somewhat circular object. The measurements were calculated in mm scale of length. Data was exported from software in a Microsoft Excel file to draw a histogram of size distributions.

2.5 Cell enumeration assays

Three different assays were used to establish cell numbers in experimental settings where hemocytometric measurements were not applicable. These fluorescence based assays included the CyQuant nucleic acid stain, Calcein-AM cytoplasmic stain, and the AlamarBlue cell viability assay. The descriptions of individual assays and their applications in this study are described below.

2.5.1 CyQuant nucleic acid fluorescent stain

The CyQuant GR assay consists of a fluorescent dye that upon intercalating with double stranded nucleic acid of ruptured cells, exhibits enhanced fluorescence. This is a destructive assay that requires cessation of sample culture for analysis, and was used for cell enumeration in cell attachment experiments. A typical assay was initiated by washing samples setup in 24-well plates three times with di-cation free PBS and cyclically freeze-thawing the culture plate at -80^oC, enclosed in plastic film, for 3 h with 30 min intervals. Samples could be assayed at 3 h or stored at -80^oC for an indefinite time. The staining was conducted by preparing a working solution of dye in lysis buffer; by diluting 1 ml stock lysis buffer in 19 ml of de-ionised water, to which were added 50 µl of the x400 concentrate of dye in DMSO. This homogenous clear dye solution was added at 150 µl per well of a 24-well plate with a micropipette and allowed to stand for 10 min at 4^oC in the dark.

Samples were then vigorously mixed with a micropipette and 100 µl of homogenate transferred to a clean well of an opaque 96-well plate. Each sample was handled with an unused micropipette tip. Fluorescence intensity was measured at excitation 530 nm and emission 590 nm. Total cell numbers were determined by extrapolating fluorescent intensities of unknown samples from a standard curve. A limitation of this assay was that the linear detection range with excitation 530 nm and emission 590 nm filters was reduced to 1x 10^4 cells. The standard curve for this assay is provided in figure 2-7.

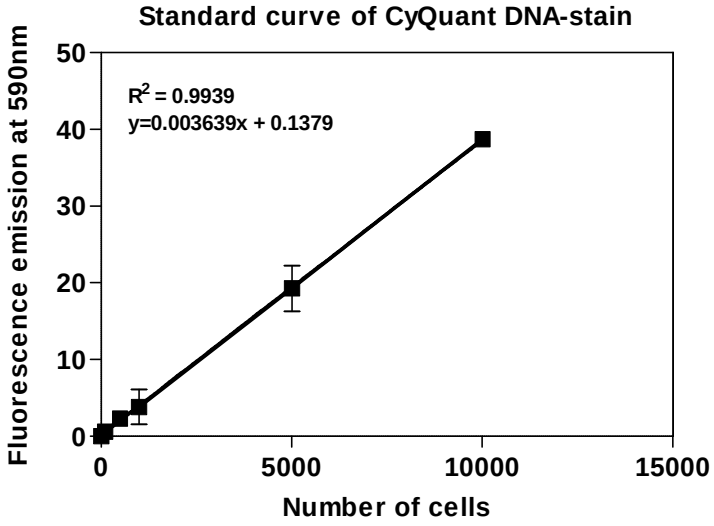

Figure 2-7 Standard curve of CyQuant

Figure shows a line graph of a six point standard curve, drawn by plotting mean fluorescence emission values on y-ais against cell numbers on the x-axis. Fluorescence values were obtained by plating calculated volumes of stock cell suspension in 24 well plates. Samples were stained and fluorometric measured made as stated in 2.5.1. Curve was drawn from zero-subtracted readings using linear regression analysis. Each point represents mean of two replicates (n=2).

2.5.2 Calcein-AM cytoplasmic esterase activated fluorescent cell label

Calcein- AM (Vybrant Cell Adhesion kit; Molecular Probes; Sigma) is a cell-permeable non-fluorescent molecule. It is hydrolysed intracellularly by cytoplasmic esterases to yield a highly fluorescent calcein anion that can be retained in the cytoplasm of living cells for up to 5 h depending on the cell type. It also has a higher fluorescence emission per cell number, making it an ideal

assay to estimate cell numbers in attachment experiments. Calcein-AM is a non-destructive assay that does not require cellular lysis. In a typical assay, cells were labeled in suspension at a proportion of 5 µM of substrate dye in serum-free GM per of 5 x 10^6 cells.ml^{-1} for 40 min in humidified conditions. Labeled cells were washed three times in divalent-cation-free PBS and viable cell numbers estimated with a haemocytometer. Viable cells were re-suspended in serum-free GM and applied to experimentation. End analysis of monolayers depended on the experimental protocol. In general, fluorescence intensity was measured by gently washing monolayers with divalent-cation-free PBS and measuring the intensity of emitted fluorescence of a whole surface at excitation 530 nm and emission 590 nm. Cell numbers were determined by subtracting the background readings of corresponding cell-free control surfaces and extrapolating the difference from a standard curve. The standard curve was formed by seeding labeled cells on TCP in a 24-well plate and measuring fluorescence intensity in situ; without washing samples (figure 2-8).

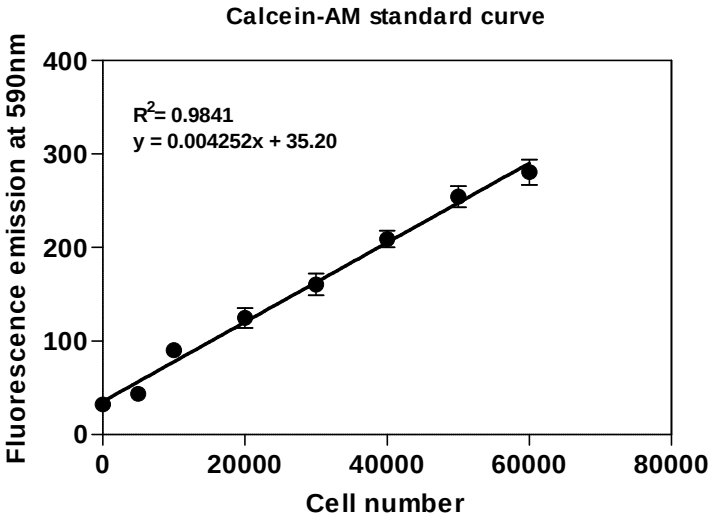

Figure 2-8 Standard curve of Vybrant calcein-AM dye

Figure shows a line graph of an eight point standard curve with mean fluorescencent emission values plotted against cell numbers. Samples were formed in 24-well plates by plating calculated volumes of stock cell suspensions. Samples were processed as stated in 2.5.2. Curve was drawn from zero-subtracted readings using linear regression analysis. Each point represents the mean±SEM of three replicates (N=3; n=3).

2.5.3 AlamarBlue fluorescent-metabolic cell substrate

AlamarBlue is dark blue water soluble solution of a non-fluorescent dye called resazurin. This is a reduction-oxidation indicator that is metabolized in cellular mitochondria to yield soluble fluorescent red colored resorufin, which can be measured with fluorescence or colorimetric spectrometry. It is an extremely easy and time efficient non-destructive assay that due to reportedly null toxicity to cells can be used for the serial analysis of changes in cell numbers of a culture over an indefinite course of time. An AlamarBlue assay would be conducted in cells cultured in 24-well plates in 1 ml of culture medium. The oxidized blue dye was added to culture at 10 % the total volume of supernatant (i.e. 100 µl dye per 1000 µl medium) and incubated for 4 h in humidified conditions. Following, 100 µl of conditioned culture supernatant of each sample would be transferred to an opaque microtitre plate, and fluorescence emission measured at excitation 530 nm and emission 590nm. The conditioned medium of cell cultures would be replaced with fresh GM for further incubation and analyses. Cell numbers were determined by extrapolating fluorescent values from a standard curve (figure 2-9).

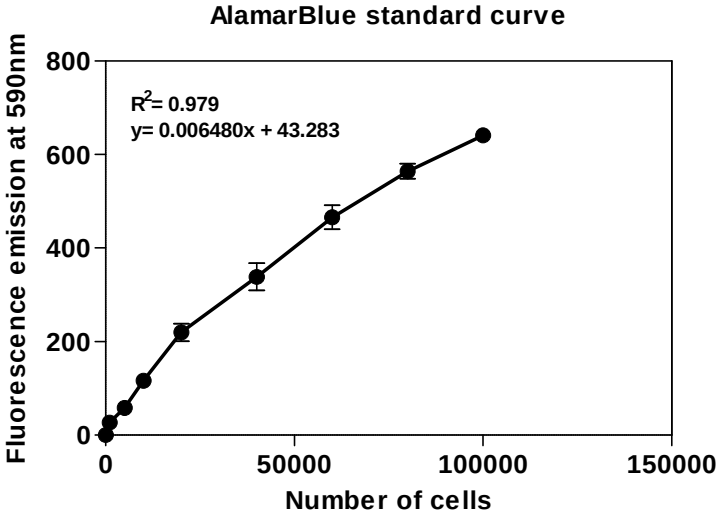

Figure 2-9 Standard curve for the AlamarBlue assay

Figure shows a line graph of a nine point standard curve with mean fluorescence emissions plotted against cell numbers. Samples were formed in 24-well plates by plating calculated volumes of stock cell suspensions. Samples were processed as stated in 2.5.3. Curve was

drawn from zero-subtracted readings using linear regression analysis. Each point represents mean±SEM, n=3.

2.6 Gene expression

Gene expression changes were analysed with real time polymerase chain reaction (RT-PCR) using the $2^{-\Delta\Delta Ct}$ method. This approach determines the 'Ct', threshold cycle, which is the cycle number at which the reaction enters log exponential phase of amplification. This method comprised three steps; the extraction of RNA, reverse transcription to cDNA and Taqman probe based RTPCR assay of relative levels of expression. Descriptions of individual steps are provided in the following sub-sections.

2.6.1 RNA extraction

Total RNA was extracted with the RNeasy Mini kit from Qiagen according to the manufacturer's instructions. These kits employ a silica membrane containing column; to which RNA adheres, and is washed and later eluted. A typical sample would consist of adherent cells cultured on a substrate in a 24-well TC plate. These were initially washed x3 with dication-free PBS and homogenized *in situ* with buffer RLT (350 µl per 1.96 cm^2). Total RNA was precipitated from homogenate by mixing with an equal volume of 70 % ethanol in distilled water, and then transferred to a silica membrane column. The membrane captured total RNA would be washed in a series of different buffers to remove excess cellular material and finally eluted from the membrane with RNAse-free water (40 µl per column). The integrity and quantity of extracted RNA was evaluated by spectrophotometry with Tecan NanoDrop at excitation 260 nm and emission 280 nm.

2.6.2 Reverse transcription

Reverse transcription was performed with first strand synthesis reactions using the High Capacity Reverse Transcription Kit from Applied Biosystems. Generally 100 µl cDNA would be prepared from 400 ng of RNA per sample combined in 1:1 with master mix according to the manufacturer's instructions. Samples were prepared in 0.2 ml PCR tubes in a thermocycler and later stored at – 80 ^{o}C.

2.6.3 Real time polymerase chain reaction

The RT-PCR reactions were performed in a 7300 Real Time PCR System from Applied Biosystems. These were undertaken in 25 µl reactions with 2.5 µl of cDNA per reaction; equivalent to 10 ng of RNA at the estimated 4 ng RNA per 1 µl of cDNA. The sample were run on a 1 h 45 min cycle to obtain the crucial 'Ct' value; it represents the point at which a particular transcript's amplification goes into exponential (log) phase of duplication. The 'Ct' values of the different markers were normalised to the GAPDH house keeping gene of the sample sample to obtain 'delta Ct' values. These were then calibrated to the reference, which comprised **Δ**Ct values of cells in suspension at time zero to obtain **ΔΔ**Ct values for each sample. Relative fold values of expression of a gene were calculated arithmetically with the formula, $2^{-\Delta\Delta Ct}$. Fold values were calculated separately for each replicate. These were then combined and used to calculate mean and error of samples with Graphpad Prism.

2.6.4 Gene expression array

Human pluripotency gene arrays consisting of 384-well Taqman RTPCR micro-fluidic cards were procured from AppliedBiosystems (Cat # 4385344); and used to evaluate global transcriptional changes in genes associated with stem cell identity. These arrays contain a reservoir on the right hand side of the plate, to which a 100 µl 1:1 mix of sample cDNA and Universal PCR master mix were added, and spun at 10, 000 x g to fill all rows. These cards were then run in a specialized RT-PCR thermocycler (AppliedBiosystems 7900 HT) at the UCL Institute of Child Health, London, UK. Data was exported in the form of Ct values, which were used to calculate relative fold differences in expression between sampled genes with Graphpad Prism. Mean fold values of three specimens were plotted in a heat map using the R software from The R Project for Statistical Computing (www.r-project.org) with a dendogram adjoining similarly expressed genes, the distance between which was calculated with Euclidean algorithm.

2.7 Assays for calcium mineralisation

The degree of osteogenic mineralisation was assessed by (i) semi-quantitative Alizarin Red S Stain dye elution method or (ii) quantitative QuantiChrom Calcium Assay. These are described below. In addition, mineralisation was assessed in a few instances with the Von Kossa and alkaline phosphatase stains.

2.7.1 Alizarin red S dye semi-quantitative monolayer stain

Alizarin red s is a red dye that has been used in histology for many years, in detecting calcifum salt deposits (Puchtler et al., 1969). At acidic pH, the dye binds Ca^{2+} in a 2:1 molar stoichiometry through a chelating process (Gregory et al., 2004). Matrix bound dye can be eluted in cetylpyridinium chloride (CPC; Sigma) and absorbance of dye measured at 562 nm in a spectrophotometer. These arbitrary units in comparison with a control provide a semi-quantitative estimate of Ca^{2+} content between samples. Moreover, the stained samples, when imaged according to the methods described in section 2.3.4, provided a visual assessment of the extent of calcium mineralisation in different experiments.

The Alizarin red S stain was carried out by washing culture monolayers gently with divalent-ion free PBS, and fixing the monolayer in 10 % formalin for 10-15 min. The monolayer would then be stained with a 2 % Alizarin Red S Solution in deionised water pH = 4.1-4.3 for 10 min followed by x4 washes with water. Samples were then allowed to air dry. Calcium bound dye was eluted with 0.5 ml of 10 % (w / v) cetylpyridinium chloride in 10 mM sodium phosphate buffer, pH=7.2. Spectrophotometric absorbance of elutant would be measured at 562 nm.

2.7.2 QuantiChrom colorimetric quantification of deposited calcium

The QuantiChrom calcium assay is a sensitive quantitative method of detecting free Calcium ions in solution. It is a colorimetric assay in which a working reagent forms a blue coloration when in contact with free-Ca^{2+}; the intensity of which depends on the concentration of the ions. This intensity was assayed by absorbance at 590 nm in a spectrophotometric plate reader. An assay was performed by washing a monolayer cultured in 1.9 cm^2 24-well TC-treated plate with dication-

free PBS, and then lysing it with 500 µl of 1 M HCl for ≤ 1 h. A 5 µl aliquot of lysate would be transferred to a clear bottom 96-well plate (duplicates per sample replicate); to which 200 µl of freshly prepared working reagent were added. The intensity of coloration was read at 562 nm. Calcium concentrations (µg / ml) were determined by interpolating zero-subtracted absorbance values from a 10 point standard curve (figure 2-10). Cells cultured on TCP in GM were used as a negative control of calcium mineralisation.

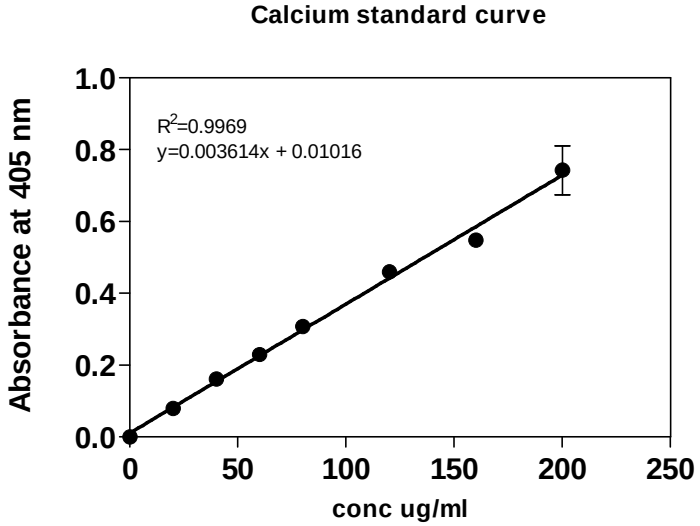

Figure 2-10 Standard curve of calcium quantification assay

Figure shows a line graph of a ten point standard curve of calcium salt formed in a 96-well plate. Samples were processed and stained as stated in 2.7.2. Curve was drawn from zero-subtracted readings using linear regression analysis. Each point represents mean±SEM, n=3.

2.7.3 Von Kossa stain

This stain has historically been used in conjunction with alizarin red s for mineralized tissue as it is specific for phosphate or carbonate anions (Puchtler et al., 1969). It is a photochemical reaction in which silver ions initially replace calcium in its salts by binding phosphate, and this complex is later photochemically degraded with ultra violet radiation to release the silver (University of Utah, 2011). The process was initiated by washing monolayers twice with divalent-ion free PBS, and fixed in 5 % glutaryldehyde (Sigma) foe 30 min. Washed samples were flooded with 5 % (w / v) silver nitrate in

water for 20 min under a 60 watt bright lamp. Samples were then washed x3 with water, and un-reacted silver removed with 5 % sodium thiosulphate for 5 min. Samples were counterstained with 0.1 % nuclear fast red in water for 5 min, followed by rinsing in water and finally an air dry.

2.7.4 Alkaline phosphatase stain

This stain was conducted as described in (Nakamura et al., 2009). Monolayers were washed with divalent-ions and fixed in 4 % glutaryldehyde in a way similar to the alizarin red s and von kossa stain. Samples were then incubated with dye, made up by combining 5 mg Naphtol AS MX-PO_4 (Sigma), 200 µl of dimethylformamide (Sigma), 25 ml of Tris-HCl (molecular weight 157.6 g / mol; initial molarity 0.2 M, pH 8.3), 30 mg red violet LB salt (Sigma) and 25 ml distilled water. Dye was filtered with Whatman's no. 1. Samples were incubated with dye for 45 min and then washed with water x3. Samples were air-dried and imaged as described in section 2.3.3.

2.8 Extracellular matrix collagen quantification

Extracellular matrix collagen was assayed with the Sircol collagen assay kit from Biocolor according to the manufacturer's instruction. An assay was conducted by homogenising a monolayer with 400 µl cold 0.5 M acetic acid (Sigma) supplemented with 100 ug/ml porcine pepsin (Sigma-Aldrich). Homogenates from three replicate wells were pooled and concentrated overnight with 200 µl Isolation and concentration reagent at near 0^{o} C. The pooling of samples was required due to the small amounts of collagen formed by cells in individual wells. Concentrated pooled replicates of a sample were centrifuged to pellet collagen; while the albumin rich supernatant was discarded. Collagen pellets were stained with Sirius red in picric acid for 30 min and later washed in acid-salt solution to remove excess unbound dye. Bound stain was eluted with 250 µl of an alkali solution. Absorbance of 200 µl of each sample was measured at 555 nm in a clear microtitre plate. Total quantities were determined by interpolating absorbance values from a 6 point standard curve (figure 2-11).

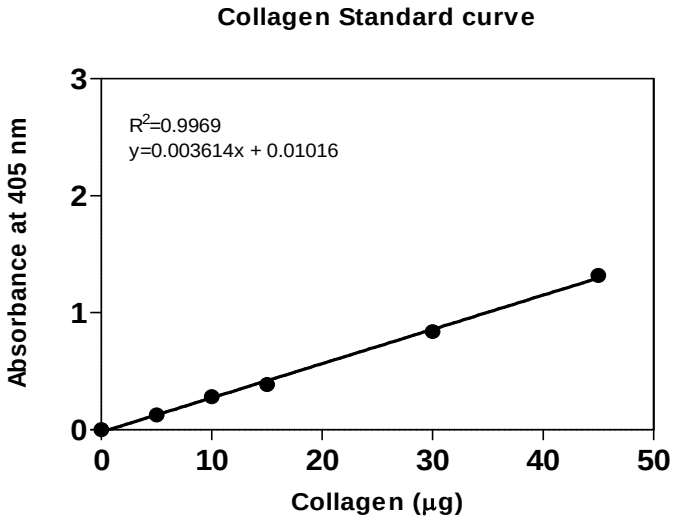

Figure 2-11 Sircol collagen assay standard curve

Figure shows a six point standard curve generated from stock (1 mg.ml^{-1}) in 1.5 ml tubes, and stained as described in 2.8. Curve was drawn from zero-subtracted readings using linear regression analysis. Each point represents mean of three replicates. Each point represents mean±SEM, n=3.

2.9 Alkaline phosphatase specific activity assay

Alkaline Phosphatase (ALP) is an enzyme that catalyzes the hydrolysis of phosphate esters (dephosphorylation) from an array of molecules to produce an organic radical and an inorganic phosphate (PO_4^{-3}). It is mainly expressed in liver and bone cells; in the latter tissue, ALP enacts to provide inorganic phosphate to a calcifying nucleation site. In this study, cellular ALP quantities were evaluated with an ALP Specific Activity assay kit (K412; Biovision) that was based on the Bassey et al method (Bassey et al., 1946). This kit provides a quantitative estimate of cellular ALP by measuring the molar rate of dephosphorylation of a colorless substrate p-nitrophenyl phosphate (pNPP) to a yellow colored product nitrophenyl phosphate (NPP) in an alkaline buffer at 37^{o}C. A typical assay would be initiated by washing a monolayer three times with dication-free PBS and then homogenising it with 200 µl of alkaline assay buffer (0.3 M 2-amino -2 methylpropane -1,3 Diol/0.002 M $MgCl_2$ in water; pH=10.25); and centrifuging homogenate at 13,000 x g for 3 min to pellet insoluble material. A 40 µl aliquot of clear lysate of a sample would be diluted 1:2 with assay buffer and incubated with 50 µl of 5mM of pNPP-substrate for 60 min at room temperature.

Reactions were stopped with a solution of 0.9 M NaOH. Absorbance of sample wells was measured at 405 nm. Absorbance units were interpolated from a 6-point standard curve of NPP to determine the quantity (umol) of product generated per sample (figure 2-12). This was used to calculate ALP specific activity by dividing the estimated quantity of NPP generated (umol) by volume of sample (ml) and then by time of reaction (min). The mean ALP specific activity per sample was normalized to mean number of cells; determined by the AlamarBlue method that is described in section 2.5.3.

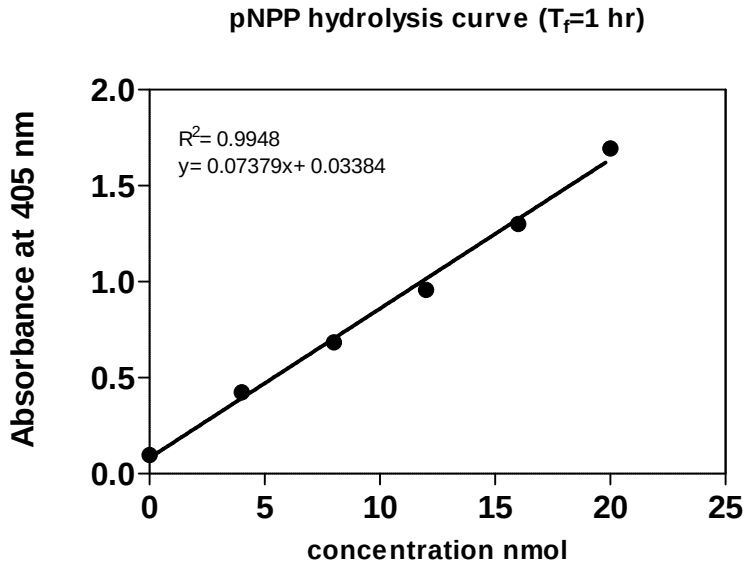

Figure 2-12 Standard curve of pNPP hydrolysis

Figure shows a six point standard curve of alkaline phosphatase substrate pNPP formed in 96-well plates by incubating with a constant amount of enzyme in alkaline buffer. Reactions were stopped after 20 min. Curve was drawn from zero-subtracted readings using linear regression analysis. Each point represents mean±SEM, n=3.

2.10 ELISA

Sandwich enzyme linked immunosorbant assay (ELISA) was used to quantify a select set of protein molecules. These colorimetric assays were procured as complete kits that could detect target proteins within a fixed linear range when used according to the manufacturer's instructions. The details of the kits used are in table 2-2.

Table 2-2 Details of ELISA kits

Protein	Type	Kit
Osteocalcin (OC)	Secreted protein	Invitrogen; KAQ1381
Osteoprotegrin (OPG)	Secreted protein	R&D; DY805
Growth differentiation factor 15 (GDF-15)	Secreted protein	R&D; DY957
Transforming growth factor β 1 (TGFβ1)	Secreted protein	R&D; DY240
Growth Arrest Specific type 6 (Gas6)	Secreted protein	R&D; Dy88g
Total extracellular Axl	Cell surface	R&D; DYC1643-2
Phosphotyrosinated extracellular Axl	Cell surface	R&D; DYC2228-2

2.10.1 General protocol

The ELISA kits from R&D Systems were based on a similar sandwich design; in which, a capture antibody would be initially adsorbed on to the base of a well of a 96-well plate (clear, tissue culture treated). A sample would be added to the capture antibody, and allowed to bind. A detection antibody conjugated with an enzyme would then bind the capture antibody bound antigen. The bound enzyme would reduce the then added substrate at a rate proportional to the quantity of adsorbed detection antibodies. The quantity of protein would be estimated by interpolating from a standard curve. All ELISA kits used in this study were provided with lyophilised antibodies and standards; apart from the osteocalcin kit, which contained pre-coated wells. The protocol applied to accomplish an ELISA is presented in table 2-3.

Table 2-3 General protocol for ELISA

Steps are intermediated by washes, which were performed by adding and removing 400 µl of 0.05 % Tween20 in PBS.

Step	Objective	Duration	Protocol
0	Preparation	~	Prepare reagents: PBS; BSA in PBS (1%); Washing buffer 0.05% Tween in PBS.
1	Capture antibody	overnight	Incubating 4 µg / ml in PBS; 100 µl to each well of a 96-well plate at room temp.
2	Blocking	< 1 hr	Incubate plate with 1% BSA in PBS.
3	Standards and sample	≤ 2 hr	Incubate samples in pre-labelled wells. Fresh prepared standards in duplicate.
4	Detection antibody	≤ 2 hr	Incubate 100 ng/ml in PBS per well.
5	Streptavidin HRP	20 min	100 µl per well.
6	Substrate	20 min	100 µl per well of 1:1 v/v hydrogen peroxide and Tetramethylbenzidine
7	Stop	~	50 µl of 2 N H_2SO_4 per well.
8	Readings	~	Absorbance measurement at 450 nm wavelength.
9	Calculations	~	Calculate standard curve with linear regression Subtract background readings from samples; and interpolate from curve. Normalise readings to cell numbers (determined with AlamarBlue).

2.10.2 Sample handling

Two different types of proteins were studied; secreted and cell surface bound. The secreted proteins included growth arrest specific 6 (Gas6), osteoprotegrin (OPG), growth differentiation factor 15 (GDF-15), transforming growth factor beta 1 (TGF-β1) and osteocalcin (OC). These were quantified in cell culture supernatant that had been conditioned by cells. The cell surface protein quantified was Axl; in monolayer homogenates of samples. All samples were collected and stored at -80^{o} C till the point of analysis. Osteocalcin, Osteoprotegrin, GDF-15 and TGF-b1 were diluted 1:10 in deionised water prior to incubating with capture antibodies in step 3 of the assay protocol. The Gas6 secreted protein was found to be expressed at minute quantities and required concentration. It was quantified by pooling supernatants from x6 replicate wells of a sample;

lyophilizing at – 80 ^{0} C in a freeze dryer; and then reconstituting the pellet with 0.5 ml distilled water, hence concentrating the samples x12 of the initial. The Axl cell surface molecules were quantified in monolayer homogenates in a pool of x6 replicate wells of a 24-well plate, homogenized in 600 µl of lysis buffer (at 100 µl homogenate per well)..

2.11 Recombinant protein techniques

The method deemed optimum to query the effects of Axl receptor deregulation was that of supplementing medium with either an Axl receptor agonist or antagonist. These had been previously applied in the initial studies linking Axl signaling with cellular mineralisation in uncommitted bovine pericytes; and were shown to be highly effective in generating a contrast response from cells (Collet et al., 2003; Collet et al., 2006). The description of the recombinant proteins and the evaluation of their dose dependent effects relevant to the study are presented in the following subsections.

2.11.1 Recombinant proteins

The human Axl/Gas6 signaling pathway was agonized or antagonized with recombinant proteins. The receptor agonist used in this study was recombinant human Gas6 (rhGas6) (885-GS; R&D Systems). This molecule was heterologously expressed as a 70.5 kDa protein in a murine myeloma cell line, NS0. The rhGas6 molecule was previously used by (Canfield et al 2003) as an agonist for Axl signaling. The protein used in this study was procured in a lyophilized form, which was re-constituted with di-cation-free PBS supplemented with 1 % (v / v) BSA (R&D Systems) to a final concentration of 100 µg / ml.

Three Axl receptor antagonists were used in conjunction to knockdown receptor signaling as much as possible. This mixture (referred in later text as MAb) included recombinant human Axl extracellular domain (Axl-ECD) (154-AL-x; R&D Systems), and blockade monoclonal antibodies against the receptor (AF154; R&D Systems) and the ligand (AB885; R&D Systems). The Axl-ECD has been used previously to knockdown receptor signaling by binding soluble ligand (Collet et al., 2003) and preventing it from inducing receptor dimerisation. It is a 71.7 kDa protein expressed in

the NS0 cell line. The Axl-ECD was supplied in PBS and was supplemented with BSA. The blockade monoclonal antibodies were raised in goats immunized with NS0 derived recombinant proteins and purified with affinity chromatography. The antibodies were supplied lyophilized and were re-constituted with divalent cation free PBS to a final concentration of 1 µg / µl. All proteins were aliquots in sterile 0.5 ml tubes and stored at – 80^0C. Aliquots were used as required. The concentration of rhGas6 used in experiments was 1 $\mu g.ml^{-1}$. The concentration of each of the three components of the receptor antagonist (MAb) was as follows; Axl-ECD, Cf = 4 $\mu g.ml^{-1}$; anti-Axl blockade monoclonal antibodies, Cf = 2.5 $\mu g.ml^{-1}$; and anti-Gas6 monoclonal antibodies, Cf = 10 $\mu g.ml^{-1}$. The concentrations of Axl-ECD and rhGas6 were experimentally determined in a dose curve described below.

2.11.2 Dose effects of recombinant proteins of cellular responses

The optimum measure of forming a scatchard plot to evaluate the dynamics of bindings of receptor ligand binding, and hence control experimental deregulation of the pathway could not be undertaken. The effects were instead evaluated as described previously (Collet et al., 2003). The dose-dependent effects of Axl-ECD and rhGas6 on mineralisation of hMSCs were assessed with a12 d osteogenic mineralisation experiment; quantifying deposited calcium, according to methods described in 2.7.2. For this experiment, hMSCs were seeded on TCP in 24 well plates at a density of ~2.5 x 10^4 cells per well in OM. The range of concentrations analysed were arbitrarily set above and below the values reported previously; Axl-ECD 4 µg/ml and rhGas6 0.25 µg/ml sufficiently affects bovine vascular pericytes. The concentration range chosen for Axl-ECD was 1, 2 and 4 $ug.ml^{-1}$; with anti-Axl blockade monoclonal antibodies, Cf = 2.5 $\mu g.ml^{-1}$; and anti-Gas6 monoclonal antibodies, Cf = 10 $\mu g.ml^{-1}$. The concentrations chosen for Gas6 were 0.125, 0.25, 0.5 and 1 µg/ml. The results are presented in figure 2-13. The low doses of Axl-MAb seemed to cause a decrease in calcium mineralisation; this effect was negated at 4 and 8, which mineralized to a similar extent. The rhGas6 affected mineralisation by causing a dose dependent decrease in mineralisation, but the concentration evaluated did not yield complete inhibition.

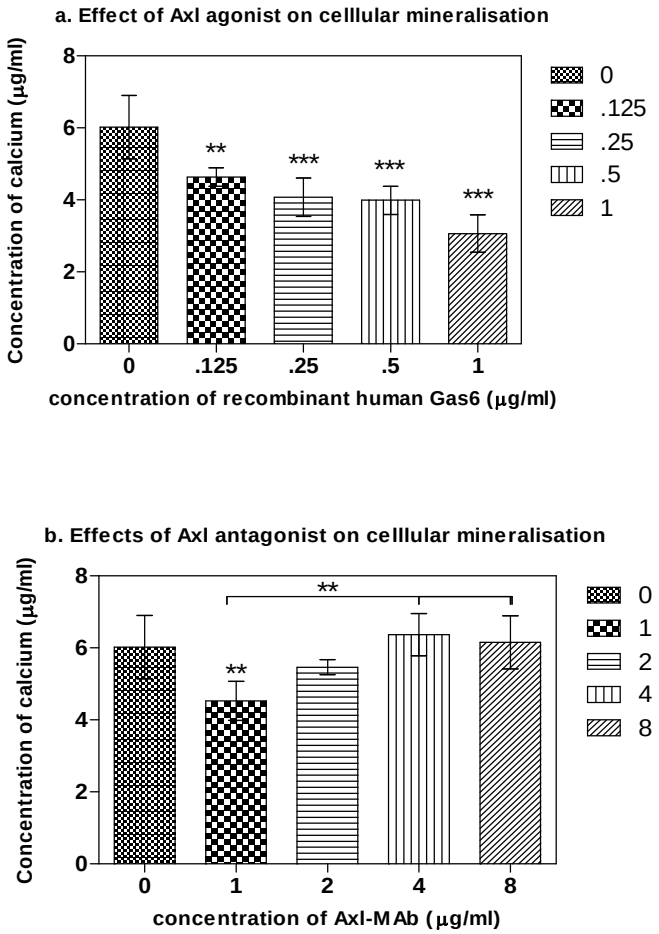

Figure 2-13 Effects of Axl receptor-signaling deregulation on hMSC mineralisation

Figure shows bar charts with mean ± 1SD N = 1, n = 3 calcium concentration readings plotted against the concentrations of Axl (a) agonist and (b) antagonist. Human MSCs were seeded at 25,000 cells per well in 24-well plates. Growth medium was replaced with osteogenic medium supplemented with recombinant proteins at 1 d post seeding, and cultures maintained till 12 d. Samples were processes as described in section 2.7.2. (a) Receptor agonist induced a significant decrease in calcium concentrations. (b) The MAb had no opposite effect on cells, which mineralised similar to the control at high doses. The experiment verified (Collet et al. 2003)'s findings that Axl signalling negatively regulates osteogenic cellular calcium mineral deposition and provided a strong reference for required receptor agonist concentrations. The lack of effect of the antagonist was considered to be due to the late time point of 12 d. *, **, *** = p < 0.05, 0.01, 0.001, respectively.

2.12 Data collection and statistics

2.12.1 Raw data analysis

Raw analytical output from quantitative assays was retrieved with Microsoft Excel. This software was used to organize data as input for statistical analyses with GraphPad Prism v5.

2.12.2 Statistical analyses

The Graphpad Prism version 5.02 statistical package was used for mathematical calculation and statistical analyses of raw data. The calculations included (i) basic statistics (mean, median, standard deviation, and frequency distribution); (ii) linear regression analysis for standard curves of quantitative colorimetric assays; (iii) a 4 parameter logistic non-linear regression for standard curves of ELISAs; (iv) interpolation of data sets from standard curves; (v) statistics for the determination of normality between data sets and (vi) evaluation of significance of the differences of means.

Statistical analyses were conducted after generating a data matrix consisting of readings from three donors with three replicates per donor (N = 3; n = 3). Data was first tested for normality with D'Agostino-Pearson normality test. This was followed by repeated measures ANOVA (analysis of variance) with a 2-way repeated measures test utilizing the Bonferonni post test comparing all variables. For samples with lesser replicate numbers or less time points, a 1 way ANOVA was used.

3 Phenotypic responses of hMSCs to modified titanium substrates

3.1 Introduction

A human marrow stromal cell (hMSC) is a strongly adherent cell that is phenotypically proliferative at the single cell level *in vitro*, seemingly under a biological pressure to attach and adapt to a substrate to initiate replication (Benayahu et al., 2007). Examinations of the phenotypic differences of committed osteoblastic cell lines to the topographically variable Ti substrates have shown that these differentiated cells adhere at relatively higher numbers to the rough surfaces than smooth, all the while adapting a relatively stretched morphology, with cytoplasmic processes emanating within the topographical spaces on the rough compared to a more spread appearance on the smooth surfaces (Wall et al., 2009; Miron et al., 2010). These cells also display altered proliferative responses, being highly restricted on the rough compared to the smooth, and thus yielding a comparatively lower number of progeny on the former over the course of time in culture (Wall et al., 2009; Schwartz et al., 2009a; Zhao et al., 2007).

The phenotypic responses of uncommitted hMSCs to modified Ti surfaces have been studied to a relatively lesser extent, but are suggested to differ from those of committed osteoblasts, based on their phylogenetic difference. The evidence at hand (Wall et al., 2009), measuring attachment at 3 to 24 h post contact has indicated no significant differences in the number of these cells to attach to the polished, SLA or modSLA surfaces. Though the study did not examine the dynamics of cellular attachment and morphology at earlier time points, when differences in these are expected to be highest, it did, however, demonstrate a stark comparison between the morphology of hMSCs on the different substrates. Cells on the modified surfaces adapt a stellate or stretched form on the rough compared to a ‘fried egg’ analogous shape of cells on the smooth. Furthermore, rough surfaces cause a significant lag in proliferation resulting in a lesser number of cells on the rough than smooth by 7 d (Olivares-Navarrete et al., 2011; Olivares-Navarrete et al., 2010a). Moreover, the rough-hydrophobic substrate modSLA also seems to challenge hMSCs with pro-apoptotic stimuli, reported in (Wall et al., 2009) to cause a concomitant increase in the number of Stro-1 positive cells.

The present, initial section of this thesis hypothesised that human MSCs exhibit different phenotypic response to the different modified Ti surfaces. It aimed to evaluate hMSC attachment, morphological and viability on all substrates at different times following initial cell contact. The specific objectives were to (i) compare cellular attachment at early time points; (ii) contrast differences in cellular morphology; (iii) compare cellular proliferative responses over the course of culture; and, (iv) examine the transcriptional activity of viability related genes, in hMSCs seeded on tissue culture plastic, polished, SLA and modSLA titanium surfaces.

3.2 Experimental protocols

In these experiments, the Ti discs were prepared as described in section 2.1.2. The cellular specimens were cultured according to the methods described in 2.2.3.

3.2.1 Cellular attachment

Cellular attachment was initially assessed at 1, 3 and 24 h post seeding; and later at various intervals within a 1 h time frame. The initial analysis was conducted to delineate the point of maximal cellular attachment while the latter as conducted to identify differences within this time frame of initial cell attachment.

3.2.1.1 Assessment of cellular attachment at 1, 3 and 24 h

The hMSCs (N = 2; n = 3) were plated on TCP, P, SLA and modSLA at a density of 1 x 10^4 cells per disc in serum free-basal αMEM. At 1, 3 and 24 h, cultures were washed twice with divalent cation-free PBS, and processed with the CyQuant nucleic acid fluorescent dye assay as described in 2.5.1.

3.2.1.2 Assessment of cellular attachment at very early times

Calcein-AM labeled hMSCs (N = 3; n = 3) were prepared as described in 2.5.2. Labeled cells were seeded on TCP, P, SLA and modSLA at a density of 1.5 x 10^4 cells.cm^{-2} in serum-free basal GM. Cell numbers were enumerated at 5, 15, 30, 60 and 180 min post seeding by washing twice with

dication-free PBS and measuring fluorescence emissions as described in 2.5.2. Un-seeded surfaces of each type immersed in 0.5 ml dication-free PBS were used for background control.

3.2.1.3 Image analysis of early cellular attachment

The calcein-AM dye assay derived samples from 3.2.1.2 were further analysed by back-scattered scanning electron microscopy (BS-SEM) to evaluate relative numbers of attached cells. For this purpose, samples were fixed in 4 % glutaryldehyde (Sigma-Aldirch) and analysed as described in 2.3.2. Furthermore, morphological differences between cells seeded on the different Ti discs were examined by sputter coating samples and examining at high resolutions with SEM, according to the methods described in section 2.3.2.

3.2.2 Cellular viability

Cellular viability of hMSCs on different surfaces was assessed by serially examining cell number changes and the expression of viability related markers over the course of culture in GM and OM. The different media were tested due to their differential phenotypic effects on uncommitted cells. The experiments conducted are detailed below.

3.2.2.1 Cellular proliferation

The effects of different surfaces on hMSC proliferation were assessed by seeding 2000 cells per 15 mm disc and serially assessing cell number changes till confluence with the AlamarBlue assay (N = 3; n = 3). This method is detailed in section 2.5.3. The initial seeding density was chosen due to the cellular specimen's phenotype: it is a highly replicative cell that forms colonies, which a high initial seeding density may inadverterntly affect due to contact inhibition of proliferation.

3.2.2.2 Gene expression analysis of viability related genes

RT-PCR was used to evaluate the expression of pro-apoptotic Caspase 3, viability/anti-apoptotic BCL-XL and proliferation related Ki-67 antigen in hMSCs. The analysis was conducted in GM and OM (N = 3; n = 3) at 1, 3, 5, 7 and 10 d post seeding. The methods applied for this analysis are detailed in section 2.6. A higher cell density was used compared to the proliferation assay as the RT-PCR analysis would have required a higher intial quantity of total RNA.

3.3 Results

3.3.1 Cellular attachment

3.3.1.1 Assessment of cellular attachment at 1, 3 and 24 h

The results of this analysis are presented in figure 3-1. It indicates the hMSCs to have attached at near-maximal numbers to all surfaces by 1 h; without undergoing any significant further increase by 24 h. The trend shows a higher number of attached hMSCs on the smooth surfaces compared to rough at all time points. The P surface displayed a significantly higher number of cells at 1 h compared to TCP; but this difference was removed by the 3 and 24 h time points. The rough SLA had a significantly higher number of cells attached compared to modSLA at 3 and 24 h.

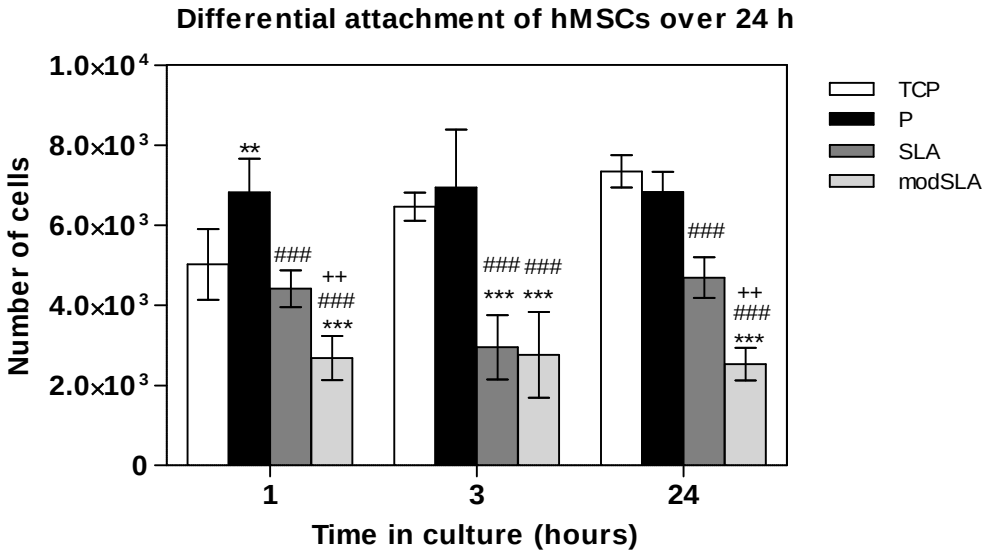

Figure 3-1 Assessment of cellular attachment at 1, 3 and 24 h

Figure shows mean ± 1SD (N = 2, n = 3) number of cells plotted against time on the x-axis. The hMSCs were plated at 10,000 cells per disc and number of attached cells evaluated with CyQuant as described in 2.5.1. Figure shows near-maximal attachment of cells at 1 h post seeding on all respective surface types. Cell numbers increased slightly on plastic but seemed to remain stagnant on other surfaces. There were significantly lower cell numbers of the rough compared to smooth surfaces. *, **, * = *p* < 0.05, 0.01, 0.001 TCP vs. Ti. #, ##, ### = *p* < 0.05, 0.01, 0.001 polished vs. SLA/modSLA. +, ++, +++ = *p* < 0.05, 0.01, 0.001 SLA vs. modSLA.**

3.3.1.2 Assessment of cellular attachment at very early times

The results of this experiment are presented in figure 3-2, It shows that the P surface had a significantly higher number of attached cells compared to TCP and rough at all time points examined in the 1 h timeframe ($p < 0.01$). There were no differences between TCP and rough surfaces in the mean number of attached cells.

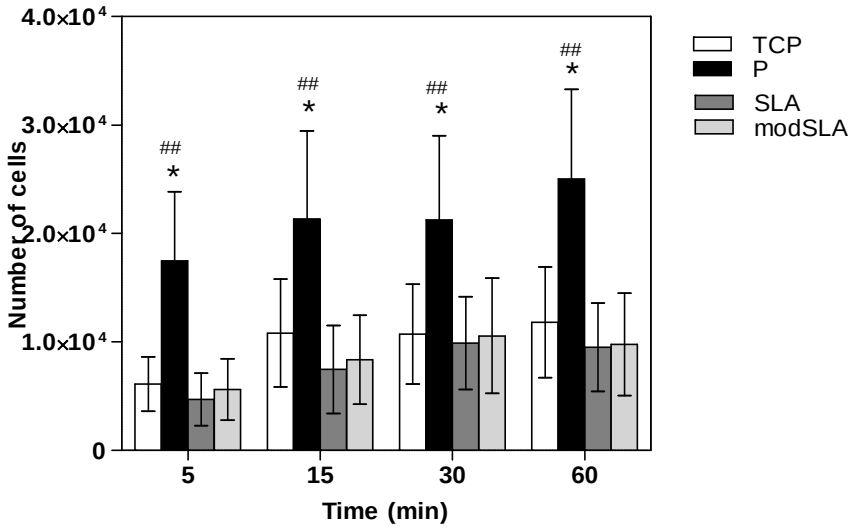

Figure 3-2 Assessment of cellular attachment at very early times

Figure shows mean ± 1SD (N = 3, n = 3) number of cells plotted against time in culture. Calcein labelled hMSCs were plated at 1.5 x 10^4 cells.cm^{-2} on tissue culture plastic, polished, SLA and modSLA Ti surfaces. Number of attached cells were determined at 5, 15, 30 and 60 min by discarding non-adherent cells and measuring fluorescence intensity as described in section 2.5.2. The number of cells attached to polished Ti was significantly higher than all other samples. There were no major differences between tissue culture plastic and the rough surfaces in this time interval. * = $p < 0.05$, TCP vs. Ti. ## = $p < 0.01$, polished vs. SLA/modSLA.

3.3.1.3 Image analysis of early cellular attachment

The Ti discs with adherent cells from 3.3.1.2 were examined with back scattered SEM. An objective software based analysis of the images could not be conducted due to the inability of the software to distinguish between the weak signals generated from certain samples, in which cells that had undergone a high degree of spreading. A set of images derived from this analysis for one donor are presented in figure 3-3. These are x100 magnification views of uncoated discs at 5, 15 and 30 min.

A subjective assessment of these images, using a manual count of dark objects, corroborated the findings presented in 3.3.1.2, which is of a higher number of cells attach to the polished surface compared to the rough at any time during the initial 30 min post seeding. This is indicated in the images in figure 3-3 as a higher number of dark objects on the P surface compared to the rough surfaces. The panel of images of adherent cells at 60 min could not be provided due to cellular spreading causing faintness in signal intensity in samples of the polished surfaces.

Morphological differences were assessed by sputter coating samples and imaging under high resolution. The images obtained are presented in figures 3-4, 3-5 and 3-6 for polished, hydrophobic SLA and hydrophilic modSLA. These indicate the human MSCs attach and spread comparatively faster and in symmetric fashion to the polished Ti substrate (figure 3-4). Cells initially have a spherical appearance at 5 min with the cytosol forming an even base under a large nucleus. These cells proceed to evenly spread their membranes and cytoplasm, and eventually acquire a flattened form, characteristic of an hMSCs in tissue culture plastic. On the rough surfaces, cells seem to initially take a rather constricted morphology, being mostly round with very few extensions trying to ‘peg’ the cell into the rough topography. These cells do not appear to alter much in form over the course of 60 min. At 3 h, the cells appear as stretched with extensions emanating from all sides to farther spots in the near vicinity, presumably to secure cellular attachment. The cells at 3 h have a smoothened upper or dorsal side. Though an analysis to view the under or ventral side could not be ascertained, it can be imagined that it would be highly asymmetric, un-even, with a lot of tension being exerted towards the cytoskeletal and nuclear apparatus. These cells appear stretched, as if they were tents held up by cytoplasmic extension ‘pegs’.

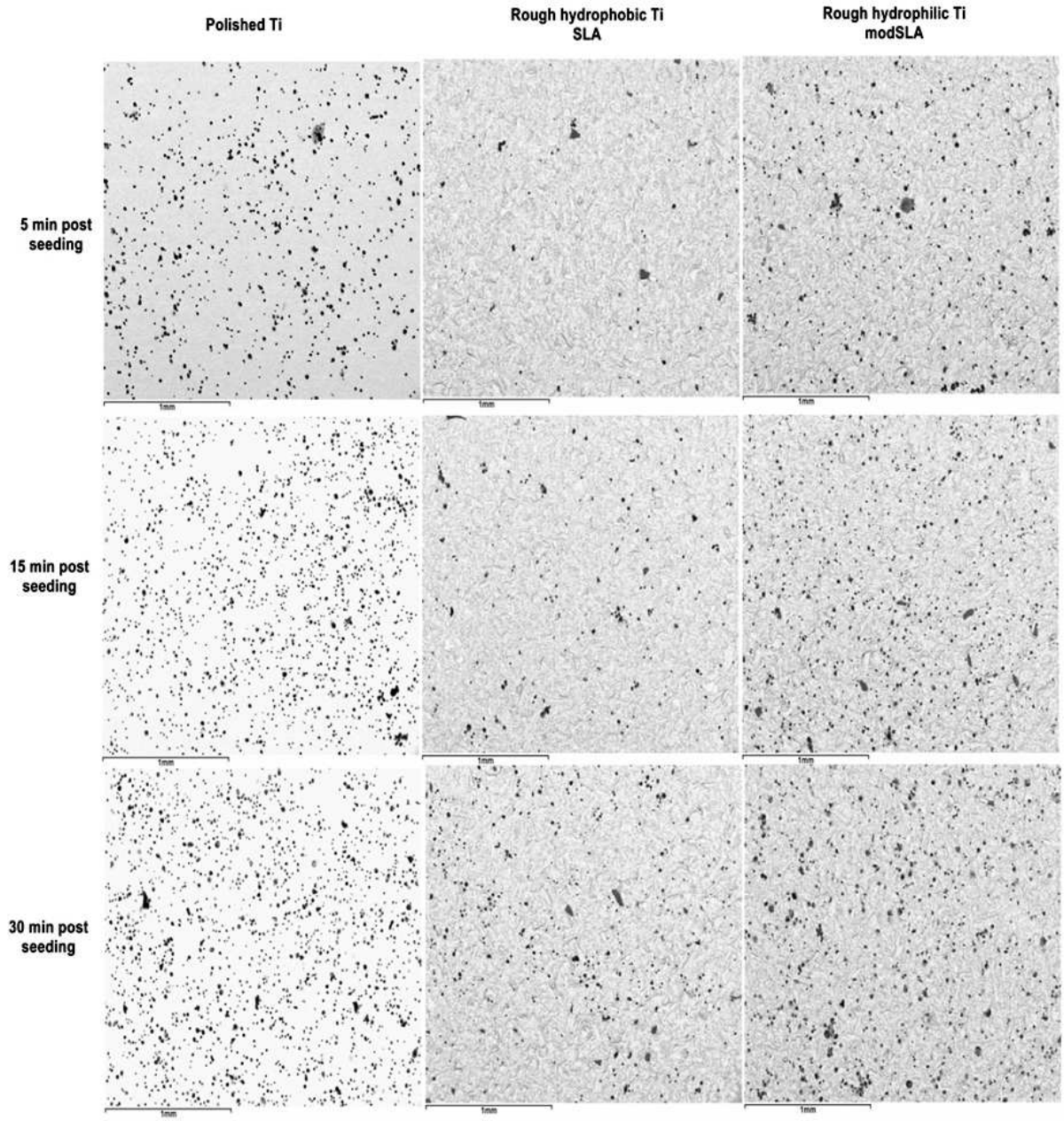

Figure 3-3 Scanning electron microscopic analysis of cellular attachment to Ti

Image is a panel of back-scattered scanning electron micrographs taken to confirm the differential attachment of human MSCs to the different surfaces. For this purpose, discs were fixed and then dehydrated. Uncoated samples were viewed at x50 magnification (bar = 1 mm). Samples at 60 min samples (not shown here) were visualised with x100 magnification due to faintness in signal resulting from cell spreading. The images confirm the previous calcein label assay that a higher number of cells attach to polished Ti than the rough SLA and modSLA surfaces in the initial instances of contact *in vitro*.

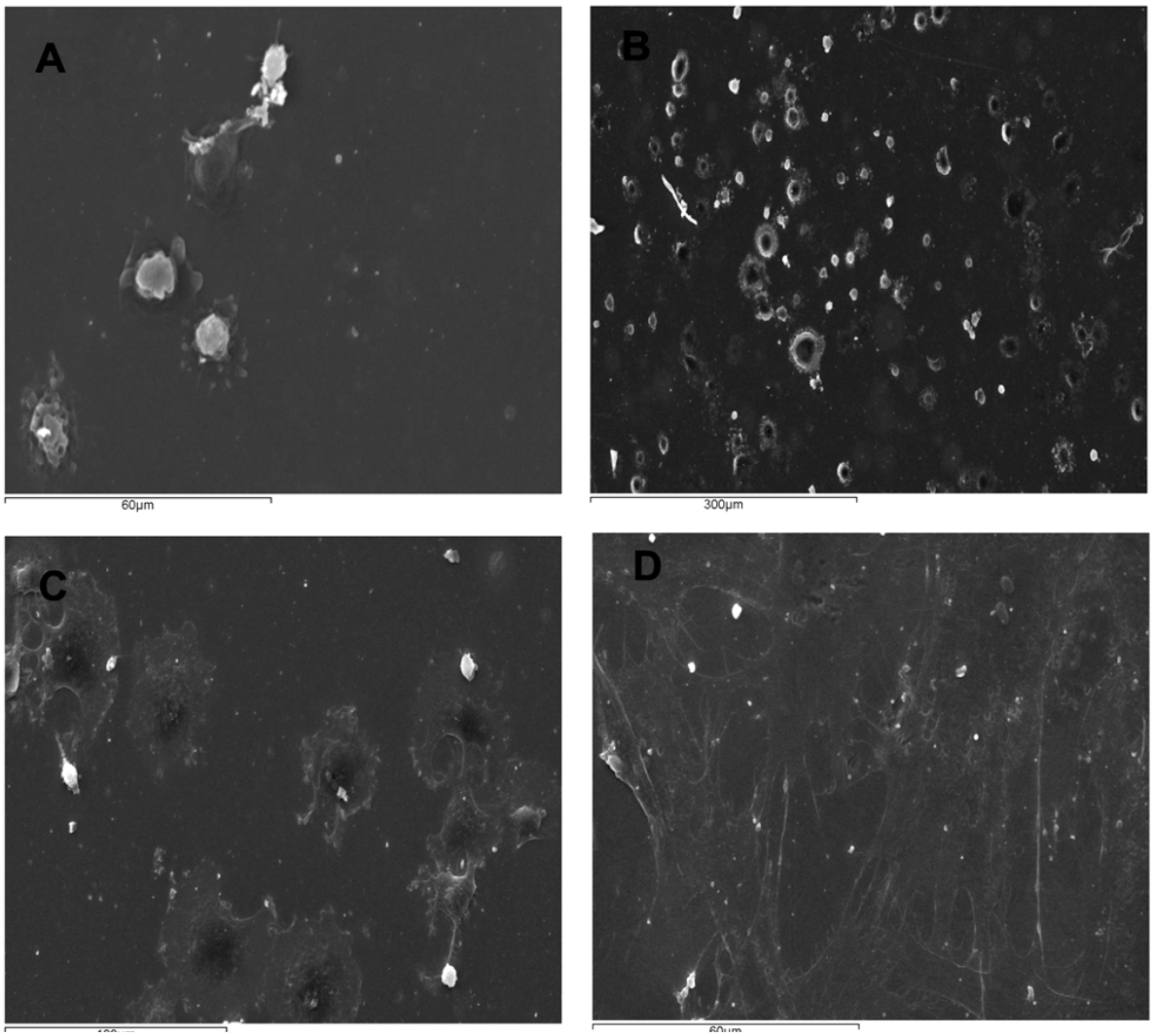

Figure 3-4 Morphology of cells on polished Ti surface

Figure is a panel of scanning electron micrographs of human MSCs that have attached to polished Ti discs. The experimental details are provided in section 3.2.1.3. (A) At 5 min after contact, cells are round with a prominent nucleus and circumferentially spread cell membranes at the base (x1500 magnification). (B) Taken at 30 min, images shows cells have spread further than at 5 min (x500 mag.). (C) Cellular spreading further increases by 60 min (x1000 mag.) leading to a confluent monolayer by 3 hours (x1500 mag.). These micrographs indicate that along with a high level of attachment, hMSCs tend to spread very early on the polished Ti surface, morphologically adapting to the surface seemingly at ease.

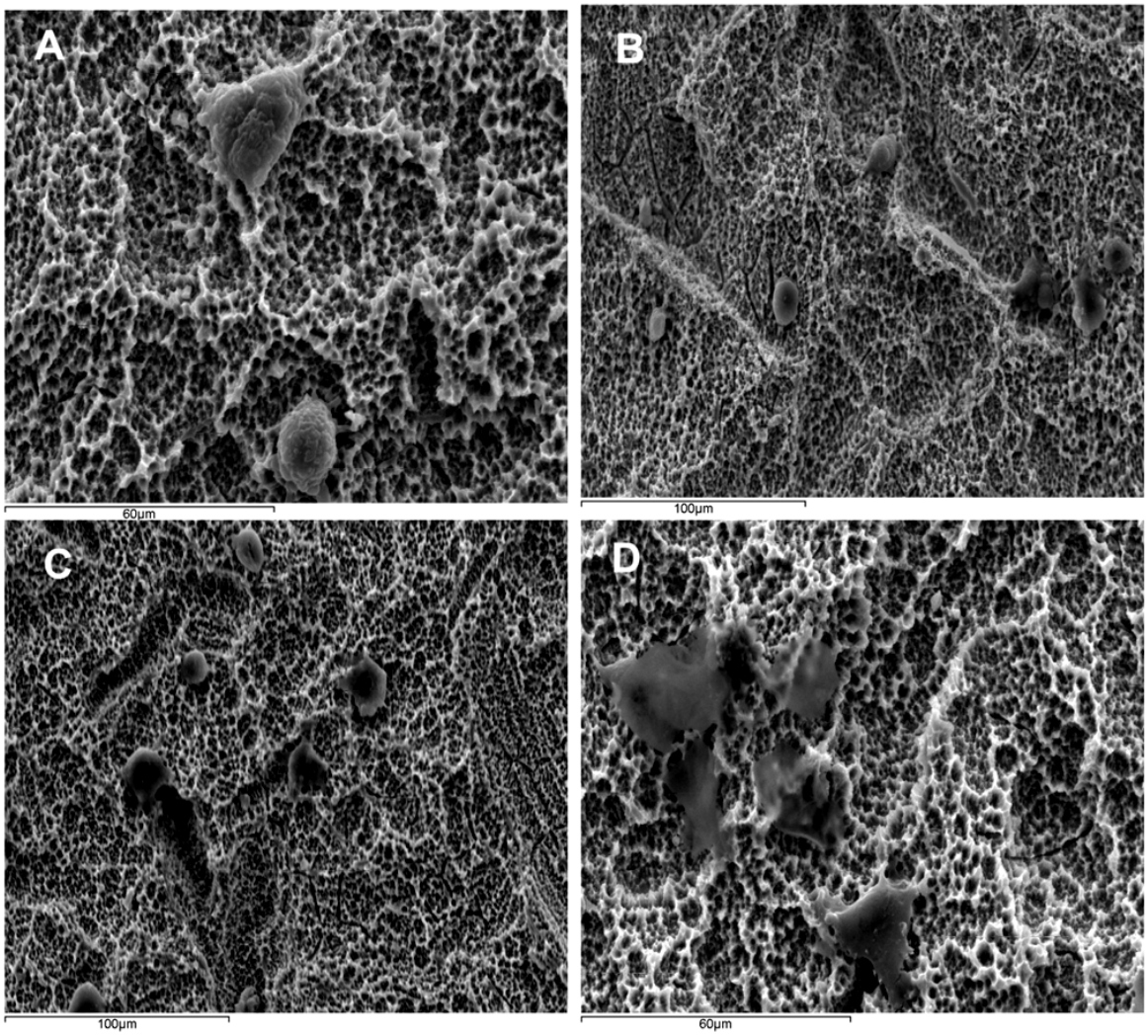

Figure 3-5 Morphology of cells on rough-hydrophobic SLA Ti surface

Figure is a panel of scanning electron micrographs of human MSCs that have attached to SLA Ti discs. Experimental details are provided in section 3.2.1.3. (A) At 5 min after contact, cells are still rounded with processes being extended towards the rough topogrphy (x1500 magnification). (B) Cells at 30 min are somewhat rounded and seem to be in the process of attachment (x500 mag.). (C) Cellular spreading does not seem to significantly increase by 60 min (x1000 mag.). (D) At 3 hours, cells have adapted to the rough topography by taking a stretched asymmetric form compared to the more spherical form on the polished in figure 3-4 (x1500 mag.). These micrographs indicate that hMSCs take longer to adapt to the rough topography of the SLA compared to polished Ti surfaces. The eventual form that the cells take is also non-symmetric, with a flattened/smoothened 'ventral' surface but an undeniably asymmetric 'dorsal' side. These morphological aspects can influence the architecture of the cytoplasmic cytoskeleton as well as influence the structure and hence probably also function, of the nucleus.

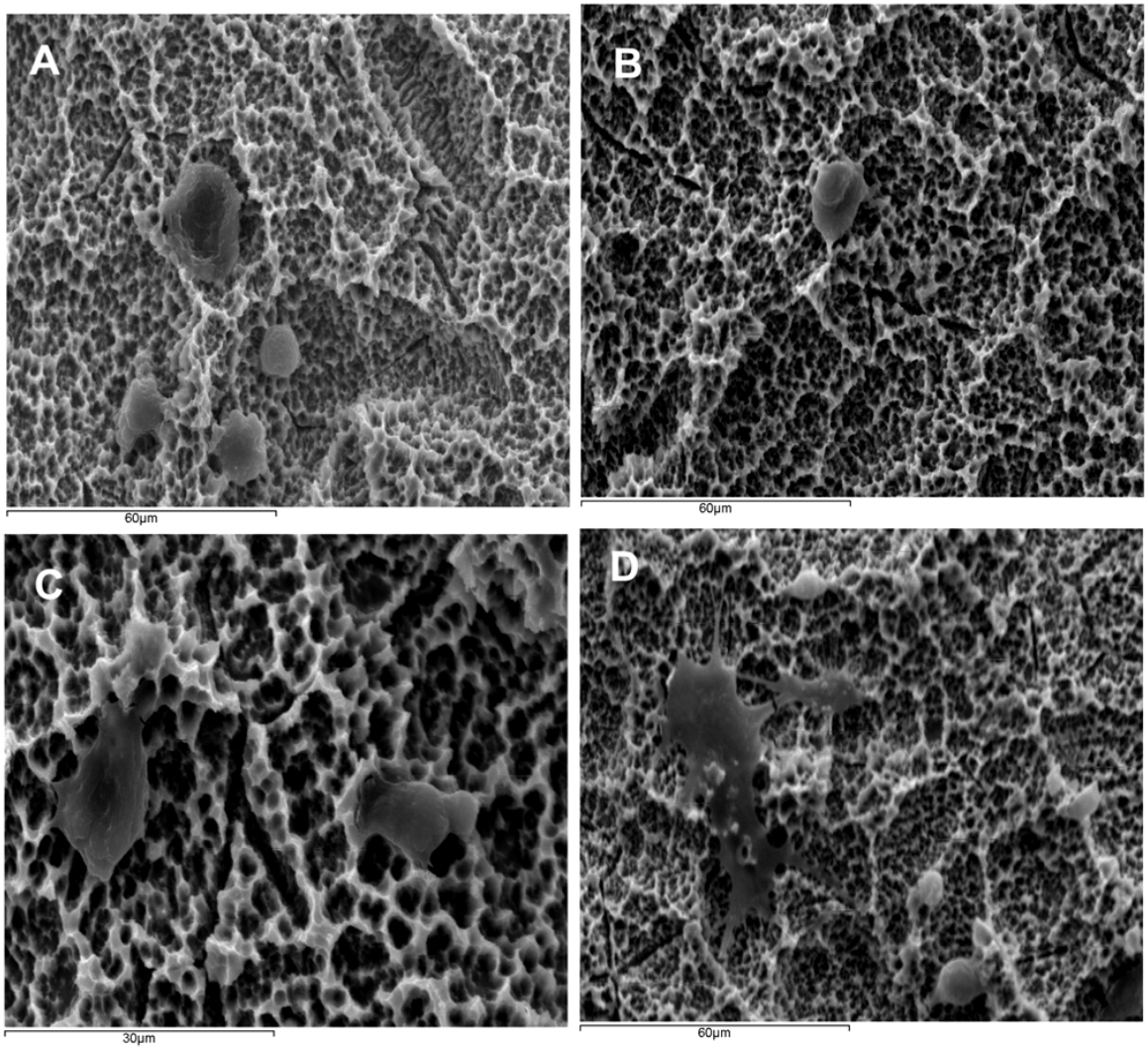

Figure 3-6 Morphology of cells on rough-hydrophilic modSLA Ti surface

Figure is a panel of scanning electron micrographs of human MSCs that have attached to modSLA Ti discs. Experimental details are provided in section 3.2.1.3. (A) The hMSCs are round at 5 min of attachment (x1500 magnification). (B) They appear to have attached with an asymmetric morphology at 30 min, but are still somewhat round (x500 mag.). (C) Cells do seem to have adapted to the rough topography by extending over the rough substrate by 60 min (x2000 mag.). (D) The cells adapt a stretched asymmetric form on the rough surfaces. Image shows two cells in the left half, which are stretched into place with extensions heading further out onto the substrate. The round objects in the right half of the image are likely dust particles (x1500 mag.). These micrographs indicate that hMSCs adapt to modSLA in a way similar to the SLA surface. Cells adhere but in an asymmetric manner, with extensions essentially hooking cells into place synonymous to the fastening of an outdoor tent. Cells seem comfortable by 3 hours and like the SLA, bear a smoothened dorsum but a surely very asymmetric/rough ventral face in direct contact with the rough topography.

3.3.2 Cellular viability

3.3.2.1 Cellular proliferation

The proliferation of 2000 cells per disc was serially examined till confluence with AlamarBlue. This analysis was conducted in GM and OM due to the differential effects of these media on cellular growth. The results of this analysis are presented in figure 3-7. The graphs indicate a similar number of cells on all surfaces at 1 d post seeding. In the later days, an increase in cell numbers takes place that is magnitudinally higher in GM than OM.

In GM (figure 3-7 A),a gradual increase in cell numbers was observed on all surfaces till 5 d. The cells cultured on TCP and P had significantly increased in numbers by several folds at 7 d in culture; and progressed at this higher rate of replication through 10 d, leading to a confluent monolayer by 14 d post seeding. The hMSCs cultured on the rough surfaces displayed a relative lag in cellular proliferation till 7 d of culture. The number of cells on the rough surfaces increased by 10 d, and cultures attained near confluent numbers by 18 d post seeding. The smooth surfaces had yielded significantly higher number of cells at all time points compared to the rough. A phenomenon of monolayer delamination was observed to occur very frequently on the TCP than Ti; particularly after the 14 d time point. This event is characterised by the detachment of the monolayer from one end and its sequestering into a stretched sheet or a compact aggregate at the opposite end.

In OM (figure 3-7 B), cellular proliferation occurred at a very slow rate on all surfaces from 1 to 7 d post seeding. Cells cultured on TCP plateaued at attaining 80 % confluence by 14 d. Cells cultured on all Ti surfaces ceased to increase in cell numbers from 7 d and displayed a similar number of cells through the remainder of culture.

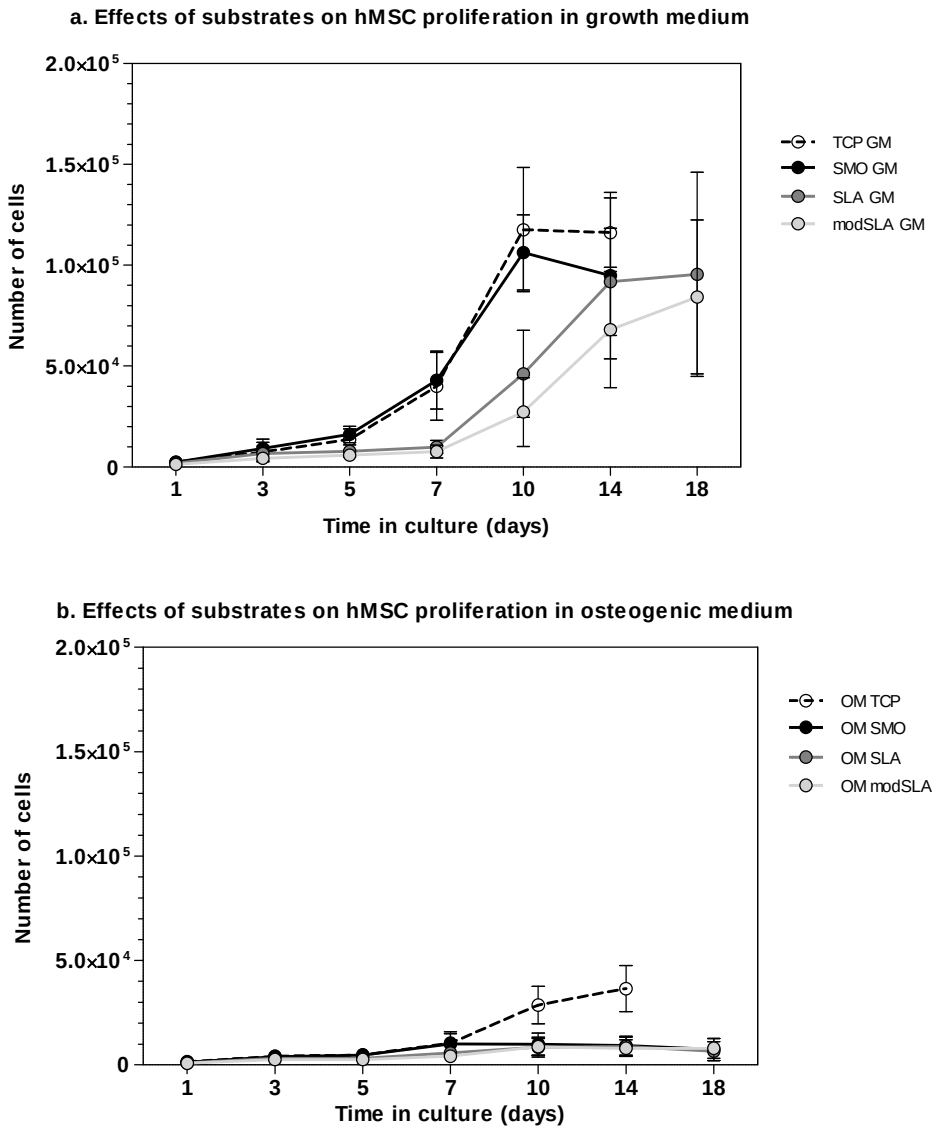

Figure 3-7 Serial analysis of cellular proliferation of hMSCs cultured on Ti surfaces

Figure shows mean ± 1SD (N = 3, n = 3) number of cells plotted against time in culture. A total of 2000 cells were seeded per disc and numbers determined till confluence. (a) In growth medium, cells proliferated at a significantly higher rate on TCP and polsihed Ti, and attained confluence by 10 days post seeding. Cells initially proliferated at similar rates on both rough surfaces but were relatively restricted on the modSLA than SLA at 10 and 14 days, attaining confluence by 18 days post seeding. (b) Osteogenic medium caused a decline in the rate of cell proliferation and changes in cell number. TCP permitted the highest cell proliferation compare to Ti from 7 to 18 days. P was similar to TCP at 5 and 7 days but plateaued with the rough Ti surfaces from 7 to 18 days. These indicate cells proliferate at higher rate on smooth surfaces and are affected by osteogenic medium supplements, which restrict proliferation at later times.

3.3.2.2 Gene expression analysis of viability related markers

The expression of viability related genes caspase 3 (pro-apoptotic), BCL-XL (anti-apoptotic) and Ki-67 antigen (proliferation association antigen) were assessed with RT-PCT through the course of the initial 10 d culture in GM and OM. The results of these analyses are presented in figures 3-8, 3-9 and 3-10, respectively. The values presented are folds relative to reference, which were cells in suspension at time zero of the experiment (reference fold value = 1).

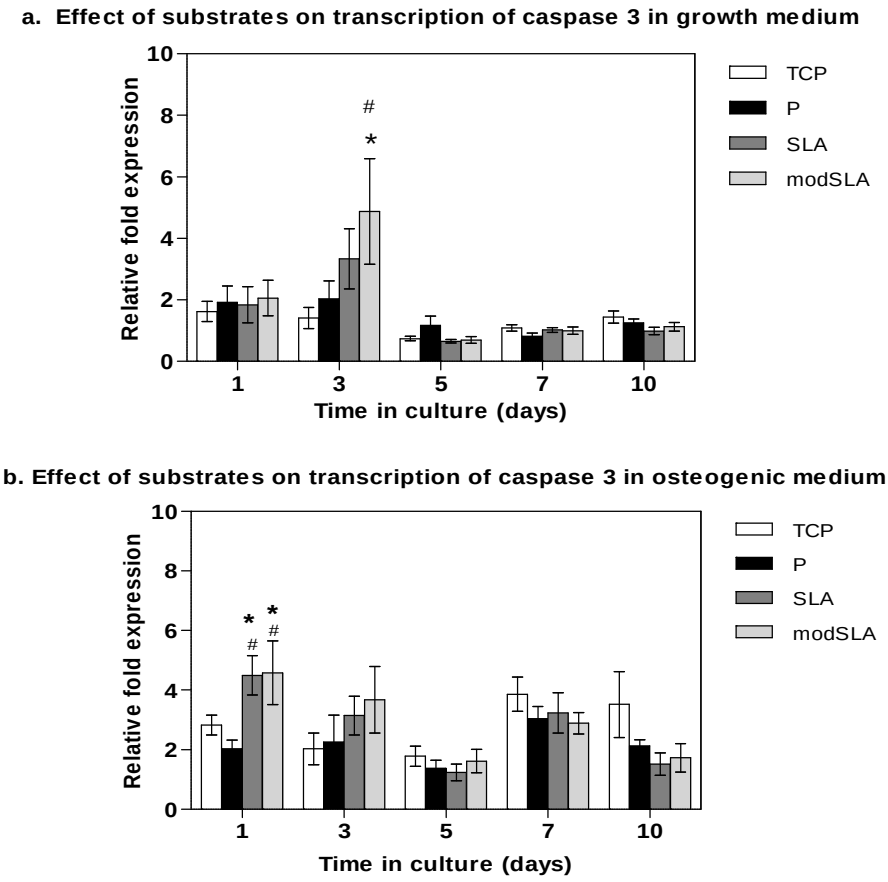

Figure 3-8 RT-PCR analysis of caspase 3 expression

Figure shows mean ± 1SD (N=3, n=3) fold expression values plotted against time in culture, evaluated in (a) growth and (b) osteogenic media. The pro-apoptotic gene was transcribed at a higher fold value by rough surfaces than smooth in the early stages of culture at 3 d in GM however, 1 d in OM. It was transcribed at a basal level in all samples through the remainder of experiment. * = $p < 0.05$, TCP vs. Ti. # = $p < 0.05$, P vs. rough.

Caspase 3 was expressed at low levels through the experiment in both media conditions (figure 3-8). In GM, caspase 3 was up-regulated by the rough substrates ($p < 0.05$, modSLA vs. TCP / polished) at 3 d post seeding. A similar significant relative up-regulation of the gene was observed in OM at 1 d post seeding on both rough surfaces. The cells displayed a similar upregulation on all surfaces at 7 d in OM. The TCP seeded cells maintained the increased expression at 10 d; while having been the Ti relatively decreased by the Ti.

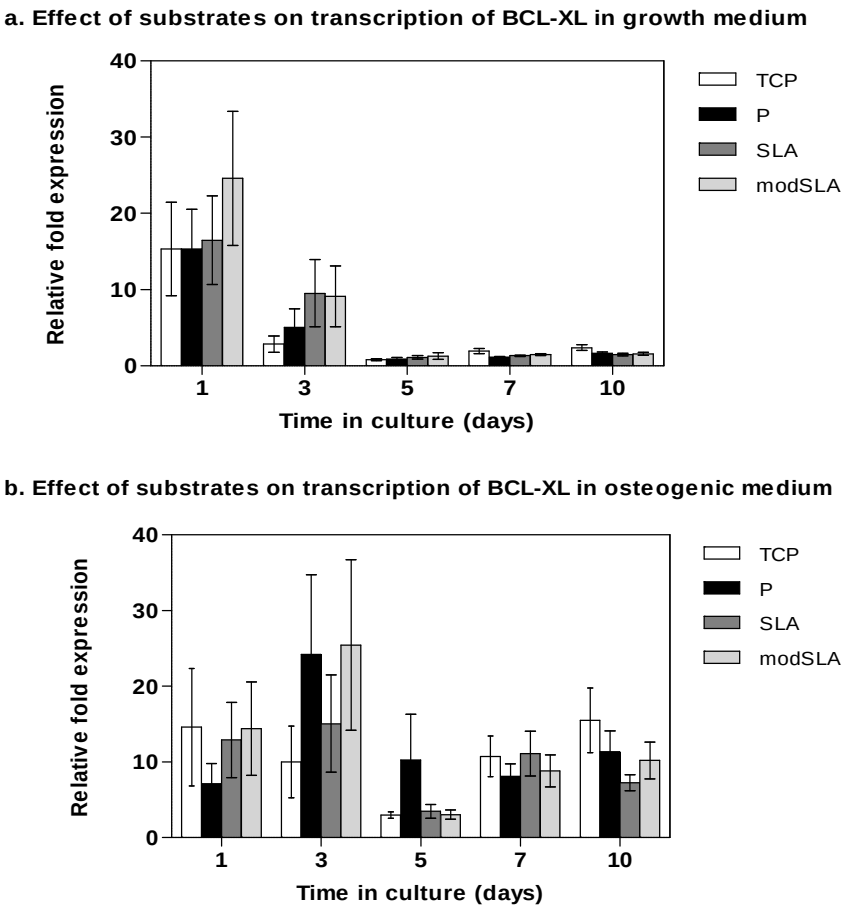

Figure 3-9 RTPCR analysis of BCL-XL expression

Figure shows mean ± 1SD (N=3, n=3) fold expression values plotted against time in culture, evaluated in (a) growth and (b) osteogenic media. The anti-apoptotic gene was transcribed in all sample at a higher fold value following early contact. Its expression in hMSCs seemed higher on the rough surfaces than smooth. It was transcribed at a basal level in all samples through the remainder of experiment, which was higher in osteogenic than growth medium.

The anti-apoptotic BCL-XL was expressed at varying levels in all samples thought the course of culture (figure 3-9). In GM, the gene was up-regulated several folds by cells on all surfaces at 1 d

post seeding, which were reduced to lower fold values from 3 to 10 d post seeding. In osteogenic medium, the gene was upregulated by all surfaces at 1 d post seeding. Its expression relatively increased on the Ti than TCP by 3 d; but was down-regulated to a similar level by 5 d. BCL-XL expression relatively increased on all surfaces to a similar level similar at 7 to 10 d post seeding in OM

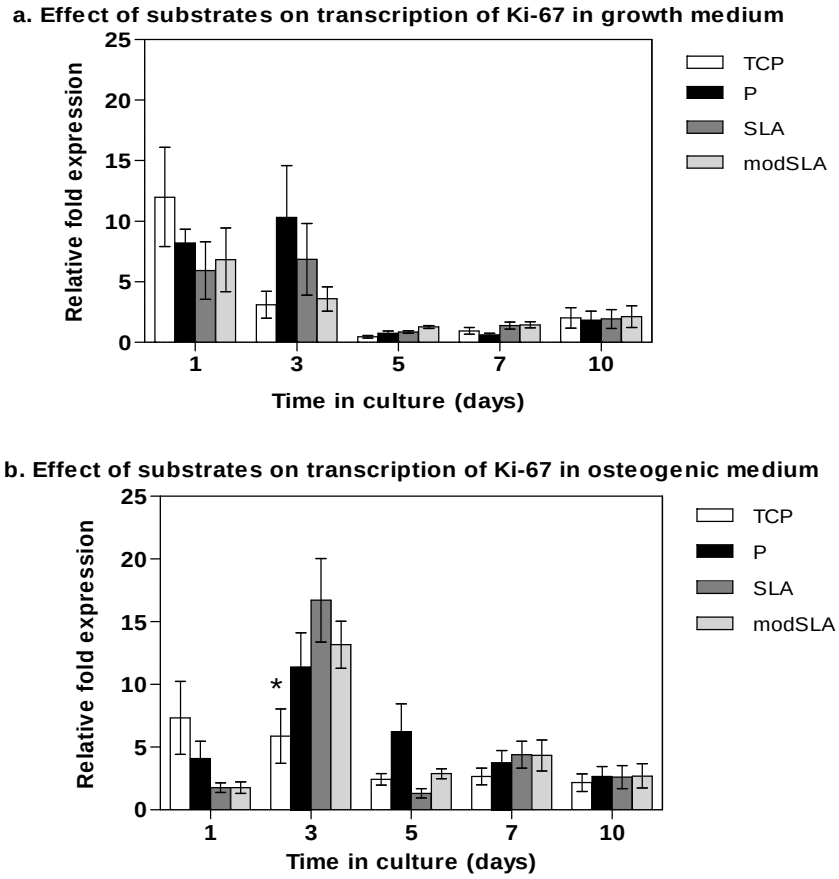

Figure 3-10 RTPCR analysis of Ki-67 expression

Figure shows mean ± 1SD (N=3, n=3) fold expression values plotted against time in culture, evaluated in (a) growth and (b) osteogenic media. (a) Ki-67 was expressed on all substrates at 1 and 3 d, but later decreased to basal levels. (b) The gene was initially transcribed higher on smooth surfaces compared to both rough surfaces. Its expression significantly increased many fold than TCP at 3 d. The expression of the gene was relatively higher in OM cultured cells than GM. * = $p < 0.05$, TCP vs. Ti surfaces.

The proliferation specific Ki-67 antigen was detected in all samples analysed (figure 3-10). In GM, it was up-regulated by cells on all surfaces at 1 d post seeding. The mean level of expression was

higher on TCP than Ti surfaces; but this difference was insignificant. The gene was expressed at relatively low levels on all surfaces through the remainder of culture. In OM, Ki-67 was upregulated by TCP compared to the Ti surfaces at 1 d post seeding. The levels of expression of the gene significantly increased on the Ti surfaces compared to TCP at 3 d; but had reduced to a relatively low level on all surfaces by 5 d. A similar upregulation was detected from 7 to 10 d.

3.4 Discussion

3.4.1 Cellular attachment

In the experimental results presented here, the hMSCs were observed to have attached at near maximal numbers by 1 h post seeding on the respective surfaces. These experiments were conducted in conditions that minimized protein interference in attachment, as is normally the case in a two dimensional *in vitro* cell culture model. In both analyses conducted, the cells displayed a higher affinity of attachment to the smooth than rough Ti surfaces by 1 h. This affinity was differentially higher for P than TCP at earlier time points. The higher affinity of the hMSC to Ti was decreased by topographical modifications of the SLA and modSLA surfaces. This differential behavior of cells to the modified Ti surfaces had extended to cellular spreading, and was most evident in the delayed spreading on SLA and modSLA compared to polished at 60 min post seeding. The micrographs of cells attached at 5, 30, 60 and 180 min exhibit this difference quite starkly.

3.4.2 Cellular viability

Similar to attachment and morphology, the viability of hMSCs was differentially affected by the various surfaces used in this study. In conditions that favored cellular proliferation (GM), the hMSCs increased to similar numbers at a higher rate on TCP and P; but displayed an extended lag on the rough Ti surfaces at all corresponding time points. However, in conditions that promoted cellular differentiation to an osteoblastic phenotype (OM), cellular proliferation took place on all surfaces; but was comparatively higher on TCP while having plateaued to a similar level on all Ti surfaces from 7 to 18 d of culture.

The early upregulation of caspase 3 in cells cultured on rough surfaces, in both media conditions, suggests a degree of apoptosis to have been faced by these cells. This upregulation of Caspase 3 is seemingly paralleled by downstream induction of anti-apoptotic BCL-XL and Ki-67; suggesting that if the caspase 3 event was an external pressure of 'death' exerted by the rough topographies on the cells, then it was countered by an intrinsic pressure to survive and proliferate by the cells. A complication derived from these results is the late upregulation of caspase 3 parallel with BCL-XL and Ki-67 at 7 to 10 d post seeding in OM; discussed below.

3.4.3 Significance of findings

The analyses conducted in this section show differences in the phenotypic responses of hMSCs, considered a highly adherent and proliferative cell type, to four different substrates. The parameters of attachment, morphology and viability are inter-related; the way cells attach affects their spreading and hence, the dynamics of their replication. Interestingly, morphological change in the form of increased stretch has been implied to instigate phenotypic differentiation in uncommitted cells (section 1.3.6). Though this last point has not been specifically evaluated here by correlating shape with gene expression, the findings clearly indicate phenotypic differences in the form of differential attachment and morphological spreading, to bear an impact on downstream phenotypic function, which in this case is cellular proliferation.

This restriction in proliferation by the rough surfaces has been suggested to be due to a degree of apoptosis that may occur very early in cell – rough surface contact, and is highest on the modSLA and then SLA compared to smooth (Wall et al., 2009). An analysis of apoptosis with a specified method, such as terminal deoxynucleotidyl transferase dUTP nick end labeling (TUNEL), may have discreetly elaborated the occurrence of apoptosis, and determined any specificity with the rough-hydrophilic modSLA surface. However, the gene expression analyses showed an early upregulation of caspase 3 followed by an upregulation of anti-apoptotic genes BCL-XL and Ki-67; which together support the notion that cells are challenged by a degree of death from the rough surfaces.

Parallel to the increased apoptosis, (Wall et al. 2009) also reported an increase in Stro-1 positive cells in samples cultured on the modSLA surface. This marker is associated with stem cell identity within the current confines of our understanding of adult stem cells, and based on which the authors implied the observed cell death to be specific to Stro-1 negative non-adult stem cells present in the heterogeneous hMSC specimen. Hence, the heterogeneity of the hMSC specimen is a further factor that complicates the observed phenotypic response of altered viability on the different surfaces.

The results suggest a synchrony between pro and anti-apoptotic activity of cells at early and late periods of culture, which may negate the exclusive association of apoptosis, or caspase 3, with non-adult stem cells of the specimen. Interestingly, caspase 3 has been assigned a function in mediating osteogenesis; indicated in the observed lack of runx2/cbfa expression in caspase 3 (-/-) (-/+) mice (Miura et al., 2004) as well as other cellular phenotypes (Lamkanfi et al., 2007). This compares the likelihood of the association of caspase 3 with apoptosis against its possible role in the enhancement of osteogenic differentiation in the hMSCs on the rough surfaces, as has been previously reported for these surfaces by several authors (see section 1.3.6), and that can be anticipated from osteogenic medium. Additionally, considering the strong possibility that an apoptotic cell may relinquish its adherent phenotype and be ‘released’ into suspension due to loss of structural integrity of the cytoskeletal apparatus, further complicates the argument of apoptosis by rough substrates and instead leans towards the idea of temporal osteogenic priming by the modified topographies.

The likely association of caspase 3 with hMSC differentiation on the rough is to a degree supported by (Wall et al. 2009)’s apoptosis analysis, in which the authors used an anti-Annexin V antibody in flow cytometric analysis of hMSCs in early contact with the different surfaces. Importantly, Annexin V occurs richly in matrix vesicles as part of their outer membranes (Arispe et al., 1996). As the anti Annexin V antibody of the kit could detect apoptotic bodies and matrix vesicles alike, it could be suggested, theoretically, that the entity detected in those experiments had likely not as much to do with apoptosis as it might have had with matrix vesicle secretion. This, in turn, could explain the

relative upregulation of caspase 3 at the later times in osteogenic medium, as the cells would have been induced and cultured for a sufficient period to express an osteogenic phenotype.

However, it is the pattern of BCL-XL and Ki-67 expression downstream to caspase 3 in both media conditions and times that underscores its likelihood with apoptotic stimuli; at least within the initial frame of contact. Accordingly, it seems the rough surfaces influence an extrinsic signal of death on hMSC cell populations, which is overcome by the downstream upregulation of anti-apoptotic and proliferative genes.

The results indicate that hMSCs are sensitive to substrate material, capable of differentially identifying Ti surfaces to TCP and rough from smooth topography. An interesting effect of the surfaces was unmasked in OM, which caused cells on all Ti surfaces to replicate uniformly; and in stark contrast to the TCP. This suggests the presence of sensory mechanisms capable of distinguishing and responding between substrate materials and topography.

3.5 Summary

The phenotypic characteristics of hMSCs are affected by substrate material, topography and chemistry.

- The hMSCs attach at higher numbers to polished than rough surfaces at earlier times, but are near similar at 3 h; indicating differences in their initial potentials to attach to the different substrates.
- The hMSCs seem to spread at a faster rate on the smooth surfaces during the initial 1 h following contact, with the rough surface seeded cells exhibiting a relatively stretched morphology. This is indicative of differences in the influence of substrate topography on cell shape (a scenario for tensegrity, influence of tension on integrity).
- Cellular proliferation at low density is comparatively restricted on the rough Ti surfaces compared to the smooth. In the presence of osteogenic inducers, Ti seeded cells proliferate similarly without surface dependent effects compared to plastic.

- Apoptosis seems to be faced by hMSCs on the rough surfaces at some time points that is responded to by the downstream upregulation of survival and proliferative factors.

4 Osteogenic responses of hMSCs to modified Ti surfaces

4.1 Introduction

Modified Ti implant surfaces promote implant integration by increasing, amongst several factors, the extent of bone-implant contact and denser bone accrual in the peri-implant zone (Wennerberg and Albrektsson, 2009). Attempts at understanding the biological basis of these observations have led investigators to examine osteoblastic cell responses to various Ti surfaces *in vitro (Mendonca G et al., 2008)*. The present evidence indicates that rough and additionally rough-hydrophilic Ti surfaces induce distinct temporal differences in the transcriptional regulation of genes key to bone-physiology, which correlate with higher matrix mineralisation and increased synthesis of osteoblast-specific factors (section 1.3.5)(Brett PM et al., 2004; Rausch-Fan et al., 2007). The biological mechanisms underlying these observations remain largely unexplained. Recent findings indicating the selective engagement of cell surface integrin molecules (ITGA2 and ITGB1) in synchrony with increased downstream osteoclastogenic regulator synthesis (Schwartz et al., 2009b). These lines of preliminary evidence are strongly suggestive that cells are capable of differentially sensing Ti substrates and topography, and may undergo a temporal and magnitudinal enhancement in osteoblastic function compared to control polished surfaces.

Although the osteoblast is functionally important in generating bone in implant integration, its existence at the bone implant interface is a derivative of migrating adult stem cells (Davies, 2003). These precursors are important reparative cells of mesenchymal tissues that are recruited very early to the site of implant placement for bone regeneration (Caplan, 2008). The importance of their early interaction with the implant surface in determining the efficacy of downstream events renders them an important position in the conundrum of osseointegration. The studies of the osteogenic responses of these cells to modified Ti surfaces have been relatively few and inconclusive. These have shown the hMSCs are affected in a way similar to osteoblastic cells by exhibiting enhanced osteogenic phenotypic expression on the modified Ti surfaces compared to plastic or polished Ti (Wall et al., 2009; Olivares-Navarrete et al., 2010a; Olivares-Navarrete et al., 2011).

This early intermediate section of the study hypothesised that rough and rough Ti implant surfaces induce an enhancement in hMSC osteogenic responses. It aimed to examine the affects of modified Ti implant surfaces on the osteogenic phenotypic differentiation of hMSCs, with the belief that a mechanism underlying the superior clinical performance and *in vitro* effects of modified Ti implant surfaces is a preferential pressure exerted on adult stem cells to acceleratedly differentiate and function as osteoblasts. The specific objectives were to comparatively (i) examine transcriptional changes in key osteogenic genes, (ii) evaluate osteogenic ECM mineralisation related parameters and (iii) assess the synthesis of osteoblastic phenotypic markers in hMSCs cultured on TCP, P, SLA and modSLA over the course of 21 d.

The genes analysed included markers representing different facets of osteogenic differentiation. These were

- the master osteogenic runt-related transcription factor (Runx2) responsible for commitment and initiation of differentiation;
- extracellular matrix vesicle associated calcium nucleating proteins osteopontin (OP / SSP1 / BSP1) and integrin dependent bone sialoprotein (IBSP / BSP2);
- osteo-specific extracellular matrix collagen (COL1A1);
- inorganic phosphate donor alkaline phosphatase (ALP);
- osteoblast specific negative regulators of osteoclastogenesis, osteoprotegrin (OPG) and growth differentiation factor type 15 (GDF-15);
- transforming growth factor beta 1 (TGF-b1) with
- the upstream integrin subunits alpha 2 (ITGA2) and beta 1 (ITGB1) implicated to be differentially modulated by Ti and furthermore, Ti surface modifications;
- bone matrix associated soluble osteocalcin or gamma-carboxyglutamic acid-containing protein osteocalcin (OC / BGLAP);
- non-canonical Wnt5a due to its implicated role in the early events of osteogenic differentiation and mechanotransduction.

In addition, the gene encoding peroxisome proliferator-activated receptor (PPARγ), a marker of adipogenic differentiation (David, 2007), was used to further compare the dynamics of phenotypic change in hMSCs on the different surfaces. The osteogenic ECM mineralisation of samples was assessed by quantifying calcium deposited in ECM monolayers cultured on the different substrates at 7, 14 and 21 d. This was paralleled by quantifications of total ECM collagen formation and relative estimation of ECM alkaline phosphatase levels. The soluble osteoblastic protein markers comparatively assessed were the osteoclastogenic inhibitors OPG and GDF-15; their implicated upstream instigator TGFb1, as well as the bone formation associated matrix molecule osteocalcin (OC / BGLAP). These parameters were analysed over the course of 21 d that is a duration considered paralleling that of an osteogenic cell in its native context.

4.2 Experimental protocols

In these experiments, the Ti discs were prepared as described in section 2.1.2. The cellular specimens were cultured according to the methods described in 2.2.3.

4.2.1 Gene expression analysis of osteogenic genes

Transcriptional changes were analysed in a set of genes associated with different parameters of osteogenic differentiation using Real time PCR. The set of genes and their importance in differentiation are tabulated in table 4-1. For this experiment, hMSCs were seeded at a density of ~2.5 x 10^4 cells.ml^{-1} in OM on TCP, P, SLA and modSLA. Analyses were conducted at 1, 7, 14 and 21 d post seeding by lysing monolayers, extracting total RNA and converting it to cDNA, followed by PCR with Taqman probes. The methods used in this experiment are detailed in section 2.6. Details of the Taqman® probes used are in table 9-10 (appendix IV).

4.2.2 Assessment of osteogenic mineralisation

The osteogenic mineralisation of hMSCs was examined in samples formed by seeding cells on TCP. P, SLA and modSLA at an initial density of ~1.25x 10^4 cells.cm^{-2} in OM. Cultures were maintained with bi-weekly medium changes. The specific parameters evaluated in these samples are described below:

4.2.2.1 Semi-quantitative assessment of mineralisation with Alizarin red S Stain

The semi-quantitative Alizarin Red S dye method was used to initially assess cellular mineralisation at 7 d post seeding. The method for this stain is detailed in 2.7.1.

4.2.2.2 Quantitative assessment of total ECM calcium deposition

A quantitative estimate of ECM deposited calcium was conducted at 7, 14 and 21 days post seeding with the QuantiChrom Calcium assay, according to the method described in 2.7.2. Cell numbers were estimated with the AlamarBlue assay described in 2.5.3.

4.2.2.3 Quantification of total ECM collagen

The total ECM collagen formed by cells was measured at 7, 14 and 21 days post seeding according to the Sircol method described in 2.8. Total collagen was not measurable within a single well due to small quantities formed by the small number of cells. Hence, collagen isolates from three replicates of a sample were pooled, concentrated with kit reagents and then stained, to obtain a reading. This was normalized to total cell numbers that were estimated with the AlamarBlue assay as in 2.5.3.

4.2.2.4 Comparison of alkaline phosphatase synthesis

The relative quantity of ECM ALP formed on individual surfaces was evaluated at 7, 14 and 21 days post seeding; by assaying ALP Specific activity per cell according to the method described in 2.9. Cell numbers of samples were estimated with the AlamarBlue assay as in 2.5.3.

4.2.3 Assessment of osteoblastic protein secretion

Secreted proteins associated with the osteoblastic phenotype were examined at 7, 14 and 21 days post seeding with specific ELISA kits; described in 2.10. The soluble proteins quantified were osteocalcin (OC), osteoprotegrin (OPG), growth differentiation factor 15 (GDF15) and transforming growth factor beta type 1 (TGF-b1). These molecules were quantified in culture supernatants of hMSCs, plated on different surfaces at an initial density of 1.25 x 10^4 cells / cm^{-2}, collected and replaced daily for 21 days. Samples were diluted x10 prior to assay in di-cation-free PBS. Cell numbers were estimated with the AlamarBlue assay as in 2.5.3.

4.3 Results

4.3.1 Gene expression analysis of osteogenic genes

The real time PCR method was used to examine temporal changes in the expression of osteogenic genes (Appendix IV, table 9-10). The results of this analysis are presented in the paragraphs below.

The Runx2 gene, shown in figure 4-1, was significantly more upregulated by rough surfaces than 1 day post seeding compared to both smooth surfaces. The gene was expressed at low level by cells on all surfaces through the remainder of culture period.

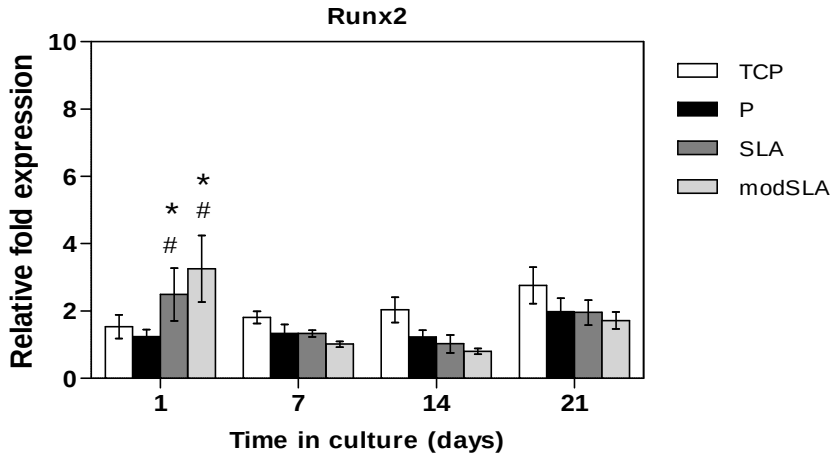

Figure 4-1 RT-PCT analysis of Runx2 expression in hMSCs

A bar chart with mean±1SD fold values of relative expression plotted against time in culture. Cells were seeded at 25,000 cell/disc and relative levels of transcripts investigated at 1, 7, 14 and 21 days in OM. Runx2 was significantly upregulated at 1 d by the rough surfaces compared to tissue culture plastic and polished Ti. It was expressed at a baseline through the remaining times. N=3, n=3; * = $p < 0.05$, TCP vs. any Ti. # = $p < 0.05$, P vs. Rough surfaces.

The bone sialoprotein type 2 (BSP2) gene was upregulated by the Ti surfaces at 1 d post seeding compared to TCP, as shown in figure 4-2. The gene was expressed at low levels on all surfaces at 7 and 14 d. It was significantly upregulated several fold on the smooth surfaces compared to rough at 21 d post seeding.

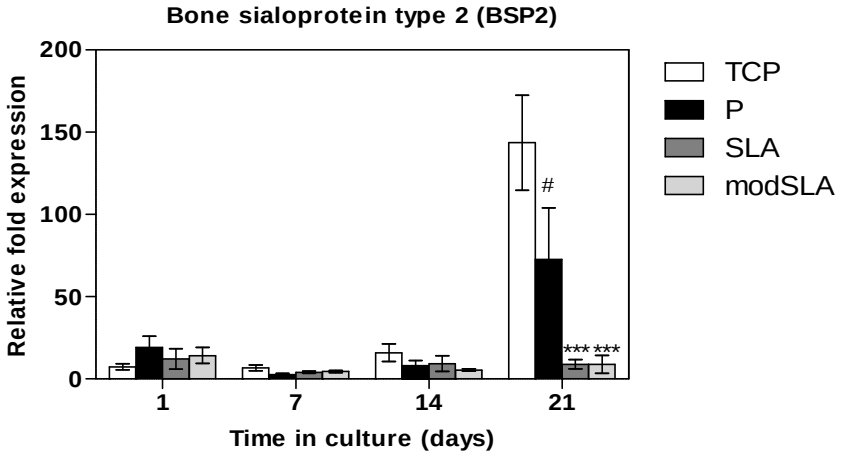

Figure 4-2 RT-PCT analysis of BSP2 expression in hMSCs

A bar chart with mean±1SD fold values of relative expression plotted against time in culture. Cells were seeded at 25,000 cell/disc and relative levels of transcripts investigated at 1, 7, 14 and 21 days in OM. BSP2 was upregulated at 1 d by the Ti surfaces compared to tissue culture plastic. The surfaces did not modulate the extracellular matrix protein until 21 d while the smooth surfaces exhibited highly significant upregulation compared to the rough surfaces. N=3, n=3; *** = $p < 0.001$, TCP vs. any Ti. # = $p < 0.05$, polished vs. rough Ti surfaces.

The osteopontin (OP) gene (figure 4-3) was significantly upregulated on the rough surfaces compared to TCP and polished at 1 day post seeding. The gene was expressed at low levels on all surfaces at 7 and 14 d. It was upregulated to a significantly higher fold value by cells on TCP and polished at 21 d post seeding compared to rough.

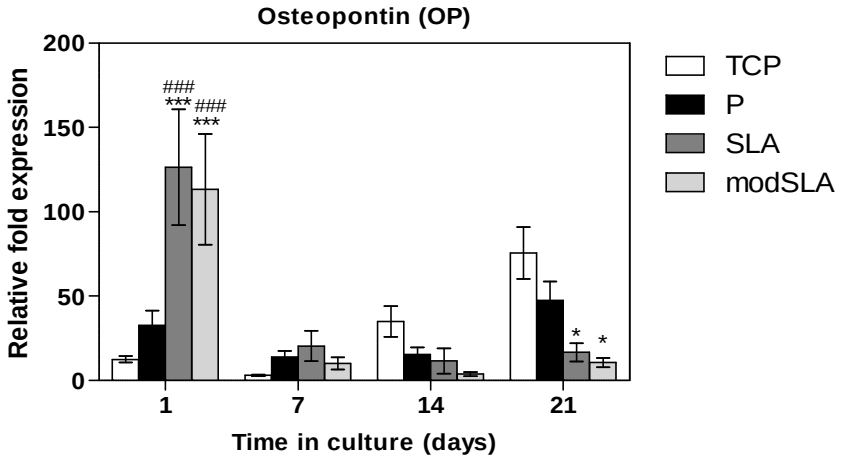

Figure 4-3 RT-PCT analysis of osteopontin expression in hMSCs

A bar chart with mean±1SD fold values of relative expression plotted against time in culture. Cells were seeded at 25,000 cell/disc and relative levels of transcripts investigated at 1, 7, 14 and 21 days in OM. OP was highly significantly upregulated at 1 day by the Ti surfaces. The cells did not modulate the extracellular matrix protein in the intermediate period of culture. At 21 days, the smooth surfaces seemingly induced a highly significant upregulation of OP compared to the rough. N=3, n=3; *** = $p < 0.001$, TCP vs. Ti surface. ### = $p < 0.001$, P vs. Rough surfaces. + = $p < 0.05$, SLA vs. modSLA.

The extracellular matrix collagen type 1 alpha chain (Col1a1) gene was upregulated several fold on the TCP compared to all Ti surfaces through the course of the experiment (shown in figure 4-4). The polished Ti seeded cells seemed to display a relative increase in Col1a1 expression till 14 d of culture. The rough surfaces displayed no change in the gene's transcription between the first and last time points.

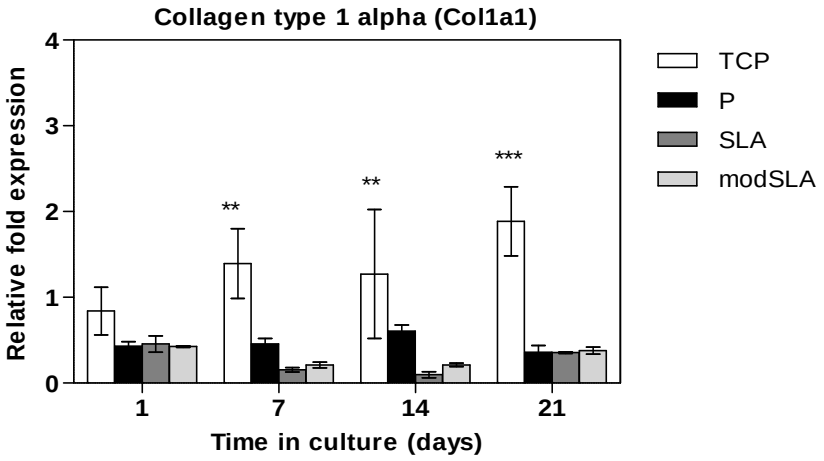

Figure 4-4 RT-PCT analysis of collagen 1 alpha 1 expression in hMSCs

A bar chart with mean±1SD fold values of relative expression plotted against time in culture. Cells were seeded at 25,000 cell/disc and relative levels of transcripts investigated at 1, 7, 14 and 21 days in OM. The Col1a1 gene was expressed significantly higher on TCP than Ti at all time points. N=3, n=3; *, **, *** = $p < 0.05, 0.01, 0.001$, respectively for TCP vs. Ti.

The ALP gene shown in figure 4-5 was expressed at similar levels on all surfaces at 1 and 14 d. It had been significantly upregulated at 7 d by TCP compared to the rest, and later at 21 d by modSLA compared to all samples.

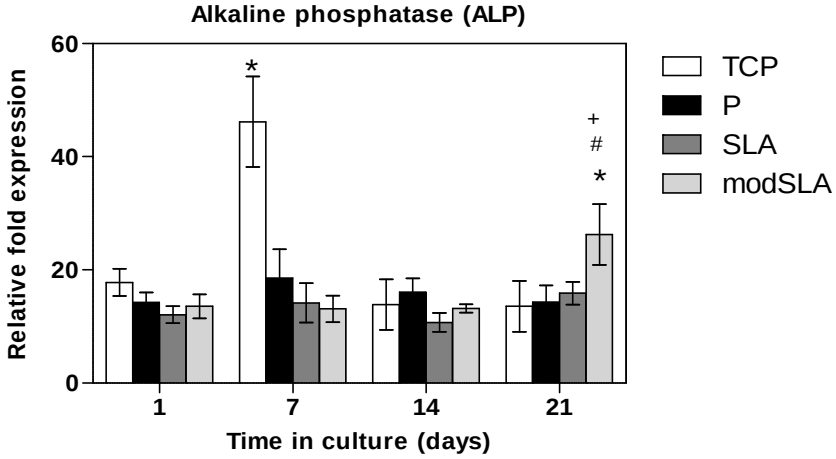

Figure 4-5 RT-PCT analysis of alkaline phosphatase expression in hMSCs

A bar chart with mean±1SD fold values of relative expression plotted against time in culture. ALP was expressed at similar levels at 1 d by all samples. Its expression had increased

significantly higher on TCP than Ti surfaces at 7 d. It was expressed at baseline levels through the remainder of culture, but was significantly upregelated more on the modSLA rough0hydrophilic Ti surfaces at 21 d. N=3, n=3; * = *p* < 0.05, TCP vs. Ti surface. # = *p* < 0.05, polished vs. rough Ti surfaces. + = *p* < 0.05, SLA vs. modSLA.

The result for OPG is shown in figure 4-6. It shows the gene was significantly upregulated by TCP and P at 3 d compared to rough surfaces. The expression of the gene increased significantly on the rough whilst decreasing on the smooth by 21 d.

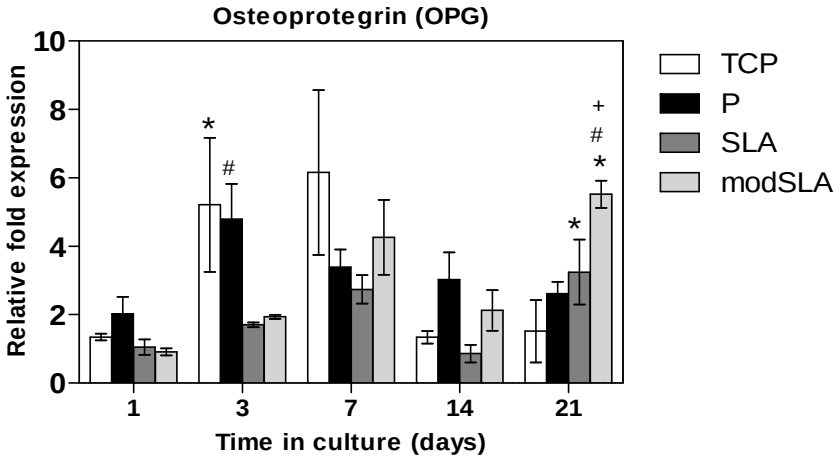

Figure 4-6 RT-PCT analysis of osteoprotegrin expression in hMSCs

A bar chart with mean±1SD fold values of relative expression plotted against time in culture. Cells were seeded at 25,000 cell/disc and relative levels of transcripts investigated at 1, 7, 14 and 21 days in OM. OPG was initially transcribed at significantly higher levels by cells on smooth than rough Ti. This trend was inversed at 21 d with stark expression of the gene in the rough surfaces than smooth. N=3, n=3; * = *p* < 0.05, TCP vs. Ti surface. # = *p* < 0.05, polished vs. rough Ti surfaces. + = *p* < 0.05, SLA vs. modSLA.

GDF-15 was, as shown in figure 4-7, was expressed at a significantly higher level on the rough surfaces at 1 d post seeding. The expression of the gene had increased on the smooth surfaces at 7 and 14 d; but had equilibrated by 21 d.

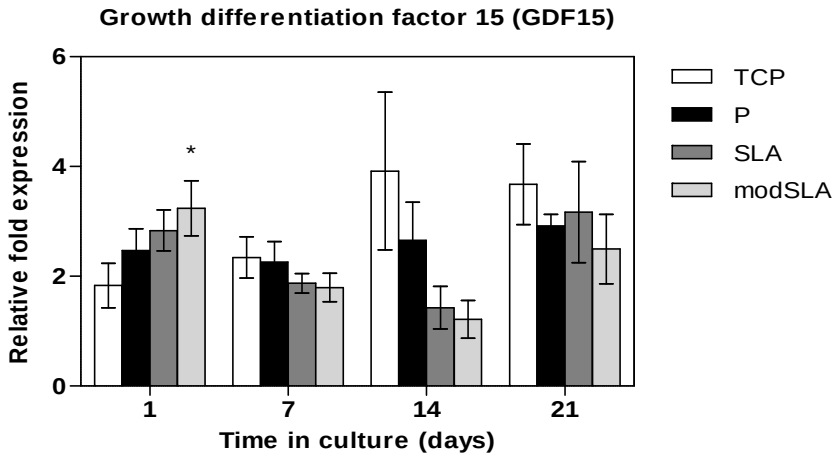

Figure 4-7 RT-PCT analysis of GDF-15 expression in hMSCs

A bar chart with mean±1SD fold values of relative expression plotted against time in culture. Cells were seeded at 25,000 cell/disc and relative levels of transcripts investigated at 1, 7, 14 and 21 days in OM. Growth differentiation factor 15 (GDF-15) was initially transcribed at significantly higher levels by cells on rough Ti than tissue culture plastic and polished Ti. The gene was seemingly transcribed at higher levels at 14 d. N=3, n=3; * = $p < 0.05$, TCP vs. Ti surface.

The results for TGF-β1 are shown in figure 4-8. The gene did not display any early differences in expression between the surfaces. It was significantly downregulated by the rough surfaces at 14 d compared to smooth, which later fell to near equal levels on all surfaces by 21 d.

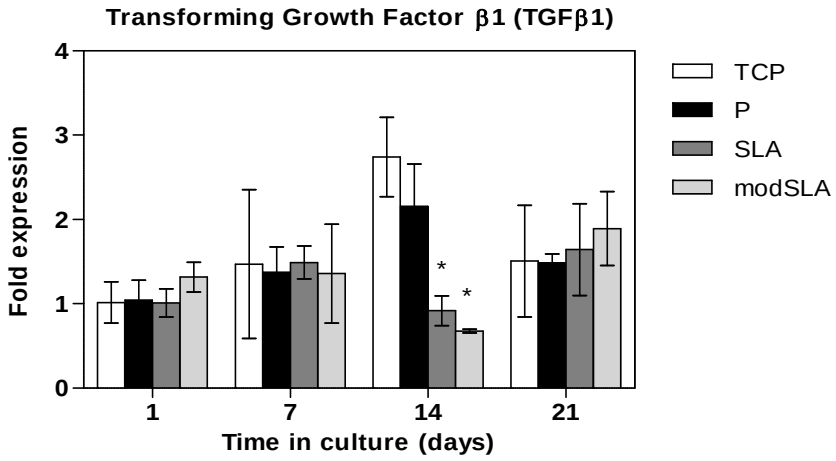

Figure 4-8 RT-PCT analysis of TGFβ1 expression in hMSCs

A bar chart with mean±1SD fold values of relative expression plotted against time in culture. Cells were seeded at 25,000 cell/disc and relative levels of transcripts investigated at 1, 7, 14 and 21 days in OM. TGFβ1 was initially transcribed at similar levels by cells at 1 and 7 d. Its expression significantly increased on the smooth by 14 d while decreasing on the rough. Levels of the gene had equilibrated by 21 d. N=3, n=3; * = $p < 0.05$, TCP vs. Ti surface.

The integrin molecules ITGα2 and ITGβ1, shown in figure 4-9, displayed a significantly higher fold expression on TCP compared to the Ti surfaces. This difference occurred late for ITGα2 but was observable very early for ITGβ1. These molecules are cell surface adhesion receptors, which have been previously suggested to be highly specific to Ti. The experiment here reveals these molecules, at the genetic level, are induced to be expressed at significantly higher fold values by the TCP than Ti,

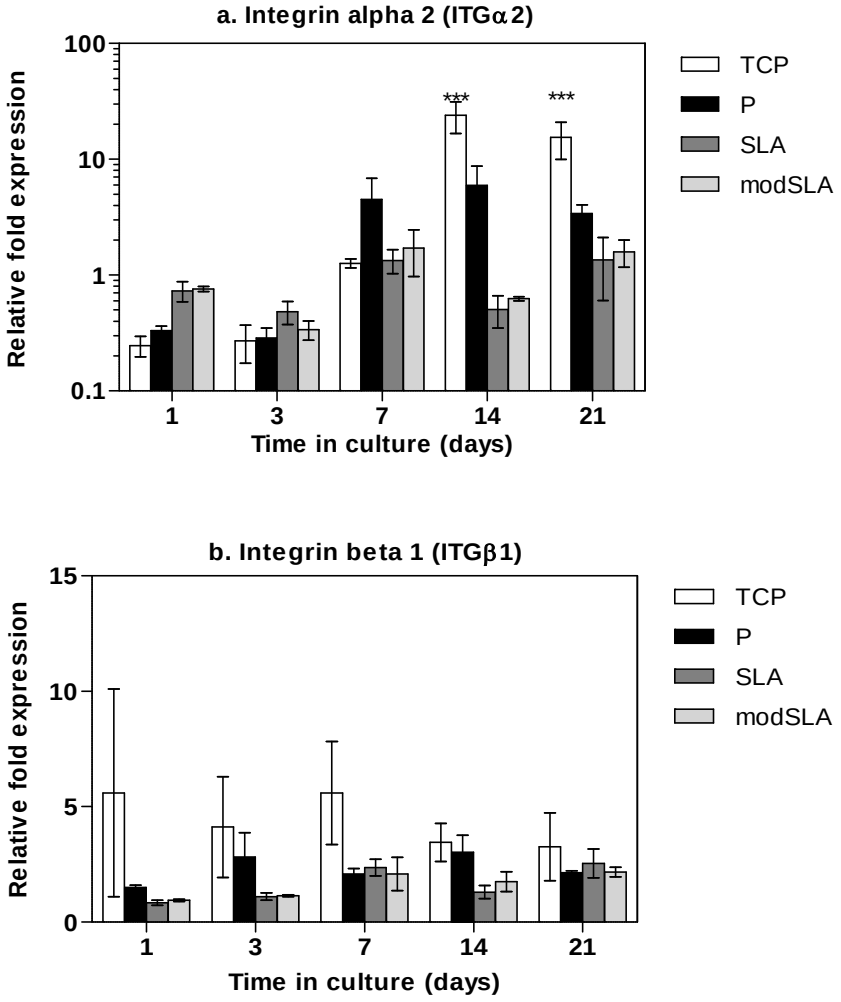

Figure 4-9 RT-PCT analysis of integrin molecules ITG α2 and β1 expression in hMSCs

A bar chart with mean±1SD fold values of relative expression plotted against time in culture. Cells were seeded at 25,000 cell/disc and relative levels of transcription examined at 1, 7, 14 and 21 days in OM. (a) A semi-log graph with relative fold expression presented as log_{10} due to the small relative values achieved for sample at 1 d. ITGα2 was seemingly upregulated by cells on the rough Ti than smooth surfaces by a very small fold value at 1 d. This upregulation was highly significant at 14 and 21 d between TCP and any Ti surface. (b) ITGβ1 was initially expressed at a slightly higher fold value in cells on TCP than Ti surfaces. Its levels of expression had equilibrated at similar levels on all surfaces by 21 days in culture. The gene was seemingly transcribed at higher levels at 14 d. N=3, n=3; *** = $p < 0.001$, TCP vs. Ti surface.

The Wnt5a pro-osteogenic molecule (figure 4-10) was comparatively upregulated by the rough surfaces at 1 d. It had decreased on the rough by 7 d. Its expression increased to similar levels on all surfaces by 21 d.

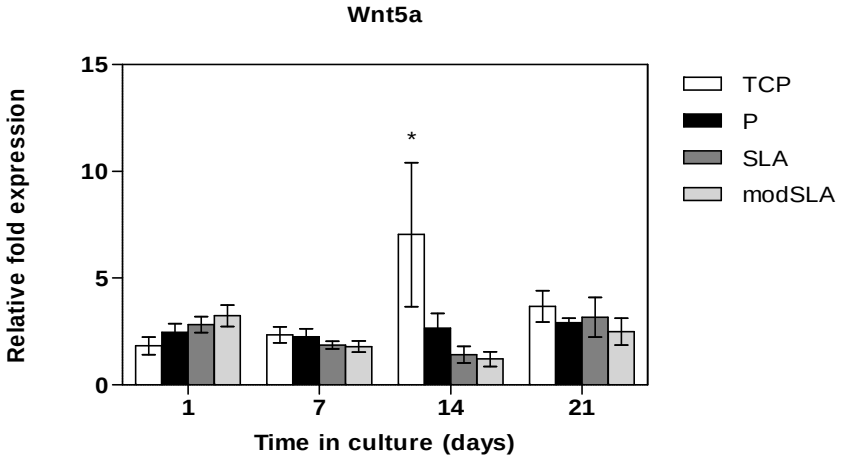

Figure 4-10 RT-PCT analysis of Wnt5a expression in hMSCs

A bar chart with mean±1SD fold values of relative expression plotted against time in culture. Cells were seeded at 25,000 cell/disc and relative levels of transcription examined at 1, 7, 14 and 21 days in OM. The Wnt5a molecule was upregulated to a relatively higher fold value by cells on modSLA than other surfaces at 1 d post seeding. The expression of the gene decreased by 7 d but was significantly upregulated by TCP compared to other surfaces by 14 d. The gene seemed to be expressed at similar levels by all samples at 21 d. N=3, n=3; * = $p < 0.05$, TCP vs. Ti surface.

The osteocalcin molecule (OC / BGLAP), as shown in figure 4-11, exhibited a relative heightened expression on the rough surfaces than smooth at 7 d, which was significantly higher at 21 d. The smooth surfaces seemingly had upregulated the gene highly significantly at 14 d, which had decreased compared to the rough surfaces by 21 d.

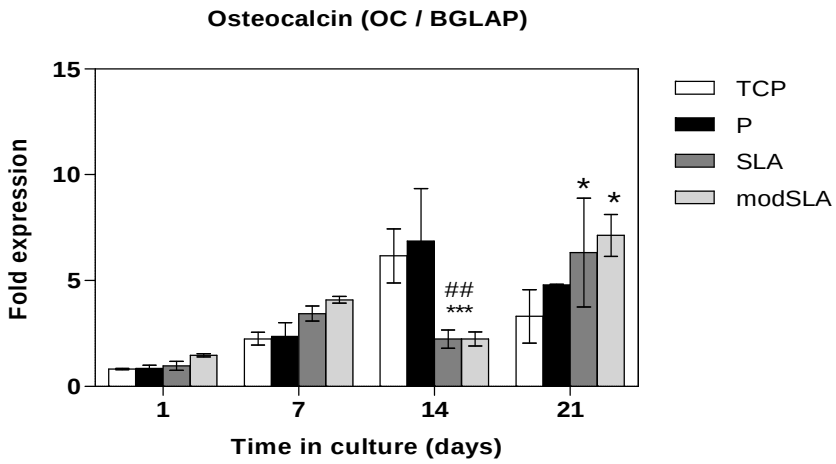

Figure 4-11 RT-PCT analysis of osteocalcin expression in hMSCs

A bar chart with mean±1SD fold values of relative expression plotted against time in culture. Cells were seeded at 25,000 cell/disc and relative levels of transcription examined at 1, 7, 14 and 21 days in OM. The molecule was initially upregulated to a relatively higher fold value by modSLA at 1 d post seeding. The expression of the gene relatively increased on the rough Ti than smooth surfaces by 7 d. A significant downregulation was observed on the rough than smooth by 14 d, which was reversed by the final time point to be significantly higher on the rough than smooth surfaces. N=3, n=3; *** = $p < 0.001$, TCP vs. Ti surface. ## = $p < 0.01$, P vs. Rough Ti surfaces.

The peroxisome proliferator-activated receptor (PPARγ) is a nuclear receptor that is a potent instigator of adipogenic differentiation. The gene seemed initially expressed higher on Ti than TCP. Its expression, shown in figure 4-12, was markedly upregulated on TCP and P compared to the rough at 3 d post seeding. Expression of the gene persisted through the culture period; and was seemingly higher on the Ti than TCP at 21 d.

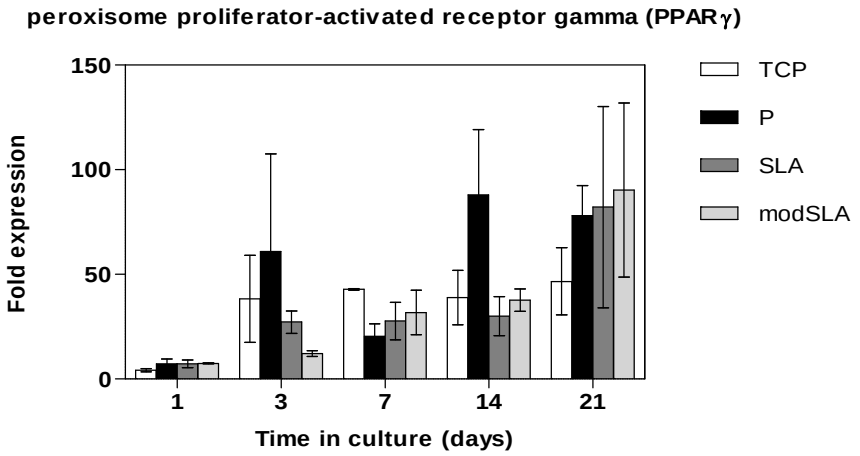

Figure 4-12 RT-PCT analysis of osteocalcin expression in hMSCs

A bar chart with mean±1SD fold values of relative expression plotted against time in culture. Cells were seeded at 25,000 cell/disc and relative levels of transcription examined at 1, 7, 14 and 21 days in OM. The molecule was detected in all samples at 1 d post seeding. Its expression had increased by 3 d, and was higher on the smooth surfaces than rough. The modSLA hydrophilic surface had relatively decreased expression than SLA at 3 d mark. The gene displayed expression through the later phases of culture. N=3, n=3.

4.3.2 Assessment of osteogenic mineralisation

4.3.2.1 Semi-quantitative assessment of mineralisation with Alizarin Red S Stain

This experiment was an initial assessment of the relative levels of calcium deposition on different surfaces at 7 d post seeding in OM. The results of this experiment at presented in figure 4-13. The results show the modSLA surface to have significantly ($p < 0.001$) induced the highest level of Alizarin red s stain compared to all surfaces. It was magnitudinally followed by SLA and then P, with the least stain present on TCP. The difference between TCP and P was much smaller than of P with SLA or modSLA; indicating a significantly higher level of calcium deposition on the rough.

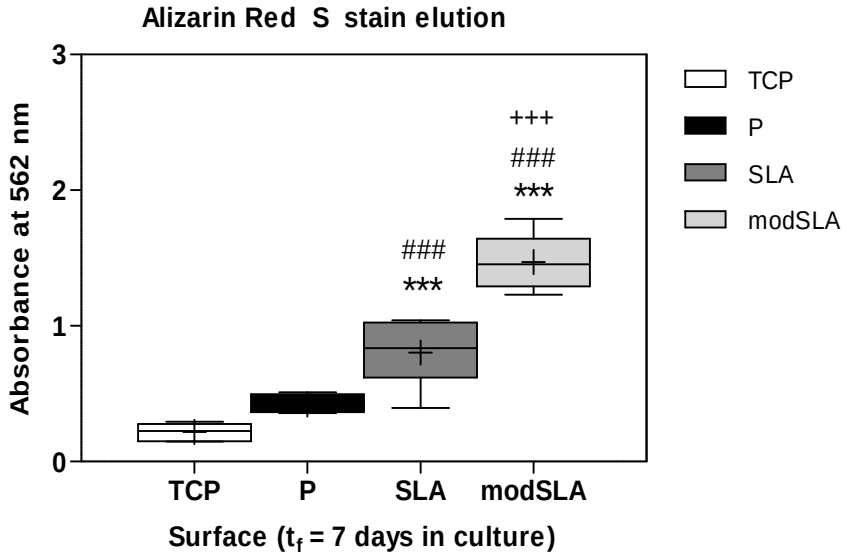

Figure 4-13 Semi-quantitative assessment of mineralisation with Alizarin Red S Stain

Box and whisker plot with minimum to maximum readings (T-bars), median (horizontal line), centre quartiles (coloured boxes above and below median) and mean depicted by centre cross (+) near median line. A total of 25,000 cells were seeded per disc. Samples were fixed and stained after 7 d culture in osteogenic medium. The rough surfaces had induced significantly higher levels of calcium deposition by this time. There were no significant differences between tissue culture plastic and polished Ti. The hydrophilic modSLA surface had caused significantly higher levels of calcium deposition than hydrophobic SLA. N = 1; n = 3. *** = $p < 0.001$, TCP vs. any Ti. ### = $p < 0.001$, P vs. rough. +++ = $p < 0.001$, SLA vs. modSLA.

4.3.2.2 Quantitative assessment of total extracellular matrix calcium deposition

The quantity of calcium deposited per cell number was evaluated at 7, 14 and 21 d post seeding. The results of this analysis are illustrated in figure 4-14. The result shows the rough surface seeded cells had deposited significantly higher levels of calcium at 7, 14 and 21 d post seeding compared to TCP and P. The P surface had induced a significantly higher level of calcium deposition at 14 and 21 d post seeding compared to TCP. The modSLA surface had significantly induced higher calcium mineralisation compared to SLA at 14 and 21 d.

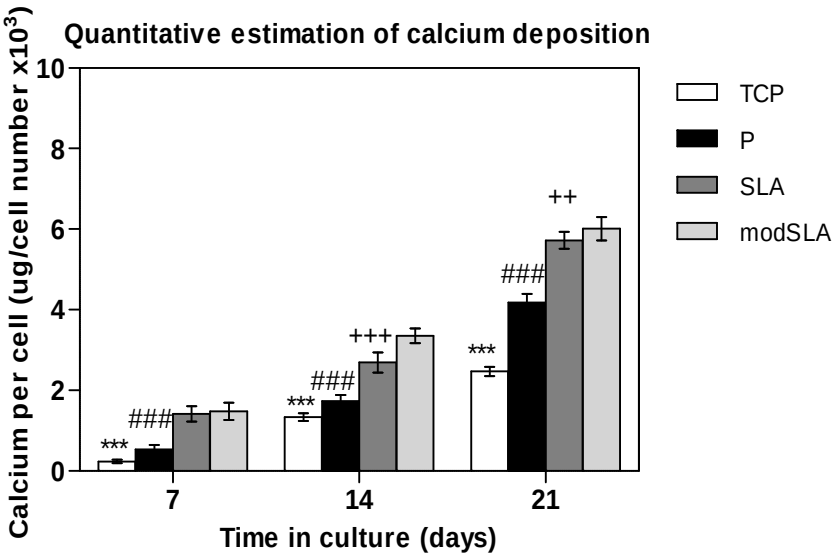

Figure 4-14 Quantitative assessment of total extracellular matrix calcium deposition

Bar chart indicating mean ± 1SD of calcium deposited per cell number per surface type. Approximately 25,000 cells were seeded per disc in OM. Quantities of deposited calcium and cell numbers were estimated at 7, 14 and 21 d post seeding in OM. The chart indicates calcium deposition was higher on rough surfaces than smooth at all time points. TCP was observably weaker in inducing calcium mineralisation compared to the Ti surfaces. N = 3, n = 3. **** = $p < 0.001$, TCP vs. any Ti. ### = $p < 0.05$, P vs. rough. ++, +++ = $p < 0.01$, 0.001 respectively, SLA vs. modSLA.

4.3.2.3 Quantification of total extracellular matrix collagen formation

The total amount of collagen formed in triplicates was normalized to total cell numbers across three wells to evaluate differences in the synthesis of the ECM molecule. The results obtained are illustrated in figure 4-15. The analysis indicates that cells on all surfaces initially formed similar levels of collagen by 7 d. This progressively increased significantly more on the TCP compared to Ti through the remainder of the experiment. The rough surfaces had induced a significantly higher level of collagen synthesis compared to polished surface at 14 and 21 d.

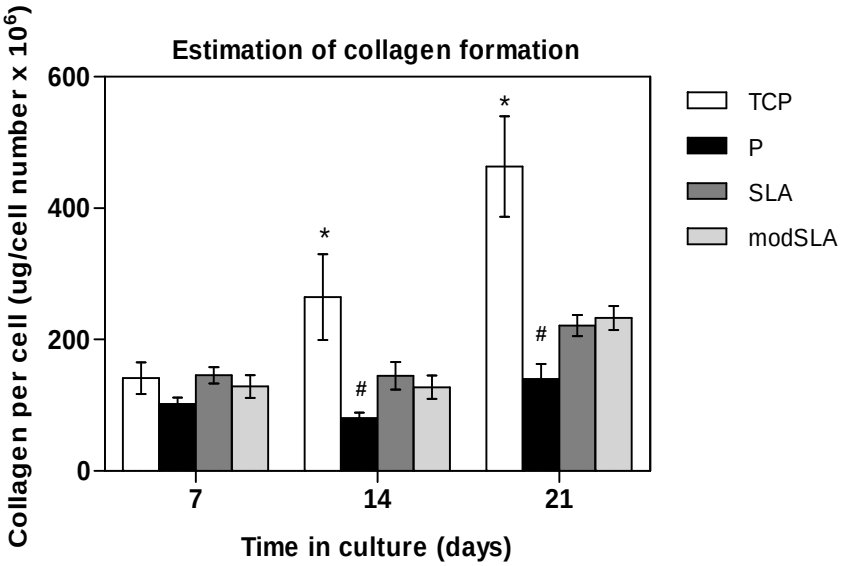

Figure 4-15 Quantification of total extracellular matrix collagen formation

Bar chart indicating mean ± 1SD of collagen formed per cell number per surface type. Approximately 25,000 cells were seeded per disc in OM. Quantities of collagen formed per cell numbers were estimated at 7, 14 and 21 d post seeding in OM. The chart indicates collagen formation was higher TCP than Ti surface. The rough surfaces had deposited significantly higher levels of collagen compared to polished Ti. N =3, n = 3. * = $p < 0.05$, TCP vs. any Ti. # = $p < 0.05$, P vs. rough.

A ratio of total calcium per collagen was calculated from data collected in 4.3.2.2 and 4.3.2.3. This was performed to assess differences in the extent of calcification of the extracellular matrix of the hMSC monolayers cultured in OM on the different surfaces. This was initiated by calculating the total amount of calcium present in three wells by summing values of the three replicates in µg. This sum was divided by the total quantity of collagen (µg) assayed in a replica pool of triplicates. This ratio was separately calculated for each of the three donors and the mean of the resulting three donors specific values calculated and plotted in a bar chart presented in figure 4-16. It shows the Ti surfaces, particularly modSLA, to have induced a significantly higher amount of calcification per collagen compared to TCP at all time points examined. This is attributed to a higher rate of collagen synthesis with a lower rate of calcium deposition on the TCP surface, and vice versa on the rough.

The ratio of calcium per collagen did not increase significantly on the rough surfaces from 14 to 21 d; but had progressively increased on the P surface, exceeding in value to the rough surfaces by 21 d. This was partly due to a relative increase in collagen levels on the rough surfaces at that time; as

well as a concomitant increase in calcium deposition on the P. Importantly, however, the pattern of increase in mineral density over the course of time implies the cells to have reached an in vitro limit of ECM calcification; deduced from the plateau formed on the rough surfaces between 14 and 21 d, which might represent a limitation of this model. The results indicate that cellular mineralisation characteristics are highly altered by material type and furthermore, substrate topography.

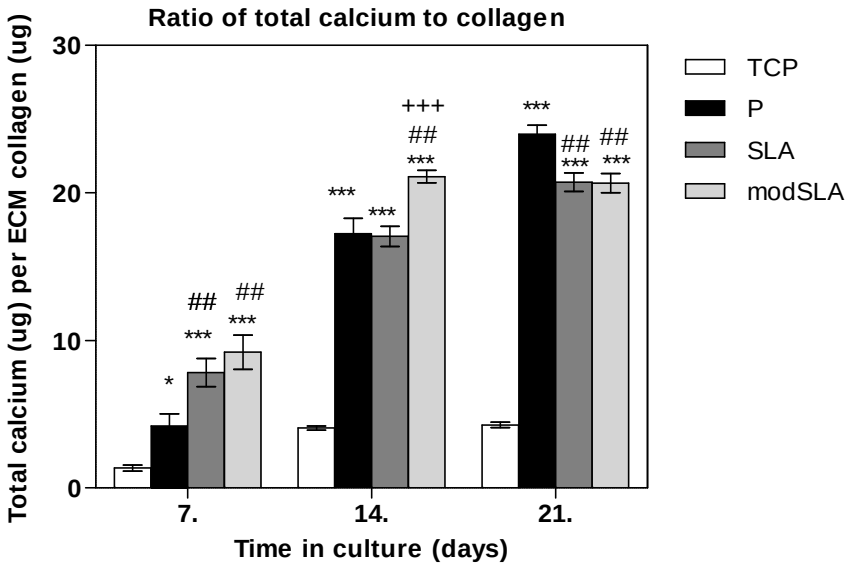

Figure 4-16 Ratio of extracellular matrix calcium per collagen

Bar chart indicating mean ± 1SD of µg calcium deposited per µg collagen in monolayers formed by hMSCs on different discs. The graph shows the Ti surfaces to have formed highly calcified extracellular matrices compared to tissue culture plastic. This calcification was significantly higher for the rough Ti surfaces compared to smooth. The hydrophilic modSLA had induced significantly higher matrix calcification than SLA at 14 d. *, **, * = *p* < 0.05, 0.01, 0.001 respectively TCP vs. any Ti. #, ##, ### = *p* < 0.05, 0.01, 0.001 P vs. Rough surfaces. +++ = *p* < 0.001, SLA vs. modSLA.**

4.3.2.4 Comparison of alkaline phosphatase activity

The specific activity of ALP per cell was examined in hMSCs cultured on the various surfaces for 7, 14 and 21 d to evaluate differences in enzyme synthesis. The results of this analysis are illustrated in figure 4-17. The enzyme was observed at a significantly higher level on the rough by 7 and 14 d in culture compared to TCP and P. Its levels decreased on all Ti surfaces at 21 d compared to TCP, which displayed a progressive increase in the enzyme's levels by this time.

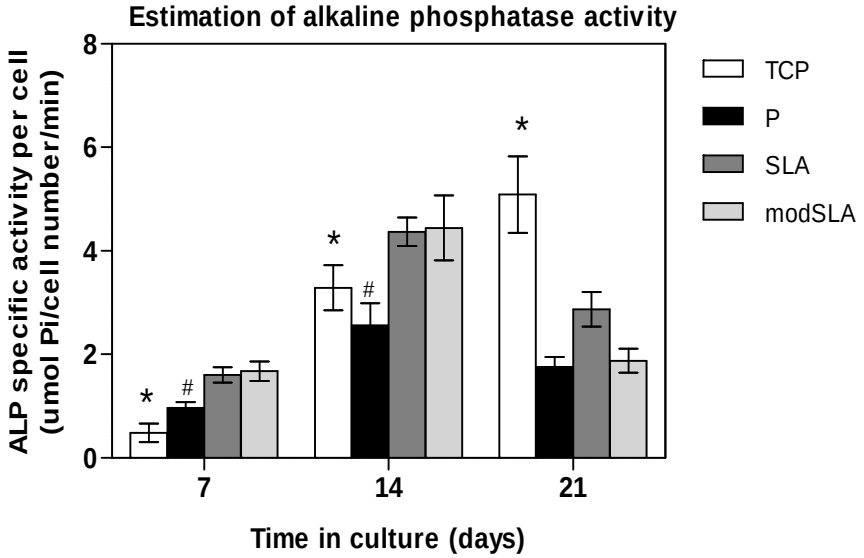

Figure 4-17 Estimation of alkaline phosphatase activity

Bar chart representing the mean ± 1SD of the estimated activity of alkaline phosphatase per cell number per surface type. 25,000 hMSCs cultured on the different discs in OM were analysed at 7, 14 and 21 d post seeding. The graph indicates the rough surfaces had induced more alkaline phosphatase expression and activity than TCP and P at 7 and 14 d. The Ti surfaces seeded cells displayed a decline in enzyme activity per cell number at 21 d compared to TCP, which progressively increased by this point. N = 1, n = 3. * = $p < 0.05$, TCP vs. any Ti. # = $p < 0.05$, P vs. rough. + = $p < 0.05$, SLA vs. modSLA.

4.3.3 Assessment of osteoblastic protein secretion

The temporal synthesis of osteoblastic protein markers osteocalin, osteoprotegrin, growth differentiation factor 15 (GDF-15) and transforming growth factor beta 1 (TGF-β1) was compared in culture supernatants, collected every 24 h over the course of 21 d. Samples at 1, 7, 14 and 21 d were examined for analysis with ELISA. Total quantities were calculated and normalized to cell numbers. The results of this experiment are presented in figure 4-18 to 4-21. The analysis indicated the following:

The osteocalin (OC) molecule, shown in figure 4-18, was detected at significantly higher levels on rough surfaces than TCP and polished through the course of culture. TCP and polished had induced low levels of the protein through 7 d, which gradually increased by 21 d but were much less

than on the rough. The peak expression on rough occurred at 7 d. The modSLA had relatively higher OC levels than SLA at 21 d.

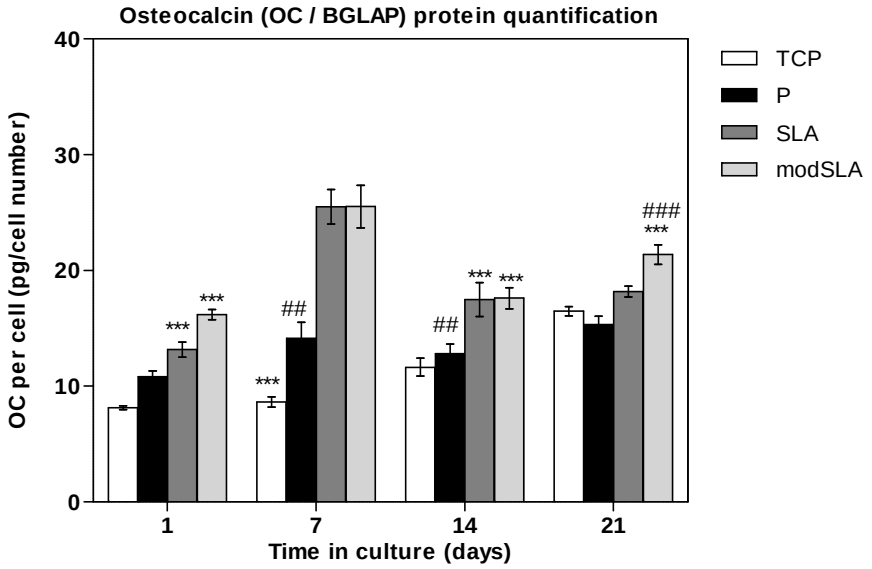

Figure 4-18 Assessment of osteocalcin secretion in hMSCs

Bar chart with mean±1SD secreted protein normalised to total cell number plotted against time in culture. Secreted protein was quantified in total culture medium collected daily for 21 d. Significantly high levels of osteocalcin were induced by cells on the rough surfaces compared to the smooth at all time points. The TCP surface, though producing detectable quantities of the molecule, displayed a small increase over the course of culture. The P surface seemed a stronger inducer than TCP by 7 d but did not display any significant differences by the 14 and 21 d time points. N=3, n=3; *, **, *** = p < 0.05, 0.01, 0.001 respectively TCP vs. any Ti. #, ##, ### = p < 0.05, 0.01, 0.001 respectively P vs. Rough surfaces.

The osteoprotegrin (OPG), shown in figure 4-19, molecule was initially expressed at similar levels on all surfaces at 1 d. Expression of the protein increased on all samples by 7 d and was seemingly higher on the rough than smooth. Levels further increased by 14 d but were highly significant on the rough vs. smooth (p < 0.001). The levels of OPG remained increased on the rough surfaces (modSLA > SLA) at 21 d while having been decreased substantially on the TCP and P.

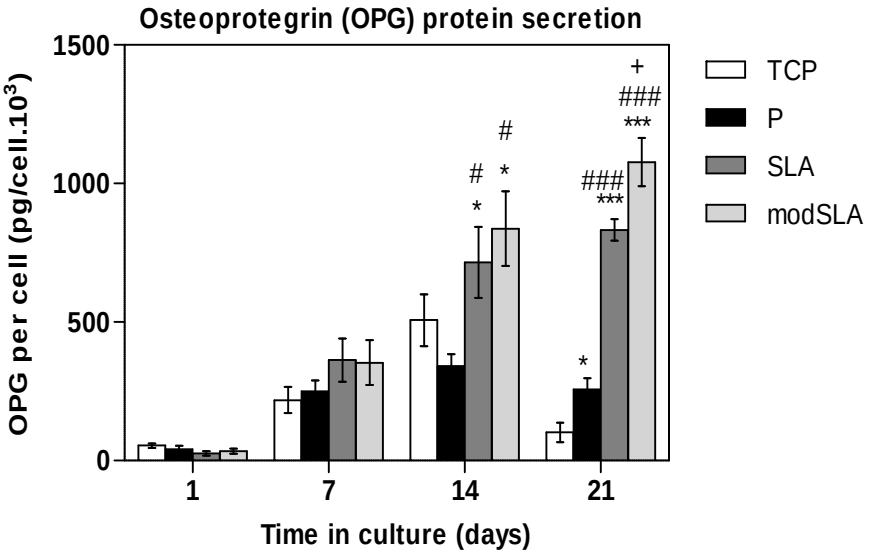

Figure 4-19 Assessment of osteoprotegrin secretion in hMSCs

Bar chart with mean±1SD secreted protein normalised to total cell number plotted against time in culture. Secreted protein was quantified in total culture medium collected daily for 21 d. Significantly high levels of osteoprotegrin were induced by cells on the rough surfaces compared to the smooth surfaces at 14 and 21 d. The TCP surface, though producing detectable quantities of the molecule, displayed a small increase over the course of culture. The P surface seemed similar in its capacity to induce OPG secretion to TCP. The hydrophilic modSLA was observed to have induced significantly higher levels of OPG than its hydrophobic counterpart. N=3, n=3; *, **, * = *p* < 0.05, 0.01, 0.001 respectively, TCP vs. any Ti. #, ##, ### = *p* < 0.05, 0.01, 0.001 respectively, P vs. Rough surfaces. + = *p* < 0.05, SLA vs. modSLA.**

Growth differentiation factor-15 (GDF-15), shown in figure 4-20, was initially expressed at a higher level by cells on the smooth surfaces (P and TCP at 7 and 14 d respectively). The rough surfaces had induced a significant increase in cytokine synthesis at 21 d compared to TCP and P. The modSLA surface induced significantly higher GDF-15 levels than SLA.

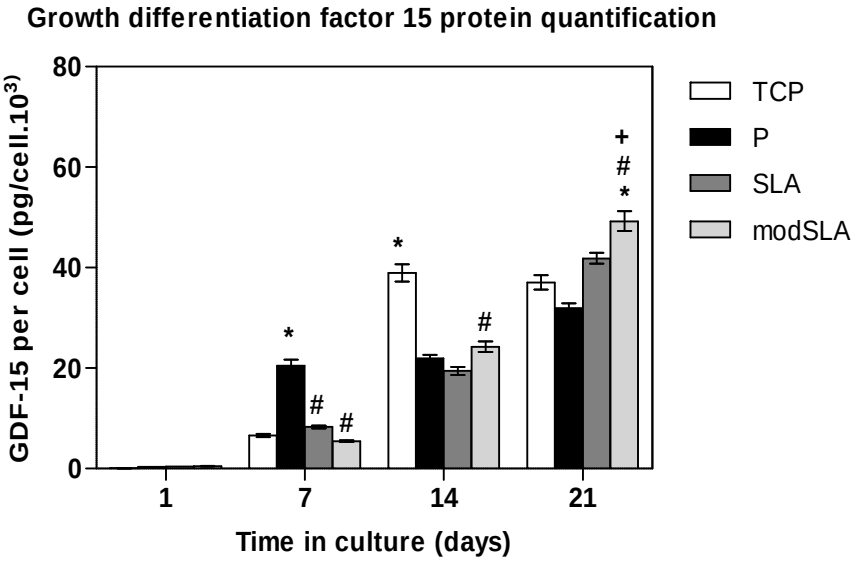

Figure 4-20 Assessment of growth differentiation factor 15 secretion in hMSCs

Bar chart with mean±1SD secreted protein normalised to total cell number plotted against time in culture. Secreted protein was quantified in total culture medium collected daily for 21 d. GDF-15 was detected at 7 d at significantly higher levels on P Ti than all others. TCP induced an increase in levels of protein by 14 d that were significantly higher than the Ti surfaces. This trend was reversed by 21 d with a higher level of protein detected on the rough surfaces. The modSLA induced significantly higher GDF-15 protein in culture supernatant than all other surfaces at 21 d. N=3, n=3; * = $p < 0.05$, TCP vs. any Ti. # = $p < 0.05$, P vs. Rough surfaces. + = $p < 0.05$, SLA vs. modSLA.

The TGFβ1 molecule, shown in figure 4-21, was detected to be expressed by cells cultured on the various surfaces at 1 d. Levels of the molecule had increased significantly on the rough compared to TCP and P by 7 d. These levels equilibrated by 14 and 21 d on all surfaces.

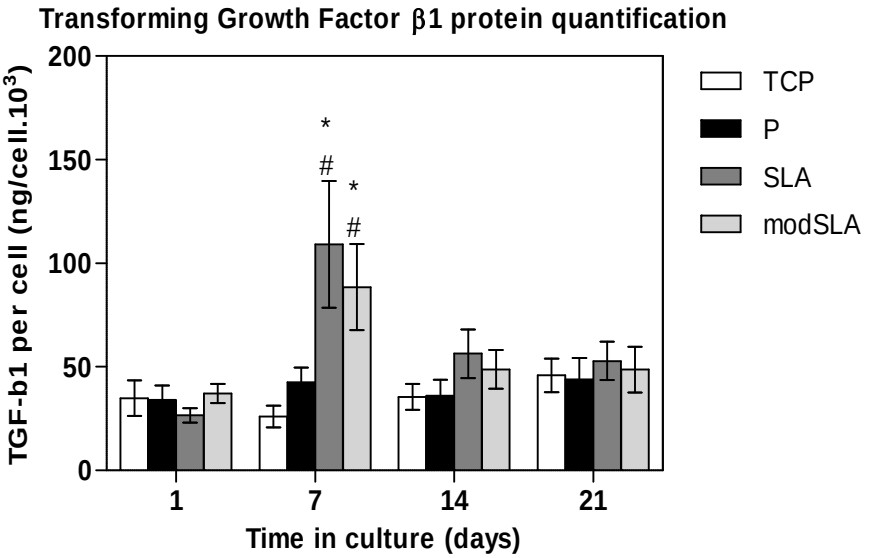

Figure 4-21 Assessment of transforming growth factor beta 1 secretion in hMSCs

Bar chart with mean±1SD secreted protein normalised to total cell number plotted against time in culture. Secreted protein was quantified in total culture medium collected daily for 21 d. TGFβ1 was detected in samples at all time points. It was significantly higher in supernatants of cells cultured on both rough Ti surfaces compared to TCP and P Ti. Quantities of the protein decreased to a baseline at 14 and 21 d marks. N=3, n=3; * = $p < 0.05$, TCP vs. any Ti. # = $p < 0.05$, P vs. Rough surfaces.

4.4 Discussion

4.4.1 Gene expression analysis of osteogenic genes

The panel of genes evaluated in 4.2.1 represents markers important to the osteogenic differentiation of hMSCs. Runx2 is a master transcription factor that up regulates genes important for progressing into the pre-osteoblastic phase of differentiation. OP and BSP 2 are important calcium nucleating proteins, secreted in matrix vesicles that induce heterogeneous calcification of the ECM (Sikavitsas et al., 2001). ALP is the enzyme that supplies inorganic phosphate to the developing calcium phosphate crystal within a matrix vesicle to when the crystal matures beyond the vesicle membranes as well as reduce local pyrophosphate levels, which are a potent inhibitor of osteogenesis. OPG and GDF-15 are osteoblast secreted negative regulators of osteoclastogenesis. TGFb1 is a multirole protein, examined here for its significance with OPG synthesis. ITGA2 and ITGB1 have been implicated in the differential response of cells to Ti, shown to be further modulated by rough topographies in human mesenchymal stromal cell (Olivares-Navarrete et al., 2010a). The Wnt5a gene was studied due to its significance with osteogenic commitment and mechanotransduction based differentiation (Santos et al., 2010).

The genes displayed differences in expression between the surfaces and time points. Most of the differences occurred either early or during the late half of culture. The differences induced by the rough surfaces indicate cells were primed to transcribe certain genes at a higher level; suggestive of a temporal enhancement in differentiation. This idea is mainly deduced from the initial significant increase in Runx2 expression by the rough surfaces. The ECM components analysed due to their association with osteogenesis displayed varied patterns of expression. BSP2 was not observed to be transcribed at high levels initially; but was upregulated at the end of the culture period by the smooth surfaces. The OP / SPP1 gene was upregulated starkly by the rough surfaces initially; but it displayed a trend similar to BSP2, by being significantly upregulated on the smooth by the end of culture period. The COL1A1 gene was highly transcribed by TCP but not Ti; in which the modified surfaces further reduced its transcription. This was also the case for ALP albeit its expression increased significantly on the rough modSLA by 21 d. These indicate that the hMSCs were

modifying their ECM microenvironments differently on the different surfaces; a loose inference would be that events occurring earlier on the rough were taking place at a later time on the smooth.

The osteoclastic modulator OPG displayed heightened expression during the early phase of culture on the smooth surfaces compared to rough. This difference was inversed by 21 d with a higher expression of the gene on the rough surfaces compared to smooth. GDF-15 synthesis displayed a variable pattern of but was comparable to the trend of OPG by being initially relatively higher on the smooth that later inversed to be relatively higher on the rough. Within the context of the biological functions of these proteins, the results suggest that the cells on the smooth surfaces were being primed to inhibit osteoclastic differentiation in the initial phase of culture; which was instigated on the rough at a much higher magnitude towards the end of the three week culture period. This notion is supported by the expression pattern of TGFb1 paralleling that of OPG and GDF-15. This molecule is assigned a role in the upstream regulation of OPG synthesis (Schwartz et al., 2009b) and its expression here is indicative of the suggested pattern of osteoclast regulator synthesis by cells on the different surfaces.

An expression analysis of the integrin subunits ITGA2 and ITGB1 showed these genes to be strongly expressed by cells on TCP and P compared to the rough surfaces. This is interesting as published literature has indicated these to be functionally Ti specific and to be highly affected by modified Ti surfaces. These molecules are receptors for molecules found in bone (laminin, collagen, fibronectin, etc.) and are expected to be co-altered with any change of the process of osteogenic differentiation of cells expressing them. However, the lack of protein evidence, may prevent the discrediting of the association of these molecules with modified Ti surfaces.

Of further interest, however, is the WNT5A gene due to the known role in mediating rock Rho mediated osteogenic differentiation (Santos et al., 2010). Its differential upregulation on the rough surfaces very early is a strong indicator of its potential association with transducing mechanical stimuli to affect osteogenic differentiation; considering the cell morphological differences reported in the previous chapter. The proposed initial enhancement in osteogenic differentiation on the rough

and the role of cellular morphology within it is supported by the parallel downregulation of the adipogenic PPAR-γ compared to the smooth surfaces.

However, it is important to state that genes and their transcriptional findings are highly dynamic, which allow an inference to be drawn but not a conclusion. This hindrance in due to a gene's possible multifunctional role complicated further by the synthetic *in vitro* environmental situation that the cell encounters and adapts to. The implications of these findings rely on the phenotypic analyses of cells on different surfaces; discussed below.

4.4.2 Assessment of osteogenic mineralisation

The effect of modified Ti implant surfaces on the osteogenic mineralisation of hMSCs *in vitro* was assessed by analysing osteogenic calcium deposition, collagen content of the ECM, and ALP levels. The results of this analysis indicate that the process of osteogenic mineralisation in hMSCs is dynamic, and can manifest differently depending on micro-environmental stimuli. Further, the results show that Ti metal increases osteogenic mineralisation compared to TCP; and that this effect is further enhanced by modified topographies.

The differential enhancement of osteogenic mineralisation by Ti compared to TCP is evident in the latter half of the culture period. This is characterised by significantly higher calcium and calcium / collagen values formed on Ti than plastic, suggestive of an earlier initiation of osteogenic matrix formation on the former. This relative enhancement in mineralisation of Ti is further significantly enhanced by the high surface roughness and energy of the SLA and modSLA surfaces in the form of a magnitudinal increase in calcium deposition, calcium/collagen and ALP expression.

The process of *in vitro* mineralisation of a cellular monolayer has limitations. One of these presented in figure 4-6, is the saturation of the ECM by calcium as seen in the form of a stagnant calcium/collagen ratio from 14 to 21 d on the rough substrates. The parallel pattern of ALP synthesis on the rough, progressing till 14 d and then decreasing by 21 d, supports this idea. It indicates cells on the rough surfaces temporally deposit higher levels of calcium than on the

smooth; and are, likely through some kind of feedback loop, informed to cease mineralisation. This inference further supports the hypothesised enhancement of differentiation and phenotypic function by the rough Ti surfaces.

4.4.3 Assessment of osteoblastic protein secretion

The secretion of osteoblastic soluble proteins OC, OPG, GDF-15 and TGF-b1 per cell number was examined in hMSCs cultured on the different surfaces in OM for 21 days. This was conducted by collecting conditioned medium daily and estimating quantities in 1, 7, 14 and 21 d samples with sandwich ELISA kits. OC is an apatite binding protein generally associated with bone formation. OPG and GDF-15 are inhibitors of osteoclastogenesis. TGF-b1 is multifunctional molecule that has been shown to be an upstream instigator of OPG secretion in cell to surface responses in addition to its wider role in osteogenic differentiation processes. The analysis indicated the differential metabolic state of cells on the different substrates in the form of variable cytokine secretion.

The OC molecule was markedly increased by the rough very early. Levels of OPG and GDF-15 were similar in all samples by 7 d; but had increased several folds on the rough in the latter half of culture. TGFb1 was increased many fold on the rough by 7 d; which did not tally with the results of OPG and GDF-15 as the latter's association with TGFb1 was considered in 4.4.1. The findings indicate that the rough substrates increase the secretion of bone formation related cytokines and also modulate the temporal synthesis of negative regulators of osteoclastogenesis.

4.4.4 Significance of findings

The results of the three sets of analyses conducted here corroborate each other in suggesting that the effect of modified Ti surfaces on hMSC differentiation is of a temporal and magnitudinal enhancement. They indicate a strong influence of modified surfaces on the differentiation of hMSCs. This influence causes cell to commit and transform relatively quicker, and deposit calcified matrix earlier on the rough than P and TCP.

In the previous chapter, differential cellular attachment and morphology were inferred to underpin the altered hMSC phenotypic responses of restricted proliferation. Three viability related markers were studied for their importance in cellular apoptosis. It was observed that caspase 3 was comparatively upregulated on the rough surfaces at early and late times of a 10 d culture period in OM. The importance of this molecule in osteogenic differentiation has been highlighted in the absence of runx2 / cbfa activity in caspase 3 null mice (Miura. et al. 2004), and based on which, it was suggested that the Caspase 3 upregulation in hMSCs in OM may have been due to an osteogenic event in cells resulting from altered attachment and morphology on the rough surfaces. The genetic and phenotypic findings in this section indirectly support this notion of Caspase 3's association with osteogenesis; as well strongly indicating the influence of modified Ti surfaces on hMSC fate determination towards an osteogenic lineage.

The results parallel the differences observed between the performance different implant surfaces *in vivo* (section 1.3.4). These further indicate that the multipotent hMSCs are highly sensitive to substrate material, topography and chemistry; as well as that Ti metal is a highly 'osteo-compatible' material that promotes osteoblastic phenotypic differentiation in comparison with the *in vitro* standard substrate, TCP.

4.5 Summary

Ti surfaces of modified topography influence a temporal and magnitudinal enhancement in the osteogenic responses of hMSCs compared to polished and plastic. The main points are.

- Genetic expression of key bone physiology related genes is differentially modulated by surface topography. Cells on the rough surfaces promote the expression of pro-osteogenic genes earlier than smooth. Osteoblastic phenotypic markers are upregulated many fold on the rough at the end of a 21 d culture period. Certain cell surface receptors implicated in the differential response to Ti were found to be upregulated on TCP and not Ti; raising a possible conflict of opinion with the investigators. The basis of possibility is due to the fluid nature of gene expression analysis; that differs starkly from the activity of its protein entity.

- Phenotypic function of the osteogenic differentiation of cells on the surfaces is highly enhanced by modified topography. This extends to calcium mineralisation and phenotypic marker secretion.

  .

5 Surface induced differential modulation of Axl/Gas6 molecules

5.1 Introduction

The hMSC is an uncommitted cell that can be induced to undergo osteogenic like differentiation *in vitro* that leads to the attainment of a phenotype, molecularly and functionally similar, but not identical, to a true osteoblast. The process of osteogenic differentiation can be affected by the material and topographical features of a substrate. The modified Ti surfaces used in this study are shown to increase various osteogenic parameters compared to control polished Ti in hMSCs, examined in chapters 4, which are suggestive of a relative temporal and magnitudinal enhancement in cellular differentiation and function by the rough Ti substrates. This differential response of cells is hypothesised to be due to the engagement of additional molecular systems by surface topography, which alter the course of cell fate, leading to comparatively earlier commitment and increased phenotypic expression.

Axl is a gene implicated to be differentially modulated by rough Ti surfaces. It has been demonstrated with global gene expression arrays to be selectively upregulated by committed human alveolar bone cells in contact with rough Ti (Brett et al. 2004). The association of the signaling pathway with various cellular functions, notably the process of cellular calcification in different biological scenarios, renders it an important and informative marker in elucidating variances in the up and downstream molecular processes of cells in contact with different substrates.

This late intermediate section of the study hypothesised that the receptor Axl and its ligand Gas6 are differentially modulated in the osteogenic responses of hMSCs (a cell type of limited phenotypic capacity) to rough Ti surfaces. It aimed to compare the modulation of the Axl and Gas6 in hMSCs cultured on the modified Ti surfaces; and then examine the effects of receptor deregulation on cell-substrate responses. The analyses were conducted in a 7 d time frame. This was due the high probability of the requirement of the receptors functioning in the initial stages of mineralisation, as inferred from previous observations (Collet et al. 2003; Collet et al. 2008).

The first aim was undertaken with genetic and protein expression analyses of Axl and Gas6 in cells cultured on the different surfaces. The genetic expression of an associated downstream effector called Twist 1 was included; due to its specified role in inhibiting osteogenic commitment (Lee et al., 1999). The second aim was to deregulate the signaling pathway with receptor agonist or antagonists, and compare differences in phenotypic parameters to the controls. The specific phenotypic parameters evaluated were cellular proliferation, osteogenic calcium deposition, collagen formation, and osteoblastic protein marker expression.

A dose curve of the effects of receptor agonist and antagonist on calcium mineralisation was performed to delineate the concentrations of reagents to be used in experiments (sub-section 2.11.2). This dose-curve analysis evaluated the effects of deregulating Axl signaling on osteogenic calcium deposition only.

5.2 Experimental protocols

5.2.1 Differential modulation of Axl/Gas6

5.2.1.1 Gene expression analysis

The genetic expression of Axl and Gas6 were investigated in hMSCs cultured on TCP, P, SLA and modSLA at 1, 3 and 7 d post seeding. This analysis was conducted in GM and OM, due to the different effects of these media on cellular function. The hMSCs (N=3, n=3) were seeded at a density of ~2.5 x 10^4 cell.disc^{-1} in 24 well plates. Samples were processed for RTPCR as described in section 2.8. In addition, a downstream effector of the Axl/Gas6 signaling pathway called Twist1 was studied due to its reported role as an inhibitor of osteogenic differentiation and hence, likelihood to modulate the pathways suggested osteo-inhibitory effects.

5.2.1.2 Protein expression analysis

The Axl and Gas6 proteins were quantified in hMSCs cultured on TCP, P, SLA and modSLA for 1, 3 and 7 d. This analysis was conducted in OM by seeding cells at a density of ~2.5 x 10^4 cell.disc^{-1} in 24 well plates. Due to minute levels of these proteins, the analyses were setup with six replicates

per sample that were pooled for measurement. For Gas6, culture supernatants were collected daily; these were pooled (Vf = 6 ml), frozen at -80^{o}C, lyophilised and finally, reconstituted with 0.5 ml of 1 % BSA in divalent cation-free PBS, to concentrate samples x12 for ELISA. The cell surface Axl was sampled by homogenising monolayers with 100 ul lysis buffer for 20 min at 4^{o}C and then pooling six replicates for storage at -80^{o}C till assay. The ELISAs were conducted to quantify total Axl protein, relative estimate of Axl tyrosine phosphorylation and supernatant Gas6. The methods used are detailed in section 2.10. Cell numbers were determined with AlamarBlue as described in section 2.5.3.

5.2.2 Effects of Axl/Gas6 recombinant proteins on cellular proliferation

The assessment of the effects of Axl signaling was conducted by incubating cells in culture medium supplemented with an agonist or antagonist of the pathway. The receptor agonist used in these experiments was recombinant human Gas6 (rhGas6), used at a concentration of 1 µg.ml^{-1} (detailed in section 2.11.2). The receptor antagonist (MAb) was a mixture of recombinant proteins: these were Axl-extra cellular domain and anti-Axl/anti-Gas6 monoclonal antibodies (MAb; Cf = 4 ug.ml^{-1} of Axl-extra cellular domain; with anti-Axl blockade monoclonal antibodies, Cf = 2.5 µg.ml^{-1}; and anti-Gas6 monoclonal antibodies, Cf = 10 µg.ml^{-1}).

The possible influence of Axl/Gas6 signaling on cellular proliferation was assessed with the AlamarBlue method. The method is detailed in section 2.5.3. This analysis was conducted by seeding cells in GM supplemented with receptor agonist or antagonist at a density of 1 x 10^{4} cells.disc^{-1} in 24 well plates. Cell numbers were estimated at 1, 3 and 7 d post seeding.

5.2.3 Effects of Axl/Gas6 recombinant proteins on cellular osteogenic responses

5.2.3.1 Osteogenic mineralisation

The effects of Axl/Gas6 signaling on cellular osteogenic mineralisation were assayed by quantifying ECM calcium deposition and collagen formation. These parameters were quantified in cultures of hMSCs incubated in OM, with agonist (Gas6) or antagonist (MAb) for 10 d on TCP, P, SLA and modSLA. Calcium deposition was examined in two instances. In the first instance, 6 x 10^{5} cells

were plated in a 9.6 cm^2 6-well plate in the following five condition; GM, OM, OM with agonist (rhGas6), OM with antagonist (MAb), and a 1:1 (v / v) mixture of the two recombinant protein supplemented media (rhGas6 + MAb); and relative calcification estimated with the Alizarin Red S stain according to the method described in section 2.7.1. In the second instance, hMSCs were cultured on TCP, P, SLA and modSLA at a density of 2.5 x 10^4 cells.$disc^{-1}$ OM, OM with agonist or OM with antagonist for 7 d. Total calcium deposited per monolayer were quantified with the QuantiChrom calcium assay, as described in section 2.7.2. Calcium quantities were normalized to total cell numbers that were estimated with the AlamarBlue assay as described in 2.5.3. The receptor agonist used in these experiments was recombinant human Gas6 (rhGas6), used at a concentration of 1 µg.ml^{-1} (detailed in section 2.11.2). The receptor antagonist (MAb) was a mixture of recombinant proteins: these were Axl-extra cellular domain and anti-Axl/anti-Gas6 monoclonal antibodies (MAb; Cf = 4 ug.ml^{-1} of Axl-extra cellular domain; with anti-Axl blockade monoclonal antibodies, Cf = 2.5 µg.ml^{-1}; and anti-Gas6 monoclonal antibodies, Cf = 10 µg.ml^{-1}).

5.2.3.2 Osteogenic ECM collagen formation

Total matrix collagen was estimated at 7 d on TCP, P, SLA and modSLA with the Sircol Collagen assay kit, according to the method described in 2.8. Cells were seeded at a density of ~2.5 x 10^4 cells.$disc^{-1}$ in 24-well plates in OM alone, and OM with agonist or antagonist. Due to the minute quantities of collagen formed in individual wells of a 24 well plate, three replicates of a sample were pooled, concentrated overnight with kit reagents and then assayed total quantities.

5.2.3.3 Osteoblastic cytokine synthesis

The effect of Axl/Gas6 signaling on osteoclastic inhibitors OPG and GDF-15 synthesis was examined by quantifying cytokines in culture supernatants of hMSCs cultured for 7 d on different surfaces. The experiment comprised seeding 2.5 x 10^4 cells.$disc^{-1}$ on TCP, P, SLA and modSLA in OM, OM with agonist and OM with antagonist. Culture supernatant was collected everyday for 7 d and assayed with ELISA according to the methods described in 2.10. Cell numbers were estimated with the AlamarBlue assay as described in 2.5.3

5.3 Results

5.3.1 Differential modulation of Axl/Gas6 in hMSCs

5.3.1.1 Gene expression analysis

The transcriptional modulation of receptor tyrosine kinase Axl, Gas6 and a likely downstream effecter called Twist1 were examined with real time PCR. The analysis was conducted at 1, 3 and 7 d post contact with the different substrates, and in GM and OM due to the differential effects of these media on cellular function. The results of this analysis are presented in figure 5-1, 5-2 and 5-3.

Analyses of the Axl gene (figure 5-1) indicate it to be expressed at similarly low levels by cells in all conditions at 1 d post seeding. The Ti surfaces significantly increased Axl transcription at 3 d compared to the TCP surface albeit in OM only and a very small relative difference. The GM did not seem to modulate the transcription of Axl, which decreased to initial levels in all samples by 7 d.

The Gas6 gene (figure 5-2) seemed transcribed at a basal level in GM through the course of the experiment. In OM, the gene was significantly upregulated by the Ti surfaces at 3 d when compared to plastic surface. The expression of Gas6 increased on all surfaces by 7 d, with the expression seemingly higher on the TCP than Ti.

Twist1 displayed varied results. Its expression was relatively higher in GM than OM. In the former, it was initially expressed at a similar level on all surfaces by 1 d. Transcription had increased several fold on the rough compared to P > TCP at 3 d but decreased by 7 d. In OM, Twist1 was initially expressed higher on the TCP compared to Ti surfaces. It gradually decreased on all surfaces by 7 d, with expression in the order of TCP > P > SLA > modSLA.

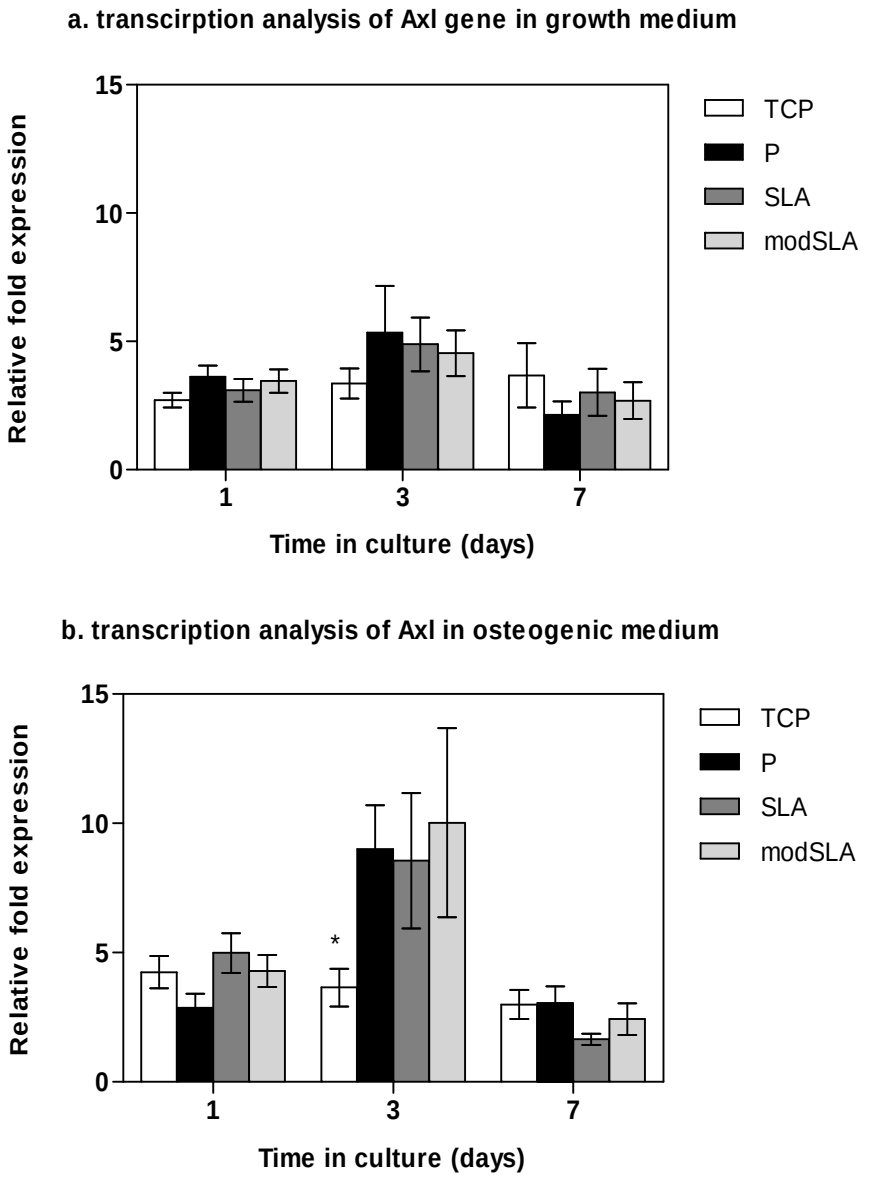

Figure 5-1 Assessing the effects of substrates on the transcription of Axl

Bar chart with mean ± SEM of the relative fold expression of Axl plotted against time in culture. A total of 25,000 cells were plated on each substrate and fold differences determined with the ΔΔCt method. (a) Growth medium did not cause a significant change in Axl expression. (b) Axl was significantly upregulated compared to the Ti surfaces at 3 d in OM. The level of transcription of the gene decreased at 7 d on all surfaces. N=3, n=1; * = $p < 0.05$, TCP vs. Ti surfaces.

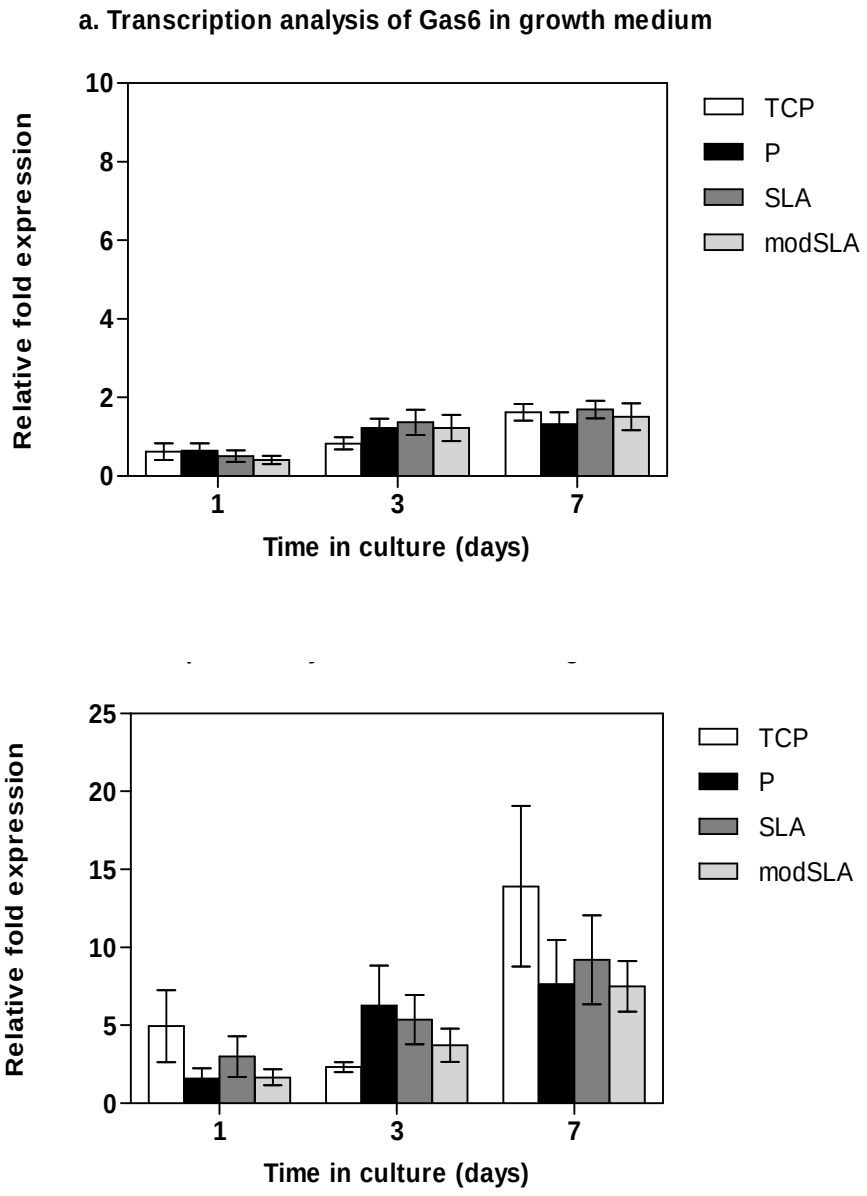

Figure 5-2 Assessing the effects of substrates on the transcription of Gas6

Bar chart with mean ± SEM of the relative fold expression of Gas6 plotted against time in culture. A total of 25,000 cells were plated on each substrate and fold differences determined with the ΔΔCt method. (a) In growth medium, Gas6 did not display any change in expression on any surface. (b) In osteogenic medium, its transcription progressively increased on all surfaces. The differences between the samples were found to be insignificant.

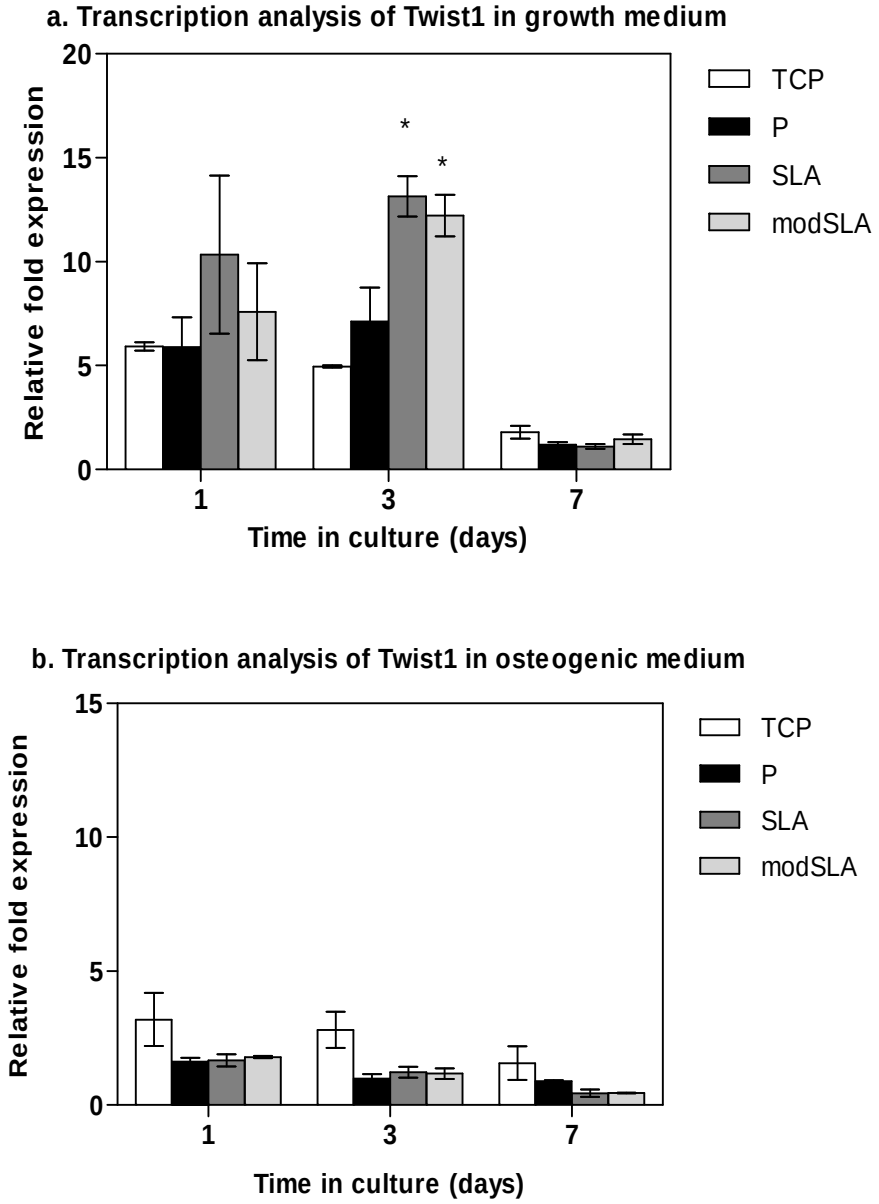

Figure 5-3 Assessing the effects of substrates on the transcription of Twist1

Bar chart with mean ± SEM of the relative fold expression of Twist1 plotted against time in culture. A total of 25,000 cells were plated on each substrate and fold differences determined with the ΔΔCt method. (a) In GM, Twist1 was found detected in all samples. Its transcription seemed higher on the rough surfaces at 1d and was significantly higher than TCP surface at 3d. Levels lowered in all samples by 7d. (b) Twist1 was detected in samples at 1 d albeit at lower levels than in GM. Its expression gradually decreased with the progression of time in osteogenic medium. Its mean value was relatively lower on the rough Ti surfaces than TCP and polished at 7 d. N=3, n=3. * = $p < 0.05$, TCP vs. Ti.

5.3.1.2 Protein expression analysis

The receptor tyrosine kinase Axl and its ligand Gas6 were quantified in pools of six replicates of hMSC specimens, cultured on TCP, P, SLA and modSLA in OM. In addition, the post translation modification of tyrosine phosphorylation was evaluated in Axl isolates. The results of this experiment are presented in figure 5-4, 5-5 and 5-6 for total Axl, phospho Axl and Gas6, respectively, protein quantities normalised to total cell numbers, In summary, the results show that the hMSCs temporally down-regulate Axl receptor quantities and phosphorylation on the rough Ti surfaces compared to TCP and polished Ti surfaces. The TCP incurs a highly significant ($p < 0.001$) progressive increase in Axl protein quantity and phosphorylation compared to Ti, comparisons between which indicate the rough surfaces to cause a significant early down regulation of the receptor compared to the polished surface by 3 and 7 d.

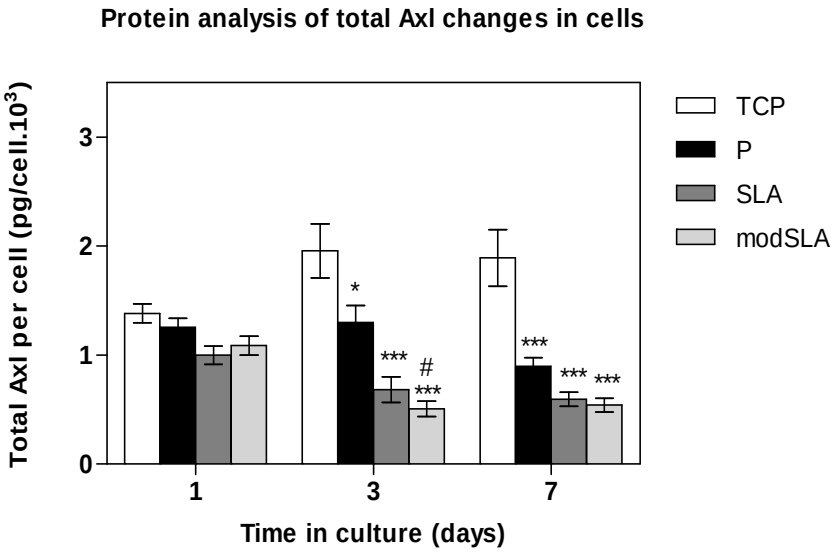

Figure 5-4 Protein expression analysis of total Axl

Bar chart of mean ± SEM of quantities of Axl protein per cell calculated for each sample plotted against time in culture. A total of 25,000 hMSCs were cultured on the different surfaces and cell surface protein quantified in a pool of six replicates with ELISA. It indicates hMSCs expressed Axl protein at initial contact with substrates. The quantities of this protein per cell increased on TCP and slightly on polished Ti by 3 d, while in comparison significantly decreasing on the rough substrates. The TCP surface supported expression of Axl protein at 7 d while it had been downregulated highly significantly by the Ti surfaces. N =

3, n = 1; *, **, *** = p < 0.05, 0.01, 0.001, respectively TCP vs. Ti surfaces. # = p < 0.05, P vs. rough surfaces.

The findings for total Axl were corroborated by relatively lower receptor phosphotyrosine estimates at 1 and 7 d on the rough vs. smooth (p < 0.05) (figure 5-5).

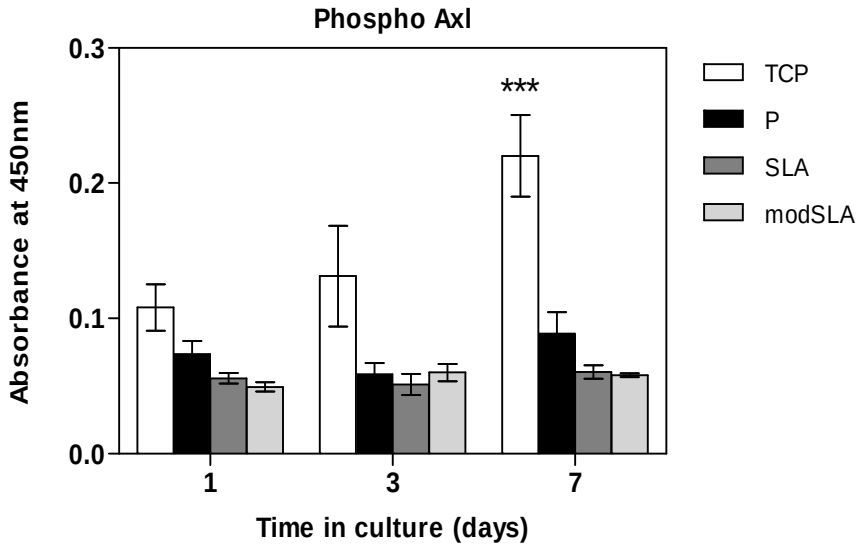

Figure 5-5 Protein expression analysis of Phospho Axl in hMSCs

Bar chart of mean ± SEM of Axl protein phosphorylation plotted against time in culture. A total of 25,000 hMSCs were cultured on the different surfaces and cell surface protein assessed for its relative degree of phosphorylation in a pool of six replicates with ELISA. Phosphorylated Axl was detected in all samples at 1 d post seeding. The relative extent of phosphorylated protein increased on the TCP while it remained at a baseline level on all Ti surfaces. The difference between TCP and the Ti surfaces was highly significant at 7 d. N=1, n=3; *** = p < 0.001, TCP vs. Ti surfaces.

The secreted cytokine Gas6 was present at similar levels on all surfaces at 1 d. Its levels increased on TCP, P and SLA surfaces at 3 d, while decreasing on the modSLA. Quantities of the cytokine decreased on all surfaces by 7 d, but were observably lower on the modSLA compared to all other surfaces.

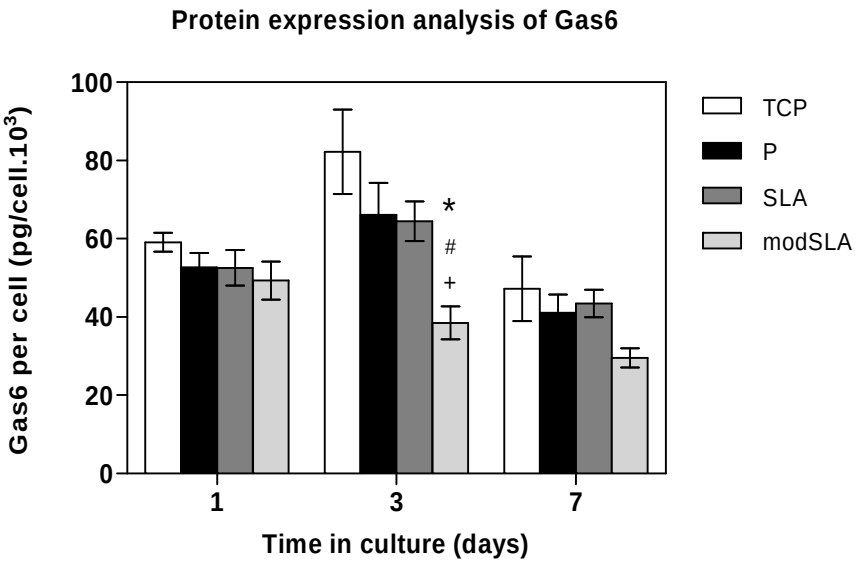

Figure 5-6 Protein expression analysis of Gas6 in hMSCs

Bar chart of mean ± SEM of Gas6 protein normalised to total cell numbers per surface plotted against time in culture. A total of 25,000 hMSCs were cultured on the different surfaces and soluble Gas6 quantified in culture supernatants by pooling medium from six replicates, conditioned with surface attached cells for 24 h. The protein was detected in all samples at 1 d. Its levels increased on all surfaces but had significantly decreased on the modSLA by 3 d. Levels of the protein decreased in all samples by 7 d in culture. N=1, n=3; * = $p < 0.05$, TCP vs. Ti surfaces; # = $p < 0.05$, P vs. rough Ti surfaces; + = $p < 0.05$, SLA vs. modSLA.

5.3.2 Effects of Axl/Gas6 recombinant proteins on cellular proliferation

The effect of Axl/Gas6 pathway deregulation on hMSC proliferation was assessed with AlamarBlue. This analysis was conducted at 1, 3 and 7 d post seeding in growth medium alone, and GM supplemented with receptor agonist or antagonist. The results of this analysis are shown in figure 5-7. It shows that the pathway does not interfere in the proliferation of cells from their normal pattern as desmonstrated in comparison with control growth medium condition. Hence, Axl receptor deregulation does not bear any obvious affect on hMSC proliferation, and is likely not involved in the differential proliferative behavior of cells on the modified Ti substrates.

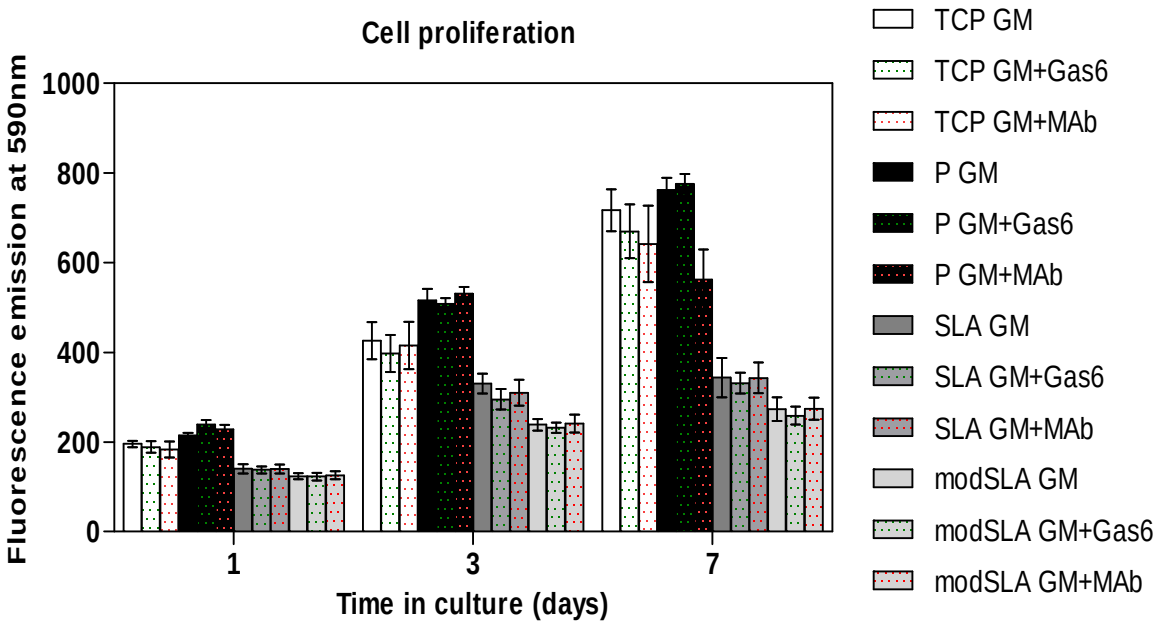

Figure 5-7 Lack of effect of Axl/Gas6 pathway deregulation on hMSC proliferation

Bar shows mean ± 1SD (N=3, n=3) of fluorescence emission values recorded for each samples plotted against time in culture. A total 10,000 cells were plated per surface in GM, GM with rhGas6 (agonist) and GM with MAb (antagonist). Cellular proliferastion was assessed with AlamarBlue fluorescence at 1, 3 and 7 d post seeding. The graphs shows that cells proliferated highly on smooth surfaces than the rough as has been previously shown in section 3. Receptor deregulation did not present any observable changes in cell numbers within any surface type relative to GM only controls.

5.3.3 Effects of Axl/Gas6 recombinant proteins on cellular osteogenic responses

5.3.3.1 ECM matrix calcification

The affects of Axl receptor deregulation on hMSC osteogenic mineralisation was assessed by an initial qualitative assessment with Alizarin Red S stain; followed by a quantitative analysis with a calcium quantification assay. In the first analysis, hMSCs were cultured in 6 well plates in the following conditions: GM, OM, OM with antagonist, OM with agonist, and a combination of both agonist and antagonist. The results of this experiment are presented in figure 5-8. The GM and OM cultured control samples displayed negative and positive stained monolayers, respectively. The OM with antagonist did display mineral, but was visibly lower than the control OM. The OM with

antagonist culture displayed a stark decline in stain compared to control and OM with antagonist. The combination of agonist and antagonist supplemented media yielded a stain intermediate in extent to both states of receptor deregulation.

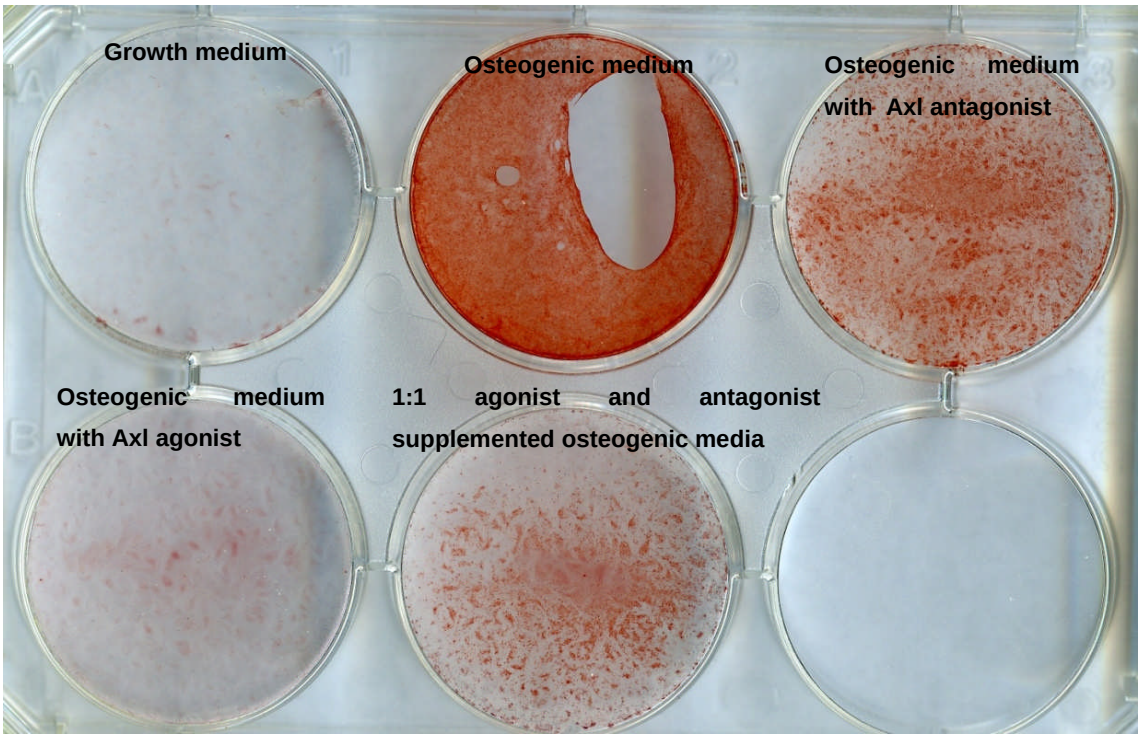

Figure 5-8 Effects of Axl signaling disruption on osteogenic ECM calcification

Image of hMSC monolayers cultured in a six well plate with growth medium (top, left); osteogenic medium (top, centre); osteogenic medium with antagonist (top, right); osteogenic medium with agonist (bottom, left) and 1:1 combination of agonist and antagonist supplemented osteogenic media (bottom, centre). Cells were cultured at 1.25 x 10^5 cells per well for 12 days. Samples were fixed in 100 % ethanol and stained with a 2 % (m / v) acqeous Alizarin Red S stain; image was taken on a flat bed scanner. The growth medium showed no retention of stain. Osteogenic medium stained intensely with a large delaminated area evident. The antagonist comparatively decreased staining while the agonist diminished it further to a level comparable with growth medium control. An intermediate level of staining was observed in the combination of both media. This indicates the involvement of the Axl receptor kinase pathway in the osteogenic mineralisation of hMSCs; seemingly in a negative regulatory manner, where its upregulated activity with the agonist certainly decreases calcium mineralisation. This is corroborated by the decrease in mineral stain in the combined media sample, although a concomitant increase in mineralisation by receptor antagonist was not evident.

In the second analysis, the amount of calcium per cell of monolayer was determined with colorimetric assays. The result of this experiment is shown in figure 5-9. It indicates the hMSCs to mineralise along a trend expected for the control condition, OM only. The addition of receptor agonist decreased the quantity of calcium per sample relative to controls; the trend of higher mineralisation on modSLA > SLA > P > TCP was still preserved, albeit the magnitude was significantly smaller.

The receptor antagonist did not affect mineralisation compared to control OM on all surfaces. The TCP and SLA cultured cells did not display any difference compared to their controls; however, P and modSLA did cause a noticeable decrease in mineralisation.

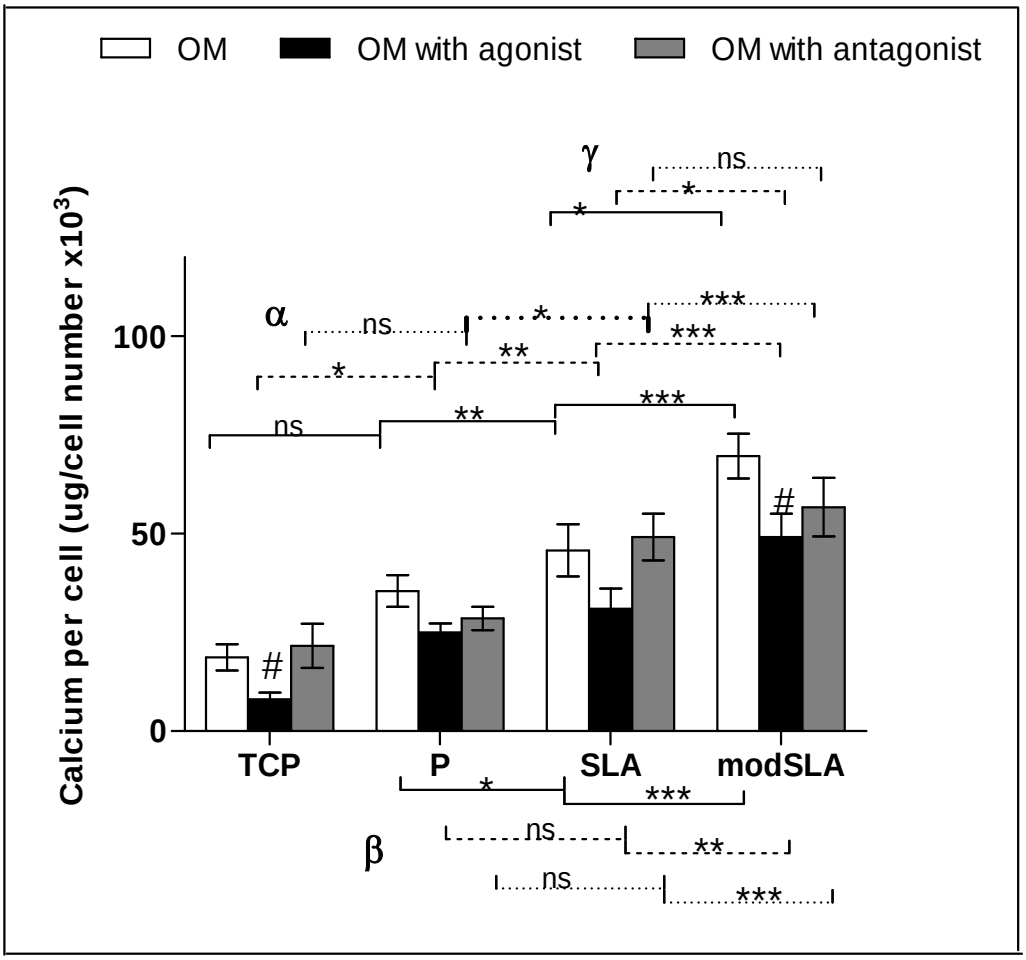

Figure 5-9 Inhibitory effects of Axl receptor deregulation on calcium mineralisation

Bars show mean ± 1SD of calcium per cell plotted against surface type. For this analysis, 25,000 cells were cultured on all surfaces in OM, OM + agonist or OM + antagonist for 7 d. Calcium quantities were determined and normalised to total cell numbers. Graph shows control OM induced mineralisation in the order of modSLA (hydrophilic-rough) > SLA (hydrophobic-rough) > P (polished Ti) > TCP (tissue culture plastic), as had been previously noted in section 4. The addition of agonist rhGas6 significantly decreased calcium mineralisation on each surface respective to controls; but did not inhibit the process. This effect was most prominent on the TCP and modSLA surfaces. The addition of antagonist did not increase mineralisation relative to controls on any surface. It did, however, decrease calcium mineralisation on P and modSLA cultured cells relative to their respective controls. N=3, n=3. # = $p < 0.05$, control vs. condition of any one surface type; *, **, *** = $p < 0.05$, 0.01, 0.001, respectively; ns represents non-significant. α represents a grouped comparison between the TCP and the Ti surfaces for each condition; 'β' between P vs. rough Ti surfaces; γ represents SLA vs. modSLA comparisons. Full lines represent control surface vs. surface comparisons; dashed lines (---) between agonist surface vs. surface; and dotted line antagonist surface vs. surface.

5.3.3.2 ECM collagen formation

The ECM collagen formed by samples was estimated at 7 d. The results of this analysis are illustrated in figure 5-10. It indicates collagen synthesis was not affected by receptor deregulation.

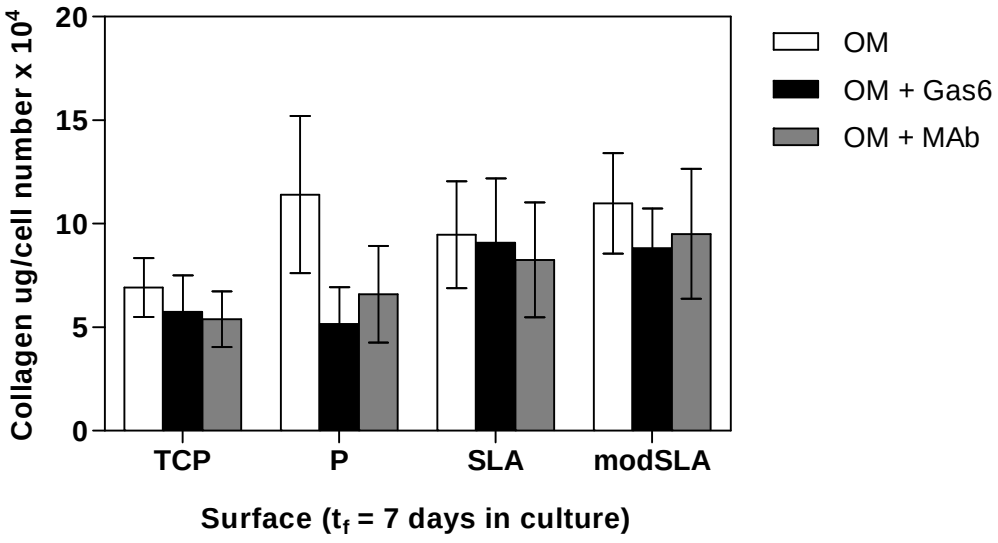

Figure 5-10 Lack of effect of Axl deregulation on cellular collagen synthesis

Bar chart with mean ± 1SD (N=3, n=1) collagen per cell number plotted against surface type. For this analysis, 25,000 cells were cultured on all surfaces in OM, OM + agonist or OM + antagonist for 7 d. Total collagen and cell numbers were estimated. The formation of

collagen was similar between the surfaces. The receptor deregulation did not affect collagen synthesis.

The ratio of extracellular matrix calcium to collagen was assessed similar to section 4.3.2.3. The results of this analysis are shown in figure 5-11. It indicates the trend observed previously for calcium per collagen ratios of samples in control conditions; modSLA > SLA > P > TCP. The receptor agonist was observed to have significantly decreased calcium to collagen ratio on TCP. A relative decrease in this ratio occurs on the rough surfaces but not on P.

The receptor antagonist increased the calcium/collagen ratio only on the modSLA; the remaining surfaces did not exhibit any significant difference.

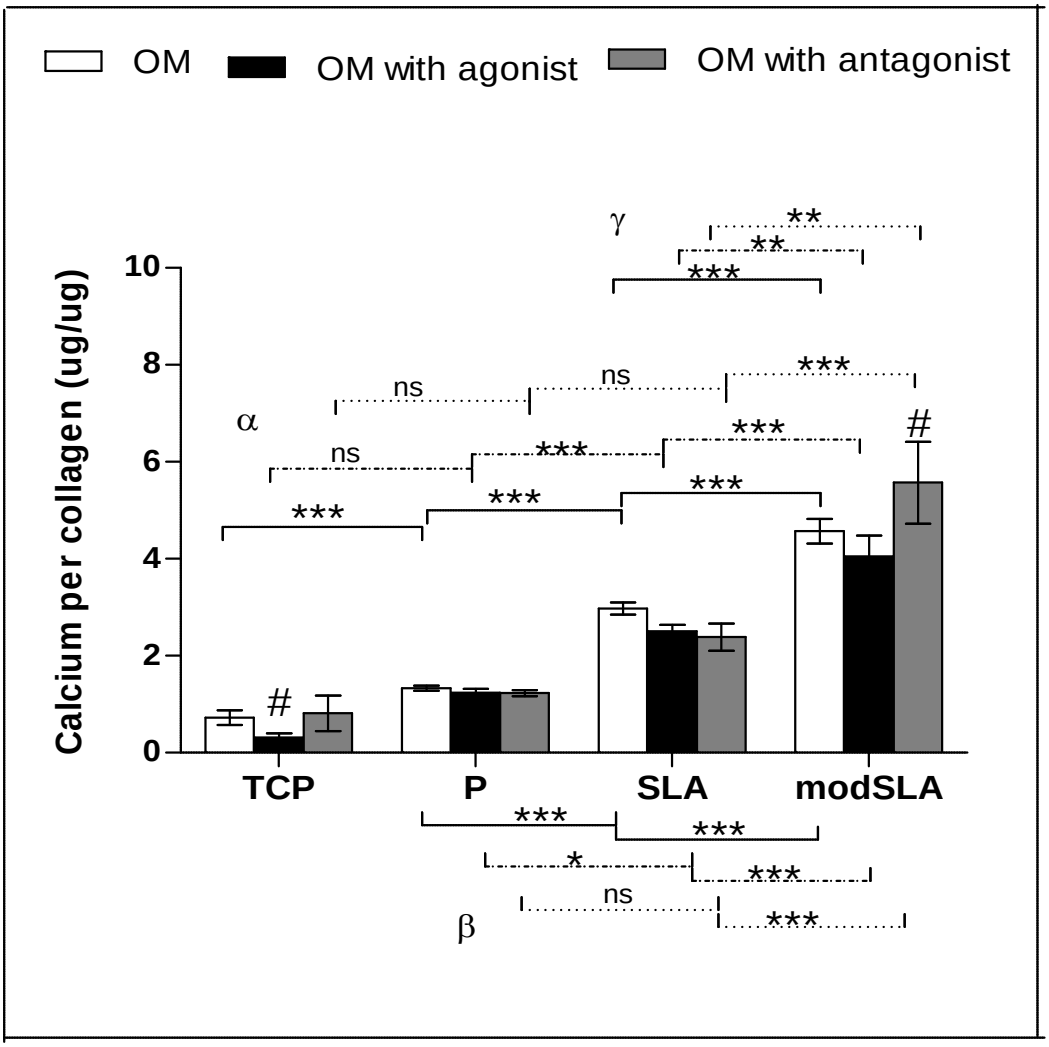

Figure 5-11 Effect of Axl deregulation on extracellular matrix Ca to collagen ratio

Bars show mean ± 1SD extracellular matrix calcium to collagen ratio values. The surfaces repeated the pattern of calcification previously observed in section 4. Receptor agonist caused a significant decrease in calcium per collagen only on TCP (tissue culture plastic). The modSLA seeded cells deposited a significantly higher calcified ECM with receptor antagonist. N=3, n=3. # = *p* < 0.05, control vs. condition of any one surface type; *, **, * = *p* < 0.05, 0.01, 0.001, respectively; ns represents non-significant. α represents a grouped comparison between the TCP and the Ti surfaces for each condition; 'β' between P vs. rough Ti surfaces; γ represents SLA vs. modSLA comparisons. Full lines represent control surface vs. surface comparisons; dashed lines (---) between agonist surface vs. surface; and dotted line antagonist surface vs. surface.**

5.3.3.3 Osteoblastic cytokine quantification

The osteoblast associated cytokines OPG and GDF-15 were quantified in culture supernatants of hMSCs on the different surfaces in control, agonist or antagonist media conditions. The results of this experiment are shown in figures 6-11 and 6-12. The OPG was expressed at a baseline by cells at this time in control medium. Both media conditions inducing receptor deregulation had modulated an increase in OPG synthesis. This increase was statistically significant for MAb compared to control, as opposed to the relatively small increase with agonist rhGas6. Additionally, the MAb cultured rough surface seeded cells secreted OPG significantly higher than TCP and P.

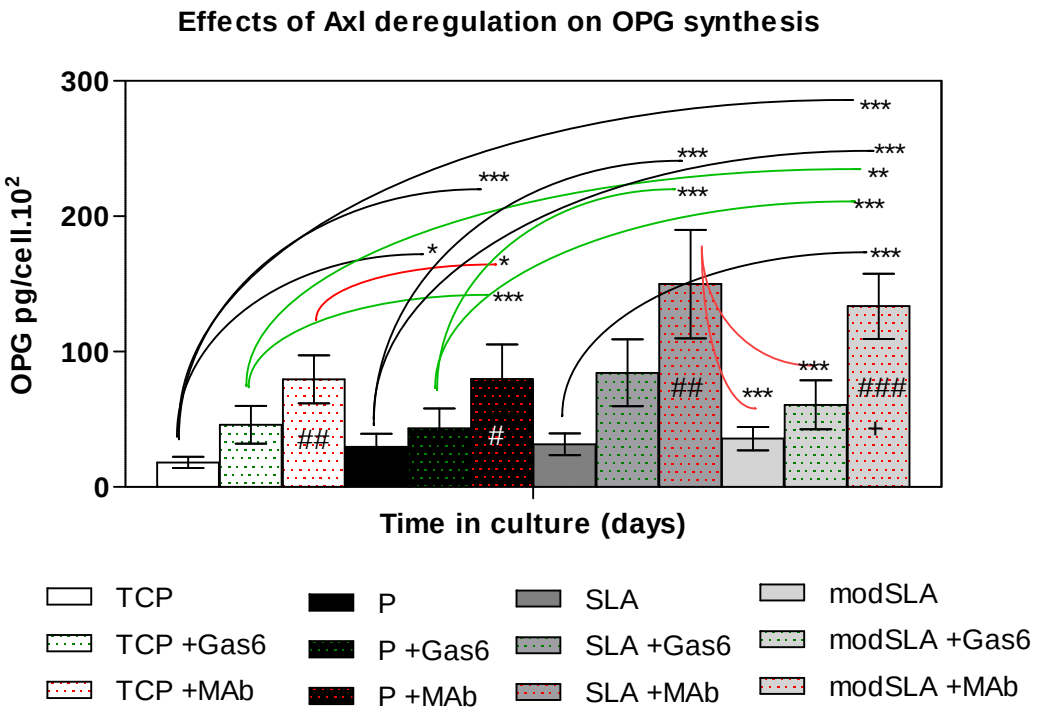

Figure 5-12 Effect of Axl receptor-deregulation on OPG synthesis

Bars show mean ± SEM; N=3, n=3. The hMSCs were cultured for 7 d on TCP, P, SLA and modSLA. Quantities of secreted OPG and cell numbers were evaluated. Results indicate receptor antagonist MAb to increase OPG levels by 7 d compared to control. #, ##, ### = *p* < 0.05, 0.01, 0.001, respectively, control vs. Condition. *, **, * = *p* < 0.05, 0.01, 0.001, respectively, samples vs. samples connected by lines. Black lines are control vs. any sample, green lines are agonist vs. any sample, and red lines are antagonist vs. any sample.**

A similar effect was obvious for GDF-15. Its secretion was relatively higher on the rough compared to smooth at 7 d in control medium. Receptor agonist did not cause any significant change compared to controls. However, the antagonist did significantly increase GDF-15 synthesis compared to control medium. Like OPG, this affect was more pronounced in cells on the rough surfaces compared to smooth.

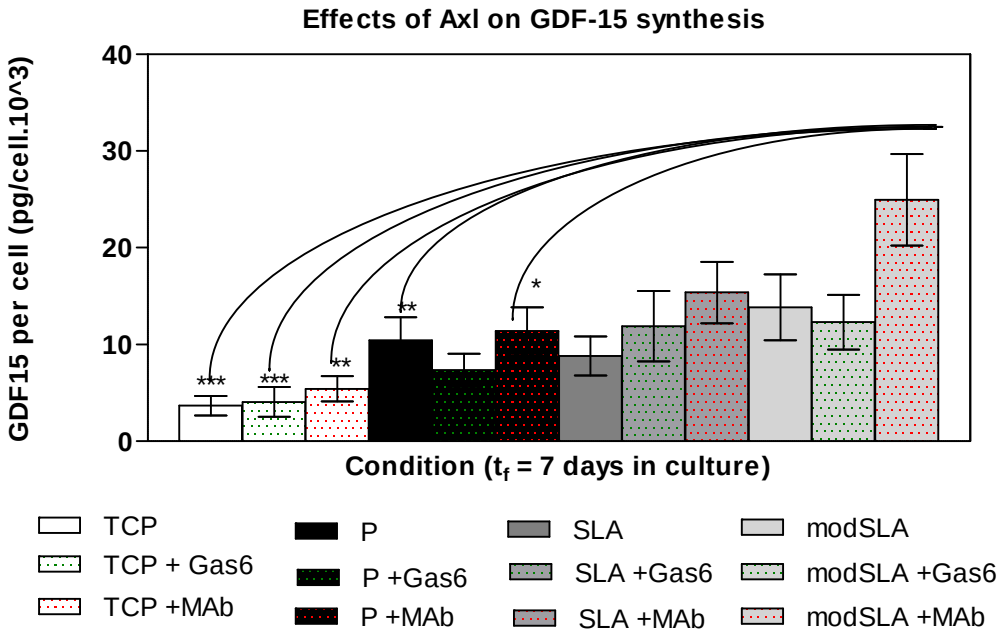

Figure 5-13 Effects of Axl receptor deregulation on GDF-15 synthesis

Bars show mean ± SEM; N=3, n=3. The hMSCs were cultured for 7 d on TCP, P, SLA and modSLA. Quantities of secreted GDF-15 and cell numbers were evaluated. Results indicate receptor antagonist MAb to increase GDF-15 levels by 7 d compared to respective control, OM only. *, **, * = *p* < 0.05, 0.01, 0.001, respectively, samples vs. modSLA connected by black lines.**

5.4 Discussion

5.4.1 Differential modulation of Axl and Gas6 in hMSCs

The expression of Axl and Gas6 was found to be influenced by surface modifications. The Axl gene was transcribed at a basal level by cells at the start of culture. Its modulation was different across the surfaces, but a general pattern comprised increasing from 1 to 3 d and then decreasing by 7d. Comparisons of Axl gene expression between the different surfaces indicate it to be temporally upregulated earlier on the rough compared to smooth; and undergoing downregulation at a similar rate in the later phase of culture.

This trend in expression of the Axl gene was also evident at the protein level. The Axl protein was detected at a lower level on the rough surfaces than smooth at 1 d, which while continually

increasing on the TCP and P, progressively decreased on the rough surfaces by 3 and 7 days. Furthermore, the state of Axl phosphorylation greatly decreased on the Ti surfaces compared to TCP through the course of culture. This state of post translational modification was relatively higher on the P than rough at 1 d but decreased to similar levels at 3 and 7 d. These indicate that cells on the rough surfaces, while probably requiring Axl receptor in the initial stage of culture, were inclined to down-regulate its activity at a comparably faster rate than on the smooth.

A similar pattern of expression was exhibited by Gas6. The molecule was nominally transcribed in GM but was markedly upregulated in OM. Its expression was similar between the surfaces at 1 d. At 3 d, it was expressed comparatively higher on the Ti than TCP. But this trend was reversed by 7 d with a higher expression of the gene on TCP than Ti. There were no significant differences between the Ti surfaces in affecting Gas6 secretion. The Gas6 protein, like the Axl molecule, was initially detected at a similar level between the samples at 1 d. Its levels increased to at 3 d on all surfaces, except for modSLA, which seemed to have had significantly decreased Gas6 synthesis at this time. The detectable levels of Gas6 decreased on all surfaces to lower level by 7 d.

The expression patterns observed for Axl and Gas6 in hMSCs on the different surfaces correspond to the trends in mineralisation recorded here, as well as in section 4. These findings suggest that the implied osteo-inhibitory function of Axl/Gas6 pathway is downregulated by the modified Ti surfaces temporally earlier than TCP or P; most likely resulting an accelerated form of phenotypic differentiation.

This notion is supported by the differential decrease in Twist1 transcription in OM over the course of culture. Its transcription follows a trend consisting of TCP > P > SLA > modSLA; inversely proportional to the extent of mineralisation achieved on these surfaces.

5.4.2 Effects of receptor deregulation on hMSC responses

The affects of deregulating the Axl/Gas6 pathway were examined on hMSC responses to the modified Ti surfaces. The responses evaluated were proliferation, osteogenic mineralisation and

cytokine secretion. The proliferation analysis indicated that receptor signaling was not important for cellular viability.

The effects of Axl deregulation were, however, starkly obvious in the experiments querying osteogenic mineralisation and osteoblastic cytokine synthesis. Osteogenic mineralisation, in terms of calcium deposited per cell, followed the similar trend observed in section 4, consisting of a higher mineral content on modSLA > SLA > P > TCP. The presence of Gas6 decreased mineralisation but did not inhibit it. This is considered largely to be due to the inefficiency of the applied method in completely blocking the paracrine release of Gas6. The agonist induced decrease in calcium mineralisation was markedly higher on TCP than the Ti. A proportionally expected increase in calcium mineralisation compared to control condition occurred only for modSLA with receptor antagonist. It also increased OPG and GF-15 synthesis in cells on the rough.

5.4.3 Significance of findings

The Axl receptor is assigned a role in cellular osteogenic differentiation. It is suggested to be important in the initial phases of osteogenic differentiation following induction but is required to be downregulated for calcium mineralisation to occur. The findings show that Axl and Gas6 are downregulated by cells during a 7 d culture period; the end time point corresponding with detectable calcium mineralisation. This downregulation is seemingly initiated earlier on the rough surfaces than smooth.

Deregulating receptor signaling can generate a contrast in cellular responses compared to control. The findings show that (i) increasing receptor signaling can impede calcium mineralisation but decreasing it does not enhance the process; (ii) decreasing receptor signaling can augment osteoclastic regulators OPG and GDF-15 secretion; and (iii) the impediment of mineralisation is higher on TCP, while augmentation of OPG and GDF-15 is higher on rough, when measured at a 7 d time point. These strongly suggest that the Axl/Gas6 pathway plays a part in the initial phases of osteogenic differentiation; in which it is steadily downregulated as the cell progresses from the state of an uncommitted state to a maturing naïve-osteoblastic phenotype.

This idea is inferred from the comparative outlook of cellular responses to the different surfaces, which reveal cells to seemingly differentiate and mineralize in a temporally enhanced manner in response to the rough surfaces compared to TCP and P. Accordingly, at the 7 d time point, whilst the cells on the rough surfaces have undergone a relatively farther level of osteogenic differentiation, those on the TCP are still in a upstream phase of differentiation; resulting in relatively higher mineral content on the rough compared to smooth at this time.

Being in a relatively precursory state than an osteoblastic phenotype, the hMSCs on the TCP seem relatively more prone to the osteo-inhibitory effects of Axl agonist on mineralisation. While this may also have been the case for the rough surfaces, the detection of this event by 7 d would not have been permissive due to the stimulus to heighten mineralisation incurred by cells on the rough. However, these do represent a state of phenotype much differentiated and mature than the TCP and P at 7 d. In these cells, mineralisation due to the relatively mature state of cells may not be affected by receptor deregulation; however, their process to synthesise and secrete osteoclastic modulators is enhanced several fold by blocking receptor signaling. This may be perceived as the effect of receptor deregulation on cells, at a farther state of osteoblastic differentiation, on the rough.

The Axl / Gas6 pathway's (i) importance in early cell-substrate events; (ii) downregulation prior to calcium mineralisation; (iii) upregulation decreasing mineral content; and (iv) enhancement of phenotypic marker synthesis in the relatively more differentiated rough surface seeded cells imply an association of the pathway with hMSC stemness, and its association with the enhanced transformation to a committed phenotype on the rough surfaces.

5.5 Summary

The Axl / Gas6 pathway is differentially modulated by hMSCs on the different surfaces. The main points are.

- The Axl receptor and its cognate ligand Gas6 are downregulated at the genetic and protein levels on the rough Ti surfaces earlier than polished and even more on plastic; suggesting that a reduction in signaling might underlie the enhancement in osteogenic parameters by modified substrates.
- The pathway affects calcium deposition but not ECM formation. The Axl agonist significantly decreases ECM calcification. This decrease is relative to the surface type.
- The pathway affects osteoblastic marker secretion. The Axl antagonist increases levels of OPG and GDF-15, which are promoted by the rough Ti surfaces.
- The collection of results suggests that hMSCs require Axl pathway initially following substrate contact; but that as the point of initiation of mineralisation approaches, it is downregulated. This downregulation is temporally enhanced on the rough surfaces.
- This implies that the pathway may be important to the pre-osteoblastic phase of a differentiating hMSC, whose function might likely be associated with stemness.

6 Differential regulation of hMSC pluripotency gene expression

6.1 Introduction

Modified Ti surfaces exert an observable enhancement on hMSC differentiation and function. This differential effect is believed to be modulated by transcriptional changes in various genetic clusters that govern specific aspects of cellular function. An aspect of interest is the cellular specimens' plasticity to functionally differentiate to an osteoblastic phenotype. Experimental evidence derived from embryonic stem cell research strongly indicates that the cohort expression of a particular set of genes imparts cellular plasticity by engaging relevant cell regulatory processes, which prevent lineage commitment and phenotypic differentiation. This is reinforced by the observation of the presence of transcripts of various lineage specifying transcription factors in un-induced or undifferentiated adult stem cells.

It is implied that if not all, then a subset of the implicated stemness genes will have to be expressed in uncommitted hMSCs to maintain their undifferentiated state. These genes will incur transcriptional change once the hMSC receives an over-writing pleiotropic stimulus from its direct microenvironment. In the context of the present study, the microenvironment constitutes medium and substrate, which due to the multiple subtypes of both variable, would variably affect the comparative loss of expression of stemness related genes.

The hypothesis of this section of the study stated that different Ti substrates would differentially down regulate stemness gene expression in hMSCs. Furthermore, it considers this differential regulation of gene expression to be modulated, in part, by the Axl/Gas6 signaling pathway; according to which, it extends to state that the differential regulation and activity of the Axl receptor and its ligand Gas6 is linked to any loss of stemness genes on the respective surfaces.

This hypothesis was evaluated by comparing the expression of a select set of 96 genes in hMSCs using Taqman microfluidic 384 well card miniarrays. These were procured with the award from the University of London Central Research Fund. The arrays comprise four sets of genes, categorized

on their implicated function: controls, maintenance of pluripotency, correlation to stemness, and differentiation markers. These genes are selected from the findings of the International Stem Cell Initiative consortium (International Stem Cell Initiative, 2007). They represent a defined set of validated genetic markers normally associated with human embryonic stem (ES) cell identity. The details of the four gene sets in the frame of stem cell science are tabulated in tables 9-11, 9-12, 9-13 and 9-14 (Appendix V), respectively.

This experiment was conducted by seeding hMSCs on the P, SLA and modSLA Ti surfaces. Analyses were conducted at 1 and 7 days post seeding comparing two different sets of conditions. Samples cultured in GM and OM only were assayed at 1 d post seeding. While samples cultured in OM, OM with agonist (rhGas6) or OM with antagonist (MAb) were assayed at 7 d. The former addressed the immediate changes caused by surface topography, while the latter evaluated Axl's possible involvement in modulating the stemness gene expression changes.

6.2 Experimental protocols

6.2.1 Miniarray RT-PCR analysis

The effects of modified Ti surfaces and of Axl/Gas6 signaling on hMSC stemness gene expression were evaluated by quantifying fold differences in the expression of cellular stemness related genes. The analysis was conducted with Taqman Stem Cell Pluripotency Microfluidic Arrays (AppliedBiosystems; 4385344). These arrays are specialized 384-well plates (8rows, 48 columns) that contain four assortments of 96 genes distributed across two 48 well rows.

The experiment was conducted by culturing hMSCs from three donors (N=3, n=1) on polished, SLA and modSLA at a density of 1.25x 10^4 cells.cm^{-2} in GM, OM, OM with receptor agonist (OM + rhGas6) and OM with receptor antagonist (OM + MAb). Samples were assayed for gene expression at 1 day (GM and OM) and at 7 days (OM, OM+Gas6 and OM+MAb) according to the methods described in section. The arrays were processed in an AppliedBiosystems 9700 Real Time PCR thermocycler at the UCL Institute of Child Health (London, UK). The receptor agonist used in these experiments was recombinant human Gas6 (rhGas6), used at a concentration of 1 µg.ml^{-1} (detailed in section 2.11.2). The receptor antagonist (MAb) was a mixture of recombinant proteins: these were Axl-extra cellular domain and anti-Axl/anti-Gas6 monoclonal antibodies (MAb; Cf = 4 ug.ml^{-1} of Axl-extra cellular domain; with anti-Axl blockade monoclonal antibodies, Cf = 2.5 µg.ml^{-1}; and anti-Gas6 monoclonal antibodies, Cf = 10 µg.ml^{-1}).

6.2.2 Miniarray data analysis

Fold values of sampled genes were calculated from the threshold cycle ‘Ct’ values, which were then computed with the 2^{-ddCt} formula to obtain relative fold differences between the genes. Samples were calibrated to the reference control, which consisted of cells in suspension prior to seeding. The gene used here as a calibrator was 18S RNA. Mean values from three donors were plotted in a heatmap with the R software. This map was composed of an x-axis with samples and y-axis with genes. The entities represented on these axes were clustered into groups on the basis of similarity.

This similarity was measured using the Euclidean distance. The default heat map colors are from red for low values, to orange or yellow or white, for medium and high values, respectively.

6.3 Results

6.3.1 Overview

A total of 43 of the 96 genes analysed were found expressed in hMSCs. These were expressed in the references sample (t = 0, cells in suspension) as well as target samples. A total of 53 genes were not detected expressed in the reference and target samples. This was considered to be due to their putative embryonic stem cell specific nature; and hence, the likelihood of not being transcribed in the hMSCs used in this study. These were in addition to the non-expression of differentiation markers incapable of being transcribed in the osteogenic inductive media.

The transcribed genes were 18S ribosomal RNA (endogenous control); ACTB; ACTC; BRIX; CD9; CGB; COL1A1; COMMD3; CRABP2; CTNNB1; DES; DNMT3B; FGF5; FLT1; FN1; GABRB3; GAPD; GATA6; GFAP; GRB7; IFITM1; IFITM2; IL6ST; IMP2; KIT; LAMA1; LAMB1; LAMC1; LIFR; Nanog ; NES; NOG; NR6A1; PECAM1; PODXL; POU5F1; RAF1; REST; RUNX2; SEMA3A; SERPINA1; SST; and SYP. The details of these genes are provided in tables 10-4, 10-5, 10-6 and 10-7 (Appendix II).

The results of this analysis are presented in two stages. A graphical representation of the collective data sets is illustrated in a heatmap in figure 7-1. This was generated with the R software courtesy of Dr Shazia Anjum of the UCL Institute of Child Health (London, UK). It represents mean fold values derived from three donor analyses (N = 3), assayed in one experimental instance (n = 1). In the presented figure, detected genes form the vertical axis and samples, arranged in an ascending order, form the horizontal axis. The genes displaying similar patterns of expression are highlighted on a dandogram drawn on the left vertical axis of the map; calculated with the Euclidean distance algorithm.

This is followed by a description of the individual gene sets (controls; maintenance of stemness; correlation of stemness; differentiation genes) with horizontal single gene bar charts depicting individual gene's expression.

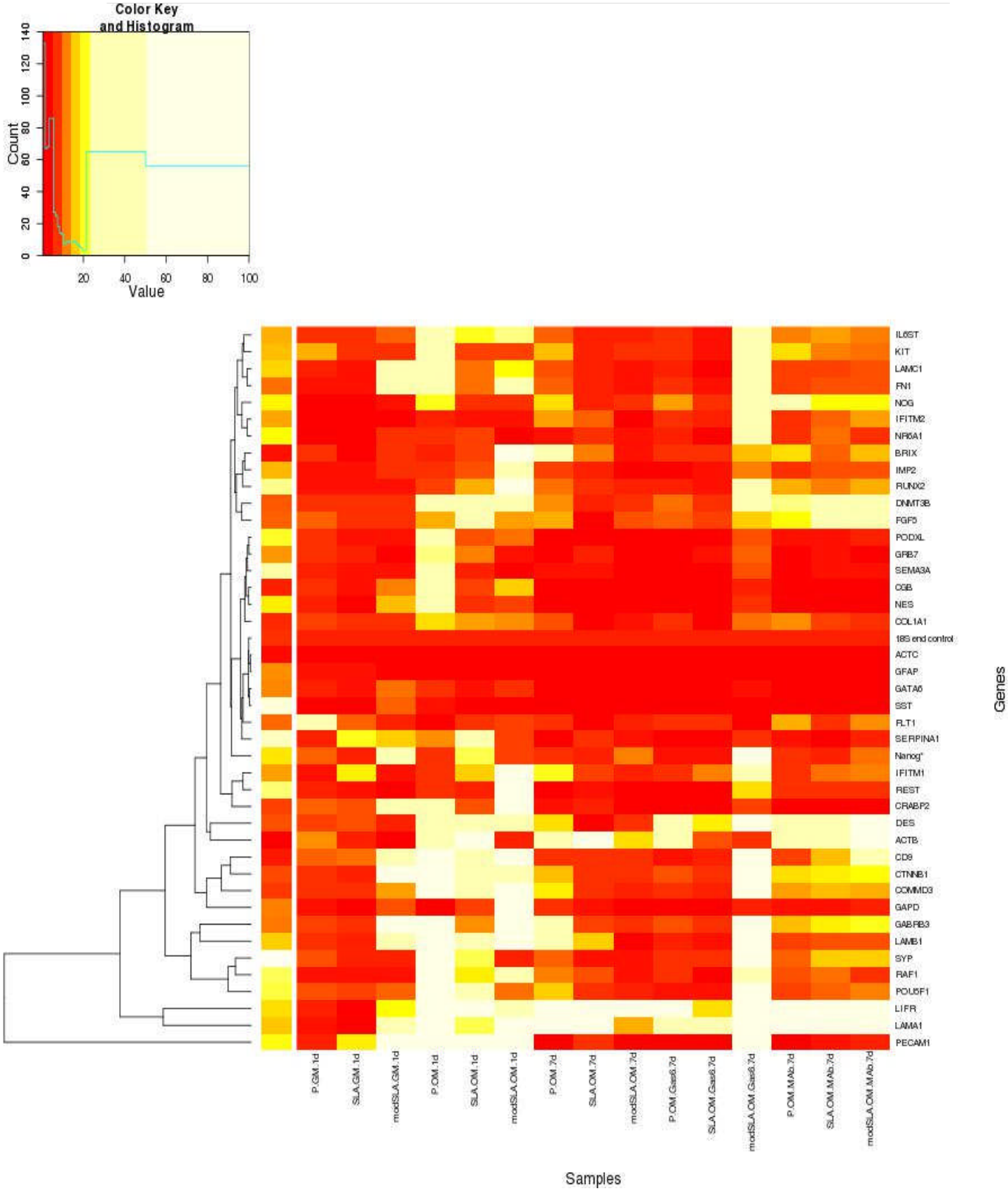

Figure 6-1 Expression values from human pluripotency miniarrays

Image is a heatmap of fold expression values derived with the $2^{-\Delta\Delta Ct}$ method. The hMSCs were cultured on P, SLA and modSLA. Gene expression was analysed at 1 d in growth and osteogenic media only, and later at 7 d between OM alone, OM with agonist Gas6 and OM with antagonist MAb. Plots represent mean values of N = 3, n = 1. Key provided top left.

6.3.2 Controls

18S RNA was used as the endogenous reference to calculate relative fold expression levels. It along with the control genes β-actin, β-catennin, GAPDH (glyceraldehyde dehydrogenase) and RAF1 oncogene were expressed in all samples analysed. The EEF1A1 gene was not detected. The 18S RNA was found to be expressed invariably in all samples whilst the remaining did display surface or condition dependent changes.

ACTB was transcribed lower in GM than OM at 1 d. It was expressed higher on polished than rough at 1 d in both media conditions. Its expression increased by 7d in OM.It was transcribed at a higher fold value on polished than rough in OM only. Axl receptor agonist decreased its expression, while Axl antagonist increased it on all surfaces.

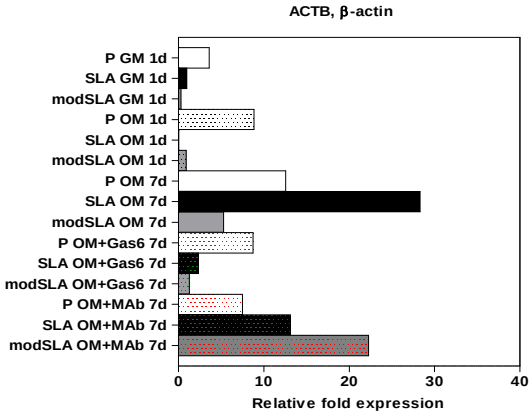

Figure 6-2 Miniarray analysis of effects of Axl signaling on ACTB gene expression

A vertical bar chart with mean relative fold expression values from three donors plotted along the x-axis (N=3, n=1) against samples on the y-axis. Gene cards define ACTB (β-actin) as a non-muscle cytoskeletal protein likely involved in cellular shape. The gene was expressed higher on the P than rough at 1 d in both media. Its expression increased on the rough at 7 vs. 1 d. Axl agonist decreased expression of the gene, particularly on the rough than P, when compared to OM. Axl antagonist increased expression on the rough relative to OM and OM with agonist. The gene, being a cytoskeletal component suggests an association of Axl signalling with modifications of cellular shape.

The expression pattern of Beta-catennin (figure 6-3) seemed condition and surface dependent. It was upregulated starkly at 1 d in cell cultured in growth medium on the modSLA but not SLA nor

polished surfaces. While expression decreased by 7 d in osteogenic medium (OM) and OM supplemented with Axl agonist, the Axl antagonist caused an increase in expression on all surfaces.

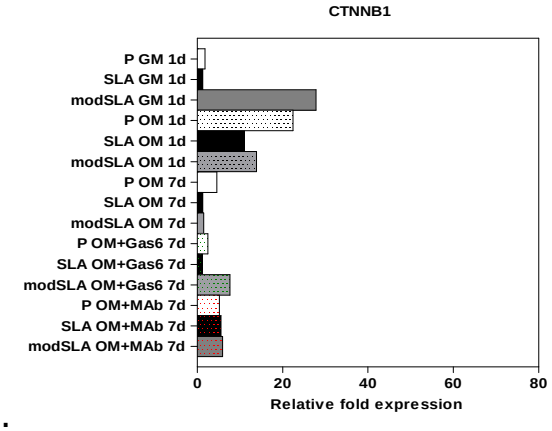

Figure 6-3 Miniarray analysis of effects of Axl signaling on CTNNB1 gene expression

A vertical bar chart with mean of the relative fold expression values from three donors plotted on the x-axis (N=3, n=1). Gene cards define CTNNB1 (cadherin-associated β-cantenin) as an adherins junction associated molecule that apart from regulating cellular adhesion, acts as a downstream effector of ligand induced canonical Wnt pathway. The gene was upregulated several fold by modSLA at 1 d in GM. Expression was raised several fold by all samples in OM. Expression had downregulated to similar levels by 7 d in OM. Agonist did not have a notable effct on P nor SLA; but did incur a small upregulation on modSLA. All surfaces were upregulated by receptor antagonist.

The GAPD gene, not shown here, had been modulated higher on the rough compared to polished but differences were absent at 7 d in all conditions. The RAF1 oncogene (figure 6-4) was found expressed in all samples. Its expression was relatively higher on the modSLA than polished and SLA at 1 d in both media conditions. Its expression was found higher on polished than both rough surfaces at 7 d in OM. The Axl agonist seemed to have reduced expression in cells cultured on polished and SLA at 7 d compared to an increase on the modSLA. The Axl antagonist had slightly increased transcription of the gene, the levels of which were similar between the surfaces.

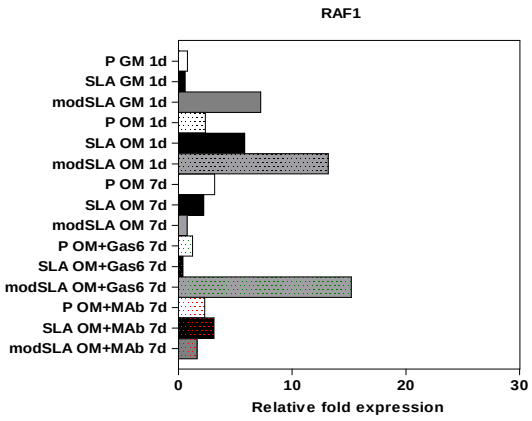

Figure 6-4 Miniarray analysis of effects of Axl signaling on RAF1 gene expression

A vertical bar chart with mean of the relative fold expression values from three donors plotted on the x-axis (N=3, n=1). Gene cards define RAF1 (MAP kinase kinase kinase) as a serine/threonine kinase that is activated by the small GTPase molecule Ras and transduces a mitogenic signals from cell membrane to the nucleus. This gene was upregulated several fold by modSLA at 1 d in GM and OM. Expression decreased in all samples by 7 d, but was relatively higher on the P than rough surfaces. Agonist seemed to decrease expression while antagonist slightly increased expression of the gene.

6.3.3 Maintenance of pluripotency

Five of the seven genes of this category were detected expressed in all samples. The expressed genes were DNMT3B, fibrobrlast growth factor 5 (FGF5), GABRB3, Nanog and POU5F1. The unexpressed genes were SOX2 and GDF3. DNMT3B (figure 6-5), FGF5 (figures 6-6) and GABRB3 (figure 6-7) displayed similar patterns of expression, comprising a relative increase on modSLA in GM and polished in osteogenic medium at 1 d. This was seemingly followed by a downregulation at 7 d in OM, with the Axl antagonist upregulating expression of genes at this time.

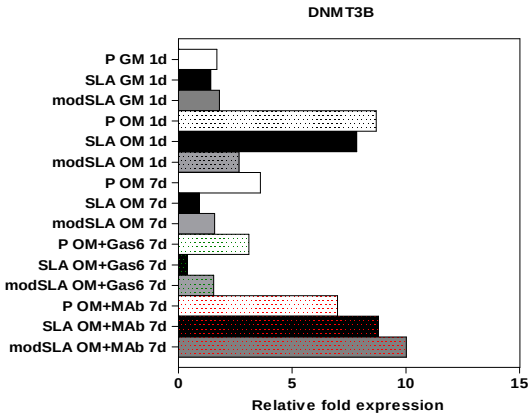

Figure 6-5 Miniarray analysis of effects of Axl signaling on DNMT3B gene expression

A vertical bar chart with mean of the relative fold expression values from three donors plotted on the x-axis (N=3, n=1). Gene cards define DNMT3B (DNA (cytosine-5-)-methyltransferase 3 beta)) as DNA methylating factor that methylates non-methylated CpG islands. this gene was upregulated several fold by modSLA at 1 d In GM. The OM showed an inverse trend to that of GM 1d with expression comparatively higher on P and SLA. Expression decreased in all samples by 7 d, but was relatively higher on the P than rough surfaces. Agonist seemed to non-affect expression while antagonist markedly increased expression of the gene in all samples.

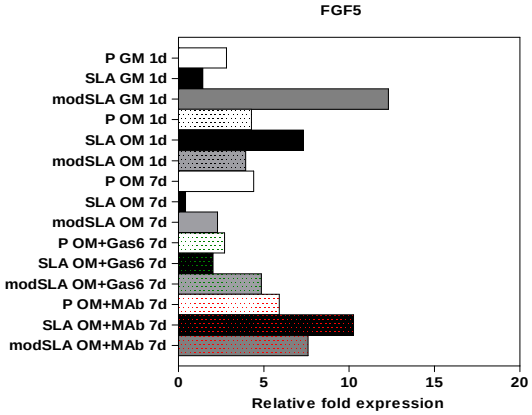

Figure 6-6 Miniarray analysis of effects of Axl signaling on FGF5 gene expression

A vertical bar chart with mean of the relative fold expression values from three donors plotted on the x-axis (N=3, n=1). Gene cards define FGF5 (fibroblast growth factor 5) as an oncogene that can transform cells upon transfection. This gene was upregulated several fold by modSLA at 1 d In GM. In OM, samples expressed the gene at near similar levels. Expression had decreased in all samples by 7 d, but was relatively higher on the polished

than rough surfaces. Agonist did not seem to affect expression while antagonist markedly increased expression of the gene in all samples.

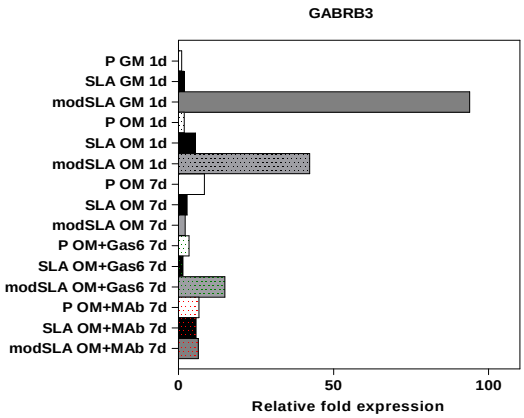

Figure 6-7 Miniarray analysis of effects of Axl signaling on GABRB3 gene expression

A vertical bar chart with mean of the relative fold expression values from three donors plotted on the x-axis (N=3, n=1). Gene cards define GABRB3 (gamma-aminobutyric acid (GABA) A receptor, beta 3) is the major inhibitory neurotransmitter in the vertebrate brain, which mediates neuronal inhibition by binding the GABA/benzodiazepine receptor and opening an integral chloride channel. This gene was upregulated several fold by modSLA at 1 d In GM and OM. The gene was detectable at low levels in all samples by 7 d in OM, with expression seemingly higher on P than the rough. Agonist did not affect expression while antagonist markedly increased expression of the gene in all samples.

The PO5F1 gene (figure 6-8) was upregulated slightly by modSLA compared to other surfaces in growth medium at 1 d. Its expression was highest on SLA, being similar on the others, in osteogenic medium at this time. Expression was higher on polished than rough at 7 d in OM. The Axl antagonist had caused an increase in levels of this gene on all surfaces by this time. Nanog, shown in figure 6-9, displayed a pattern of expression similar to POU5F1.

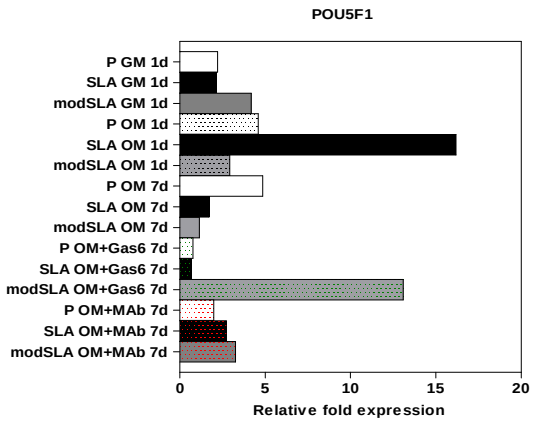

Figure 6-8 Miniarray analysis of effects of Axl signaling on POU5F1 gene expression

A vertical bar chart with mean of the relative fold expression values from three donors plotted on the x-axis (N=3, n=1). Gene cards define POU5F1 (POU class 5 homeobox 1) forms a trimeric complex with SOX2 and controls the expression of a number of genes involved in embryonic development. This gene was expressed at similar levels by cells at 1 d in GM and OM, apart from an unexpected increase by the SLA. Its expression remained high on the P by 7 d, while having decreased several fold on the rough. Agonist did not affect expression apart from an upregulation on modSLA. Antagonist increased experssion of the gene compared to the 7d control samples.

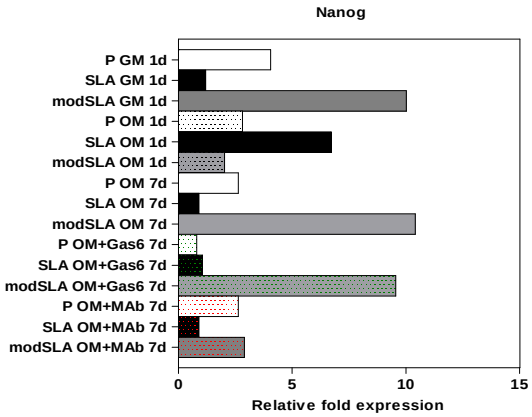

Figure 6-9 Miniarray analysis of effects of Axl signaling on NANOG gene expression

A vertical bar chart with mean of the relative fold expression values from three donors plotted on the x-axis (N=3, n=1). Gene cards define NANOG as a transcription factor that regulates inner cell mass and embryonic stem cell proliferation and self-renewal. This gene was expressed higher on the modSLA in GM and SLA in OM at 1 d. Expression seemed to be retained at a higher level by 7 d on modSLA but had decreased on the P and SLA surfaces. The agonist and antagonist relatively decreased expression of the gene compared to 7 d controls.

6.3.4 Correlation with stemness

A total of fifteen genes were detected expressed in this category. These were BRIX, CD9, COMMD3, CRABP2, GRB7, IFITM1, IFITM2, IL6ST, IMP2, KIT, LIFR, NOG, NR6A1, PODXL, and REST.

BRIX was transcribed at 1 d in all samples (figure 6-10). It was not differentially modulated at 1 d in GM, but was increased several fold on the modSLA in OM. Its expression was detected at 7 d in OM; higher on polished than SLA than modSLA. This trend in expression was not present in presence of Axl agonist; expression was downregulated. The Axl antagonist had caused an observable increase in expression.

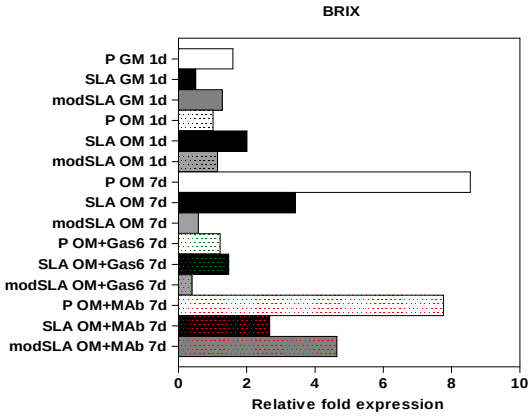

Figure 6-10 Miniarray analysis of effects of Axl signaling on BRIX gene expression

A vertical bar chart with mean of the relative fold expression values from three donors plotted on the x-axis (N=3, n=1). Gene cards define BRIX as a protein required for the biogenesis of the 60S ribosomal subunit. This gene was expressed at similarly low levels in cells cultured on all surfaces. Expression had increased on the P and SLA surfaces compared to modSLA t 7 d. Agonist reduced expression while antagonist increased it.

CD9 (figure 6-11) and COMMD3 (6-12) displayed similarities in expression patterns, although the expression of CD9 was magnitudinally several fold higher. These genes were modulated relatively higher on modSLA than other surfaces at 1 d in GM. OM caused an upregulation in all samples compared to GM. Expression levels of both genes were detectable at 7 d in OM but at relatively

lower levels than the initial time point. The addition of Axl agonist caused a decrease in expression whereas Axl antagonist caused an upregulation, which in the case of CD9 seemed surface dependent being higher on modSLA than SLA than polished.

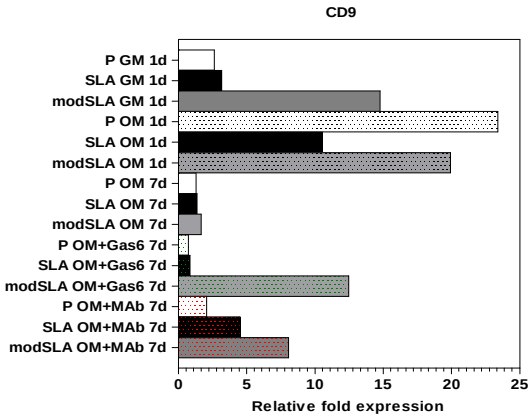

Figure 6-11 Miniarray analysis of effects of Axl signaling on CD9 gene expression

A vertical bar chart with mean of the relative fold expression values from three donors plotted on the x-axis (N=3, n=1). Gene cards define CD9 as a member of the tetraspanins, a class of cell surface glycoproteins with four transmembrane domains that form multimeric complexes with other cell surface, and are involved in differentiation, adhesion, and signal transduction. The gene was markedly upregulated by modSLA than polished and SLA at 1 d in GM. The OM caused an upregulation in all samples. Expression of the gene had decreased to lower levels in all samples by 7 d. Agonist generally seemed to have decreased expression compared to controls; it displayed increased expression on modSLA. Antagonist increased expression in all surfaces relative to OM only; this increase was higher for modSLA than the other surfaces.

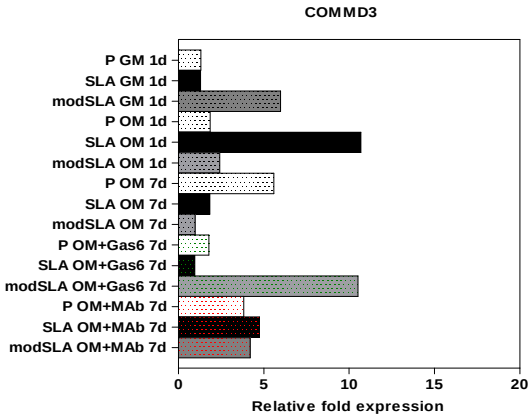

Figure 6-12 Miniarray analysis of effects of Axl signaling on COMMD3 gene expression

A vertical bar chart with mean of the relative fold expression values from three donors plotted on the x-axis (N=3, n=1). Gene cards define COMMD3 (COMM domain containing 3) is a protein that may negatively regulate the activation of NF-kappa-B by associating with a homolog, COMMD1. Expression of COMMD3 was present at 1 d in all samples, being comparatively higher on the modSLA and SLA surfaces in GM and OM, respectively. Expression was detected at low levels in all samples at 7 d. Agonist seemed to decrease while antagonist increased expression.

CRABP2 (figure 6-13) and GRB7 (6-14) displayed similarities in expression patterns. These genes were comparatively expressed higher on modSLA at 1 d post seeding in GM but in a reverse trend in OM with polished displayed higher fold expression than both rough surfaces. The genes seemed expressed very similarly at 7 d post seeding. Expression had decreased at this time in osteogenic medium only. Axl agonist seemed to have had no effect but a slight upregulation was detectable for CRABP2, while GRB7 seemed selectively downregulated in rough surface seeded cells by the Axl agonist and antagonist at this time point.

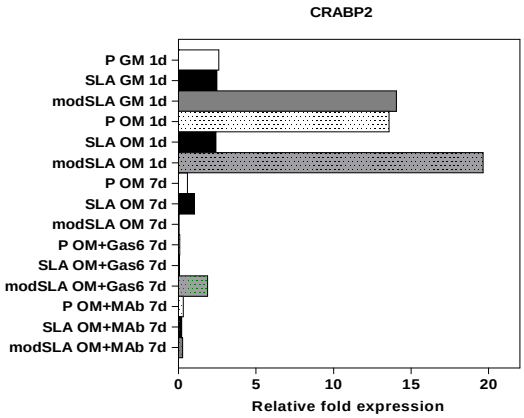

Figure 6-13 Miniarray analysis of effects of Axl signaling on CRABP2 gene expression

A vertical bar chart with mean of the relative fold expression values from three donors plotted on the x-axis (N=3, n=1). Gene cards define CRABP2 as a cytosol-to-nuclear shuttling protein that transports retinoic acid to its cognate receptor. The gene was expressed at 1 d in all samples. At 1 d in GM, it was expressed highest on modSLA while OM caused an increase in expression in both P and modSLA samples. Expression had decreased starkly by 7 d with no-transcripts detected for modSLA. Agonist abolished expression of the gene in P and SLA while increasing it on modSLA, when compared to OM only controls. Antagonist starkly reduced expression of the gene in all samples.

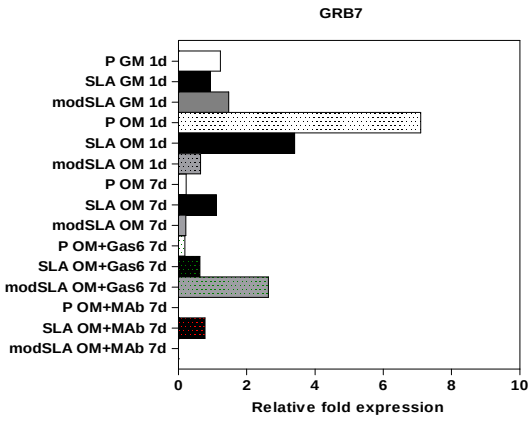

Figure 6-14 Miniarray analysis of effects of Axl signaling on GRB7 gene expression

A vertical bar chart with mean of the relative fold expression values from three donors plotted on the x-axis (N=3, n=1). Gene cards define GRB7 (growth factor receptor-bound protein 7) as an adaptor molecule that interacts with the cytoplasmic domains of tyrosine kinases, mainly epidermal growth factor receptor and ephrin receptors. GRB7 was detected at similar levels at 1 d in GM in all samples. Its expression was markedly increased by the P in OM than both rough surface, which differed with a higher comparative expression on SLA. Expression of the gene was present at 7 d in OM. Agonsit increased expression on modSLA but antagonist seemed to abolish expression in P and modSLA while not affecting cell on SLA.

IFITM1 (figure 6-15) and IFITM2 (figure 6-16) displayed similar expression at 7 d in OM; being higher on P than the rough. Agonist and antagonist increased expression on rough compared to P. At 1 d, however, the genes were different. The former was transcribed higher in OM on the rough. The latter was not initially expressed.

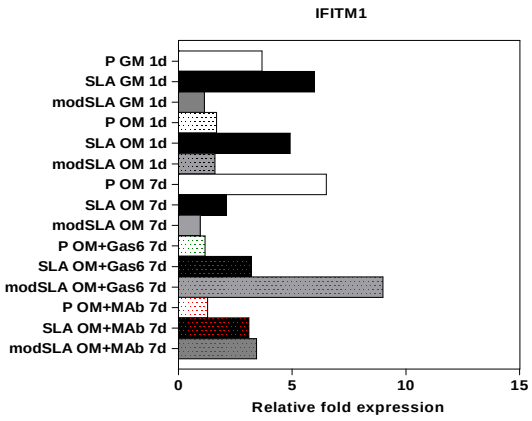

Figure 6-15 Miniarray analysis of effects of Axl signaling on IFITM1 gene expression

A vertical bar chart with mean of the relative fold expression values from three donors plotted on the x-axis (N=3, n=1). Gene cards define IFITM1 (interferon induced transmembrane protein 1) as an antiviral protein that mediate cellular innate immunity, multimeric complex involved in the transduction of antiproliferative and homotypic adhesion. IFITM1 was expressed higher on P and SLA in GM at 1 d. OM had reduced expression of the gene but not on the SLA surface. Expression at 7 was highest on P > SLA > modSLA. Agonist and antagonist increased expression on the rough surfaces while reducing its expression on the P surface.

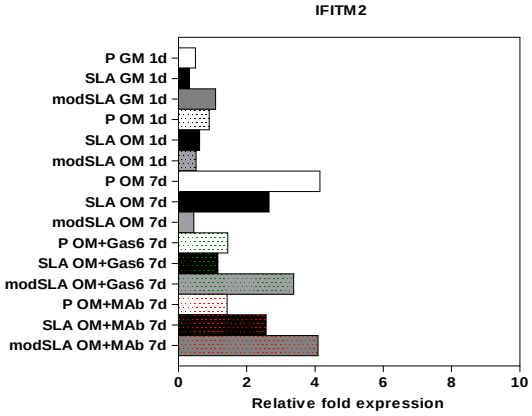

Figure 6-16 Miniarray analysis of effects of Axl signaling on IFITM2 gene expression

A vertical bar chart with mean of the relative fold expression values from three donors plotted on the x-axis (N=3, n=1). Gene cards define IFITM2 (interferon induced transmembrane protein 2) is a protein similar to IFITM1 but also implicated in the Induction of cell cycle arrest and apoptosis by caspase activation independent of p53. Its expression was at a similarly low level on all surfaces at 1 d in both media. Its expression had increased

by 7 d on P than rough, and was higher on SLA than modSLA. Agonist and antagonist increased expression on the rough surfaces compared to P.

The analysis grouped IL6ST, IMP2, KIT, NOG and NR6A1 genes together. This was due to similarities in their patterns of expression at certain times and condition. The IL6ST gene, shown in figure 6-17, seemed modulated higher in osteogenic than growth medium at 1 d. It was expressed relatively higher on modSLA in GM and P in OM. Its expression had decreased by 7 d in OM on all surfaces. Addition of Gas6 did not affect gene expression (considering modSLA OM+Gas6 7d as possibly erroneous). However, receptor antagonist did cause notable increase in expression relative to OM and OM + Gas6 in all samples.

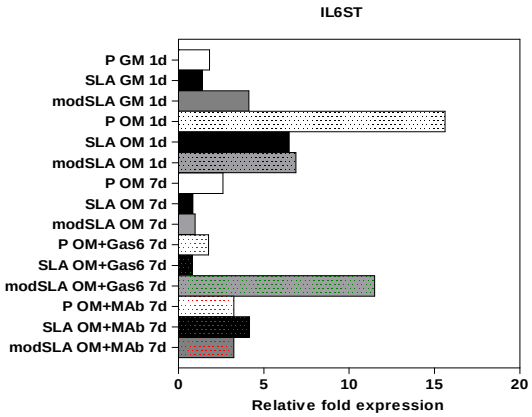

Figure 6-17 Miniarray analysis of effects of Axl signaling on IL6ST gene expression

A vertical bar chart with mean of the relative fold expression values from three donors plotted on the x-axis (N=3, n=1). Gene cards define IL6ST (interleukin 6 signal transducer) as a signal transduction molecule, associated with the receptors for key immunity related cytokines. IL6ST was expressed at a higher level by P cultured cells in OM. Its expression had decreased by 7 d on all surfaces. While agonist seemed to induce a downregulation, antagonist caused an upregulation of the gene at 7 d.

IMP2 (figure 6-18) was modulated very small fold relative to time zero reference. It was expressed lower in GM than OM; being higher on modSLA on the former, while bearing an inverse trend in OM. Peak expression of the gene occurred on P at 7 d in OM only, which was higher than SLA and then modSLA. Receptor Axl deregulation decreased expression across all samples relative to OM.

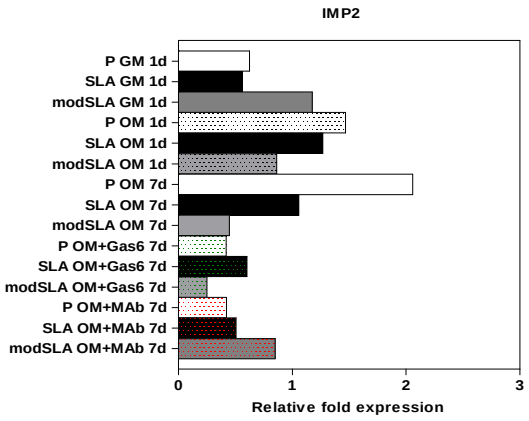

Figure 6-18 Miniarray analysis of effects of Axl signaling on IMP2 gene expression

A vertical bar chart with mean of the relative fold expression values from three donors plotted on the x-axis (N=3, n=1). Gene cards define IMP2 as the enzymatic sub-unit of an inner mitochondrial protein complex, which cleaves transit peptides and facilitates the targeting of the molecules to the inner mitochondrial matrix. IMP2 was found expressed comparatively higher on the modSLA and P in GM and OM, respectively. Expression of the gene was retained by 7 d with higher fold expression on the P than rough. Agonist and antagonist decreased expression on P but did not affect the rough surface seeded cells.

KIT (figure 6-19) was similar in their patterns of expression. It was upregulated by P compared to rough in GM and OM at 1 d. It remained upregulated on P compared to rough at 1 d in OM. Agonist decreased expression on P but not rough. Axl agonist increased expression in all samples.

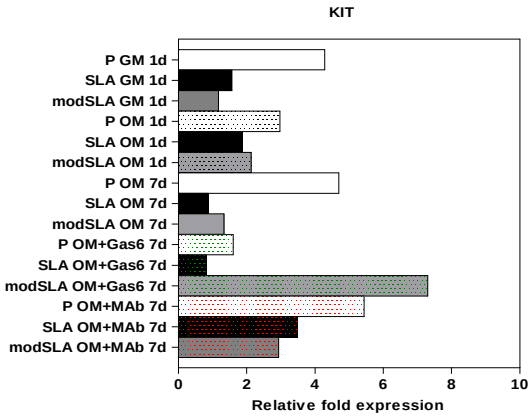

Figure 6-19 Miniarray analysis of effects of Axl signaling on KIT gene expression

A vertical bar chart with mean of the relative fold expression values from three donors plotted on the x-axis (N=3, n=1). Gene cards define KIT as a tyrosine kinase protein that acts as a receptor for stem cell factor. Kit was expressed higher on P surface at 1 d in both media types. Expression was retained at similar levels by 7 d on P but had decresed on the rough in OM only. Agonist decreased expression on P and SLA but not modSLA. Antagonist increased expression in all samples.

The NOG (figure 6-20) and NR6A1 (figure 6-21) genes displayed similar expression patterns. Both genes were upregulated comparatively by modSLA in GM and polished in OM at 1 d. Genes were expressed at high levels on P at 7 d in OM compared to rough. Axl agonist decreased expression on polished but not rough. Axl antgonist increased expression in all samples.

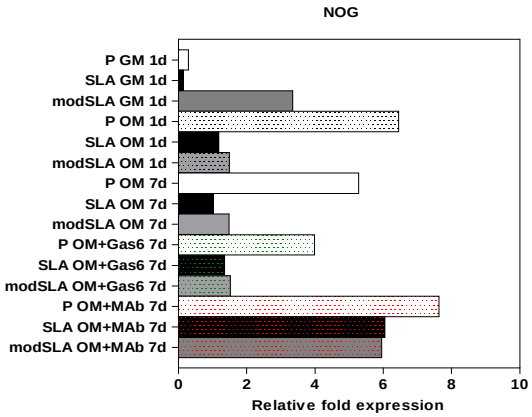

Figure 6-20 Miniarray analysis of effects of Axl signaling on NOG gene expression

A vertical bar chart with mean of the relative fold expression values from three donors plotted on the x-axis (N=3, n=1). Gene cards define NOG (noggin) as a polypeptide which negatively regulates transforming growth factor beta family members, such as bone morphogenic protein type 4, and thus inhibits bone formation. It is considered to be important for cartilage formation. NOG was expressed high on modSLA than others in GM at 1 d. But its expression was greatly reduced in OM, with a higher fold value on P than both rough surfaces. The P surface retained expression by 7 d, which had lowered on the rough surfaces compared to OM 1 d. Agonist seemed to not affect expression but antagonist starkly upregulated the gene.

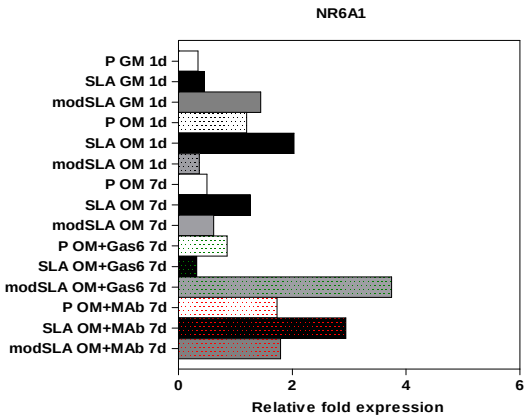

Figure 6-21 Miniarray analysis of effects of Axl signaling on NR6A1 gene expression

A vertical bar chart with mean of the relative fold expression values from three donors plotted on the x-axis (N=3, n=1). Gene cards define NR6A1 (nuclear receptor subfamily 6, group A, member 1) as a nuclear receptor that may be involved in neurogenesis and germ cell development. Its expression was comparatively higher on modSLA at 1 d in GM, the pattern of which was reversed with a relatively lower expression of the gene on modSLA in OM at 1 d. All samples retained expression by 7 d. Agonist did not have a stark affect on the expression of the gene, apart from an upregulation on modSLA. Antagonist increased expression relative to OM 7 d controls.

LIFR (figure 6-22) was transcribed higher in OM at 1 and 7 d. It was modulated higher on modSLA only at 1 d in GM. The Axl antagonist upregulated expression in polished surface cultured cells at 7 d.

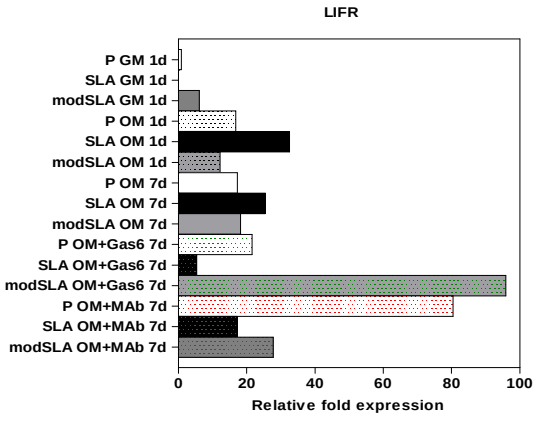

Figure 6-22 Miniarray analysis of effects of Axl signaling on LIFR gene expression

A vertical bar chart with mean of the relative fold expression values from three donors plotted on the x-axis (N=3, n=1). Gene cards define LIFR (leukemia inhibitory factor receptor alpha) as subunit of a complex that mediates the action of the leukemia inhibitory factor, a polyfunctional cytokine that is involved in cellular differentiation, proliferation and survival in the adult and the embryo. This gene was strongly modulated by OM than GM at 1 d. In GM, expression was detectable on modSLA but not on the other surfaces. Expression was similar on all surfaces by 7 d. Agonist seemed to increase expression of the gene but only on modSLA. Antagonist increased expression of the gene but only on P, when compared to OM 7 d controls.

PODXL was not modulated in GM (figure 6-23). In osteogenic medium, it was higher on polished than rough. It was not transcribed at 7 d in osteogenic medium only. Axl antagonist caused a relative upregulation compared to 7 d control medium.

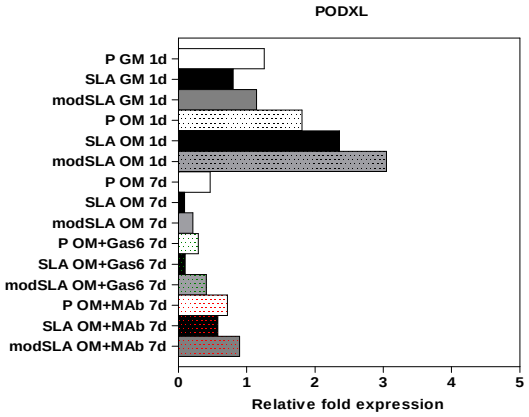

Figure 6-23 Miniarray analysis of effects of Axl signaling on PODXL gene expression

A vertical bar chart with mean of the relative fold expression values from three donors plotted on the x-axis (N=3, n=1). Gene cards define PODXL (podocalyxin-like) as a protein that regulates cell adhesion and morphology, and affects cancer progression. PODXL was expressed a similar levels at 1 d in GM. Its expression had increased several fold on modSLA than others in OM at 1 d. Expression of the gene had decreased on all surfaces by 7 d in OM. Antagonist seemed to affect an increase in the expression of the gene on all surfaces.

6.3.5 Differentiation

The genes detected in this category were ACTC, CGB, COL1A1, DES, FLT1, FN1, GATA6, GFAP, LAMA1, LAMB1, LAMC1, NES, PECAM1, RUNX2, SEMA3A, SERPINA1, SST, and SYP. ACTC

(figure 6-24) and GFAP (figure 6-25), myogenic markers, were unexpressed. CGB, GATA6 and SST, markers associated with lunch epithelium development (Zhang et al., 2008) and embryonic hepatic cell migration (Jung et al., 2006) respectively, were initially expressed at 1 d in both media conditions similarly on all surfaces. Genes were unexpressed at later time point and conditions.

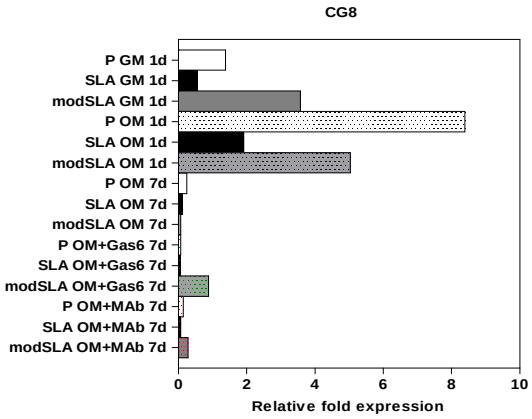

Figure 6-24 Miniarray analysis of effects of Axl signaling on CG8 gene expression

A vertical bar chart with mean of the relative fold expression values from three donors plotted on the x-axis (N=3, n=1). Gene cards define CG8 (peroxisomal biogenesis factor) as a molecule required for protein import into peroxisomes. CG8 was expressed higher on the modSLA than others in GM but was modulated many fold higher in OM, with highest expression on P than others. Expression had decreased by 7 d in OM. Agonist increased expression on modSLA only; while antagonist increased expression by a very small fold value on all surfaces.

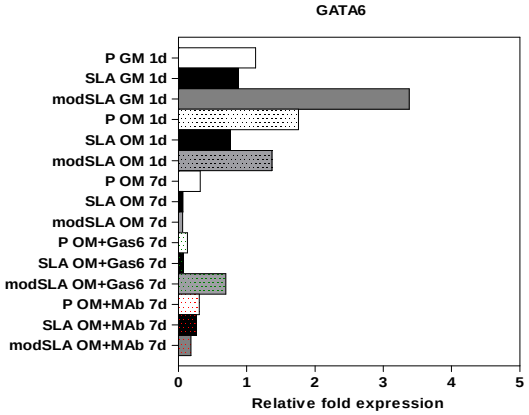

Figure 6-25 Miniarray analysis of effects of Axl signaling on GATA6 gene expression

A vertical bar chart with mean of the relative fold expression values from three donors plotted on the x-axis (N=3, n=1). Gene cards define GATA6 as a transcription factor that regulates terminal differentiation in different tissue cells such as cardiac myocytes, intestinal stroma etc. Its expression was higher on the modSLA than the similarly expressed levels on P and SLA at 1 d in GM. It was expressed relatively higher on the P and modSLA surfaces than SLA at 1 d in OM. The P surface retained expression of GATA6 by 7 d, with a very low expression on the rough surfaces. Agonist did not alter expression apart from on modSLA but antagonist did increase expression compared to OM only in all samples.

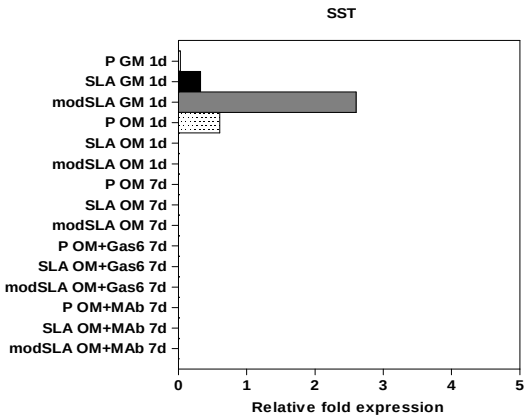

Figure 6-26 Miniarray analysis of effects of Axl signaling on SST gene expression

A vertical bar chart with mean of the relative fold expression values from three donors plotted on the x-axis (N=3, n=1). Gene cards define SST (Somatostatin) as a peptide hormone that inhibits secondary hormones and hence regulated the endocrine system. The SST gene was detected at 1 d in GM. Its expression was highest on the modSLA than SLA and P, the latter exhibiting very minute expression fold values. Its expression was detected in the P cultured cells in OM at 1 d. The gene lacked any expression in the later samples.

COL1A1 (figure 6-27), FN1 (figure 6-28), NES (figure 6-29) and SEMA3A (figure 6-30), markers of osteogenic, angiogenic (Online Mendelian Inheritance in Man, 2011), neural and neural/lung (Becker et al., 2011) respectively, were expressed lower in growth than osteogenic medium at 1 d with higher fold expression on polished than rough surfaces. Expression of these genes had reduced by 7 d in osteogenic medium on all surfaces. The Axl antagonist increased expression on polished compared to rough surfaces.

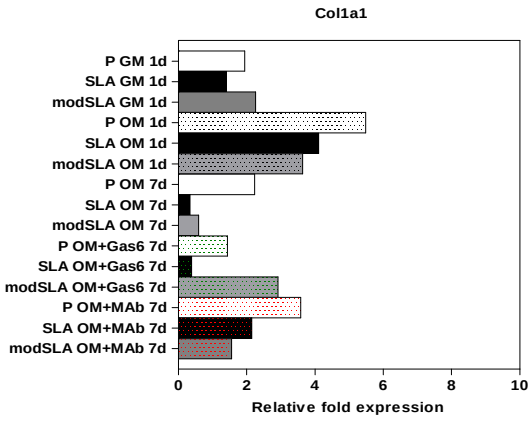

Figure 6-27 Miniarray analysis of effects of Axl signaling on Col1a1 gene expression

A vertical bar chart with mean of the relative fold expression values from three donors plotted on the x-axis (N=3, n=1). Gene cards define Col1a1 (collagen type 1, alpha sub-unit 1) as an extracellular matrix molecule, which forms the collagenous matrix of bone. Its expression was detected at similar levels at 1 d in GM, while OM seemed to cause an upregulation of the gene on P compared to the rough surfaces. The P surface retained expression by 7 d. Agonist did not affect expression apart from on modSLA. Antagonist increased expression in all samples.

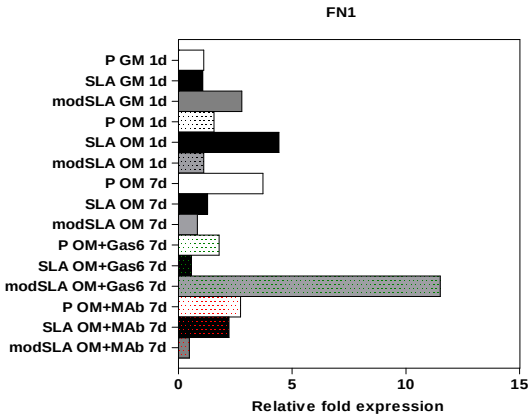

Figure 6-28 Miniarray analysis of effects of Axl signaling on FN1 gene expression

A vertical bar chart with mean of the relative fold expression values from three donors plotted on the x-axis (N=3, n=1). Gene cards define FN1 (fibronectin 1) as an extracellular matrix and soluble protein important for cell adhesion and survival. FN1 was detected in alls samples at 1 d. Its expression had decreased on the rough than P by 7 d in OM only. Agonist did not seem to affect expression, while antagonist increased expression on P and SLA but not on modSLA.

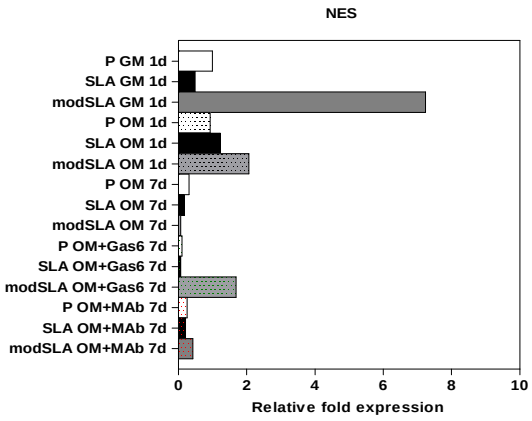

Figure 6-29 Miniarray analysis of effects of Axl signaling on NES gene expression

A vertical bar chart with mean of the relative fold expression values from three donors plotted on the x-axis (N=3, n=1). Gene cards define NES (nestin) as a filamentous molecule expressed predominantly in stem cells of the central nervous system in the neural tube that is downregulated and replaced by neurofilaments upon terminal differentiation. Its expression was observed higher on modSLA than other surfaces at 1 d in GM. This pattern was repeated in OM but with lower magnitude. Expression was observed at 7 d OM at very low levels. Expression increased slightly in presence of antagonist.

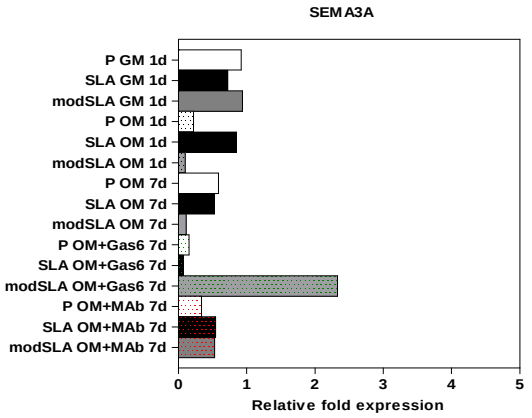

Figure 6-30 Miniarray analysis of effects of Axl signaling on SEMA3A gene expression

A vertical bar chart with mean of the relative fold expression values from three donors plotted on the x-axis (N=3, n=1). Gene cards define SEMA3A as a soluble growth protein that can function as either a chemorepulsive agent, inhibiting axonal outgrowth, or as a chemoattractive agent, stimulating the growth of apical dendrites. This gene was expressed at basal levels in all samples.

DES (figure 6-31), a myogenic marker, was expressed at a detectable level in cells. Expression was lower in GM than OM. They was expressed higher on P than rough in GM and OM at 1 d. Expression noticeably decreased on rough by 7 d and was still expressed high on P. Receptor Axl deregulation increased expression levels across all samples.

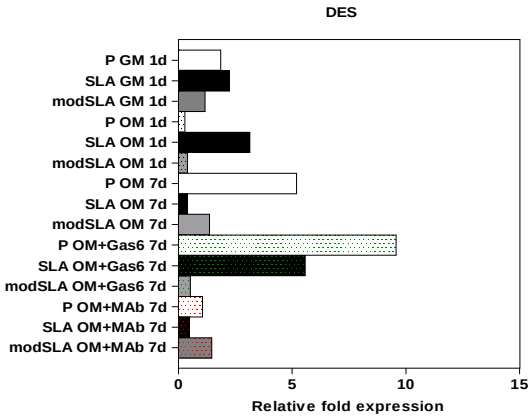

Figure 6-31 Miniarray analysis of effects of Axl signaling on BRIX gene expression
A vertical bar chart with mean of the relative fold expression values from three donors plotted on the x-axis (N=3, n=1). Gene cards define NANOG as a transcription factor that regulates inner cell mass and embryonic stem cell proliferation and self-renewal. This gene was expressed higher on the modSLA in GM and SLA in OM at 1 d. Expression seemed to be retained at a higher level by 7 d on modSLA but had decreased on the P and SLA surfaces. The agonist and antagonist relatively decreased expression of the gene compared to 7 d controls. Bars show mean; N = 3, n = 1.

LAMA1, LAMB1, LAMC1, and SYP, all markers of neuronal development (Online Mendelian Inheritance in Man, 2011) displayed a similar trend in expression as shown in figures 6-32, 6-33, 6-34 and 6-35. These genes were modulated higher by SLA in OM at 1 d compared to other surfaces. In all cases, receptor Axl antagonist increased expression at 7 d.

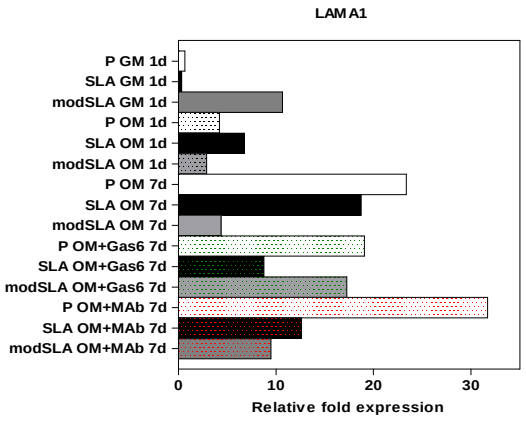

Figure 6-32 Miniarray analysis of effects of Axl signaling on LAMA1 gene expression
A vertical bar chart with mean of the relative fold expression values from three donors plotted on the x-axis (N=3, n=1). Gene cards define LAMA1 (laminin, alpha 1) is part of an extracellular matrix molecule that manages the attachment and organization of cells into tissues. This gene was expressed higher on modSLA than others at 1 d in GM. Expression was similar in all samples at 1 d OM. At 7 d, expression had increased many times on the P and SLA but not modSLA. Agonist and antagonist did not seem to affect the expression of the gene apart from on the P surface.

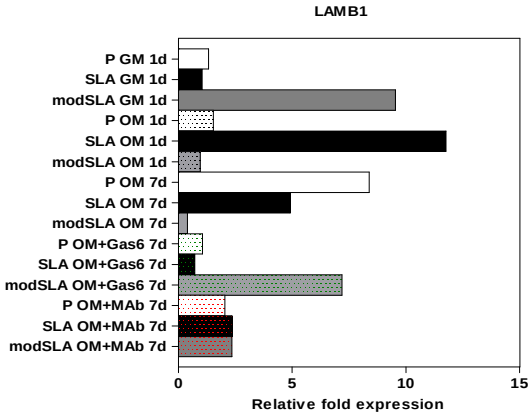

Figure 6-33 Miniarray analysis of effects of Axl signaling on LAMB1 gene expression
A vertical bar chart with mean of the relative fold expression values from three donors plotted on the x-axis (N=3, n=1). Gene cards define LAMB1 (laminin, beta 1 subunit) is part of an extracellular matrix molecule that manages the attachment and organization of cells into tissues. This gene was modulated higher on modSLA and SLA in GM and OM, respectively, 1 d post seeding. Expression of the gene was highest on P and then SLA at 7 d in OM, while being very low on modSLA. The agonist increased expression of modSLA but reduced it in P

and SLA samples. Antagonist decreased expression on all surfaces compared to 7 d OM only controls.

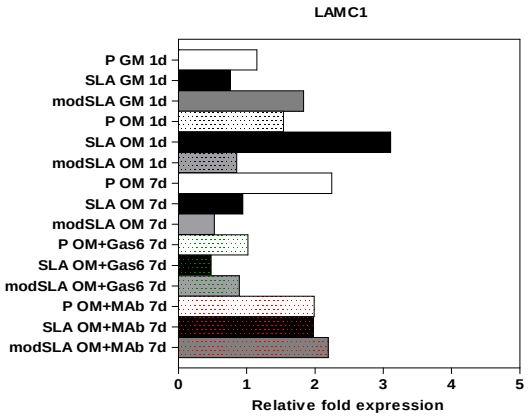

Figure 6-34 Miniarray analysis of effects of Axl signaling on LAMC1 gene expression
A vertical bar chart with mean of the relative fold expression values from three donors plotted on the x-axis (N=3, n=1). Gene cards define LAMC1 (laminin, gamma 1 subunit) is part of an extracellular matrix molecule that manages the attachment and organization of cells into tissues. Its expression changes took place in a small window of magnitude, with it being similar on all surfaces by 1 d but being downregulated by 7 d. Agonist decreased while antagonist increased expression.

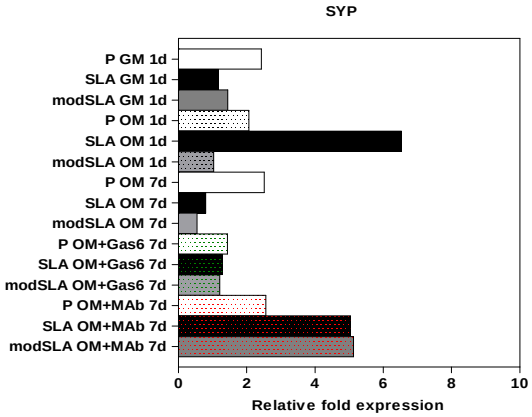

Figure 6-35 Miniarray analysis of effects of Axl signaling on SYP gene expression
A vertical bar chart with mean of the relative fold expression values from three donors plotted on the x-axis (N=3, n=1). Gene cards define SYP (synaptophysin) as a molecule that is part of the membrane of small synaptic vesicles in brain and endocrine cells, and is believed have a structural function in neural cells. Its expression was similar in all samples. The antagonist increased expression on the rough surfaces relative to OM only.

FLT1 (figure 6-36) and SERPINA1 (figure 6-37), markers of angiogenesis and were expressed higher on P than rough in GM 1d. OM decreased expression but was higher on rough than P. Genes were downregulated at 7 d in OM on all surfaces. Axl antagonist caused increase in expression on all surfaces.

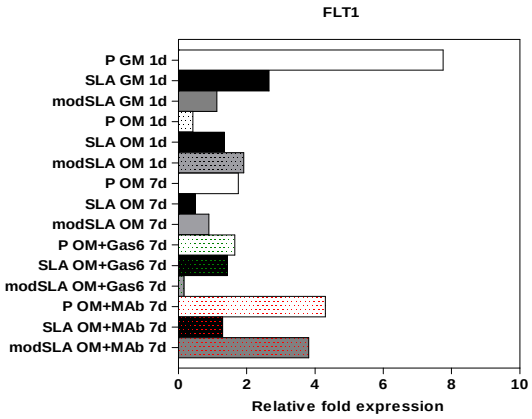

Figure 6-36 Miniarray analysis of effects of Axl signaling on FLT1 gene expression
A vertical bar chart with mean of the relative fold expression values from three donors plotted on the x-axis (N=3, n=1). Gene cards define FLT1 (vascular endothelial growth factor/vascular permeability factor receptor tysoine kinase 1) as a molecule regulating angiogenesis and now-vasculogenesis. FLT1 was highly expressed by P in GM at 1 d compared to the rough surfaces. Its expression was low in OM at 1 d, with a higher fold value for modSLA than SLA than P surfaces. Agonist seemed to decrease expression while antagonist seemed to increase expression of the gene relative to control OM only.

SERPINA1 (figure 6-37), was expressed at similar levels by cells in GM. Expression was variable in osteogenic medium; it was detected higher on SLA only than others. Expression had diminished by 7 d in all conditions. PECAM1 (figure 6-38), a hematopoietic marker, was expressed higher on rough than polished in GM at 1 d. Expression was similarly high on all surfaces in OM at 1 d. Expression decreased at 7 d on all surfaces. Expression was not observably affected by receptor Axl deregulation.

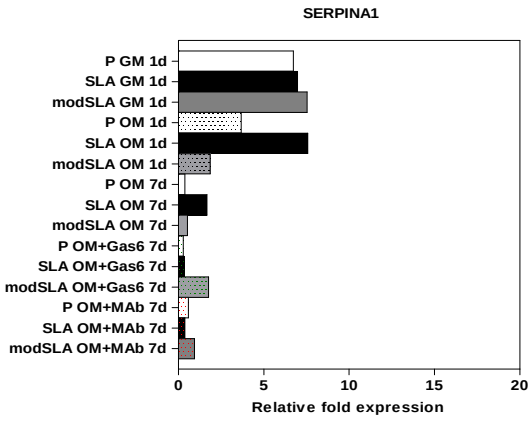

Figure 6-37 Miniarray analysis of effects of Axl signaling on SERPINA1 gene expression
A vertical bar chart with mean of the relative fold expression values from three donors plotted on the x-axis (N=3, n=1). Gene cards define SERPINA1 (serine proteinase inhibitor) as a soluble protease inhibitor for molecules like trypsin, elastin, thombin etc. Its expression was detected highest at 1 d in GM in all samples. Its expression deceased in all samples by 7 d in OM only. Agonist and antagonist did not seem to affect expression of this gene in comparison with the controls.

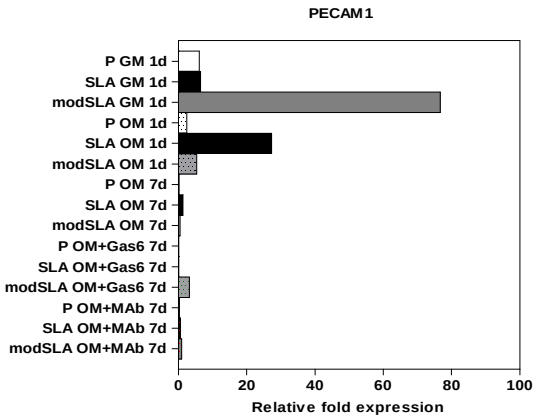

Figure 6-38 Miniarray analysis of effects of Axl signaling on PECAM1 gene expression
A vertical bar chart with mean of the relative fold expression values from three donors plotted on the x-axis (N=3, n=1). Gene cards define PECAM1 (platelet/endothelial cell adhesion molecule) as a member of the immunoglobulin superfamily, involved in leukocyte migration, angiogenesis, and integrin activation. Its expression was detected highest on modSLA compared to P and SLA at 1 d in GM. Expression was detected in OM without a clear trend. Expression had reduced by 7 d to near zero levels. Antagonist seemed to cause a tiny increase in expression fold values.

RUNX2, the master osteogenic regulator, was not expressed in growth medium at 1 d post seeding. It was upregulation by modSLA higher than SLA and polished in osteogenic medium at 1 d. Its expression decreased by 7 d and appeared higher on polished than the rough surfaces. The antagonist increased expression by a small fold value compared to Axl agonist and control.

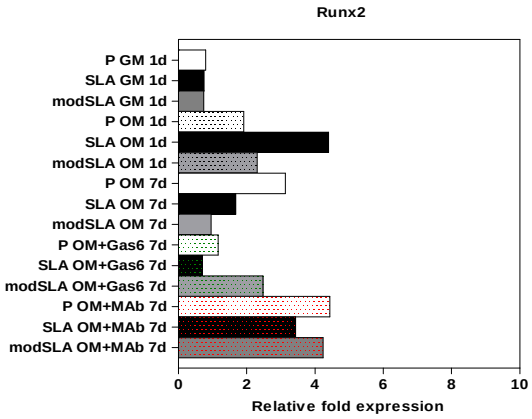

Figure 6-39 Miniarray analysis of effects of Axl signaling on RUNX2 gene expression
A vertical bar chart with mean of the relative fold expression values from three donors plotted on the x-axis (N=3, n=1). Gene cards define RUNX2 (runt related type 2) as a transcription factor that positively drives the osteogenic differentiation of stem cells. Its expression was very low in growth medium. In contrast osteogenic medium had caused a slight upregulation that seemed higher on the rough than P surfaces. Its expression was retained at a higher level on the P surface and then rough surfaces at 7 d in OM. Agonist did not starkly affect expression but antagonist comparatively increased expression of the gene relative to 7 d controls.

6.3.6 Inter-relation of samples

An analysis was conducted to order samples according similarities calculated by Euclidean distance algorithm. The results of this analysis are shown in figure 6-40. This figure is extracted from a heatmap shown in figure 6-1 with the exception that samples are arranged in an order of similarity.

Figure 6-40 indicates the sample ‘P OM 1d’ related to all samples. A limitation of this analysis was that those specific instances attributing the sample with overlap could not be highlighted.

The ‘primary’ cluster branching from ‘P OM 1d’ consists of a small and large group. The small group included ‘modSLA GM 1d’ and ‘modSLA OM 1d’. The larger cluster was secondarily divided to ‘modSLA OM + Gas6 7 d’ against the remaining samples.

This cluster forming the remaining samples was further divided into two groups. The first contained ‘P GM 1d’ and ‘SLA GM 1d’ linked to ‘SLA OM + Gas6 7d’; related to ‘P OM + Gas6 7d’ and ‘modSLA OM 7d’ and ‘SLA OM 7d’.

The second consisted of the pairing of ‘P OM 7d’ and ‘SLA OM + MAb 7d’; in an ascending hierarchy with ‘modSLA OM + MAb 7d’ and ‘P OM + MAb 7d’ to ‘SLA OM 1d’.

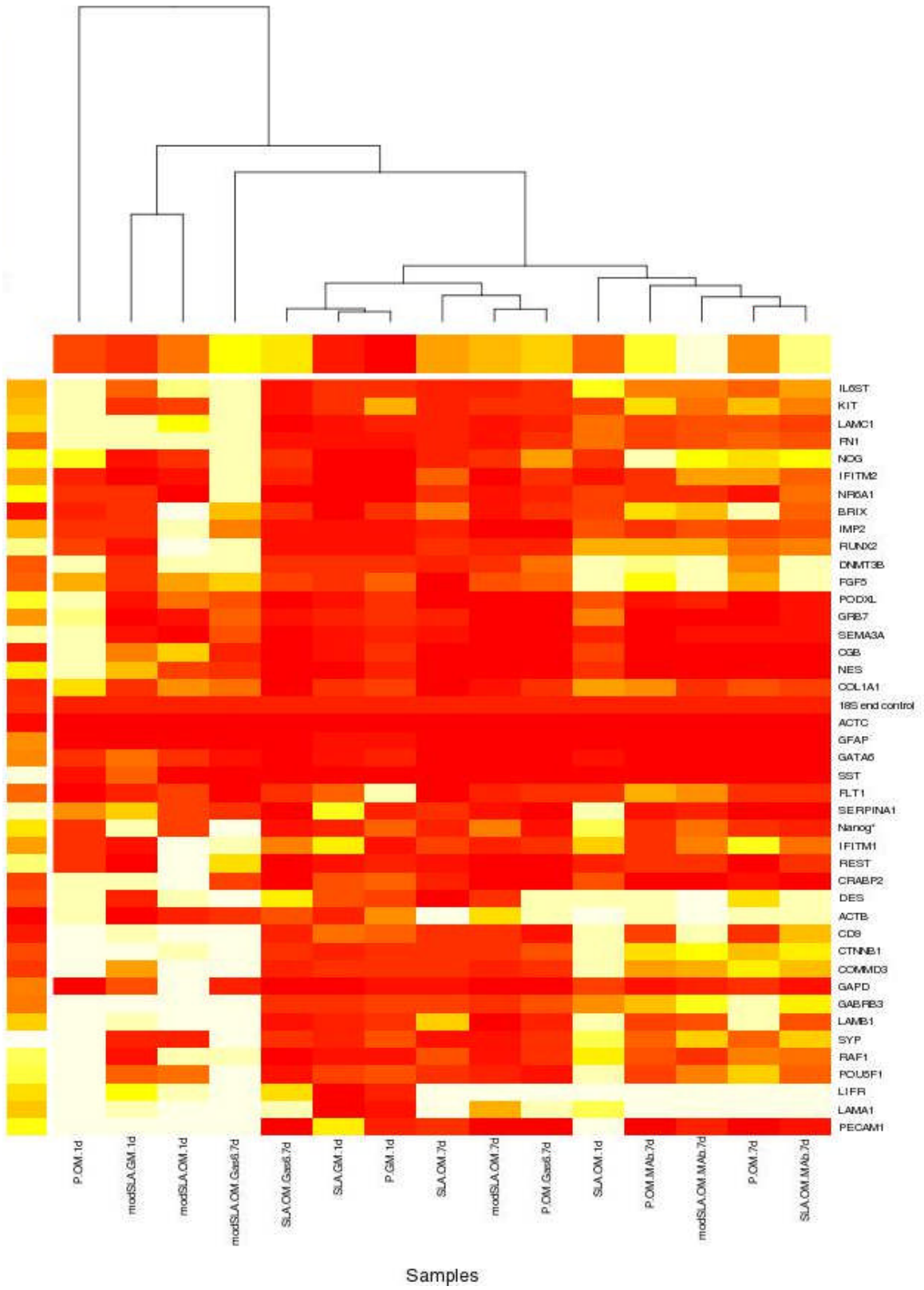

Figure 6-40 Evaluation of similarities between substrate and conditions

6.4 Discussion

6.4.1 Unexpressed genes

The unexpressed genes were largely differentiation markers for neuronal, myogenic, endothelial, and angiogenic differentiation. Their lack of expression in the calibrator reference of time zero indicates the difference in the gene expression pattern of hMSCs and embryonic stem cell markers.

6.4.2 Controls

The process of real time PCR calculates the fold of difference in expression of a target gene in relation to an internal control. This control is usually assumed to be a ubiquitous gene, constitutively expressed at a constant rate in a specimen of cells; and largely unaffected in the proposed experimental system. The results indicate here that 18S RNA, a main requirement for cellular systems' protein synthesis apparatus; and GAPD, a vital metabolic effector, were unaffected by any variables tested.

However, ACTB, CTNNB1 and RAF1 were modulated differently. These genes were upregulated more in OM than in GM. Their responses to the surfaces differed; however a common overlap was their increased expression on the smooth surface relative to the rough; and their comparative upregulation by cells cultured with receptor antagonist. The functions of these molecules suggest that cells were either approaching or actively enacting a level of

6.4.3 Maintenance of pluripotency

These gene exhibited expression in the hMSCs, indicative of the specimens' uncommitted and undifferentiated nature; although different to a similar state in embryonic stem cells, as seen in absence of expression of the critical SOX2 gene.

The common trend observed was of increased expression in OM within the initial phase of culture; with a higher expression on P than the rough surfaces. This relative difference between the surface types was maintained by 7 d; albeit at a lower magnitude. This decrease was attenuated by receptor antagonist, which increased gene expression.

6.4.4 Correlation with stemness

These genes seemed largely modulated in the early phase of culture. In general, their increase was higher in OM than in GM and on P than rough. Like the previous genes, these were increased in expression by receptor antagonist.

6.4.5 Differentiation genes

This was the most critical section of the experiment; querying the expression of genes known to induce or drive phenotypic differentiation to a lineage other than osteoblastic. The majority of markers seemed expressed early in culture. These markers seemed to be expressed higher on P than the rough surfaces. The osteogenic marker Runx2 displayed a pattern somewhat interpretable within the context of the experiment. The lack of expression of the gene at 1 d in GM was as expected. Its upregulation at 1 d in OM on modSLA > SLA > P had been independently observed within this study in a previous experiment (section 4). Its relative high level on P compared to rough at 7 d probably suggests that at this early interval in osteogenic differentiation, the gene was still being transcribed on P. This is, however, confounded by the observation of increase in expression by receptor antagonist.

6.4.6 Inter-relation of samples

The similarities drawn between the different samples with the Euclidean algorithm indicated two solitary and four grouped samples. The first solitary sample was P OM 1d. It was found comparable to all samples but closely linked to ‘modSLA GM 1 d’ and ‘modSLA OM 1 d’. The modSLA surface enhances osteogenic responses, and as such is highly osteogenic and low stemness; hence, their grouping together might be indicative of being primed for (osteogenic) differentiation. This is indicated in the decreased expression of various correlation and maintenance of stemness genes on this surface.

The second solitary sample is ‘modSLA OM Gas6 7 d’. It is comparable to the remainder of samples, organised into three groups. The first groups comprises ‘SLA OM Gas6 7d, ‘SLA GM 1 d’ and ‘P GM 1 d. These are low osteogenic and high stemness; the similarities between which imply

their relative higher expression of stemness markers. The second group, directly related to the preceding ‘higher stemness group’, includes ‘SLA OM 7 d’, ‘modSLA OM 7 d’ and ‘P OM Gas6 7d’. This is an unexpected relation, as the initial two samples of this group are known through previous experiments as being highly osteogenic and hence, low stemness. However, hypothetically, ‘P OM Gas6 7d’ is a high stemness representing sample, influenced by the relative lag in osteogenic differentiation compared to rough seen in previous experiments and the presence of Axl promoting Gas6, theoretically an inhibitor of mineralisation.

The third is a hierarchical group of five samples. The initial two are ‘P OM 7 d’ and ‘SLA OM MAb 7 d’. This relationship is unexplained as, theoretically, the expression of stemness genes on the latter would be expected to be lower than on the former. The pair is related to ‘modSLA OM MAb 7d’, which is then related to ‘P OM MAb 7 d’ and then ‘SLA OM 1 d’. The similarities between these three imply a similar loss of stemness gene expression.

6.4.7 Significance of findings

The experiment shows a differential pressure on hMSC differentiation on the various surfaces and conditions. The analyses at 1 d indicate that the hMSCs are in an uncommitted state with a high level of expression of correlation, maintenance and differentiation genes in cells on all surfaces. The expression of these genes is relatively downregulated by the rough than polished surface at this initial time. The expression of most genes expectedly decreases with time in inductive medium. Interestingly, the addition of receptor agonist and antagonist alter the pattern of gene expression in many genes. This association of receptor de-regulation with the stem cell transcriptome suggests that Axl signaling might be important to the state of stemness of hMSCs. In the case of β-catennin and Runx2, the effect of a relative small fold upregulation at 7 d by antagonist compared to controls, is indicative of the effect expected from the attenuation of this pathway; positive signaling inhibits mineralisation and vice versa. A further indication of these results is of a ‘silencing’ effect that the agonist seems to be causing in the case of many genes (Matt Dalby, Univ. of Glasgow, personal communication). This may be the reason causing a down instead of an up regulation of the stemness genes.

6.5 **Summar**y

The expressions of a subset of genes implicated in imparting a cell with pluripotency are differentially regulated by modified Ti surfaces. The polished surface promotes stemness gene expression relatively more than rough. OM causes a decrease in overall stemness gene expression over time. The inhibition of Axl signaling, for unknown reasons, promotes the expression of several of these stemness genes at the 7 d time point.

7 Discussion

7.1 The hypothesis

The question posed by this thesis queried whether the Axl receptor is differentially modulated in cellular osteogenic responses to rough Ti implant surfaces compared with a control polished surface. There were two main sets of observations that led to the posed question.

The first was the differential promotive effects of modified Ti surfaces, used in this study, which in summary can be suggested to cause an accelerated form of osteogenic differentiation in cells. The results leading to this notion have been presented in several studies examining cell-substrate interactions on these very surfaces, i.e. polished, rough-hydrophobic SLA and rough-hydrophilic modSLA (described in sections 1.3.4 and 1.3.5). These studies have applied a wide range of analyses at the genetic and molecular levels, as well as cell types, including committed osteoblastic cells, osteogenic cancer cell lines, immune cells, and various stem cells. The *in vitro* evidence indicates differences in the capacity of each surface to alter osteogenic differentiation and function. These suggest an order based on magnitudinal differences in effects with rough-hydrophilic modSLA relatively more promotive than rough-hydrophobic SLA, which is than polished, which is in turn is than tissue culture plastic (TCP) in terms of their ability to support and promote osteogenic activity (Miron et al., 2010; Wall et al., 2009) Mendonca et al. 2008 (Mendonca G et al., 2008) (Olivares-Navarrete et al., 2011; Olivares-Navarrete et al., 2010a; Wennerberg and Albrektsson, 2009).

The second was the selective upregulation, detected by global gene expression analyses with microarrays, of a receptor tyrosine kinase Axl in cells cultured on rough-hydrophobic SLA surface (Brett et al. 2004). This molecule and its ligand, Gas6, are implicated in the negative regulation of the differentiation of uncommitted bovine pericytes cultured in osteogenic inductive medium (Collet et al., 2007; Collet et al., 2003). Specifically, the receptor is thought to be important in the pre-osteogenic phase of differentiation and is down-regulated prior to calcium deposition by cells (Collet

et al., 2007) suggesting it a probable role in the differential response of cells to the modified Ti surfaces.

7.2 Overview of thesis

The study was conducted in two parts. The first part evaluated the phenotypic and osteogenic response of human mesenchymal stromal cells (hMSCs) to the different substrates. The second examined the modulation of receptor kinase Axl and ligand Gas6 at the transcript and protein level in control conditions, and later examined the effects of receptor de-regulation on the previously assessed cellular phenotypic and osteogenic parameters. Receptor de-regulation was achieved with recombinant proteins and monoclonal antibodies; upregulation with receptor agonist and down-regulation with antagonist. This method was used due to its simplicity. It was thought of as an optimum point of initiating the study of Axl's potential role in differential cellular responses to different substrates, particularly with respect to the cellular specimens multipotent nature; the very factor that renders these the preferred cell type for evaluating the pathway's importance in substrate influenced cell developmental processes.

The hMSCs are known to gradually lose their multipotentiality with time in culture, and this can veru easily be further affected by the variable stresses cellular cultures undergo *in vitro* (Shanti et al., 2007; Tuan, 2011). As the applied method did not require the biochemical manipulation of cells, i.e. transfection with expression vectors etc, or gene knock out procedures, the possibilities of any alterations in the specimens' normal behavior were relatively reduced, as were the possibilities of ambiguity in the findings derived from them. The importance of the specimens' nature was even more significant due to the perceived higher dependence of these multipotent cells on the Axl pathway's osteo-inhibitory effects.

The experiments were conducted on three topographically and chemically different Ti surfaces with tissue culture plastic used as a control for material based differences. The Ti surfaces were manufactured by Straumann AG, a Swiss company that specialises in dental products. They re-produced the implant topographies on 15 mm discs. These substrates have been previously

characterised by (Rupp et al., 2006), who demonstrated an average roughness measure (R_a, arithmetic mean of lowest and highest point in a surface profile) of < 0.5 µm compared to ~ 4.2 µm for the rough-hydrophobic SLA/hydrophobic modSLA, respectively. (Rupp et al., 2006) also evaluated advancing contact angle measurements to be 0^o for the modSLA compared to 138.3 $\pm$ 4.2^o angles for SLA and 96 ^{o} angle for P surface (Buser et al., 2004; Zhao et al., 2007). The rough surfaces, though different in their potential to adsorb water, had the same topography. An easy way to describe their roughness is as a surface resorbed by osteoclasts, with large craters formed by the blasting of alumina particles, which is superimposed by many tiny 'crypt' like indentations formed by acid etching that collectively yield a highly uneven topography (Schwartz et al., 2009a; Ferguson et al., 2006; Rupp et al., 2006). The comparative findings of this thesis are discussed in the following sub-sections.

7.2.1 Phenotypic responses to modified Ti surfaces

The phenotype of a mesenchymal stromal cell is that of a strongly adherent and mitotic cell. It is seemingly under pressure to attach to a substrate in order to divide to form larger progeny numbers (DiGirolamo et al., 1999). When the attachment of an hMSC is tested on the different substrates studied in this thesis, they seem to attach preferentially and at a higher affinity to the polished surface, upon which the hMSC begins to attain stability by spreading over the surface at a faster rate taking a near uniform spherical morphology with a central nucleus, resembling the appearance of a fried egg. This was similar to what was reported in (Wall et al. 2009) at 3 h.

This does not happen on the rough, which present a topography that the cells need to adapt to. The cells attach to the roughened surfaces at a rate relatively lower than on the polished, resulting in a lower number of cells in the initial instances of contact (5 to 60 min). In addition, the cells adapt an irregular morphology, seemingly constrained or stretched, with cytoplasmic processes emanating in various directions. The cells, as shown in figure 3-5 and 3-6, seem to resemble a tent pegged to the ground on all sides. These figures also show that the final state the cell adapts on the rough surfaces at 3 h is quite different to their earlt appearance, which is highly spherical with very few

attachment processes. It may have been highly interesting to have evaluated cytoskeletal changes in the cells per time, with emphasis paid on the positioning of the nucleus.

The differential events of attachment and spreading are followed by stark differences in cellular viability and proliferation. While the hMSC on a polished surface would initiate proliferation after adhering stably, forming a higher number of progeny over the course of culture, the cells on the roughened surfaces exhibit a lag in replication before cell numbers increase significantly in the intermediate to end stages of a 21 day culture. This relative replicative lag on the rough compared to polished or tissue culture plastic is considered to be partly due to the events of apoptosis and necrosis occurring in the specimen at early cell-rough substrate contact as reported in (Wall et al. 2009); and partly due to substrate induced metabolic changes in cells, believed to manifest in the form of altered fate determination in these cells. The occurrence of apoptosis is inferred from the patterns of cellular proliferation observed on the different surfaces combined with that of caspase 3, BCL-XL and Ki-67 transcriptional upregulation on the rough at very early times in culture. The metabolic differences induced by the rough surfaces resulting in altered cellular responses, primarily related to the osteogenic activity of the cells on the rough substrates is also implicated from the transcriptional upregulation of caspase 3; but through its reported association with osteogenic differentiation in mice and mice MSCs (Miura et al. 2004). It seems that the cells which survive this ‘selective’ process, through either apoptosis or metabolic enhancement, ultimately are capable of exhibiting heightened osteogenic activity. This may translate as an induction by rough surface on cellular ability of producing better quality bone and might therefore be responsible for the better *in vivo* performance of the rougher surfaces.

7.2.2 Osteogenic responses to modified Ti surfaces

The metabolic activity taking place in an hMSC differentiating on the rough surface is suggested to be different than that cultured on the smooth surfaces. The rough surfaces offer a very different set of variables for the cell to sense and respond to. The effect of these differences appears to induce the undifferentiated cells to differentiate earlier, adopting an osteoblastic phenotype that is probably most suited for the detected microenvironment. The cell, being a constituent of the organism’s

anatomy, would bear a memory and capability of responding to only what it could face in its cognate microenvironment within the organism; and certainly not an innate object such as Ti metal. However, it seems that the cell can distinguish Ti metal from TCP and differentiate more profoundly on the metal, and even more on the modified Ti surfaces. The events taking place on the rough surfaces apparently occur later on the polished and are further delayed on the TCP. The outcome of each of these varied processes is the formation of a calcified ECM, reminiscent of true bone formation *in vivo*. The rough Ti surfaces apparently induce an increase in the measured parameters, which can only suggest an increase in cellular differentiation and hence, bone formation.

These variations in the cell's behavior on the different substrates are largely down to a differential set of stimuli received by the cell over time (Tuan, 2011). These stimuli seem pleiotropic in nature. They can be immediate and direct in the form of topography, chemistry, medium, physical properties (temperature, humidity, etc), as biological in the form of cell type, context of experiment etc., and as late culminations of the effects of the initial set of stimuli. This seems true for the cell attaching and spreading on the rough surfaces, which might engagement extra cell fate determination mechanisms; supported from the observed pattern of Wnt5a that is a known effector of osteogenic differentiation the engagement of cell architectural assemblies associated Rock/Rho GTPase signaling system in MSC like cells (Santos et al., 2010). Though the exact activity of mechanotransduction elements was not examined in this study, the results strongly suggest that the hMSC on the rough surfaces uses its genes and molecular systems very differently to the cells the polished and tissue culture plastic.

7.2.3 Differential modulation of Axl/Gas6 pathway by modified Ti surfaces

The receptor Axl is expressed by osteogenic cells but has not been widely studied in the context of osteogenic differentiation. However, its significant effects on this process have been demonstrated experimentally in the context of vascular ossification, which is deemed to be developmentally overlapping with skeletal osteogenesis (Johnson et al., 2006). It is known that Axl is needed in the

pre-osteoblastic phase of an osteogenic cell's life cycle and is downregulated nearing the initiation of cellular mineralisation (Collet et al. 2003; 2006).

The findings of this study demonstrate that an hMSC cultured on the rough Ti surfaces induces this downregulation earlier than on polished and TCP. This hMSC would have engaged several different mechanisms in response to the early direct and late indirect stimuli that seem to affect the downregulation of Axl. The contrast generated by deregulating receptor signaling suggests it to be part of cell physiological events preceding the initiation of mineralisation. Specifically, it seems to be regulating cellular maturation, inferred from 7^{th} day culture observations of receptor deregulation on cellular osteogenic responses. The experiment showed the downregulation of mineralisation to be highest on TCP. Though the Ti surfaces did show a decrease in mineralisation, it was substantially less compared to control conditions. A factor here is Ti metal, which seemed to have been a significant contributor to the heightened mineralisation of the cells.

Moreover, while the rough substrates do not respond significantly to the Axl agonist, they exhibit a higher synthesis of osteoblast secreted soluble regulators of osteoclastogenesis (osteoprotegrin and growth differentiation factor 15). In simple terms, according to the suggestion of an enhancement in osteogenic differentiation on the rough surfaces, the finding of an enhancement in OPG and GDF15 may indicate a possible association of Axl with the promotive effects of the substrates on cellular differentiation.

The correlation of Axl signaling with the hMSC pluripotency apparatus is also evident in the differences seen in the expression of stem cellness associated genes in chapter 6. The experiment revealed cells variably regulate the expression of stemness genes. Most of the genes correlating with the maintenance of stemness and those indicative of cellular pluripotency displayed a higher expression on the polished that rough at 1 day post seeding. The effects of media were evident, and several trends observed in growth medium were reversed in osteogenic inductive medium. However, crucially, the expression of genes at 7 day in control, agonist and antagonist cultured cells were different. Most of these genes were downregulated by all surfaces in control osteogenic

medium. The agonist seemed to have caused a similar effect but mostly keeping the expression of these genes at a low relative fold value. However, it was the antagonist that seemed to have positively modulated the expression of several genes. Of particular significance are β-catennin and Runx2, both of which have been shown to bear an importance in the process of osteogenesis. The patterns of these genes, being lowered or raised, in comparison to osteogenic medium only controls at 7 days, by agonist and antagonist respectively, is an encouraging find that supports the notion of Axl causing an osteoinhibitory effect: receptor de-regulation by agonist increases Axl signaling and may underpin the relative lower fold expression of the said genes, while their relative upregulation by antagonist could be representative of the effect of decreasing the pathway's signaling. In correlation with the observed pattern of receptor downregulation on the rough, the arrays, too, suggest that that it is the temporal downregulation of the receptor that the hMSC pursues in response to osteogenic medium and that the cell on the rough is under a stronger pressure to decrease the activity of this pathway in order to differentiate and mineralise comparatively faster than on polished surfaces.

7.3 Correlations and disagreements with other studies

The findings presented in this thesis agree with many of the previous discoveries in cell-implant interactions concerning the SLA and modSLA surfaces described in section 1.3.5 and 1.4.6. The studies cited in these sections had shown the differential regulation of alternate cell regulatory and fate determination systems that instigate enhanced osteogenic differentiation and function on the rough surfaces. Their comparative highlights between with this study are listed below.

1. Phenotypic responses
    a. As reported in (Miron et al. 2010; Wall et al. 2009), cells of a mesenchymal lineage spread highly on the P and are stretched on the rough. These studies do not indicate differences in the potential of cells to adhere to the different surfaces. Those differences have been shown here to manifest in a higher number of attached cells on the polished than rough at very early times. In addition, this study provides evidence that the stretched morphology of cells on the rough is a fate that

the cell would reach at 3 h post contact. Prior, the hMSCs seem to be in a restricted, non-spread, and spherical shape with fewer cytoplasmic processes fixing the cell onto the substrate compared to the later time point.

b. The reduction in cellular viability on SLA and modSLA observed here has been reported previously in (Olivares-Navarrete et al. 2010; Wall et al. 2009; Rausch-fan et al. 2007). (Wall et al., 2009) indicated that this loss of viability may be due to apoptosis and necrosis occurring in cells on the rough surfaces. The occurrence of apoptosis in the cultures used in this study can be anticipated with the finding of a transcriptional upregulation of caspase 3 and related factors at early times on the rough compared to smooth. However, a possibility exists that the authors may have detected Annexin V of matrix vesicles as opposed to that of apoptotic cells, due to the kits specificity for this antigen. Indeed, the association of caspase 3 with osteogenesis, as suggested by the knockout and knockdown experiments of (Miura et al., 2004), though not sufficiently strong evidence, can also be indicative of a metabolic change occurring in cells. This, in the context of the present set of results and the observers' views, could likely be representative of a heightened osteogenic differentiation as opposed to cell death suggested by (Wall et al., 2009).

2. Osteogenic responses

a. The study agrees with the observations of (Rausch-fan et al. 2007; Olivares-Navarrete et al. 2010) of the increased synthesis of alkaline phosphatase, osteocalcin, and osteoprotegrin molecules on the rough surfaces. However, the dynamics of their synthesis has been evaluated here in a larger time frame that provides a wider perspective of this process. The temporal effects of the surfaces on the expression of these molecules, in particular the downregulation on the Ti surfaces compared to tissue culture plastic at 21 d of ALP (section 4) that parallel's the substrates' significantly higher mineralisation compared to tissue culture plastic, are demonstrated with relative higher contrast.

b. The results here agree with (Miron et al. 2010; Wall et al. 2009) that calcium deposition is higher on the rough than smooth. The results here, however, provide a quantitative assessment of ECM mineralisation as opposed to a comparative view. In addition, those studies did not provide an assessment of the state of density of calcification in the extracellular matrix. Combining the quantification of calcium and collagen in the extracellular monolayer, this study managed to provide an additional aspect of mineralisation in the form of density of calcium per matrix collagen.

c. The differential involvement of Integrins ITGA2 and ITGB1 with Ti and Ti modified surfaces in regulating TGF-b1 and OPG (Schwartz et al 2009) could not be ascertained by the gene expression findings of this study. A comparison at the protein level may have been more informative of this relationship.

3. Differential Axl modulation

a. The trend of Axl quantity and phosphotyrosination decrease suggested by (Collet et al. 2003; Collet et al. 2006) in pericytic cells was found true. This study provides a further view consisting of the effects of this pathway on osteoprotegrin and growth differentiation factor 15 synthesis in the proposed heightened state of osteogenic differentiation on the rough substrates.

b. De-regulation of this pathway and its effects on stem cellness gene expression had not been proposed prior. The results in this thesis may serve as a starting point in querying the association of Axl with human stem cell transcriptome.

A point of contention in this study has been the occurrence of apoptosis on the rouigh substrates, which the expression of caspase 3 and related survival genes at early times combined with its potential role in the program of osteogenic differentiation, demonstrated by decreased bone mineral density due to decreased runx2 expression in caspase 3 null mice (Miura et al. 2004), have made difficult to solve. (Wall et al., 2009) proposed the apoptosis to be specific to Stro-1 negative cells, leading to a comparative increase in the number of Stro-1 positive cells on the rough, which were

further hypothesised to underpin the enhanced mineralisation on the rough. This study could not evaluate the relative change in Stro-1 positive cells between the populations. The methods applied in the thesis could not distinguish between the different sub-sets in an hMSC samples. But it did observe an up regulation of the caspase 3 gene at times and in conditions that relate more to differentiation than to apoptosis. This is supported by a retrospective view of the apoptosis related annexin V flow cytometric kit used by (Wall et al. 2009), which suggests that the entity studied by the authors may have been matrix vesicles that are also rich in Annexin v (Anderson et al., 2005).

There is a disagreement with methodological shortcomings in other studies (Olivares-Nevarrate et al. 2010; Schwartz et al. 2009) and related publications, in which experiments have been conducted by seeding cells on the surfaces in growth medium with TCP as a reference to evaluate cellular confluence. Medium would be changed from growth to osteogenic when cellular confluence was found in the TCP samples and parameters such as osteoblastic protein marker expression etc. would be quantified and compared. Whilst this may test the effects of the rough surfaces on the immediate activity of cells, it negates consideration of substrate influence immediately initiated at the point of contact, and followed through over the following days in culture. Accordingly, cells would have sustained many unknown changes, particularly considering the nature of the cells examined.

In addition, the authors have stated that the calcium mineralisation assay is not an appropriate method to assay osteogenic differentiation due to the influence of different medium stimulants (Olivares-Nararrete et al. 2010). This is strongly disagreed here; the use of the calcium mineralisation assay applied in this study is supported by the parallel trend observed in mineralization and osteoclastogenic regulator synthesis in hMSCs cultured on the different surfaces. These findings provide strong evidence that validates the application of this assay. In addition, the formulation of OM used here did not lead to the suggested destruction of cell numbers; instead a steady growth of cells, at low and high initial seeding densities, was observed. The model is not true osteogenic mineralisation; but it can been deemed ‘authentic in an artificial setting’, with

finite capacity, as seen in the form of a plateau in the ratios of ECM calcium to collagen at 14 d compared to 21 d on the rough surfaces.

7.4 Conclusion

In conclusion, the findings here implicate the differential sensing of substrate material and hence, response to substrate topography by osteogenic cells. This differential behavior of cells is a reflection of the temporal variation in osteogenic events on the different surfaces. The study proposes that surface topography of the SLA and modSLA 'accelerates the osteogenic differentiation of MSCs through some sort of alternative mechanism of phenotypic induction and differentiation. This temporal and magnitudinal enhancement by the rough surfaces includes the variable modulation of Axl tyrosine kinase. The pathway is expressed in uncommitted cells implying its importance to that cellular state. It is downregulated as the cell progresses through commitment to the state of mineralisation. The faster the process of differentiation, as exemplified by modSLA, the faster the downregulation of this receptor system, and vice versa.

7.5 Significance of findings and Future directions

The present study, like any form of research, has several implications depending on the perspective of the observer. It views the human body as a composite of overlapping systems, with the 'regenerative system' being one such system that has not been well characterised yet but will be highlighted in the near future, considering the present drive for ever new therapeutic developments. It can be loosely seen to consist of cells of an uncommitted / plastic nature, sequestered in tightly regulated pockets within various forms of tissue (mostly highlighted in blood, bone, muscle), which are mobilized by cytokines associated with reparative responses to the site of damage with the intent of repair. Papers from the late 1880s and the post World War 2 eras, periods that saw major progress in developmental biology, extensively use the term stem cells. Indeed, in many contexts the use of this term was correct as the investigators were querying the phylogenetic linkage between cellular entities of a system, notably the hematopoietic system. However, the same scrutiny at the single cell level has not been demonstrated with the MSC. This is being said not to discourage the crucial findings of the past but to encourage a consensus for deciphering their

biological truth that may prove very fruitful in the present momentum of biotechnological advancement.

The present theoretical implication of MSCs considers them participants in tissue repair that are limited in the capacity to regenerate but may be sufficient with human intervention in the form of biomaterials. Ti has been long known to be a biocompatible biomaterial. The exact biological mechanism(s) that achieve osseointegration are unknown but not for long. *In vitro* studies have demonstrated cell phenotypic responses to modified surfaces and will continue to do so- and will produce much useful to help dissect the important events in osteogenesis leading to the design of novel molecular therapies.

The therapeutic implications of Ti in the short term would include (i) its use as an *in vitro* substrate for the evaluation of osteogenic events and (ii) biomaterial design for bone related tissue engineering purposes. The long term implications surround identifying relevant sub-cellular target pathways, which may be manipulated to gain the desired osteogenic outcome with a high degree of specificity and efficiency. The Axl system is an example of a putative therapeutic target. This may not be apparent in the present framework but with Axl as a reference point, elucidation of the dynamics of osteogenic differentiation would identify targets of therapeutic interest.

7.6 Limitations

The relationship between cellular morphology and phenotypic differentiation is an area of study that is gaining in significance. It would have been interesting to query the structural differences in cells while attached to different surfaces, and assess in parallel, the relevant components of the currently known mechanotransduction apparatus in those samples. This could be conducted by confocal microscopy techniques and immuno staining of various structural and signaling molecules.

In a similar way, it would be interesting to compare the quantitative and qualitative state of key osteogenesis associated proteins such as Runx2, bone morphogenic proteins and receptors, bone sialoprotein subtypes etc. at the protein level with western blots. Gene expression is difficult to

interpret as it does not provide information at the protein level. Proteins levels in some instances may present more accurate information of an actual event as increased mRNA levels do not always lead to an increase in the effector molecules (proteins). The accurate identification of the effector molecules actually participating in the difference could help identify upstream molecular systems.

Different methods of Axl receptor deregulation could have been used to increase the contrast of cellular responses. The methods used here were sufficient to disrupt the normal activity, above (agonist) or below (antagonist) the required threshold. However, the method was not highly efficient in inhibiting receptor activity through binding endogenous Gas6 resulting in only incomplete inhibition of signaling, and therefore smaller variations in the measured responses. It would have been ideal to further assess the present findings using (i) transfection of expression vectors with receptor kinase variants (wild type vs. deficient); (ii) RNA interference to knock-down Gas6 synthesis; (iii) Axl or Gas6 knock-out mice. The disadvantages of these methods largely pertain to time constraints but may also manifest in altered cellular behavior due to the specimens sensitive nature. The Axl signaling initiates at the cell surface and progresses through different sub-cellular systems before generating its transcriptional effect, leading to phenotypic changes in the cells. Knowledge of the downstream effectors in this cascade would have made it possible to screen for changes in the protein levels of these molecules and therefore help to elucidate the end-effector and its concise biological function.

8 References cited

Reference List

Albrektsson,T., Branemark,P., Hansson,B., and Lindstorm,J. (1981). Osseointegrated titanium implants. Requirements for ensuring a long-lasting, direct bone-to-implant anchorage in man. Acta Orthop Scand *52*, 155-170.

Albrektsson,T. and Johansson,C. (2001). Osteoinduction, osteoconduction and osseointegration. Eur Spine J *10*, S96-S101.

Almaguer-Flores,A., Olivares-Navarrete,R., Wieland,M., Ximenez-Fyvie,L., Schwartz,Z., and Boyan,B. (2011). Influence of topography and hydrophilicity on initial oral biofilm formation on microstructured titanium surfaces in vitro. Clin Oral Impl Res *doi: 10.1111/j.1600-0501.2011.02184.x.*.

Anderson,H., Garimella,R., and Tague,S. (2005). The role of matrix vesicles in growth plate development and biomineralisation. Front Biosci *10*, 822-837.

AR Guntur and CJ Rosen (2011). The skeleton: a multi-functional complex organ. New insights into osteoblasts and their role in bone formation: the central role of PI3Kinase. J Endocrinol *211*, 123-130.

Arispe,N., Rojas,E., Genge,B., Wu,L., and Wuthier,R. (1996). Similarity in calcium channel activity of annexin V and matrix vesicles in planar lipid bilayers. Biophys J *71*, 1764-1775.

Aslan,H., Zilberman,Y., Kandel,L., Liebergall,M., Oskouian,R., Gazit,D., and Gazit,Z. (2006). Osteogenic differentiation of non-cultured immuisolated marrow derived CD105+ cells. Stem Cells *24*, 1728-1737.

Assender,H., Bliznyuk,V., and Porfyrakis,K. (2012). How surface topography relates to materials' properties. Science *209*, 973-976.

Aubin,J.E. (2001). Regulation of Osteoblast formation and function. Rev Endocr Metab Disord *2*, 81-94.

Barry,F., Boynton,R., Murphy,M., Haynesworth,S.E., and Zaia,J. (2001). The SH-3 and SH-4 Antibodies Recognize Distinct Epitopes on CD73 from Human Mesenchymal Stem Cells. Biochem Biophys Res Commun *289*, 519-524.

Bassey,O., Lowry,O., and Brock,M. (1946). A method for the rapid determination of alkaline phosphatase with five cubic millimeters of serum. J Biol Chem *164*, 321-329.

Becker,P., Tran,T., Delannoy,M., He,C., Shannon,J., and McGrath-Morrow,S. (2011). Semaphorin 3A contributes to distal pulmonary epithelial cell differentiation and lung morphogenesis. PLoS One *6*, e27449.

Benayahu,D., Akavia,U.D., and Shur,I. (2007). Differentiation of bone marrow stroma derived mesenchymal cells. Curr Med Chem *14*, 173-179.

Berk,B.C. (2001). Vascular Smooth Muscle Growth: Autocrine Growth Mechanisms. Physiol Rev *81*, 999-1030.

Bornstein,M., Valderrama,P., Jones,A., Wilson,T., Seibl,R., and Cochran,D.L. (2008). Bone apposition around two different sandblasted and acid-etched titanium implant surfaces: a histomorphometric study in canine mandibles. Clin Oral Impl Res *19*, 233-241.

Bornstein,M., Wittneben,J., Bragger,U., and Buser,D. (2010). Early loding at 21 days of non-submerged titanium implamts with a chemically modified sandblasted and acid-etched surface: 3-year results of a prospective study in the posterior mandible. J Periodontal *81*, 809-818.

Bosshardt,D., Salvi,G., Huynh-Ba,G., Ivanovski,S., Donos,N., and Lang,N. (2011). The role of bone debris in early healing adjacent to hydrophilic and hydrophobic implant surfaces in man. Clin Oral Impl Res *22*, 357-364.

Boyan,B., Lossdorfer,S., Zhao,G., Wang,L., Lohmann,C., Cochran,D.L., and Schwartz,Z. (2003a). Osteoblasts generate an osteogenic microenvironment when grown on surfaces with rough microtopographies. Eur Cell Mater *6*, 22-27.

Boyan,B., Schwartz,Z., Lohmann,C., Sylvia,V., Cochran,D.L., Dead,D., and Puzas,J. (2003b). Pretreatment of bone with osteoclasts affects phenotypic expression of osteoblast-like cells. J Orthop Res *21*, 638-647.

Branemark,P., Aspergren,K., and Breine,U. (1964). Microcirculatory studies in man by high resolution vital microscopy. Angiology *15*, 329-332.

Branemark,P., Hansson,B., Adell,R., Lindstorm,J., Hallen,O., and Ohman,A. (1977). Osseointegrated implants in the treatment of the edentulous jaw. Experience from a 10-year period. Scand J Plast Reconstr Surg *16*, 1-132.

Branemark,P. and Harders,H. (1963). Intravital analysis of microvascular form and function in man. Lancet *7*, 1197-9.

Branemark,P. (1983). Osseointegration and its experimental background. J of prosthetic dentistry *50*, 399-410.

Branemark,P. (2005). The osseointegration book. Quintessence books).

Branemark,P., Breine,R., Adell,R., Hansson,B., Lindstorm,J., and Ohlsson,A. (1969). Intra-osseous anchorage of dental prosthesis. Scand J Plast Reconstr Surg *3*, 81-100.

Brett PM, Harle,J., Salih,V., Mihoc,R., Olsen,I., Jones,F.H., and Tonetti,M. (2004). Roughness response genes in osteoblasts. Bone *35*, 124-133.

Brunette,D., Tengvall,P., Textor,M., and Thomsen,P. (2000). Titanium in medicine. Springer).

Budagian,V. (2005a). A promiscuous liasion between IL-15 receptors and Axl receptors tyrosine kinase in cell death control. EMBO *24*, 4260-4270.

Budagian,V. (2005b). Soluble Axl is generated by ADAM10 dependent cleavage and associates with Gas6 in mouse serum. Mol Cell Biol *25*, 9324-9339.

Buser,D., Broggini, Wieland, Schenk, Denzer, Cochra, Hoffmann, Lussi, and Steinemann (2004). Enhanced Bone Apposition to a Chemically Modified SLA Titanium Surface. J Dent Res *83*, 529-533.

Buser,D., Schenk, Steinemann, Fiorellini, Fox, and Stich (1991). Influence of surface characteristics on bone integration of titanium implants. A histomorphometric study in miniature pigs. J Biomed Mater Res A *25*, 889-902.

Caetano-Lopes,J., Canhao,H., and Fonseca,J.E. (2007). Osteoblasts and bone formation. Acta Reum Port *32*, 103-110.

Caplan,A. (2008). All MSCs are preicytes? Cell Stem Cell 229-230.

Caterson,E., Nesti,L., Danielson,K., and Tuan,R. (2002). Human marrow-derived mesenchymal progenitor cells Isolation, culture expansion, and analysis of differentiation. Mol Biotech *20*, 245-256.

Chen,N., O'Neill,K., Chen,X., and Moe,S. (2008). Annexin-Mediated Matrix Vesicle Calcification in Vascular Smooth Muscle Cells. J Bone Miner Res *23*, 1798-1805.

Chung,U., Kawaguchi,H., Takato,T., and Nakamura,K. (2004). Distinc osteogenic mechanisms of bones of distinct origins. J Orthop Sci *9*, 410-141.

Clarke,B. (2008). Normal bone anatomy and physiology. J Am Soc Nephrol *3*, S131-S139.

Collet,G.D.M., Sage,A.P., Kirton,J.P., Alexander,M.Y., Gilmore,A.P., and Canfield,A.E. (2006). Axl/phosphotidylinositol 3-kinase signalling inhibits mineral deposition by vascular smooth muscle cells. Circulation Research.

Collet,G.D.M., Sage,A.P., Kirton,J.P., Alexander,M.Y., Gilmore,A.P., and Canfield,A.E. (2007). Axl/phosphotidylinositol 3-kinase signalling inhibits mineral deposition by vascular smooth muscle cells. Circ Res *100*, 502-509.

Collet,G.D.M., Wood,A., Alexander,M.Y., Varnum,B.C., Boot-Handford,R.P., Ohanian,J., Ohaniuan,V., Fridel,Y., and Canfield,A.E. (2003). Receptor Tyrosine Kinase Axl Modulates the Osteogenic Differentiation of Pericytes. Circ Res *92*, 1123-1129.

Colter,D.C., Class,R., DiGirolamo,C.M., and Prockop,D.J. (2000). Rapid expansion of recycling stem cells in cultures of plastic-adherent cells from human bone marrow. PNAS *97*, 3213-3218.

Colter,D.C., Sekiya,I., and Prockop,D.J. (2001). Identification of a subpopulation of rapidly self-renewing and multipotential adult stem cells in colonies of human marrow stromal cells. PNAS *98*, 7841-7845.

Crisan,M. (2008). A Perivascular Origin for mesenchymal stem cells in multiple human organs. Cell Stem Cell *3*, 301-313.

Curtis,A. and Wilkinson,C. (1998). Topographical control of cell migration. In Motion analysis of living cells, D.Soll and D.Wessels, eds. (New York: Wiley-Les Inc), pp. 141-156.

David,V. (2007). Mechanical loading down-regulates peroxisome proliferator-activated receptor gamma in bone marrow stromal cells and favors osteoblastogenesis at the expense of adipogenesis. Endocrinology *148*, 2553-2562.

Davies,J. (1998). Mechanisms of endosseous integration. Int J Prosthodont *11*, 391-401.

Davies,J. (2003). Understanding Peri-implant endosseouns healing. J Dent Edu *67*, 932-949.

Davies,J. (2007). Bone bonding at natural and biomaterial surfaces. Biomaterials *28*, 5058-5067.

De Silva Merielles,L. (2008). In search of the in vivo identity of mesenchymal stem cells. Stem Cells *26*, 2287-2299.

Demer,L.L. and Tintut,Y. (2008). Vascular calcification: pathobiology of a multifaceted disease. Circ Res *117*, 2938-2948.

DiGirolamo,C.M., Stokes,D., Colter,D.C., Phinney,D.G., Class,R., and Prockop,D.J. (1999). Propagation and sensescence of human marrow stromal cells in culture: a simple colony fomring assay identifies samples with the greatest potential to propagate and differentiate. Br J Haematol *107*, 275-281.

Dimitriou,R., Tsiridis,E., and Giannoudis,P. (2005). Current concepts of molecular aspects of bone healing. Int J Dev Biol *36*, 1392-1404.

Farrington-Rock,C., Crofts,N., Doherty,M., Ashton,B., Griffin-Jones,C., and Canfield,A. (2004). Chondrogenic and angiogenic potential of microvascular pericytes. Circ Res *110*, 2226-2232.

Fazzalari,N. (2011). Bone fracture and bone fracture repair. Osteoporos Int *22*, 2003-2006.

Ferguson,S., Broggini,N., Wieland,M., de Wild,M., Rupp,F., Geis-Gerstorfer,J., Cochran,D.L., and Buser,D. (2006). Biomechanical evaluation of the interfacial strength of a chemically modified sandblasted and acid-etched titanium surface. J Biomed Mater Res A *78*, 291-297.

Fujita,K. and Janz,S. (2007). Attenuation of WNT signalling by DKK-1 and -2 regulates BMP2-induced osteoblasti differentiation and expression of OPG, RANKL and M-CSF. Mol Cancer *6*, 71-84.

Fukumoto,S. and Martin,T. (2009). Bone as an endocrine organ. Trends Endocrinol Metab *20*, 230-236.

Gene Cards, Weizmann Institute of Science. http://www.genecards.org/ . 2011.

Gene Ontology Project, Gene Ontology Consortium. www.geneontology.org/ . 2011.

Gilbert,S. (2000). Developmental biology. (Massachusetts: Sinauer Associates Inc Publishers).

Goruppi,S., Chiaruttini,C., Ruaro,M., Varnum,B.C., and Schneider,C. (2001). Gas6 induces growth, beta-catenin stabilisation, and t-cell factor transcriptional activation in contact-inhibited C57 mammary cells. Mol Cell Biol *21*, 902-915.

Gotfredsen,K., Wannerberg,A., Johansson,C., Skovogard,L., and Hjorting-Hansen,E. (1995). Anchorage of TiO2 blasted, HA-coated and machined implants; an experimental study with rabbits. J Biomed Mater Res A *29*, 1223-1231.

Gregory,C., Gunn,W., Peister,A., and Prockop,D.J. (2004). An Alizarin red-based assay of mineralization by adherent cells in culture: comparison with cetylpyridinium chloride extraction. Anal Biochem *329*, 77-84.

Gronthos,S., Zannettino,A.C.W., Hay,S.J., Shi,S., Graves,S.E., Kortesdis,A., and Simmons,P.J. (2003). Molecular and cellular characterisation of highly purified stromal stem cells derived from human bone marrow. J Biol Sci *116*, 1827-1835.

Guehennec,L.L., Soueidan,A., Layrolle,P., and Amouriq,Y. (2007). Surface treatments of titanium dental implants for rapid osseointegration. Dental Materials *23*, 844-854.

Hafizi,S. and Dahlback,B. (2006). Signalling and functional diversity within the Axl subfamily of receptor tyrosine kinases. Cytokine Growth Factor Rev *17*, 295-304.

Hall,B. (2005). Bones and cartilage: developmental and evolutionary skeletal biology. Elsevier Academic Press).

Hansson,S. and Norton,M. (1999). The relation between surface roughness and interfacial shear strength for bone-anchored implants. A mathematical model. J Biomech *32*, 829-836.

Harle,J., Salih,V., Olsen,I., Brett PM, Jones,F., and Tonetti,M. (2004). Gene Expression Profiling of Bone Cells On Smooth and Rough Titanium Surfaces. J Mater Sci Mater Med *15*, 1255-1258.

Harrison,R. (1911). On the stereotropism of embryonic cells. Science *34*, 279-281.

Hattori,T., Muller,C., genhard,S., Bauer,E., Pausch,F., Schlund,B., Bosl,M., Hess,A., Surmann-Schmitt,C., mark,H., Crombrugghe,B., and Mark,K. (2010). Sox9 is a major negative regulator of cartilage vascularisation, bone marrow formation and endochondral ossification. Development *137*, 901-911.

Honczarenko,M., Le,Y., Swierkowski,M., Ghiran,I., Glodek,A., and Silberstein,L. (2006). Human Bone Marrow Stromal Cells Express a Distinct Set of Biologically Functional Chemokine Receptors. Stem Cells *24*, 1030-1041.

Horwitz,E., Le Blanc,K., Dominici,M., Mueller,I., Slaper-Cortenbach,I., Marini,F., Deans,R., Krause,D., and Keating,A.K. (2005). Clarification of the nomenclature for MSC: The International Society for Cellular Therapy position statement. Cytotherapy *7*, 393-395.

International Stem Cell Initiative (2007). Characterization of human embryonic stem cell lines by the International Stem Cell Initiative. Nat Biotech *25*, 803-816.

Ivanovski,S., Hamlet,S., Salvi,G., Huynh-Ba,G., Bosshardt,D., Lang,N., and Donos,N. (2011). Transcriptional profiling of osseointegration in humans. Clin Oral Impl Res *22*, 373-381.

Javazon,E.H., Beggs,K., and Flake,A. (2004). Mesenchymal stem cells: Paradoxes of passaging. Exp Hematol *32*, 414-425.

Johnson,R.C., Leopald,J.A., and Loscalzo,J. (2006). Vascular calcification pathobiological mechanisms and clinical implications. Circ Res *99*, 1044-1059.

Jones,E. and McGonagle,D. (2008). Human bone marrow mesenchymal stem cells in vivo. Rheumatology *47*, 126-131.

Jung,Y., Oh,S., Zheng,D., Shupe,T., Witek,R., and Petersen,B. (2006). A potential role of somatostatin and its receptor SSTR4 in the migration of hepatic oval cells. Lab Invest *86*, 477-489.

Kolf,C.M., Cho,E., and Tuan,R.S. (2007). Biology of adult mesenchymal stem cells: regulation of niche, self-renewal and differentiation. Arthritis Res Ther *9*, 204.

Kou,P., Schwartz,Z., Boyan,B., and Babenesee,J. (2011). Dendritic cell responses to surface properties of clinical titanium surfaces. Acta Biomater *7*, 1354-1363.

Kuznetsov,S.A., Mankani,M.H., Gronthos,S., Satomura,K., Bianco,P., and Robey,P.G. (2008). Circulating skeletal stem cells. J Cell Biol *153*, 1133-1140.

Lai,H., Zhuang,L., Liu,X., Wieland,M., Zhang,Z., and Zhang,Z. (2009). The influence of surface energy on early adherent events of osteoblast on titanium substrates. J Bone Miner Res *93*, 289-296.

Lamkanfi,M., Festjens,N., Declercq,W., Vande Berge,T., and Vandenabeele,P. (2007). Caspases in cell survival, proliferation and differentiation. Cell death and differentation *14*, 44-55.

Lazennec G and Jorgensen,C. (2008). Adult Multipotent stromal cells and cancer: rish or benefit? Stem Cells *26*, 1387-1394.

Lee,M., Lowe,G., Strong,D., Wergedal,J., and Glackin,C. (1999). TWIST, a basic helix-loop-helc transcription factor can regulate the human osteogenic lienage. J Biol Chem *75*, 566-577.

Lekholm,U., Zarb,G., and Albrektsson,T. (1985). Patient selection and preparation. (Chicago: Quintessence Publishing Co Inc).

Lindhe,J., Land,P., and Karring,T. (2000). Proceedings of the 3rd European workshop on periodontology. Quintessence).

Linger,R.M.A., Keating,A.K., Earp,S., and Graham,D.G. (2008). TAM receptor tyrosine kinases: biological functions, signalling and potential therapeutic targeting in human cancer. Adv Cancer Res *100*, 35-83.

Liu,E., Hjelle,B., and Bishop,J.M. (1988). Transforming genes in chronic myelogenous leukemia. PNAS *85*, 1952-1956.

Liu,X., Chu,P., and Ding,C. (2004). Surface modification of titanium, titanium alloys, and related materials for biomedical applications. Mat Sci Eng *47*, 49-121.

Loeffler,M. and Roeder,I. (2002). Tisasue stem cells: definition, plasticity, heterogeneity, self-organisation and models- a conceptual approach. Cells Tissues Organs *171*, 8-26.

Mackie,E., Tatarczurch,L., and Mirams,M. (2011). The skeleton: a multi-functional complex organ. The growth plate chondrocyte and endochondral ossification. J Endocrinol *211*, 109-121.

Marco,F., Milena,F., Gianluca,G., and Vittoria,O. (2005). Peri-implant osteogenesis in health and osteoporosis. Micron *36*, 630-644.

Marie,P. (2008). Transcription factors controlling osteoblastogenesis. Arch Biochem Biophys *473*, 98-105.

Masaki,C., Schneider,G.B., Zaharias,R., Seabold,D., and Stanford,C. (2005). Effects of implant surface microtopohgraphy on osteoblast gene expression. Clin Oral Impl Res *16*, 650-656.

McBeath,R., Pirone,D.M., Nelson,C.M., Bhadriraju,K., and Chen,C.S. (2004). Cell shape, cytoskeletal tension and RhoA regulate stem cell lineage commitment. Dev Cell *6*, 483-495.

McCloskey,P., Fridell,Y.W.C., Attar,E.C., Villa,J., Varnum,B.C., and Liu,E. (1997). Gas6 mediates adhesion of cells expressing the receptor tyrosine kinase Axl. J Biol Chem *272*, 23285-23291.

McNutt,M. and Chou,C. (2003). Current trends in immediate osseous dental implant case selection criteria. J Dent Edu *67*, 850-859.

Mendonca G, Mendonca D, Aragao,F., and Cooper,L. (2008). Advancing dental implant surface topography - from micron to nanotopography. Biomaterials *29*, 3822-3835.

Miron,R., Oates,C., Molenberg,A., Dard,M., and Hamilton,D. (2010). The effect of enamel matrix proteins on the spreading, proliferation and differentiation of osteoblasts cultured on titanium surfaces. Biomaterials *31*, 449-460.

Miura,M., Chen,X., Allen,M., Bi,Y., Gronthos,S., Seo,B., Lakhani,S., Flavell,R., Feng,X., Roey,P., Young,M., and Shi,S. (2004). A crucial role of caspase-3 in osteogenic differentiation of bone marrow stromal stem cells. J Clin Invest *114*, 1704-1713.

Nakamura,A., Dohi,Y., Akahane,M., Ohgushi,H., Nakajima,H., Funaoka,H., and Takakura,Y. (2009). osteocalcin secretion as an early marker of in vitro osteogenic differentiation of rat mesenchymal stem cell. Tissue Eng C *15*, 169-180.

Neubauer, A, Burchert, A, Maiwald, C Gruss H J, Serke, S, Huhn, D, Wittig, B, and Liu, E. Recent progress on the role of Axl, a receptor tyrosine kinase, in malignant transformation of myeoloid leuikemias. Leuk Lymphoma 25[1], 91-96. 1997.

Nishimoto,S.K., Nishimoto,M., Park,S., Lee,K., Kim,H., Koh,J., Ong,J., Liu,Y., and Yang,Y. (2007). The effect of titanium surface roughening on protein absorption, cell attachment and cell spreading. Int J Oral Maxillofac Implants *23*, 675-680.

Novack,D. and Teitelbaum,S. (2008). The osteoclast: friend or foe? Annu Rev Pathol Mech Dis *3*, 457-484.

O'Bryan,J.P., Frye,R.A., Cogswell,P.C., Neubauer,A., Kitch,B., Prokop,C., Espinosa,R., LE Beau,M.M., Earp,H.S., and Liu,E. (1991). axl, a transforming gene isolated from primary human myeloid leukemia cells, encodes a novel receptor tyrosine kinase. Mol Cell Biol *11*, 5016-5031.

Olivares-Navarrete,R., Hyzy,S., Hutton,D., Erdman,C., Wieland,M., Boyan,B., and Schwartz,Z. (2010a). Direct and indirect effects of microstructured titanium substrates on the induction of mesenchymal stem cell differentiation towards the osteoblast lineage. Biomaterials *31*, 2728-2735.

Olivares-Navarrete,R., Hyzy,S., Park,J., Dunn,G., Haithcock,D., Wasilewski,C., Boyan,B., and Schwartz,Z. (2011). Mediation of osteogenic differentiation of human mesenchymal stem cells on titanium surfaces by a Wnt-integrin feedback loop. Biomaterials *Epud ahead of print*.

Olivares-Navarrete,R., Hyzy,S., Wieland,M., Boyan,B., and Schwartz,Z. (2010b). The roles of Wnt signaling modulators Dickkopf-1 (Dkk1) and Dickkopf-2 (Dkk2) and cell maturation state in osteogenesis on microstructured titanium surfaces. Biomaterials *31*, 2015-2024.

Online Mendelian Inheritance in Man, OMIM McKusick-Nathans Institute of Genetic Medicine Johns Hopkins University Baltimore MD. http://omim.org/ . 2011.

Orlic,D., Kajstura,J., Chimenti,S., Bodine,D., Leri,A., and Anversa,P. (2003). Bone marrow stem cells regenerate infacted myocardium. Pediatr Transplantation *7*, 86-88.

Orlic,D., Kajstura,J., Chimenti,S., Jokoniuk,I., Anderson,S., Li,B., Pickel,J., McKay,R., Nadal-Ginard,B., Bodine,D., Leri,A., and Anversa,P. (2001). Bone marrow cells regenerate infarcted myocardium. Nature *410*, 701-705.

PANTHER, Gene Classification System. http://www.pantherdb.org. 2011.

Pavlako FM, Norvell,S., Burr,D., Turner,C., Duncan,R., and Bidwell,J. (2003). A model for mechanotransduction in bone cells: the load bearing mechanosomes. J Cell Biochem *88*, 104-112.

Pittenger,M., Mackay,A., Beck,S., Jaiswal,R., Douglas,R., Mosca,J., Moorman,M., Simonetti,D., Craig,S., and Marshak,D. (1999). Multilineage Potential of Adult Human Mesenchymal Stem Cells. Science *284*, 143-147.

Puchtler,H., Meloan,S., and Terry,M. (1969). On the history and mechanism of alizarin and alizarin red s stains for calcium. J Hist Cyto *17*, 110-124.

Puelo,D. and Nanci,A. (1999). Understanding and controlling the bone–implant interface. Biomaterials *20*, 2311-2321.

Raghavendra,S., Wood,M., and Taylor,T. (2005). Early wound healing adjacent to endosseous dental implants: A review of the literature. Int J Oral Maxillofac Implants Eprint.

Rausch-Fan,X., Qu,Z., Wieland,M., Matejka,M., and Schedle,A. (2007). Differentiation and cytokine synthesis of human alveolar osteoblasts compared to osteoblast like cells in response to titanium surfaces. Dental Materials *24*, 102-110.

Rupp,F., Schneider,C., Olshanska,N., de Wild M, Wieland,M., and Geis-Gerstorfer,J. (2006). Enhancing surface free energy and hydrophilicity through chemical modification of microstructured titanium implant surfaces. J Biomed Mater Res A *76*, 323-334.

Sakka,S. and Coulthard,P. (2011). Implant failure: Etiology and complications. Med Oral Patol Oral Cir Bucal *1*, e42-44.

Santos,A., Bakker,A., De Blied-Hogervorst,J., and Klein-Nulend,J. (2010). WNT5a induces osteogenic differentiation of human adipose stem cells cia rho associated kinase Rock. Cytotherapy *12*, 924-932.

Santos,M., Campos,M., and Line,S. (2002). Early dental implant failure: a review of the literature. Braz J Oral Sci *1*, 101-111.

Schneider,C., King,R., and Philipson,L. (1988). Genes specifically expressed at growth arrest of mammalian cells. Cell *9*, 787-793.

Schwartz,F., Sager,M., Kadeka,I., Ferrari,D., and Becker,J. (2010). Influence of titanium implant surface characteristics on bone regeneration in dehiscence type defects: an experimental study in dogs. J Clin Periodontol *37*, 466-473.

Schwartz,F., Wieland,M., Schwartz,Z., Zhao,G., Rupp,F., Geis-Gerstorfer,J., Schedle,A., Broggini,N., Schedle,A., Bornstein,M., Buser,D., Ferguson,S., Becker,J., Boyan,B., and Cochran,D.L. (2009a). Potential of chemically modified hydrophilic surface characteristics to support tissue integration of titanium dental implants. J Biomed Mater Res A *88B*, 544-557.

Schwartz,Z., Lohmann,C., Oefinger,J., Bonewald,L., Dead,D., and Boyan,B. (1999). Implant Surface Characteristics Modulate Differentiation Behavior of Cells in the Osteoblastic lineage. Adv Dent Res *13*, 38-48.

Schwartz,Z., Olivares-Navarrete,R., Wieland,M., Cochran,D.L., and Boyan,B. (2009b). Mechanisms regulating increased production of osteoprotegrin by osteoblasts cultured on microstructured titanium surfaces. Biomaterials *30*, 3390-3396.

Sekiya,I., Larson,B.L., Smith,J.R., Pochampally,R., Cui,J., and Prockop,D.J. (2002). Expansion of human adult stem cells from bone marrow stroma: conditions that maximise yields of early progenitors and evaluate their quality. Stem Cells *20*, 530-541.

Sennerby,L., Thomsen,P., and Ericson,L. (1992). Ultrastructure of bone-titanium interfce in rabbits. J Mat Sci *3*, 262-271.

Shankar S L (2006). Gas6/Axl signalling activates the phophatidylinositol 3-kinase/Akt1 survival pathway to protect oligodendrocytes from tumor necrosis factor alpha-induced apoptosis. J Neurosci *26*, 5638-5648.

Shanti,R.M., Li,W.J., Nesti,L.J., Wang,X., and Tuan,R.S. (2007). Adult Mesenchymal Stem cells: Biological properties, characteristics, and applications in maxillofacial surgery. J Oral Mazillofac Surg *65*, 1640-1647.

Shapiro,F. (2008). Bone development and its relation to fracture repair. The role of mesenchymal osteoblasts and surface osteoblasts. Eur Cell Mat *15*, 53-76.

Shore,E., Xu,M., Fieldman,G., Frenstermacher,D., Cho,T., Choi,I., Connor,J., Delai,P., Glaser,D., LeMerrer,M., Morhard,R., Rogers,J., Smith,R., Tfiffitt,J., Urtizberea,J., Zasloff,M., Brown,M., and Kalplan,F. (2006). A recurrent mutation in the BMP type I receptor ACVR1causes inherited and sporadic fibrodysplasia ossificans progressiva. Nat Gen *38*, 525-527.

Sikavitsas,V., Temenoff,J., and Mikos,A. (2001). Biomaterials and bone mechanotransduction. Biomaterials *22*, 2581-2593.

Simmons,P.J. and Torok-Storb,B. (1991). Indentification of stromal cell precursors in human bone marrow by a novel monoclonal antobody stro-1. Blood *78*, 55-62.

Soejitno,A., Wihandani,D., and Kuswardhani,R. (2010). Clinical applications of stem cell therapy for regenerating the heart. Acta Med Indones *42*, 243-257.

Son,B., Kozaki,K., Iijima,K., Eto,M., Kojima,T., Ota,H., Senda,Y., Maemura,K., Nakano,T., Akishita,M., and Ouchi,Y. (2006). Statins protect human aortic smooth uscle cells from inorganic phosphate induces calcification by restoring Gas6-Axl survival pathway. Circ Res *98*, 1024-1031.

Song,L. and Tuan,R. (2004). Transdifferentiation potential of human mesenchymal stem cells derived from bone marrow. FASEB *18*, 980-982.

Stenfelt,S. (2011). Acoustic and physiologic aspects of bone conduction hearing. Adv Otorhinolaryngol *71*, 10-21.

Stewart,K., Mond,P., Walsh,S., Jefferiss,C., Letchford,J., and Beresford,J. (2003). STRO-1, HOP-26 (CD63), CD49a and SB-10 (CD166) as markers of primitive human marrow stromal cells and their more differentiated progeny: a comparative investigation in vitro. Cell Tissue Res *313*, 281-290.

Stitt,T., Conn,G., Goret,M., Lai,C., Brunno,J., Radzlejewski,C., Mattsson,K., Fisher,J., Gies,D., Jones,P., Masiakoski,P., Ryan,T., Tobkes,N., Chen,D., DiStefano,P., Long,G., Basilico,C., Goldfarb,M., Lemke,G., Glass,D., and Yancopoulous,G. (1995). The anticoagulation factor protein S and its relative, Gas6, are ligands for the Tyro 3/Axl family of receptor tyrosine kinases. Cell *80*, 661-670.

Takahashi,N., Maeda,M., Ishihara,A., Uehara,S., and Kobayashi,Y. (2011). Regulatory mechanisms of osteoclastogenesis by RANKL and Wnt signals. Front Biosci *1*, 21-30.

Tinsley,D., Watson,C., and Ogden,A. (1999). Implant Surface Characteristics Modulate Differentiation Behavior of Cells in the Osteoblastic. Journal of Oral Rehabilitation *26*, 14-18.

Tortora,G. and Derrickson,B. (2009a). The skeletal system: bone tissue. In Principles of anatomy and physiology, John Wiley & Sons. Inc.), pp. 176-1991.

Tortora,G. and Derrickson,B. (2009b). The skeletal system: The axial skeleton. In Principles of anatomy and physiology, (Hoboken: John Wiley & Sons), pp. 198-234.

Tuan,R. (2011). Role of adult stem/progenitor cells in osseointegration and implant loosening. Int J Oral Maxillofac Implants *26*, 50-62.

Tzouvelekis,A., Antoniadis,A., and Bouros,D. (2011). Stem cell therapy in pulmonary fibrosis. Curr Opin Pulm Med *17*, 368-373.

Ulf Bagge (1989). The Branemark Titanium Chamber for Intravital Microscopy of the human microcirculation. In The Branemark Osseointegrated Implant, pp. 21-23.

University of Utah, WebPathology. Von Kossa stain. http://library.med.utah.edu/WebPath/HISTHTML/MANUALS/VONKOSSA.PDF 2011.

Valeria,S. (2009). Mesenchymal stem cell homing capacity. Transplantation *87*, S42-S45.

Vassilios,I., Temenoff,J., and Mikos,A. (2001). Biomaterials and mechanotransduction. Biomaterials *22*, 2581-2593.

Vattikut,R. and Towler,D. (2004). Osteogenic regulation of vascular calcification. Am J Physiol Endocrinol Metab *286*, E686-E696.

Vlacic-Zischke,J., Hamlet,S., Friis,T., Tonetti,M., and Ivanovski,S. (2010). The influence of surface microroughness and hydrophilicity of titanium on the up-regulation of TGFb/BMP signalling in osteoblasts. Biomaterials *32*, 665-671.

Wall,I., Donos,N., Calqvist,K., Jones,F., and Brett,P. (2009). Modified titanium surfaces promote accelerated osteogenic differentiation of mesenchymal stromal cells in vitro. Bone EPub ahead of print.

Wall,M.E., Bernaki,S.H., and Loboa,E.G. (2007). Effects of serial passaging on the adipogenic and osteogenic differentiation potential of adipose derived human mesenchymal stem cells. Tissue Eng *13*, 1291-1298.

Wannerberg,A., Albrektsson T, Johansson,C., and Andersson,B. (1996). Experimental study of turned and grit blasted screw shaped implants with special emphasis on effects of blasting material andsurface topography. Biomaterials *17*, 15-22.

Wennerberg,A. and Albrektsson,T. (2009). Effects of titanium surface topography on bone integration: a systematic review. Clin Oral Impl Res *20*, 172-182.

Williams,A. and Hare,J. (2011). Mesenchymal stem cells: Biology, pathophysiology, translational findings, and therapeutic implications for cardiac disease. Circ Res *109*, 923-940.

Zhang,Y., Andrukhov,O., berner,S., Matejka,M., Wieland,M., Rausch-Fan,X., and Schedle,A. (2010). Osteogenic properties of hydrophilic and hydrophobic titanium surfaces evaluated with osteoblast like cells in coculture with umbilical vein endothelial cells. Dent Mat *26*, 1051.

Zhang,Y., Goss,A., Cohen,E., Kadzik,R., Lepore,J., Muthkumaraswamy,K., Yang,J., DeMayo,F., Whilsett,J., Parmacek,M., and Morrisey,E. (2008). A Gata6-Wnt pathway required for epithelial stem cell development and airway regeneration. Nat Genet *40*, 862-870.

Zhao,G., Raines,A., Wieland,M., Schwartz,Z., and Boyan,B. (2007). Requirement for both micron and sub-micron scale structure for synergistic responses of osteoblasts to substrate energy and topography. Biomaterials *31*, 2728-2735.

Ziros,P., Basdra,E., and Papavassiliou,A. (2008). Runx2: of bone and stretch. Int J Biochem Cell Biol *40*, 1659-1663.

Zuk,P., Zhu,M., Ashjin,P., Ugarte,D., Huang,J., Mizuno,H., Alfonso,Z., Fraser,J., Benhaim,P., and Hedrick,M. (2002). Human adipose tissue is a source of multipotent stem cell. Mol Biol Cell *13*, 4279-4295.

9 Appendices

9.1 Appendix I: Stem cell identity markers

The appendix I contains tables for cell surface markers presently considered as either positive, negative or neutral for flow-cytometry based cell identification procedures. These are tables 9-1, 9-2, and 9-3, respectively.

Table 9-1 Positive human mesenchymal stromal cell markers

These molecules are strongly associated with the positive identification of mutlipotent fibroblastic cells isolated from bone marrow. Gene annotations obtained from (Gene Cards, 2011).

Molecular marker	Description	General function	Reference
Stro 1	A tryspin resistant unidentified antigen	unknown	(Simmons and Torok-Storb, 1991)
CD 13	Alanyl (membrane) Aminopeptidase	Integrin family membrane receptors	(Honczarenko et al., 2006)
CD 29	Fibronectin Receptor, Integrin beta 1	Involved in cell adhesion and recognition	(De Silva Merielles, 2008)
CD 44	Extracellular matrix receptor-III, Cell Surface Glycoprotein	Involved in cell adhesion and recognition	(Gronthos et al., 2003)
CD 63	Lysosomal Membrane Glycoprotein; Melanoma 1 Antigen	regulation of cell development, activation, growth and motility	(Stewart et al., 2003)
CD 73	Purine 5-Prime-Nucleotidase	Catalyses conversion of purine 5-prime mononucleotides to	(Barry et al., 2001)
CD 90	Thy-1 membrane glycoprotein precursor	Cell-Cell Interactions	(Honczarenko et al., 2006)
CD 105	Endoglin	Component of the transforming growth factor beta receptor complex	(Honczarenko et al., 2006)
CD 166	Activated Leucocyte Cell Adhesion Molecule	Implicated in cell to cell adhesion through homophilic and heterphilic binding	(Wall et al., 2007)
CD 217	IL17RA	A ubiquitous type I membrane glycoprotein that binds with low affinity to interleukin 17A	(Jones and McGonagle, 2008)

Table 9-2 Negative expressed human mesenchymal stromal cell marker

Gene annotations obtained from (Gene Cards, 2011)

Molecular marker	Description	General function	Reference
CD11b	Integrin Alpha M	Cell-Cell Interactions	(De Silva Merielles, 2008)
CD14	Monocyte Differentiation Antigen	Lipopolysaccharide and apoptotic cell binding surface protein, expressed on monocytes/lymphocyte precursors	(Pittenger et al., 1999)
CD19	B-lymphocyte antigen	Cell surface molecule which assembles with the antigen receptor of B lymphocytes in order to decrease the threshold for antigen receptor-dependent stimulation.	
CD31	Platelet/Endothelial Cell Adhesion Molecule	Cell adhesion molecule expressed on platelets and at endothelial cell intercellular junctions	(Pittenger et al., 1999)
CD34	Hematopoietic Progenitor Cell Antigen	A monomeric cell surface antigen selectively expressed on human hematopoietic progenitor cells	(Online Mendelian Inheritance in Man, 2011)
CD45	Leukocyte-common antigen	Required for T-cell activation through the antigen receptor	(Zuk et al., 2002)
CD59	T cell-activating protein	Regulates complement-mediated cell lysis and is involved in lymphocyte signal transduction	(Javazon et al., 2004)
CD79-alpha	B-cell antigen receptor complex-associated protein alpha chain	CD79B for initiation of the signal transduction cascade activated by binding of antigen to the B-cell antigen receptor complex	(Valeria, 2009)
c-Kit		Hematopoietic Stem Cell Growth Factor Receptor	(Orlic et al., 2001)
HLA-DR	Major Histocompatibility Complex Class 2	Presentation of Antigens to CD8+ T-Cells	(De Silva Merielles, 2008)

Table 9-3 Variably expressed cell surface markers on hMSCs

Gene annotations obtained from (Gene Cards, 2011)

Molecular marker	Description	General function	Reference
hTert	Human Telomerase Enzyme Reverse Transcriptase	Enzymatic subunit of telomere length maintaining protein present in early aged cells	(Colter et al., 2001)Colter et al 2001
Flk-1	Vascular Endothelial Growth Factor. Expressed on RS cells but not on mMSCs.	Receptor for VEGF or VEGFC. Has a tyrosine-protein kinase activity.	(Colter et al., 2001)
CD106	Vascular cell adhesion molecule	low expression relative to high Stro1; a cell surface sialoglycoprotein expressed by cytokine-activated endothelium	(Gronthos et al., 2003)
Ki-67	Cell Proliferation Antigen	Absent in fresh isolates	(Orlic et al., 2003)

9.2 Appendix II: Types of serum tested for culture optimisation

The table 9-4 shows the type, source and batch number of the six different sera types used for the experiments conducted in section 2.2.4.

Table 9-4 Types of FBS tested for hMSC culture

Type	Serum Source	Serum catalogue/Batch No
A	Gibco-A	41F8061K
B	Gibco-B	41F3083K
C	Lonza-A	DE14-801C-B0002
D	Lonza-B	DE14-870C-B0001
E	Biosera	05464 S1810
F	PAA (Control)	A15-151-1570

9.3 Appendix III: Tabulation of cell culture materials

The tables 9-5 to 9-9 tabulate details of the various equipment and materials used in this project.

Table 9-5 Cell culture environment

Item No.	Equipment	Manufacturer	Application
1	Laminar Flow Cabinet	NUAIRE Class II with UV-tube	Confined clean work environment; pre-cleaned with 70% ethanol spray and propanol wipes prior to every use
2	Incubator	Nuaire NU-5500 DH AutoFlow Co2 Incubator	Set at 5% CO_2 and 37^0C for cell incubation; cleaned every fortnight with bleaches.
3	Cryogenic cell storage	Thermo Scientific	Liquid nitrogen containing chamber with removable lid and six vertical racks, each capable of containing 5 x 96 sample cryo-boxes. Re-stocked with liquid nitrogen every fortnight.
4	Water bath	ETI 800 series	Weekly cleaned 50 L chamber with adjustable thermostat, set at 37^0C
5	Inverted microscope	Olympus CXK31	Standard device with fixed binocular observation tube and 4, 10, 40 and 100x magnification objective lenses.
6	Hemocyto-meter with trypan blue	Sigma	Standard 9x (1 x1 mm) grid with cover slip.
7	Centrifuge	Different	Tissue culture purposed large centrifuge. Microcentrifuge for smaller samples.
8	Pipettes	Qiagen	Calibrated pipette ‘gun’ and 1000, 200, 20 and 10 uL micropipettes.

Table 9-6 Cell culture consumables

Item No.	Equipment	Manufacturer	Applications
1	Flasks	Fluka	Enclosed polystyrene flasks with a negatively charged inner substratum for cell culture. Three sizes used in this study: 150, 75 and 25 cm^2 flasks. Inner space accessed through an air-permeable screw-able cap.
2	Plates	Nunc	Treated polystyrene multi-well plates with removable lid. Three types used depending on individual well size: 9.6 cm^2 6-well; 1.9 cm^2 24-well; and 0.19 cm^2 96 well plates.
3	Tubes	Nunc	Sterile polystyrene tubes for various cell culture purposes. Sizes used: 50, 15, 2 and 1.5 ml.
4	Microtubes	Nunc	Sterile plastic tubes of 500 and 100 uL.

5	Cryopreservation tubes	Nunc	Male-screw sterile plastic vials of 2 ml volume for cryopreserving cells.
6	Tube Racks	Generic	Autoclavable plastic racks of various sizes.

Table 9-7 Cell culture reagents

Abbreviations of reagents used in text are provided in the corresponding row under the applications column.

Item No.	Reagent	Manufacturer	Applications
1	Alpha minimal essential medium	Gibco	**αMEM**; L-Glutamine supplemented basal medium for hMSC propagation and growth.
2	Dulbecco's modified eagle's medium	PAA Lab.	**DMEM**; L-Glutamine supplemented low-glucose (1 g / L) basal medium for hABC growth. Also used as basal medium for forming osteogenic inductive medium.
3	Trypsin/EDTA	PAA Lab.	A solution of 0.05 % / 0.002 % Trypsin/EDTA in calcium and magnesium free phosphate buffered saline.
4	Ca^{2+} Mg^{2+} free Phosphate Buffered Saline	PAA Lab.	**Dication-free PBS**; an isotonic solution of NaCl in water used for cell washing, and dilutions.
5	Fetal Bovine Serum (FBS)	Gibco	**FBS**; heat inactivated serum sourced from South America, supplemented to basal medium to nourish cells whilst in culture.
6	Antibiotics	PAA Lab.	A mixture of Penicillin 10 Units / ml and Streptomycin 10 mg / ml in dication-free PBS. This was occasionally supplemented with the fungicide Amphotericin B at 0.2 % of culture medium.
7	DMSO	Sigma	Dimethyl sulfoxide; used as a cryoprotectant for cryopreserving cells.
8	Dexamethasone	Sigma	Water soluble glucocorticoid molecule complexed with Cyclodextrin in osteogenic differentiation.
9	β-glycerophosphate	Fischer	Water soluble phosphate donor in osteogenic differentiation.
10	Asorbate-3-phsphate	Fischer	Metabolite used for collagen synthesis in osteogenic differentiation.

Table 9-8 Sterilisation equipment

Item No.	Equipment	Manufacturer	Applications
1	Alcohols	Various	Industrial methylated spirit at 70 % in water and used as a sterilizing spray. Propanol wipes (Azowipes) were used also applied to clean large surfaces.
2	Autoclave		Pressurised steam sterilizer set at 126 ^{o} C for 20 min.
3	Ultra violet radiation	Steristorm	UV light cabinet set at 255 nm wavelength of radiation.
4	Bunsen burner	Various	Portable flame burner used for heat sterilisation of mainly metallic instruments, such as forceps, scalpels.

Table 9-9 Volume of medium used per surface area of culture vessel

Cell culture vessel	Surface area of culture substrate (cm^2)	Volume of liquid (ml)
Large culture flask T150	150	25
Medium culture flask T75	75	10
Small culture flask T25	25	5
6-well multiwall treated plate	9.6	3
24-well multiwall treated plate	1.96	1
96-well multiwall treated plate	0.3	0.2

9.4 Appendix IV: Taqman probes for osteogenic markers

Table 9-10 List of genes examined in hMSC responses to Ti surfaces

Category	Genes	Information	Probe serial number
Transcription factors	Runx2	Master osteogenic regulator	Hs01047975_m1
Extracellular Matrix components	OP,	Bone matrix component protein	Hs00959010_m1
	BSP2	Bone matrix component protein	Hs00913377_m1
	Col1a1	Primary organic phase of bone	Hs00164004_m1
	ALP	inorganic phosphate synthesis by cleavage from pyrophosphate	Hs01029144_m1
Secreted osteogenic regulators	Wnt5a	Regulation of BMP expression	Hs00998537_m1
	OC/BGLAP	Calcium binding molecule	Hs01587814_g1
	OPG, GDF-15	Negative regulators of osteoclastogenesis	Hs00900358_m1; Hs00171132_m1
	TGF-b1	Regulator of osteoblastic differentiation	Hs00998133_m1
Cell surface integrins	ITGα2, ITGβ1	Implicated Ti-specific cell surface regulators of cell function	Hs00158127_m1 Hs00559595_m1
Adipogenic marker	PPARγ	Nuclear protein, important for adipogenic differentiation	Hs01115513_m

9.5 Appendix V: Stem cell gene array

Four sets of genes were represented on the AppliedBiosystems Human Pluripotency Microfluidic miniarrays. The details of the genes and their functions are tabulated in tables 9-11, 9-12, 9-13 and 9-14 for controls, maintenance of stem cellness, pluritpotency and differentiation genes, respectively.

These tables consist of five columns; entitled gene symbol, description, molecule type, process and gene function. The first and second columns provide information re: gene identity. The third is the designate of molecule type, extracted from the PANTHER Classification System (Protein ANalysis Through Evolutionary Relationships)(PANTHER, 2011). The process column states the biological processes the gene is suggested to be involved in, and these were derived from the Gene Ontology project (Gene Ontology Project, 2011; PANTHER, 2011) . The presented processes represent the significance of gene function in the context of stem cell differentiation. Biological descriptions are derived from NCBI (Online Mendelian Inheritance in Man, 2011) or Gene Cards v 3 (Gene Cards, 2011). These descriptions do not represent the entire repertoire of possible functions of the genes, but those that are observably significant to stem cell biology. These reference databases were accessed April, 2011.

Table 9-11 Miniarray: control genes

Molecule type obtained from (PANTHER, 2011). Process obtained from (Gene Ontology Project, 2011). Gene function obtained from NCBI (Online Mendelian Inheritance in Man, 2011).

Gene symbol	Description	Molecule type	Process	Gene function
18S	Ribosomal RNA	ribozyme	translation	Part of the small ribosomal subunit. Aides in catalyzing amino acid transfer from tRNAs
ACTB	actin, beta	cytoskeletal protein	cytoskeletal	a non-muscle cytoskeletal actin; major constituent of the contractile apparatus
CTNNB1	beta catennin	cell adhesion molecule	cell fate specification	Involved in the regulation of cell adhesion and canonical Wnt signalling pathway
EEF1A1	eukaryotic translation elongation factor 1 alpha 1	translation elongation factor activity	protein biosynthesis	an isoform of the alpha subunit of the elongation factor-1 complex, which is responsible for the enzymatic delivery of aminoacyl tRNAs to the ribosome
GAPD	glyceraldehyde-3-phosphate dehydrogenase	dehydrogenase	carbohydrate metabolism	catalyzes the reversible oxidative phosphorylation of glyceraldehyde-3-phosphate in the presence of inorganic phosphate and nicotinamide adenine dinucleotide
RAF1	murine leukemia viral oncogene homolog 1	Non-receptor serine/threonine protein kinase	activation of MAPKK activity ; signal transduction	transduction of mitogenic signals from the cell membrane to the nucleus

Table 9-12 Miniarray: maintenance of stem cell genes

Gene symbol	Description	Molecule type	Process	Gene function
NANOG	Homeobox transcription factor Nanog	Transcription factor	Regulation of somatic stem cell maintenance; embryonic development	transcription regulator influencing embryonic stem cells proliferation and self-renewal. Imposes pluripotency on ES cells by preventing differentiation. Overexpression increases proliferation
POU5F1	POU class 5 homeobox 1	Transcription factor	cardiac cell fate determination; somatic stem cell maintenance; morphogenesis	translocation of this gene with the Ewing's sarcoma gene has been linked to tumor formation
TDGF1	teratocarcinoma-derived growth factor 1	Growth factor	cardiac muscle cell differentiation	an extracellular, membrane-bound signaling protein that plays an essential role in embryonic development and tumor growth. Mutations in this gene are associated with forebrain defects
DNMT3B	DNA (cytosine-5-)-methyltransferase 3, beta	DNA methyltransferase	positive regulation of neuron differentiation	essential for the establishment of DNA methylation patterns during development
GABRB3	gamma-aminobutyric acid (GABA) A receptor, beta 3	ligand-gated ion channel	signal transduction ; synaptic transmission	is one of at least 13 distinct subunits of a multisubunit chloride ion channel that serves as the receptor for gamma-aminobutyric acid, the major inhibitory transmitter of the nervous system
GDF3	Growth differentiation factor type 3	cytokine	growth	regulator of cell growth and differentiation in both embryonic and adult tissues
Sox2	SRY (sex determining region Y)-box 2	transcription factor	negative regulator of osteoblast differentiation ; positive regulation of neuroblast proliferation	is required for stem-cell maintenance in the central nervous system

Table 9-13 Correlation with stemness genes

Gene symbol	Description	Molecule type	Process	Gene function
BRIX	biogenesis of ribosomes, homolog	Ribosomal protein	ribosome and protein biogenesis	Required for biogenesis of the 60S ribosomal subunit
CD9		Cell surface glycoprotein	Signal transduction; stem cell maintenance	functions in many cellular processes including differentiation, adhesion, and signal transduction
COMMD3	COMM domain containing 3			unclear
CRABP2	cellular retinoic acid binding protein 2	Transfer/carrier protein	epidermis development ; embryonic forelimb morphogenesis	a cytosol-to-nuclear retinoic acid binding shuttling protein, which facilitates RA binding to its cognate receptor complex
EBAF	endometrial bleeding associated factor			secreted member of the TGF-beta family of proteins; implicated in Left-Right axis formation
FGF4	fibroblast growth factor 4	Signaling molecule	chondroblast differentiation	suggested a function in bone morphogenesis and limb development through the sonic hedgehog (SHH) signaling pathway
FGF5	fibroblast growth factor 5	Signaling molecule	nervous system development	involved in a variety of biological processes, including embryonic development, cell growth, morphogenesis, tissue repair, tumor growth and invasion.
FOXD3	forkhead box D3	Transcription factor	cartilage development ; melanocyte differentiation ;	Required for maintenance of pluripotent cells in the pre-implantation and peri-implantation stages of embryogenesis
GAL	galanin prepropeptide	Peptide hormone	response to stress ; nervous system development ;	modulating diverse physiologic functions; primarily as a neurotransmitter. It causes negative regulation of lymphocyte proliferation
GBX2	gastrulation brain homeobox 2	Transcription factor	hindbrain development ; autonomic nervous system development	transcription factor for cell pluripotency and differentiation in the embryo
GRB7	growth factor receptor-bound protein 7	Trans-membrane receptor	signal transduction ; epidermal growth factor	Interacts with the cytoplasmic domain of the epidermal growth factor receptor which is then inhibited

			pathway	
IFITM1	interferon induced transmembrane protein 1	receptor signaling protein activity	negative regulation of cell proliferation ; response to biotic stimulus	Implicated in the control of cell growth. Component of a multimeric complex involved in the transduction of anti-proliferative and homotypic adhesion signals
IFITM2	interferon induced transmembrane protein 2	Miscellaneous function	immune response ; response to biotic stimulus	IFN-induced antiviral protein that mediates cellular innate immunity; Induces cell cycle arrest and mediates apoptosis by caspase activation and in p53-independent manner
IL6ST	interleukin 6 signal transducer	Cytokine receptor	positive regulation of cell proliferation ; positive regulation of osteoblast differentiation	a signal transducer shared by many cytokines; Knockout studies in mice suggest that this gene plays a critical role in regulating myocyte apoptosis
IMP2	IMP2 inner mitochondrial membrane peptidase-like			catalytic subunits of the IMP complex; complex generates mature, active proteins in the mitochondrial intermembrane space
KIT	v-kit Hardy-Zuckerman 4 feline sarcoma viral oncogene homolog	Tyrosine protein kinase receptor	lymphoid progenitor cell differentiation ; hemopoiesis ; somatic stem cell maintenance; germ cell programmed cell death	This gene encodes the human homolog of the proto-oncogene c-kit. Mutations in this gene are associated with gastrointestinal stromal tumors, mast cell disease, acute myelogenous lukemia, and piebaldism.
LEFTB	left-right determination factor 1	Signaling molecule	development ; somatic stem cell division ; positive regulation of long-term neuronal synaptic plasticity	This gene encodes a member of the TGF-beta family of proteins. A similar secreted protein in mouse plays a role in left-right asymmetry determination of organ systems during development.
LIFR	leukemia inhibitory factor receptor alpha	Cytokine receptor	organ regeneration	This protein combines with a high-affinity converter subunit, gp130, to form a receptor complex that mediates the action of the leukemia inhibitory factor, a polyfunctional cytokine that is involved in cellular differentiation, proliferation and survival in the adult and the embryo. Mutations in this gene cause Schwartz-Jampel syndrome type 2, a disease belonging to the group of the bent-bone dysplasias.
LIN28	lin-28 homolog A	Nucleic acid binding	stem cell maintenance ; stem cell differentiation	Acts as a 'translational enhancer', driving specific mRNAs to polysomes and thus increasing the efficiency of protein synthesis. Essential for skeletal muscle differentiation program through the translational up-regulation of IGF2 expression.

NODAL	nodal homolog	Cytokine	mesoderm formation ; nervous system development ; stem cell maintenance ; embryonic heart tube development	protein encoded by this gene is a member of the TGF-beta superfamily. Studies of the mouse counterpart suggested that this gene may be essential for mesoderm formation and subsequent organization of axial structures in early embryonic development
NOG	noggin	Extracellular matrix cytokine	embryonic development	The secreted polypeptide binds and inactivates members of the transforming growth factor-beta (TGF-beta) superfamily signaling proteins, such as bone morphogenetic protein-4. By diffusing through extracellular matrices more efficiently than members of the TGF-beta superfamily, this protein may have a principal role in creating morphogenic gradients.
NR5A2	nuclear receptor subfamily 5, group A, member 2	Nuclear hormone receptor	embryonic development	a critical cis-element of gene expression and regulation. May contribute to the regulation of pancreas-specific genes and play important roles in embryonic development
NR6A1	nuclear receptor subfamily 6, group A, member 1	Nuclear hormone receptor	gametogenesis ; spermatogenesis	This gene encodes an orphan nuclear receptor which is a member of the nuclear hormone receptor family. Its expression pattern suggests that it may be involved in neurogenesis and germ cell development.
PODXL	podocalyxin-like	Extracellular matrix glycoprotein	epithelial tube formation ; negative regulation of cell adhesion	biological activities include: binding in a membrane protein complex with Na+/H+ exchanger regulatory factor to intracellular cytoskeletal elements, playing a role in hematopoetic cell differentiation, and being expressed in vascular endothelium cells.
PTEN	phosphatase and tensin homolog	Protein phosphatase	central nervous system development ; heart development	is a phosphatidylinositol-3,4,5-trisphosphate 3-phosphatase. It contains a tensin like domain as well as a catalytic domain similar to that of the dual specificity protein tyrosine phosphatases. It negatively regulates intracellular levels of phosphatidylinositol-3,4,5-trisphosphate in cells and functions as a tumor suppressor by negatively regulating AKT/PKB signaling pathway.
REST	RE1-silencing transcription factor	transcriptional repressor	negative regulation of neuron differentiation	a transcriptional repressor that represses neuronal genes in non-neuronal tissues. The protein is also found in undifferentiated neuronal progenitor cells and it is thought that this repressor may act as a master negative regular of neurogenesis.
SEMA3A	sema domain, immunoglobulin domain (Ig), (semaphorin) 3A	Membrane-bound signaling molecule	nervous system development	This secreted protein can function as either a chemorepulsive agent, inhibiting axonal outgrowth, or as a chemoattractive agent, stimulating the growth of apical dendrites. In both cases, the protein is vital for normal neuronal pattern development.
SFRP2	secreted frizzled-related protein 2	Signaling molecule	positive regulation of fat cell differentiation ; cartilage development ; bone morphogenesis	homologous to the putative Wnt-binding Frizzled proteins. SFRPs act as soluble modulators of Wnt signaling.

TERT	telomerase reverse transcriptase	Reverse transcriptase	telomere maintenance ; replicative senescence	Telomerase is a ribonucleoprotein polymerase that maintains telomere ends by addition of the telomere repeat TTAGGG.
TFCP2L1	transcription factor CP2-like 1	Transcription factor	epithelial cell morphogenesis	Transcriptional suppressor. May suppress UBP1-mediated transcriptional activation. Modulates the placental expression of CYP11A1
UTF1	undifferentiated embryonic cell transcription factor 1	Transcription factor	male gonad development	Acts as a transcriptional coactivator of ATF2. Implicated in embryonic stem cell maintenance.
Xist	X (inactive)-specific transcript (non-protein coding)			The XIST gene is expressed exclusively from the XIC of the inactive X chromosome. The transcript is spliced but apparently does not encode a protein. The transcript remains in the nucleus where it coats the inactive X chromosome.
ZFP42	zinc finger protein 42 homolog (mouse)	Transcription factor	meiosis male gonad development	Involved in self-renewal property of ES cells

Table 9-14 Differentiation genes

ACTC	actin, alpha, cardiac muscle 1	Cytoskeletal protein	cardiac myofibril assembly; cardiac muscle morphogensis	one of three main groups of actin isoforms, alpha, beta, and gamma. The alpha actins are found in muscle tissues and are a major constituent of the contractile apparatus.
AFP	alpha-fetoprotein	metal ion binding	sexual reproduction; pancreas development; organ regeneration	The protein is thought to be the fetal counterpart of serum albumin, and the alpha-fetoprotein and albumin genes are present in tandem in the same transcriptional orientation on chromosome 4.
CD34	CD 34 molecule	Cell surface	regulation of immune response; immune cell migration	CD34 is a monomeric cell surface antigen with a molecular mass of approximately 110 kD that is selectively expressed on human hematopoietic progenitor cells
CDH5	cadherin 5, type 2 (vascular endothelium)	Cell surface	Cell adhesion molecule; negative regulation of cell proliferation	encoded protein is a calcium-dependent cell-cell adhesion glycoprotein comprised of five extracellular cadherin repeats, a transmembrane region and a highly conserved cytoplasmic tail. Functioning as cadherin by imparting to cells homophilic bindings, may play an important role in endothelial cell biology through control of the cohesion and organization of the intercellular junctions.
CDX2	caudal type homeobox 2	transcription factor	blood vessel development; blastocyst development; trophectodermal cell differentiation	The proteins LMX1 (MIM 600298) and CDX3 are homeodomain proteins that bind an A/T-rich sequence in the insulin promoter and stimulate its transcription
CGB	chorionic gonadotropin, beta polypeptide	Peptide hormone	female gamete generation	CG is produced by the trophoblastic cells of the placenta and stimulates the ovaries to synthesize the steroids that are essential for the maintenance of pregnancy.
COL1A1	collagen, type I, alpha 1	Extracellular matrix structural protein	skeletal development; blood vessel development; osteoblast differentiation	Type I is a fibril-forming collagen found in most connective tissues and is abundant in bone,
COL2A1	collagen, type II, alpha 1	Extracellular matrix structural protein	skeletal development ; cartilage condensation; tissue homeostasis; endochondral ossification; chondrocyte differentiation	This gene encodes the alpha-1 chain of type II collagen, a fibrillar collagen found in cartilage
DDX4	DEAD (Asp-Glu-Ala-Asp) box polypeptide 4	RNA helicase	development ; sperm motility	members of this family are believed to be involved in embryogenesis, spermatogenesis, and cellular growth and division

DES	desmin	Cytoskeletal protein	muscle contraction; cytoskeleton organization and biogenesis	encodes a muscle-specific class III intermediate filament.
EOMES	eomesodermin	Transcription factor	endoderm formation ; mesoderm formation ; cell differentiation involved in embryonic placenta development	gene disrupted in mice is shown to be essential during trophoblast development and gastrulation
FLT1	fms-related tyrosine kinase 1	Protein kinase receptor	sprouting angiogenesis ; development ; pregnancy ; cell differentiation	gene encodes a member of the vascular endothelial growth factor receptor (VEGFR) family. This protein binds to VEGFR-A, VEGFR-B and placental growth factor and plays an important role in angiogenesis and vasculogenesis. Expression of this receptor is found in vascular endothelial cells, placental trophoblast cells and peripheral blood monocytes.
FN1	fibronectin 1	Cell adhesion molecule	angiogenesis	gene encodes fibronectin, a glycoprotein present in a soluble dimeric form in plasma, and in a dimeric or multimeric form at the cell surface and in extracellular matrix; involved in cell adhesion and migration processes including embryogenesis, wound healing, blood coagulation, host defense, and metastasis.
FOXA2	forkhead box A2	Transcription factor	embryonic development;; lung development ; neuron fate specification	gene encodes a member of the forkhead class of DNA-binding proteins. These hepatocyte nuclear factors are transcriptional activators for liver-specific genes and also interact with chromatin.
GATA4	GATA binding protein 4	Transcription factor	positive regulation of cardioblast differentiation	gene encodes a member of the GATA family of zinc-finger transcription factors; protein is thought to regulate genes involved in embryogenesis and in myocardial differentiation and function. Mutations in this gene have been associated with cardiac septal defects
GATA6	GATA binding protein 6	Transcription factor	endoderm development; cardiac muscle cell differentiation	Thought to be important for regulating terminal differentiation and/or proliferation
GCG	glucagon	Peptide hormone	cell proliferation ; regulation of insulin secretion	plays a key role in glucose metabolism and homeostasis; stimulates intestinal growth and up-regulates villus height in the small intestine, concomitant with increased crypt cell proliferation and decreased enterocyte apoptosis.
GCM1	glial cells missing homolog 1	Transcription factor	cell differentiation involved in embryonic placenta development	Transcription factor that is necessary for placental development. Binds to the trophoblast-specific element 2 (TSE2) of the aromatase gene enhancer

GFAP	glial fibrillary acidic protein	Cytoskeletal protein	structural constituent of cytoskeleton	gene encodes one of the major intermediate filament proteins of mature astrocytes. It is used as a marker to distinguish astrocytes from other glial cells
HBB	hemoglobin, beta	Transfer/carrier protein	positive regulation of cell death	Involved in oxygen transport from the lung to the various peripheral tissues
HBZ	hemoglobin, zeta	Transfer/carrier protein	erythrocyte maturation	The zeta chain is an alpha-type chain of mammalian embryonic hemoglobin, synthesized primarily in the yolk sac
HLXB9	motor neuron and pancreas homeobox 1	Transcription factor	morphogenesis ; post-embryonic development	Putative transcription factor involved in pancreas development and function
IAPP	islet amyloid polypeptide	Peptide hormone	endocrine pancreas development ; negative regulation of bone resorption	can induce apoptotic cell-death in particular cultured cells, an effect that may be relevant to the development of type II diabetes
INS	insulin	Peptide hormone	carbohydrate metabolism ; positive regulation of cell proliferation	Insulin decreases blood glucose concentration.
IPF1	pancreatic and duodenal homeobox 1	Transcription factor	positive regulation of cell proliferation ; organ morphogenesis	The encoded nuclear protein is involved in the early development of the pancreas and plays a major role in glucose-dependent regulation of insulin gene expression
ISL1	ISL LIM homeobox 1	Transcription factor	generation of precursor metabolites and energy	The encoded protein is central to the development of pancreatic cell lineages and may also be required for motor neuron generation. Mutations in this gene have been associated with maturity-onset diabetes of the young
KRT1	keratin 1	Structural protein	epidermis development ; regulation of angiogenesis	heterotypic keratin chains coexpressed during differentiation of simple and stratified epithelial tissues. This type II cytokeratin is specifically expressed in the spinous and granular layers of the epidermis
LAMA1	laminin, alpha 1	Extracellular matrix linker protein	cell adhesion ; substrate adhesion-dependent cell spreading	laminin is thought to mediate the attachment, migration and organization of cells into tissues during embryonic development by interacting with other extracellular matrix components
LAMB1	laminin, beta 1	Extracellular matrix linker protein	cell adhesion; substrate adhesion-dependent cell spreading ; odontogenesis ;	laminin is thought to mediate the attachment, migration and organization of cells into tissues during embryonic development by interacting with other extracellular matrix components

LAMC1	laminin, gamma 1	Extracellular matrix linker protein	protein complex assembly ; cell adhesion ; extracellular matrix disassembly ; adhesion-dependent cell spreading	Embryos of transgenic mice in which both alleles of the gamma 1 chain gene were inactivated by homologous recombination, lacked basement membranes, indicating that laminin, gamma 1 chain is necessary for laminin heterotrimer assembly.
MYF5	myogenic factor 5	Transcription factor	muscle cell differentiation ; muscle cell fate commitment	Involved in muscle differentiation (myogenic factor). Induces fibroblasts to differentiate into myoblasts.
MYOD1	myogenic differentiation 1	Transcription factor	muscle development ; myoblast cell fate determination	gene encodes a nuclear protein that belongs to the basic helix-loop-helix family of transcription factors and the myogenic factors subfamily. It regulates muscle cell differentiation by inducing cell cycle arrest, a prerequisite for myogenic initiation.
NES	nestin	Cytoskeletal protein		It is expressed predominantly in stem cells of the central nervous system in the neural tube. Upon terminal neural differentiation, nestin is downregulated and replaced by neurofilaments
NEUROD1	neurogenic differentiation 1	Transcription factor	positive regulation of neuron differentiation ; neurogenesis	Differentiation factor required for dendrite morphogenesis and maintenance in the cerebellar cortex.
NPPA	natriuretic peptide A	Peptide hormone	negative regulation of cell growth	Natriuretic peptides are implicated in the control of extracellular fluid volume and electrolyte homeostasis. Mutations in this gene have been associated with atrial fibrillation familial type 6
OLIG2	oligodendrocyte lineage transcription factor 2	Transcription factor	nervous system development	The protein is an essential regulator of ventral neuroectodermal progenitor cell fate
PAX4	paired box 4	Transcription factor	organ morphogenesis	These genes play critical roles during fetal development and cancer growth. The paired box 4 gene is involved in pancreatic islet development and mouse studies have demonstrated a role for this gene in differentiation of insulin-producing beta cells
PAX6	paired box 6	Transcription factor	central nervous system development	known to bind DNA, and function as regulators of gene transcription. This gene is expressed in the developing nervous system, and in developing eyes.
PECAM1	platelet/endothelial cell adhesion molecule	Cell adhesion molecule	cell recognition ; cell adhesion	encoded protein is a member of the immunoglobulin superfamily and is likely involved in leukocyte migration, angiogenesis, and integrin activation
PTF1A	pancreas specific transcription factor, 1a	Transcription factor	embryonic development tissue development	gene encodes a protein that is a component of the pancreas transcription factor 1 complex; and is known to have a role in mammalian pancreatic development.

RUNX2	runt-related transcription factor 2	Transcription factor	skeletal development	gene is a member of the RUNX family of transcription factors and encodes a nuclear protein; protein is essential for osteoblastic differentiation
SERPINA1	serpin peptidase inhibitor, clade A	Serine protease inhibitor	response to organic cyclic substance	protein encoded by this gene is secreted and is a serine protease inhibitor whose targets include elastase, plasmin, thrombin, trypsin, chymotrypsin, and plasminogen activator.
SOX17	SRY (sex determining region Y)-box 17	Transcription factor	cardiac cell fate determination	gene encodes a member of the SOX (SRY-related HMG-box) family of transcription factors involved in the regulation of embryonic development and in the determination of the cell fate
SST	somatostatin	Peptide hormone	negative regulation of cell proliferation induction of apoptosis by hormones	This hormone is an important regulator of the endocrine system through its interactions with pituitary growth hormone, thyroid stimulating hormone, and most hormones of the gastrointestinal tract. Somatostatin also affects rates of neurotransmission in the central nervous system and proliferation of both normal and tumorigenic cells
SYCP3	synaptonemal complex protein 3	DNA binding	cell division	encodes an essential structural component of the synaptonemal complex. This complex is involved in synapsis, recombination and segregation of meiotic chromosomes
SYP	synaptophysin	Membrane traffic regulatory protein	regulation of long-term neuronal synaptic plasticity ; synaptic vesicle maturation	Synaptophysin (p38) is an integral membrane protein of small synaptic vesicles in brain and endocrine cells
T	T, brachyury homolog	Transcription factor	vasculogenesis somitogenesis neural plate morphogenesis	Encodes an embryonic nuclear transcription factor that binds to a specific DNA element, the palindromic T-site. The protein is localized to notochord-derived cells
TAT	tyrosine aminotransferase	Synthase	biosynthesis ; response to organic cyclic substance	encodes a mitochondrial protein tyrosine aminotransferase which is present in the liver and catalyzes the conversion of L-tyrosine into p-hydroxyphenylpyruvate.
TH	tyrosine hydroxylase	Oxygenase	heart development	gene is involved in the conversion of tyrosine to dopamine.
WT1	Wilms tumor 1	Transcription factor	heart development ; vasculogenesis ; ureteric bud development	Transcription factor that plays an important role in cellular development and cell survival. Regulates the expression of numerous target genes, including EPO. Plays an essential role for development of the urogenital system.

9.6 Appendix VI: Specimen characterisation data sheets

The attached documents are of the pre-liminary characterizations of human mesenchymal stromal cells, isolated from human bone marrow aspirates at Tulane University, New Orleans, USA. The data sheets are for donors 7032, 7043 and 7081.

9.7 Appendix VII: Copy of University of London Central Research Fund application

9.8 Appendix VIII: Academic activities

9.8.1 Papers

The differential modulation of key bone matrix components by modified Ti surfaces. MR Khan, N Donos, V Salih, PM Brett. Bone 2012; 50 (1): 1-8.

Deregulation of the Axl tyrosine kinase pathway in human mesenchymal stromal cell responses to rough implant surfaces. MR Khan, N Donos, V Salih, PM Brett (submitted).

Differential attachment and morphology of human mesenchymal stromal cells to modified Titanium surfaces. MR Khan, N Donos, V Salih, N Mordan, M Parkar, PM Brett (in preparation).

9.8.2 Presentations

Oral. Examining Axl receptor tyrosine kinase in cell osteogenic responses to modified surfaces. European Calcified Tissue Society, Postgraduate course. Rome, Italy. 1-4 September, 2008.

Oral. Investigating the role of tyrosine kinase Axl in modulating Marrow Stromal Cell responses to Rough Titanium Implant Surfaces. MPhil to PhD upgrade examination. UCL Eastman Dental Institute, London, UK. 5 November, 2008.

Oral. Modulation of Tyrosine Kinase AXL in Marrow Stromal Cells by Rough Titanium Implant Surfaces. Presentation to visiting team from Straumann AG (Switzerland). London, UK.15 December, 2008.

Oral. Accelerated osteogenic responses of human marrow stromal cells to modified Ti surfaces. Biomaterials and tissue engineering Departmental Seminar. UCL Eastman Dental Institute, London, UK. 8 July, 2009.

Oral. Tissue engineering and future therapeutics. Guest speaker at the surgeons club. Al Khobar, Saudi Arabia. 9 September, 2009.

Oral. Differential responses of cells to Ti implant surfaces. Presentation to visiting team from Straumann AG (Switzerland). 13 October, 2009.

Poster. Novel assessment of mesenchymal stromal cells to modified implant surfaces. International Association of Dental Research annual meeting. Barcelona, Spain. Date 14-17 July, 2010. Candidate for Young Investigator Prize.

9.8.3 Reports

Report for MPhil to PhD upgrade to Prof Mark Lewis and Dr Farlan Veraitch. 5 November, 2008 and with modification on 5 May, 2009.

Study completion report for International Team for Implantology and Straumann AG.

Extended abstract for IADR 2010 Young Investigator Award.

9.8.4 Conferences

UCL Stem Cell Day; October 2007.

Pan European Federation International Association for Dental Research, PEF-IADR. London, UK. Dates: September 10 - 12, 2008.

International Association for Dental Research, IADR. Barcelona, Spain. Dates: July 13 – 17, 2010.

9.8.5 Sponsorship / Grants

University of London, Central Research Fund (CRF) award; total = £ 4,250.00.

UCL Eastman Dental Institute conference fund; total = £ 400.00.

UCL Graduate School Conference fund; total = £ 350.00.